ASSESSMENT OF THE DISPERSION ERROR AND GOAL-ORIENTED ADAPTIVITY FOR WAVE PROBLEMS

Lindaura Maria Steffens

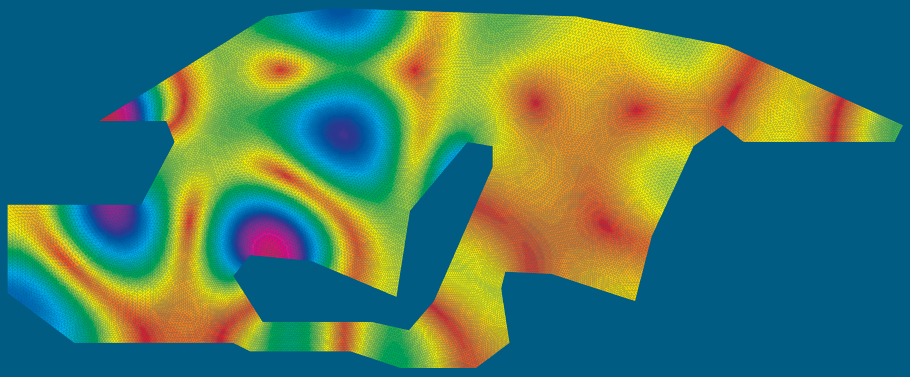

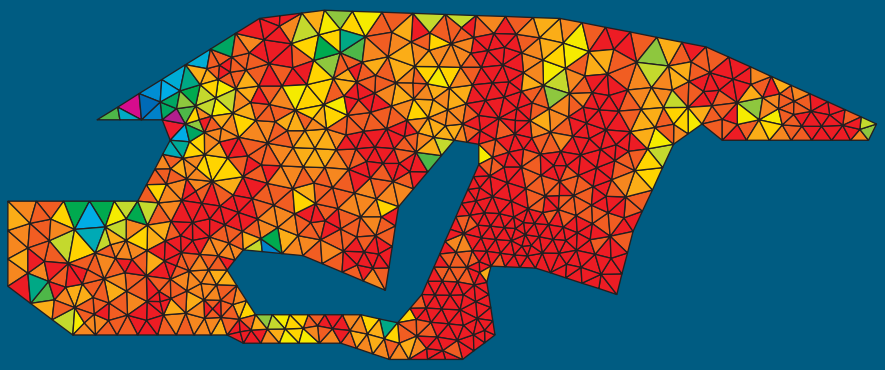

Doctoral Thesis
Barcelona, July 2010

ASSESSMENT OF THE DISPERSION ERROR AND GOAL-ORIENTED ADAPTIVITY FOR WAVE PROBLEMS

Lindaura Maria Steffens

Doctoral Thesis
Advisors: Pedro Díez and Núria Parés
Barcelona, July 2010

Departament de Matemàtica Aplicada III
Programa de Doctorat de Matemàtica Aplicada

Aos meus pais Elvino e Maria,

à minha amiga Cris,

e especialmente à minha irmã Edi.

Um homem precisa viajar.
Por sua conta, não por meio de histórias, imagens, livros ou televisão.
Precisa viajar por si, com seus olhos e pés, para entender o que é seu.
Para um dia plantar as suas próprias árvores e dar-lhes valor.
Conhecer o frio para desfrutar o calor. E o oposto.
Sentir a distância e o desabrigo para estar bem sob o próprio teto.

Um homem precisa viajar para lugares que não conhece para quebrar essa

arrogância que nos faz ver o mundo como o imaginamos,
e não simplesmente como é ou pode ser.

Que nos faz professores e doutores do que não vimos,

quando deveríamos ser alunos,
e simplesmente ir ver.
(Amyr Klink)

Contents

APPENDED PAPERS

Paper A

Steffens, L. and Díez, P. (2009), A simple strategy to assess the error in the numerical wave number of the finite element solution of the Helmholtz equation, *Comput. Methods Appl. Mech. Engrg.* 198, 1389-1400.

Paper B

Steffens, L., Parés, N. and Díez, P. (2010), Estimation of the dispersion error in the numerical wave number of standard and stabilized finite element approximations of the Helmholtz equation, *Internat. J. Numer. Methods Engrg.* Accepted for publication.

Paper C

Steffens, L., Parés, N. and Díez, P. (2010), Goal oriented *h*-adaptivity for the Helmholtz equation: error estimates, local indicators and refinement strategies, *Comput. Mech.* Submitted for publication.

Acknowledgements

The work developed in this thesis has been possible thanks to the support, guidance, motivation and suggestions of many people. Without these people, this thesis would never have been completed. I wish to express my thanks to everyone who has contributed in one way or another to accomplishing this work.

Gostaria de agradecer aos professores da Universidade Federal de Santa Catarina pelo incentivo e encorajamento em realizar meus estudos em Barcelona, em especial ao professor e orientador Marcelo Krajnc Alves. Obrigada por todo seu apoio e seus sábios conselhos.

Mis sinceros agradecimientos a mis tutores y directores de tesis, Pedro Díez y Núria Parés, por vuestras innumeras ideas y sugestiones constructivas. Agradezco vuestra paciencia, dedicación y magnifica dirección durante estos años, que han hecho posible llevar a buen término este trabajo.

Al Pedro, a quien considero un gran ejemplo como profesional, investigador y persona, le quiero dar las gracias porque siempre me ha brindado su total apoyo, seriedad y responsabilidad, por los conocimientos que me ha transmitido, por los buenos consejos que me ha dado, por el buen sentido del humor que siempre me ha tratado, por la manera especial que ha tenido para dirigir mi tesis doctoral, pero sobre todo por darme la oportunidad de vivir esta grande experiencia tanto en nivel profesional como personal.

A la Núria no puc estar-li més agraïda. Suposo que haver estat la seva primera doctoranda no hi haurà estat una tasca fàcil, però amb aquestes línies vull expressar la meva gratitud més sincera. Agraeixo la seva ajuda, la seva disponibilitat, la seva direcció rigorosa i plena de criteri, els seus comentaris sempre encertats i seva excel·lent intuïció. Gràcies al tot el temps que hem passat juntes he après molt i m'he

convertit en una professional millor. A més, li vull agrair les mil i una hores que ha passat corregeint-me una i altra vegada els escrits que he realitzat. De fet, sense la seva ajuda no hauria pogut escriure aquesta tesi. Amb tota la meva admiració i respecte: Gràcies de tot cor!

Pedro i Núria, moltes gràcies per haver supervisat als meus primers passos com a investigadora, ha estat un veritable plaer i un honor haver treballat amb vosaltres tots aquests anys.

También deseo agradecer al profesor Antonio Huerta por haberme permitido venir e incorporarme al grupo de investigación LaCàN (Laboratori de Càlcul Numèric). Tampoco puedo olvidarme de los profesores del grupo con los cuales he cursado asignaturas, seminarios y he compartido conversaciones y discusiones productivas, en especial agradezco a Antonio Rodríguez, Josep, Marino, Sonia, Rubén y Esther. Muchas gracias a Imma, a Àngels, a Carmen Lopez y Carme Capdevila, por solucionar las cuestiones administrativas y burocraticas, y a David por su ayuda y soporte técnico.

Evidentemente ocupan un lugar muy especial los amigos y compañeros de doctorado. No voy a nombrarlos, por miedo a dejarme a alguno fuera. Sin embargo quiero detallar algunos momentos especiales que seguro nos habrán marcado mucho y nos dejaran recuerdos para el resto de nuestras vidas. Con ellos he compartido muchos momentos de trabajo, dificultades y también de diversión y alegrías. Las horas del almuerzo, cafés, las largas discusiones y conversaciones sean de métodos numéricos, vida personal o incluso de futbol, quedarán para siempre en mis memorias.

Agradezco a todos los amigos que me hayan apoyado, acompañado y aconsejado durante mi estancia en Barcelona. Ha sido en verdad un placer haber compartido este tiempo de mi vida con todos ustedes.

He de agradecer a la Programa Alβan (European Union Programme of High Level Scholarships for Latin America, scholarship no. E06D100641BR) por haberme concedido una beca durante los tres primeros años y al LaCàN por proporcionarme financiación con un proyecto del plan nacional durante el último año.

Agradeço a todos meus familiares e amigos, que mesmo a distância sempre acompanharam minha trajetória, apoiando e acreditando na minha capacidade. Obrigada pela compreensão nos momentos que precisaram de mim e estive ausente.

À Mari, por sua amizade desde o primeiro dia de Barcelona. Obrigada por sua energia e otimismo. Nestes anos compartilhamos mais que um apartamento, compartilhamos nossas vidas, com suas alegrias e dificuldades, e principalmente, nossa saudade de casa. Obrigada por tudo!

Ao meu ogro predileto, Gustavo, por seu apoio, amizade e capacidade de tranquilizar-me, e especialmente por seu amor. ♫ *Although I've traveled far I always hold a place for you in my heart...*♫

Não posso deixar de agradecer a minha melhor amiga Cris, que mesmo estando longe sempre está junto comigo, dando-me alegrias, carinho e seu amor incondicional. ♫ *A distância, a saudade e a sua falta me fazem amar você ainda mais. Você estará comigo até o fim!*♫

O meu muitíssimo obrigado a minha *piquitita*, por embarcar nesta 'aventura', por me aguentar nos dias de desânimo e mau humor, apoiando-me nos momentos difíceis e vibrando com minhas conquistas. Obrigada simplesmente por estar sempre ao meu lado. ♫ *I remember how we'd fight We made up and laughed all night Wish we were kids again My sister my friend...*♫

Por último, mas não menos importante agradeço e dedico esta tese aos meus queridos pais, a quem devo minhas vitórias, meus valores e acima de tudo a pessoa que sou. ♫ *...e não há nada pra comparar para poder lhe explicar como é grande o meu amor por você Nem mesmo o céu nem as estrelas nem mesmo o mar e o infinito não é maior que o meu amor por você Nunca se esqueça nem um segundo que eu tenho o amor maior do mundo Como é grande o meu amor por você!* ♫

Barcelona — Lindaura Maria Steffens

Julho, 2010

Abstract

This thesis presents an *a posteriori* estimator for the error in the wave number in the context of finite element approximations of the Helmholtz equation, both for standard and stabilized formulations. We also introduce a new goal-oriented adaptive strategy using post-processing techniques.

The simple strategy assessing the error in the wave number is based on the determination of the numerical wave number that better accommodates the numerical solution. Compared to other goal-oriented error estimation strategies, the approach proposed in this work is innovative because it adopts a new paradigm.

A distinctive feature of this method is that the error estimation procedure is devoted to obtain the numerical wave number, corresponding to the approximate solution, instead of the exact one, which is known as part of the data of the problem. Thus, the error in the wave number is consistently defined as the outcome of a global minimization problem. This problem is computationally unaffordable and, for practical error estimation purposes, is approximated. An enhanced approximation is obtained from the finite element solution using a simple local least-squares technique. Once the enhanced solution is obtained, the associated numerical wave number is readily recovered using a simple closed expression. An alternative improved recovery technique is developed to take advantage of the nature of the solutions of wave problems. The standard polynomial least-squares technique is replaced by a new exponential fitting, yielding much sharper results in most cases.

The proposed new goal-oriented adaptive strategy is based on post-processed solutions and is valid both for linear and non-linear quantities of interest. In the non-linear case the linear contribution to the quantity of interest is assumed to be the leading term. Two different representations to recover the error in the quantity

of interest are studied, both providing similar results in the adaptive procedures. It has been shown that the accuracy of these representations, which involve the post-processing of either the primal or adjoint finite element approximations, is related to the dispersion error of its corresponding problems. Moreover, the adaptive procedure leads to a faster reduction of the error when compared with a uniform refinement. The proposed error estimate properly identifies the areas most contributing to the error in the quantity of interest and consequently the adaptive procedure yields adapted meshes that provide accurate results.

Key words: *Wave problems, Helmholtz equation, Error estimation of wave number, A posteriori error estimation, Dispersion/pollution error, Goal-oriented adaptivity, Local indicators, Finite element method, Stabilized methods.*

Chapter 1

Introduction and state-of-the-art

1.1 Motivation and objectives

Computational numerical methods are becoming an increasingly requested tool for solving different types of problems in all branches of engineering and applied sciences. However, any numerical method yields an approximated solution to the problem. The numerical solutions are affected by errors coming from different sources. The *modeling error* is accounting for the discrepancy between the mathematical model and the physical reality. In this work we concentrate in assessing the *discretization error* which is associated with the numerical accuracy obtained in solving the mathematical problem. The discretization error can be computed approximately using *a posteriori* error estimators. Besides providing information about the global accuracy of a simulation, error estimates describe the spatial distribution of the error and consequently allow developing adaptive schemes.

In this context, it is worth highlighting the particular difficulty in solving wave propagation problems. The numerical solution of these problems has been an active area of research since the early sixties. This area is common to various fields of application: acoustics, geophysics, meteorology, electromagnetics, shallow water, fluid dynamics, among others. Unfortunately, standard numerical methods can not cope with wave phenomena characterized by high frequencies (large wave numbers) without requiring a prohibitive computational effort.

Recently, Bouillard, Almeida, Decouvreur and Mertens (2008) have considered that the simulation of the wave propagation phenomenon is one of the most chal-

lenging amongst computational mechanics. In wave propagation problems, many questions are still unsolved, namely: derivation of more accurate numerical methods in order enlarge the properly simulated frequency range; definition of artificial boundary conditions to effectively deal with unbounded domains; and finally, formulation and implementation of reliable error estimators, preferably in local or engineering quantities and their application to methods to adaptive methods.

The reference cited above shows that the key to face all these issues is the control of the so-called pollution effect, associated mainly with the dispersive nature of the numerical waves. To control such errors in an effective way is a major ongoing challenge.

This work aims precisely at discussing error estimation and adaptivity for wave propagation problems, specifically for the Helmholtz model. The original motivation was to tackle the shallow water problem, and then we started studying the Helmholtz equation, since it is a simplified version of the former. Thus, we concentrated in deriving error estimates for the pollution/dispersion error in the Helmholtz equation as a first step (and currently unsolved) to proceed further.

Shallow water problems describe the behavior of water flow in rivers, lakes and shallow seas in zones with smooth variation of the depth and with waves of small amplitude. They are also applied to the study of many physical phenomena of interest, such as, environmental effects, commercial activities on fisheries and coastal wildlife, remediation of contaminated bays and estuaries for the purposes of improving water quality. To efficiently perform these simulations, it is needed to develop systems and programs of high technological level.

A mathematical model for the simulation of shallow water problems is given by the *mild slope* or Berkhoff equation (Berkhoff, Booy and Radderc 1982):

$$\boldsymbol{\nabla} \cdot (cc_g \boldsymbol{\nabla} u) + \kappa^2 cc_g u = 0. \tag{1.1}$$

This model is based on the theory of simple harmonic linear waves. The equations of the hydrodynamics (mass balance or continuity equation and momentum equation) are used to describe the motion in fluid dynamics. The effects of nonlinearity, such as energy dissipation by friction or breaking, are not taken into account. Equation (1.1) accounts simultaneously the phenomena of refraction and diffraction. It is an elliptic equation and, for constant depth (constants c and c_g) it

reduces to the Helmholtz equation:

$$\boldsymbol{\Delta} u + \kappa^2 u = 0.$$

Despite its simplicity, many of the fundamental models for wave propagation in science and engineering are based on the Helmholtz equation. The active control of sound is an example of an important practical problem where models based on this equation play a fundamental role. Besides, to satisfy acoustic requirements is nowadays important in many sectors, such as the aerospace, automotive and building industries, among others.

The attempts of introducing error estimators for assessing the dispersion error in the Helmholtz problem have not been successful in the past, as explained later. Most of these estimators are global (energy norm) and they have the tendency to underestimate the error for high wave numbers, obtaining good estimates only when the pollution error is negligible. Moreover, error estimators in quantities of interest have not been explored to measure and control the dispersion error and often only in an one-dimensional setup.

The main goal of this thesis is to assess and control the errors in the context of finite element approximations of the Helmholtz equation. In this scenario the following partial goals are considered:

- **Obtaining a methodology to assess the dispersion error:** the goal is to develop a simple and inexpensive *a posteriori* technique to assess the error in the wave number and generalize the procedures developed for others discretization methods, aiming at controlling the dispersion error;

- **Strategies for obtaining goal-oriented error estimates and *h*-adaptivity:** the goal is to analyze the error for linear and non-linear outputs and to define outputs of interest for acoustic problems. Furthermore, to define local indicators and refinement strategies in order to implement an adaptive process.

To reach these goals, we accomplished the following tasks:

- analysis of the physical phenomena described by shallow water models, deduction of Berkhoff model and the simplified model, given by the Helmholtz equation;

- study of the dispersion and pollution effects, in order to propose more efficient procedures related to the convergence rate, estimates and control errors;
- study of other discretization methods for the Helmholtz equation, to improve the accuracy by reducing the dispersion error;
- building an inexpensive approximation through recovery techniques, so that it can be exploited in *a posteriori* error assessment;
- analysis of the behavior of the proposed and applied methods in order to compare the performance of the results obtained.

The first part of the goals is mainly related to the assessment of the dispersion error. This work and its results are detailed in (Steffens and Díez 2009), (Steffens, Parés and Díez 2010*a*) and also in chapter 2. The second part is related to goal-oriented error estimates and *h*-adaptivity. These partial goals are developed and presented in (Steffens, Parés and Díez 2010*b*) and in chapter 3.

1.2 Model problem - The Helmholtz equation

The propagation of acoustic waves through a fluid medium is governed by the wave equation

$$\frac{1}{c^2}\frac{\partial^2 P}{\partial t^2} = \boldsymbol{\Delta} P,$$

where c stands for the speed of sound in the medium. This equation describes the evolution of the acoustic pressure P as a function of the position $\mathbf{x}$ and time t. In order to reduce the complexity of the simulations, it is often assumed that the acoustic waves are harmonic in time. In this case, the acoustic pressure associated to an angular frequency ω is $P(\mathbf{x}, t) = u(\mathbf{x})e^{i\omega t}$ where $u(\mathbf{x})$ is the complex spatial distribution of the acoustic pressure and $i = \sqrt{-1}$ is the imaginary unit, and the wave equation reduces to the homogeneous Helmholtz equation:

$$\boldsymbol{\Delta} u + \kappa^2 u = 0, \tag{1.2}$$

where $\kappa = \omega/c \in \mathbb{R}$ stands for the wave number. It is worth nothing that the wave number κ characterizes the oscillatory behavior of the solution: the larger the value of κ, the stronger the oscillations.

Wave propagation problems are usually classified as interior or exterior, depending on whether one is interested in the sound field in bounded or unbounded regions in space.

The remainder of this section is devoted to provide an overview of interior and exterior problems for future reference.

1.2.1 Interior problems

Interior problems deal with acoustic phenomena in enclosed regions of space, such as cavity or room acoustics problems. The unknown $u(\mathbf{x})$ is the physical pressure, taking values for $\mathbf{x} \in \Omega \subset \mathbb{R}^d$ (d being the number of spatial dimensions, d =1, 2 or 3). The boundary of the domain Ω is denoted by $\partial\Omega$.

A complete definition of the problem to be solved, requires adding to equation (1.2) proper boundary conditions. For interior acoustic problems, three types of boundary conditions are considered: Dirichlet, Neumann and Robin (or mixed).

Dirichlet boundary conditions prescribe the values of the pressure on a part of the boundary $\Gamma_{\mathrm{D}} \subset \partial\Omega$. Namely,

$$u = u_D \qquad \text{on } \Gamma_{\mathrm{D}}.$$

On the Neumann part of the boundary $\Gamma_{\mathrm{N}} \subset \partial\Omega$ the normal component of the velocity is prescribed, namely

$$\boldsymbol{\nabla} u \cdot \mathbf{n} = g \qquad \text{on } \Gamma_{\mathrm{N}}.$$

If the Neumann boundary condition is produced by a vibrating rigid wall wich vibrates with the normal velocity v_n, producing a sound propagation in the medium, the Neumann data g is given by $g = -i\rho c\kappa v_n$, where ρ is the density of the medium. It is worth noting that for time-harmonic waves of the form $P(\mathbf{x}, t) = u(\mathbf{x})e^{-i\omega t}$ the Neumman data becomes $g = i\rho c\kappa v_n$ (note the change in sign).

Finally, the most general form of boundary condition is embodied in the Robin part of the boundary $\Gamma_{\mathrm{R}} \subset \partial\Omega$ as

$$\boldsymbol{\nabla} u \cdot \mathbf{n} = mu \qquad \text{on } \Gamma_{\mathrm{R}},$$

with $m = -i\rho c\kappa A_n$, where the coefficient A_n denotes the field admittance in the normal direction and represents the structural damping. The value of A_n depends on the nature of the enclosure and is associated with absorbent panels. For $A_n = 0$ it turns out to be an homogeneous Neumann boundary condition, standing for a perfectly reflecting panel or rigid wall. In the limit case as $A_n \to \infty$, the wall is said to be acoustically soft and one recovers the homogeneous Dirichlet boundary condition $u = 0$. For $0 < A_n < 1$, the wall acts as an absorbing surface, and the Robin condition is usually referred to as an absorbing boundary condition. Finally, for $A_n = 1/\rho c$ the boundary condition describes a fully absorbent panel, also called anechoic situation.

In order to get a well posed problem these three parts of the boundary must cover the whole boundary, that is $\partial\Omega = \overline{\Gamma_{\mathrm{D}} \cup \Gamma_{\mathrm{N}} \cup \Gamma_{\mathrm{R}}}$, see figure 1.1.

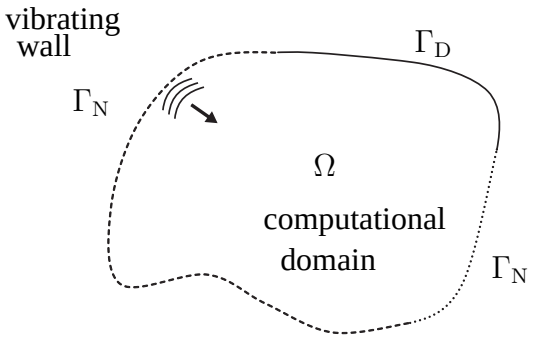

Figure 1.1: Acoustic problems in an interior region Ω.

To summarize, the general form of interior acoustic problems consists in finding the spatial component of the acoustic pressure field $u : \Omega \to \mathbb{C}$ such that

$$
\begin{aligned}
-\boldsymbol{\Delta} u - \kappa^2 u = 0 \qquad & \text{in } \Omega, \\
u = u_D \qquad & \text{on } \Gamma_{\mathrm{D}}, \\
\boldsymbol{\nabla} u \cdot \mathbf{n} = g \qquad & \text{on } \Gamma_{\mathrm{N}}, \\
\boldsymbol{\nabla} u \cdot \mathbf{n} = mu \qquad & \text{on } \Gamma_{\mathrm{R}}.
\end{aligned}
$$

1.2.2 Exterior problems

Exterior problems are concerned with the characterization of the acoustic field in the surrounding space of a given structure. The main difficulty in dealing with this class of problems is that the domain is unbounded in space and, therefore, a bounded computational domain has to be introduced. Examples of exterior problems are radiation, scattering and transmission problems. Figure 1.2 shows an example of a scattering problem, where an obstacle D is hit by a plane wave. It also shows the computational domain Ω.

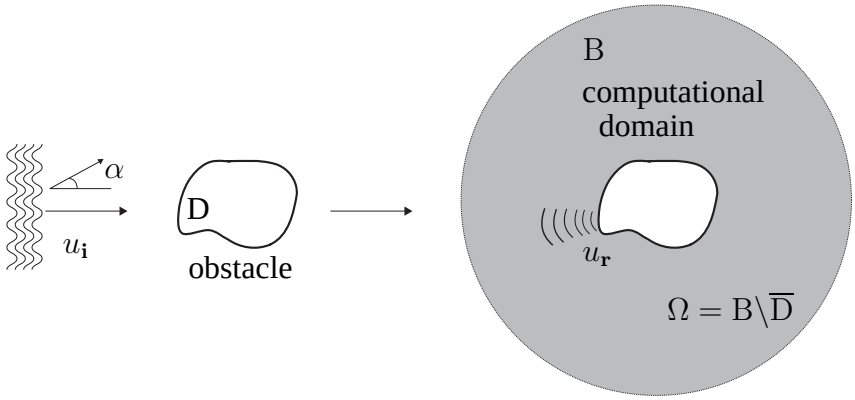

Figure 1.2: Scattering problems: a plane wave hits an obstacle D. The computational domain $\mathrm{B}\backslash\overline{\mathrm{D}}$ is obtained by introducing a sufficiently large ball B.

Consider first the radiation problem. Let $\mathrm{D} \subset \mathbb{R}^d$, $d = 1, 2$ or 3, be the region occupied by a body embedded in a homogeneous isotropic medium at rest, with smooth boundary $\partial\mathrm{D}$. Suppose that the walls of the body vibrate with normal velocity v_n and that the radiated waves propagate in space, see figure 1.3. The physical requirement that all radiated waves can not be reflected at infinity leads to the Sommerfeld radiation condition (Ihlenburg 1998)

$$\lim_{r\to\infty} \mathrm{r}^{\frac{d-1}{2}}(\boldsymbol{\nabla} u \cdot \mathbf{r} - i\kappa u) = 0,$$

where $\mathrm{r} = |\mathbf{x}|$ and $\boldsymbol{\nabla} u \cdot \mathbf{r}$ denotes the derivative in the radial direction. Imposing the Sommerfeld radiation condition requires solving the Helmholtz equation in an infinite domain and prevents the immediate use of traditional computational methods designed for bounded domains, such as the finite element method.

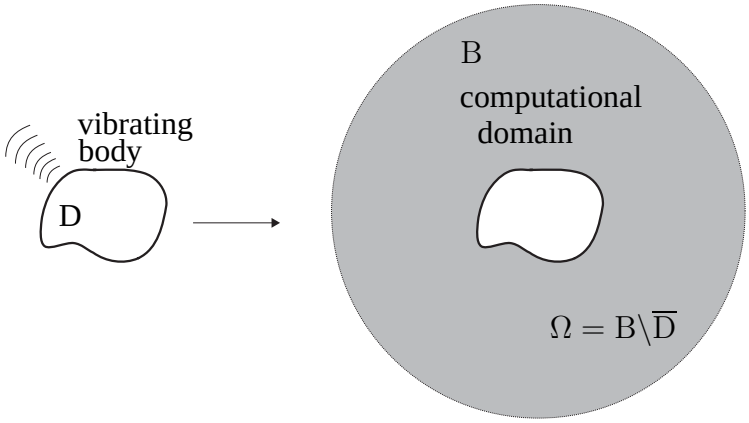

Figure 1.3: Radiation problem: a body D vibrates and the radiated waves propagate in the space.

To overcome this difficulty, one introduces a sufficiently large circle $\mathrm{B} \subset \mathbb{R}^d$, containing the obstacle D. Using the Dirichlet-to-Neumann map (DtN) technique, one can approximate the Sommerfeld condition at infinity by the Robin-type boundary condition on $\partial\mathrm{B}$,

$$\boldsymbol{\nabla} u \cdot \mathbf{n} = m_{\mathrm{B}} u \qquad \text{on } \partial\mathrm{B}, \tag{1.4}$$

where m_{B} is the linear operator DtN that defines an absorbing boundary condition on the artificial boundary $\partial\mathrm{B}$. Therefore, the computational domain reduces to the region $\Omega = \mathrm{B} \setminus \overline{\mathrm{D}} \subset \mathbb{R}^d$, with boundary $\partial\Omega = \partial\mathrm{B} \cup \partial\mathrm{D}$. On the artificial boundary, one can prescribe absorbing boundary conditions that incorporate (exactly or approximately) the far-field behavior into the finite element model. For different conditions considered see Djellouli, Farhat, Macedo and Tezaur (2000) and Harari and Djellouli (2004) and references therein.

Then, the radiation problem for a vibrating body consists in finding the acoustic pressure $u : \Omega \to \mathbb{C}$ such that:

$$\begin{aligned} -\boldsymbol{\Delta} u - \kappa^2 u &= 0 && \text{in } \Omega, \\ \boldsymbol{\nabla} u \cdot \mathbf{n} &= g && \text{on } \partial\mathrm{D}, \\ \boldsymbol{\nabla} u \cdot \mathbf{n} &= m_{\mathrm{B}} u && \text{on } \partial\mathrm{B}. \end{aligned}$$

Recall that if the wall of the body D vibrates with normal velocity v_n, the Neu-

mann data is $g = -i\rho c\kappa v_n$. Also, note that Dirichlet or Robin boundary conditions may also be prescribed on parts of the boundary $\partial\mathrm{D}$. Finally, the expressions for the first and second DtN boundary conditions are

$$m_{\mathrm{B}} = -i\kappa u + \frac{\zeta}{2}u \quad \text{and} \quad m_{\mathrm{B}} = -i\kappa u + \frac{\zeta}{2}u - \frac{\zeta^2}{8(\zeta - i\kappa)}u - \frac{\partial}{\partial s}\left(\frac{1}{2(\zeta - i\kappa)}\frac{\partial u}{\partial s}\right),$$

where ζ is the curvature of the surface of the scatterer, and s is the curvilinear abscissa defined on the surface of the scatterer.

Let's now move to the scattering problem. In this case an incident plane wave $u_{\mathrm{i}}(x) = e^{i\kappa(\cos\alpha x + \sin\alpha y)}$ is scattered by an obstacle D, where α denotes the incident direction of the plane wave, see figure 1.2. The reflected wave is given by u_{r} and the total solution is $u = u_{\mathrm{r}} + u_{\mathrm{i}}$. The total solution u, the incident plane wave u_{i} and the reflected wave u_{r}, all satisfy the Helmholtz equation in $\mathbb{R}^d \setminus \mathrm{D}$. Similarly to the radiation problem, the infinite outer region is restricted to a circle B on which the reflected wave u_{r} satisfies the absorbing boundary condition (1.4).

A perfectly sound-soft obstacle leads to the Dirichlet condition $u = 0$, or $u_{\mathrm{r}} = -u_{\mathrm{i}}$. For an acoustically rigid scatterer, acoustic waves satisfy the Neumann boundary condition $\boldsymbol{\nabla} u \cdot \mathbf{n} = 0$, or equivalently $\boldsymbol{\nabla} u_{\mathrm{r}} \cdot \mathbf{n} = -\boldsymbol{\nabla} u_{\mathrm{i}} \cdot \mathbf{n}$. Finally, obstacles characterized by an acoustic admittance A_n will satisfy the Robin boundary condition $\boldsymbol{\nabla} u \cdot \mathbf{n} = mu$, where $m = -i\rho c\kappa A_n$. Naturally, Dirichlet, Neumann and Robin boundary conditions may also be prescribed on parts of the boundary $\partial\mathrm{D}$, where $\partial\mathrm{D} = \overline{\Gamma_{\mathrm{D}} \cup \Gamma_{\mathrm{N}} \cup \Gamma_{\mathrm{R}}}$. Hence the general formulation of the scattering problem consists in finding the spatial component of the scattered acoustic pressure $u_{\mathrm{r}} : \Omega \to \mathbb{C}$ such that:

$$\begin{aligned}
-\boldsymbol{\Delta} u_{\mathrm{r}} - \kappa^2 u_{\mathrm{r}} &= 0 && \text{in } \Omega, \\
u_{\mathrm{r}} &= -u_{\mathrm{i}} && \text{on } \Gamma_{\mathrm{D}} \subset \partial\mathrm{D}, \\
\boldsymbol{\nabla} u_{\mathrm{r}} \cdot \mathbf{n} &= -\boldsymbol{\nabla} u_{\mathrm{i}} \cdot \mathbf{n} && \text{on } \Gamma_{\mathrm{N}} \subset \partial\mathrm{D}, \\
\boldsymbol{\nabla} u_{\mathrm{r}} \cdot \mathbf{n} + \boldsymbol{\nabla} u_{\mathrm{i}} \cdot \mathbf{n} &= m(u_{\mathrm{r}} + u_{\mathrm{i}}) && \text{on } \Gamma_{\mathrm{R}} \subset \partial\mathrm{D}, \\
\boldsymbol{\nabla} u_{\mathrm{r}} \cdot \mathbf{n} &= m_{\mathrm{B}} u_{\mathrm{r}} && \text{on } \partial\mathrm{B}.
\end{aligned}$$

Note that the reflected solution u_{r} also verifies the homogeneous Helmholtz equation in Ω since the incident wave satisfied $-\boldsymbol{\Delta} u_{\mathrm{i}} - \kappa^2 u_{\mathrm{i}} = 0$.

Finally, the transmission problem, also called elastic scattering problem, differs from the scattering problem since the incident sound is allowed to penetrate the obstacle. If the obstacle D is made of another fluid with different sound speed and density, the transmission problem leads to a coupled problem in which the total pressure $u = u_{\mathrm{r}} + u_{\mathrm{i}}$ outside of D and the interior pressure in D both satisfy the Helmholtz equation and on the boundary $\partial\mathrm{D}$ the pressure and normal velocities are assumed to be continuous. We refer to (Ihlenburg 1998) for details of the formulation.

1.3 Numerical schemes

The finite element method (FEM) is probably the most well known numerical scheme to solve Helmholtz equation. This method performs satisfactory for low and medium frequencies, but one of the major computational challenges nowadays is dealing with high-frequencies. Recently, considerable efforts have been devoted to obtain more accurate numerical solutions, by extending the finite element method to a frequency range able to simulate practical applications. The key is to control the pollution error, originated mainly from the dispersive nature of the numerical waves.

The development of numerical methods to solve the Helmholtz equation, which behaves robustly with respect to the wave number, is a topic of vivid research. Many enhancements and extensions of the finite element method have been proposed in the last decade to improve the accuracy of the simulations, but none of them being totally *dispersion-free*. Amongst them, one finds the stabilized Galerkin schemes, high-order approximants, multi-scale variational methods, and other discretization techniques. The number is too large to discuss all of them, so, only the most relevant ones will be briefly revised.

1.3.1 The finite element method

The use of the finite element method for time-harmonic acoustics governed by the Helmholtz equation has been an active research area for almost half a century. Initial applications focused on interior problems, but in the recent years, huge progress has

been also achieved on exterior problems in unbounded domains. The main difficulty of applying the standard Galerkin finite element method to the Helmholtz equation is to accurately resolve the oscillating wave solutions for higher wave numbers. This section summarizes the main properties of the finite element method for the Helmholtz equation. However, the reader is referred to Ihlenburg (1998) and Harari (2006) for a deep insight of the issues, properties, applications and methodologies related to the finite element method for time-harmonic acoustics.

The Helmholtz problem both for interior and exterior problems can be formulated as: find $u : \Omega \to \mathbb{C}$ such that

$$-\boldsymbol{\Delta} u - \kappa^2 u = f \qquad \text{in } \Omega, \tag{1.7a}$$

$$u = u_D \qquad \text{on } \Gamma_{\mathrm{D}}, \tag{1.7b}$$

$$\boldsymbol{\nabla} u \cdot \mathbf{n} = g \qquad \text{on } \Gamma_{\mathrm{N}}, \tag{1.7c}$$

$$\boldsymbol{\nabla} u \cdot \mathbf{n} = mu \qquad \text{on } \Gamma_{\mathrm{R}}, \tag{1.7d}$$

where Ω is the either the true domain or the computational domain for exterior problems. Note that, in most applications, as the ones show in the previous section, $f = 0$. However a non-zero source term may appear in acoustic problems, where the non-homogeneous Helmholtz equation models time-harmonic wave propagation in free space due to a localized source. For instance,a non-zero source term may appear in the study of a vibrating string where a force is applied to drive a wave on this string.

The boundary value problem defined by equations (1.7) is readily expressed in its weak form using the corresponding natural functional spaces. The space for the trial functions is $\mathcal{U} = \{u \in \mathcal{H}^1(\Omega), u|_{\Gamma_{\mathrm{D}}} = u_D\}$ while the space for the test functions is $\mathcal{V} = \{v \in \mathcal{H}^1(\Omega), v|_{\Gamma_{\mathrm{D}}} = 0\}$, where $\mathcal{H}^1(\Omega)$ is the standard Sobolev space of complex-valued square integrable functions with square integrable first derivatives.

The weak form of the problem then reads: find $u \in \mathcal{U}$ such that

$$a(u, v) = \ell(v) \quad \forall v \in \mathcal{V}, \tag{1.8}$$

where the sesquilinear form $a(\cdot, \cdot)$ and the antilinear form $\ell(\cdot)$ are defined as follows

$$a(u,v) = \int_\Omega \nabla u \cdot \nabla \bar{v}\, d\Omega - \int_\Omega \kappa^2 u \bar{v}\, d\Omega - \int_{\Gamma_{\mathrm{R}}} m u \bar{v}\, d\Gamma, \tag{1.9a}$$

$$\ell(v) = \int_\Omega f \bar{v} + \int_{\Gamma_{\mathrm{N}}} g \bar{v}\, d\Gamma, \tag{1.9b}$$

and the symbol $\bar{\cdot}$ denotes the complex conjugate. Recall that this formulation is also valid for exterior problems where Robin boundary conditions are applied the fictitious boundary $\partial\mathrm{B} \subset \Gamma_{\mathrm{R}}$.

The classical Galerkin finite element discretization is applied to the variational formulation of the Helmholtz equation (1.8). For this, let the discrete counterparts of $\mathcal{U}$ and $\mathcal{V}$ be the finite element spaces $\mathcal{U}_H \subset \mathcal{U}$ and $\mathcal{V}_H \subset \mathcal{V}$ associated with a mesh of characteristic element size H and degree p for the complete interpolation polynomial base. The discrete finite element solution is $u_H \in \mathcal{U}_H$ such that

$$a(u_H, v) = \ell(v) \quad \forall v \in \mathcal{V}_H.$$

where u_H is expressed in terms of the basis-functions $\{N^j\}_{j=1,\ldots,\mathtt{n}_{\mathtt{np}}}$ spanning $\mathcal{U}_H$, $\mathtt{n}_{\mathtt{np}}$ being the number of nodes of the mesh. Namely,

$$u_H = \sum_{j=1}^{\mathtt{n}_{\mathtt{np}}} N^j u_H^j = \mathbf{N}\mathbf{u}_H, \tag{1.10}$$

where u_H^j is the complex nodal value associated with the mesh node $\mathbf{x}^j$, $\mathbf{N} = [N^1, N^2, \ldots, N^{\mathtt{n}_{\mathtt{np}}}]$ and $\mathbf{u}_H^{\mathsf{T}} = [u_H^1, u_H^2, \ldots, u_H^{\mathtt{n}_{\mathtt{np}}}]$.

The accuracy of the Galerkin finite element approximation is characterized by the *dispersion* error. The dispersion error is related to the phase difference between the exact solution and its finite element approximation, that is, the difference between the wave number κ associated with the exact solution u and the numerical wave number associated with numerical solution u_H, namely denoted by κ_H. This effect has been deeply analyzed in Ihlenburg and Babuška (1995a), Ihlenburg and Babuška (1995b), Ihlenburg (1998) and Babuška and Sauter (2000).

Sharp error estimates for the dispersion error have been obtained under the assumption that the magnitude κH is small. In particular, Ihlenburg and Babuška (1995a) showed that the relative error of the finite element solution in the $\mathcal{H}^1$-

seminorm is controlled by a sum of two contributions depending on the wave number. Specifically, for linear elements

$$\frac{|u - u_H|_1}{|u|_1} \leq C_1 \kappa H + C_2 \kappa^3 H^2, \tag{1.11}$$

where

$$|u|_1 = \sqrt{\int_\Omega \left(\frac{du}{dx}\right)^2}$$

stands for the $\mathcal{H}^1$-seminorm and C_1, C_2 are constants independent of κ and H. This result is fundamental for understanding the nature of the approximation error. The first term of equation (1.11) represents the interpolation error (difference between the exact solution and its best approximation in the space $\mathcal{U}_H$) and the second term is the pollution or dispersion error (difference between the best approximation in $\mathcal{U}_H$ and the finite element approximation). The interpolation error is the classical error arising in elliptic problems and pertains to the ability of the discretization to properly approximate the exact solution, whereas the pollution error is the responsible of the phase lag of the finite element approximation, see figure 1.4.

Note that the interpolation error is bounded if κH is constant, which is the so-called *rule of the thumb* and corresponds to taking a certain fix number of elements per wavelength. However, as can be seen in equation (1.11), this rule is not sufficient to keep the pollution error under control, as it increases with κ. Thus, to obtain an accurate approximation, the second term also needs to be controlled. In practice, standard Galerkin methods are not competitive for high wave numbers because controlling the pollution term requires using extremely fine meshes. The enhancements and extensions of the finite element method focus on overcoming this drawback.

1.3.2 Stabilized finite element methods

Stabilized finite element methods were originally developed for fluid problems. The first upwind-type stabilized methods (Hughes and Brooks 1979) subsequently gave rise to consistent stabilization techniques - ensuring that the exact solution is also a solution of the weak stabilized problem. Amongst these techniques, the Galerkin least-squares method (GLS) has been successfully applied both to fluids (Hughes,

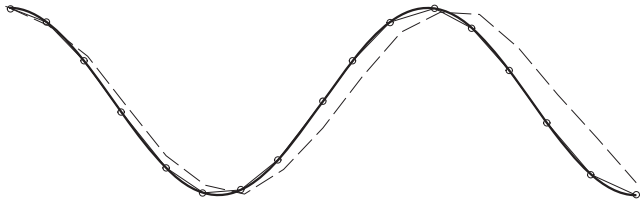

Figure 1.4: Illustrative example of the errors arising in the finite element approximation. Exact solution (thicker solid line), best approximation in $\mathcal{U}_H$ (solid thinner line with circles) and the finite element approximation (dashed line). The finite element approximation reproduces approximately the shape of the wave with a larger wavelength.

Franca and Hulbert 1989, Donea and Huerta 2003) and to the Helmholtz equation (Harari and Hughes 1992, Harari and Nogueira 2002).

Stabilized methods are one of the most popular techniques because they provide a significant reduction in the dispersion error with an extremely simple implementation. These approaches belong to the first class of methods aiming at reducing the dispersion for Helmholtz equation. This is achieved by including additional residual terms in the sesquilinear form $a(u, v)$ of the weak formulation. For instance, the Galerkin least-squares method (Harari and Hughes 1992, Thompson and Pinsky 1995) includes an additional stabilization term which is a function of the residual of the Helmholtz equation, namely,

$$a(u, v) - (\mathcal{L}u - f, \tau_H \mathcal{L}\bar{v})_{\widehat{\Omega}} = \ell(v),$$

whereas the Galerkin gradient least-squares method (Harari 1997) includes the gradient of this residual, namely,

$$a(u, v) - (\nabla(\mathcal{L}u - f), \tau_H \nabla\mathcal{L}\bar{v})_{\widehat{\Omega}} = \ell(v).$$

In the previous equations $\mathcal{L}u = -\Delta u - \kappa^2 u$ is the indefinite Helmholtz operator, $\widehat{\Omega}$ is the union of element interiors of the mesh and τ_H represents the stabilization parameter. The selection of an optimal stabilization parameter completely eliminates the dispersion error in the one-dimensional problem. Unfortunately, this is not the case for higher-dimensional problems, where the selection of an optimal stabilization parameter can only eliminate the dispersion error in certain preferred directions. In two or three dimensions, the pollution effect is substantially reduced but can not be completely eliminated.

1.3.3 Higher-order finite element methods

In order to reduce the effect of numerical dispersion: when approximating the solution using the finite element method, one can consider stabilized formulations which only involve a simple modification of the code while substantially improving the accuracy of the results with no additional computational cost. However the standard finite element method also offers another possibility to improve the precision of simulations: the combination of h and p-refinement in which the mesh size h and the polynomial degree p are allowed to vary among the elements. The number of elements per wavelength to obtain a given discretization error strongly depends on the p, order of the finite element basis functions. Since higher-order elements generally provide greater computational efficiency, fewer degrees of freedom are generally needed to achieve a given discretization error, even for oscillatory wave solutions.

A dispersion analysis similar to the standard analysis for linear elements can be carried out for high-order polynomials of order $p \geq 2$ and a dispersion relation in the same form as equation (1.11) is obtained. In particular, Ihlenburg (1998), shows that, under certain assumptions, the $\mathcal{H}^1$-seminorm of the finite element error can be bounded by

$$\frac{|u - u_H|_1}{|u|_1} \leq C_1 \left(\frac{\kappa H}{2p}\right)^p + C_2 \kappa \left(\frac{\kappa H}{2p}\right)^{2p},$$

C_1 and C_2 being constants independent of κ, H and p, which shows that the pollution effect for $p \geq 2$ is significantly reduced if the mesh is fine enough such that $\kappa H/2p < 1$.

Various authors have shown the advantages of using higher-order finite element method. Thompson and Pinsky (1994) studied the dispersive and attenuation properties of finite element method for the one-dimensional scalar Helmholtz equation up to fifth order approximations. Harari and Avraham (1997) applied these methods to stabilized formulations, in order to develop robust methods in which stability properties are enhanced while maintaining higher-order accuracy. Ainsworth (2004) generalizes the *a priori* estimates obtained by Ihlenburg and Babuška (1997) by deriving explicit expressions for the dispersion error of $h - p$ methods.

1.3.4 Meshless methods

Two of the main advantages of meshless methods are that they do not require to construct a mesh fitting the computational domain and that it is possible to use high-order shape functions of arbitrary continuity. These methods have been extensively investigated by Belytschko, Lu and Gu (1994), Belytschko, Krongauz, Organ, Fleming and Krysl (1996), and have been applied in various branches of engineering: fluids, solids, biomechanics, etc.

In acoustics applications, both the possibility of using high-order interpolations and the case of enriching the interpolation space with information on the wave characteristics make of the meshless methods a particularly attractive alternative to finite element. Specifically, the can exploit known analytical solutions such as plane waves, trigonometric functions, or other analytical solutions to define or enrich the approximate solution space.

Bouillard and Suleau (1998) have shown that the meshless methods, in particular the element-free Galerkin (EFG) method based on the moving least-squares approximation (MLS), are very general and accurate approaches for interior acoustic problems.

Suleau and Bouillard (2000) investigate the problem of the dispersion effect in one-dimensional setting. Interesting developments of the theory of dispersion error concerning acoustic problems were presented by the same authors in Suleau, Deraemaeker and Bouillard (2000) and Bouillard, Lacroix and De Bel (2004). In particular, Bouillard et al. (2004) focuses on analyzing the dispersion phenomena and manages to achieve accurate results on academic as well as real-life three-dimensional problems within a large frequency range.

In the case of the Helmholtz equation, it is advantageous that the local basis functions of the element-free Galerkin method can naturally contain terms of trigonometric type (Lacroix, Bouillard and Villon 2003). Indeed, since the pressure is a complex valued field, it is useful to introduce sine and cosine functions in the meshless basis, depending on the value of the propagation angle (α) or phase of the pressure field at each point of the domain. It is worth noting that α is unknown *a priori*. Thus, first, an approximation of the problem using a standard element-free Galerkin basis functions is computed which is subsequently enriched with *a*

posteriori knowledge of the solution.

It is shown that the use of α-dependant local meshless basis involves a significant reduction of the dispersion error in comparison with the corresponding finite element method. In the one-dimensional case, it is possible to construct shape functions that are better suited to represent the solution of the wave propagation problem, especially for high wave numbers. These shape functions include an oscillatory behavior, enabling to completely eliminate the dispersion. In the two-dimensional case, it is not possible to completely eliminate the dispersion error, but, as what occurs in stabilized finite element methods, it can be minimized in a user-prescribed direction, α, and substantially reduced for closer values.

1.3.5 Generalized finite element methods

Another class of very popular methods, conceptually very close to meshless ideas, and which allow the incorporation of local known information of the solution into the approximation space, are the generalized methods based on the partition of unity, first proposed by Babuška and Melenk (1997).

This section briefly discusses the two main methods which fall in this category: the partition of unity method (PUM) and the generalized finite element method (GFEM). Both methods are based on an enrichment of the standard polynomial finite element basis with *local* solutions of the corresponding homogeneous problem.

The main capabilities of these methods are: first, the possibility of using meshes which are partially or totally independent of the domain and, second, the potentiality of enriching the approximation by any special functions of interest. These methods aim at reducing the dispersion by incorporating *a priori* knowledge about the global behavior of the solution in the local approximation field.

Partition of unity method

The partition of unity method can be seen as a generalized finite element method where the core ideas are the construction of proper interpolation spaces with desirable local approximation properties and the conformity of these spaces.

The interpolation space associated to the partition of unity method is defined using two sets of functions.

First a decomposition of the domain is used to define a set of functions being a partition of unity on this decomposition. For simplicity of representation, assume that a finite element mesh is given, and let $\{N^j\}_{j,\ldots,\mathrm{n_{np}}}$ denote the standard linear finite element basis. It is well known that the functions N^j form the partition of unity on Ω, namely

$$\sum_{j=1}^{\mathrm{n_{np}}} N^j(\mathbf{x}) = 1 \quad \forall \mathbf{x} \in \Omega$$

and that the shape functions have a local support. Indeed, the support of N^j is denoted by ω_j and consists of all elements containing node $\mathbf{x}^j$. It is worth noting that other decompositions of the domain and other partition of unity may be defined.

Once the partition of unity and the associated patches ω_j are introduced, a suitable approximation space $\mathcal{W}^j$ is defined in each patch. Note that the spaces $\mathcal{W}^j$ can contain known local information of the solution. Usually, the local spaces $\mathcal{W}^j$ are set to be equal in all the patches, unless specific information is known about the local behavior of the solution at a particular patch.

In Helmholtz context, two sets of spaces are generally used: plane-wave functions and wave-band functions (Strouboulis and Hidajat 2006). Specifically, the local space of wave-plane functions associated to a parameter m is given by

$$\mathcal{W}(m) = \text{span}\left\{ e^{i\kappa(x\cos\theta_n + y\sin\theta_n)}, \theta_n = \frac{2\pi n}{m}, n = 0, \ldots, m-1 \right\},$$

which includes the linear combinations of plane waves traveling in the directions $\theta_n = 2\pi n/m, n = 0, \ldots, m-1$. It is worth noting that if *a priori* knowledge of the solution in a particular patch ω_j is at hand, the local space $\mathcal{W}^j$ can be modified to better fit the information.

Once the partition of unity $\{N^j\}_{j,\ldots,\mathrm{n_{vp}}}$ and the local spaces $W^j = \mathcal{W}(m)$ are defined, the partition of unity approximation is defined as

$$u_H = \sum_{j=1}^{\mathrm{n_{np}}} N^j \left(\sum_{n=0}^{m} e^{i\kappa(x\cos\theta_n + y\sin\theta_n)} u_H^{jm} \right),$$

where u_H^{jm} represent the unknowns of the partition if unity method.

Note that this expression is particular for the specific choice of the partition of unity and local interpolation spaces that has been considered. However, the general approximation is obtain in an analogous way.

The locally defined spaces $\mathcal{W}^j$ contain *a priori* knowledge about the local behavior of the solution and the partition of unity guarantees the inter-element continuity. The application of the partition of unity method associated to the set of plane-wave functions shows an improved computational efficiency compared with stabilized methods. However, the treatise of essential boundary conditions and the numerical integration require special attention. Furthermore, the set of algebraic equations becomes ill-conditioned for a large dimension of the case $\mathcal{W}^j$ (m in the space of the plane-wave functions).

Babuška and Melenk (1997) apply the partition of unity method to the Laplacian, the elasticity, the Helmholtz and a general class of elliptic problems. In this work, the method is analyzed and *a priori* and *a posteriori* estimates are derived.

Strouboulis and Hidajat (2006) presents a numerical study of the method for the Helmholtz equation. The authors study the effect of the choice of the local interpolation spaces, the quadrature, and also discuss the *a posteriori* estimation of quantities of interest. In the particular, *a posteriori* error estimates are used to find out when the pollution becomes negligible. The partition of unity method provides good accuracies but there is a need for developing theoretical results of the reduction of the pollution in terms of as the number of plane-waves or wave-bands employed in the local interpolation spaces $\mathcal{W}^j$.

Generalized finite element method

The generalized finite element method for the Helmholtz equation is a direct extension of the classical finite element method which involves an enrichment of the solution using the partition of unity method (Strouboulis, Babuška and Hidajat 2006).

The generalized finite element approximation is obtained by adding to the standard finite element approximation, the partition of unity method approximation. Namely, for the particular example of the partition of unity method described above,

the generalized finite element approximation is

$$u_H = u_H^{\text{FE}} + \sum_{j=1}^{\text{n}_{\text{np}}} N^j \left(\sum_{n=0}^{m} e^{i\kappa(x\cos\theta_n + y\sin\theta_n)} u_H^{jm} \right),$$

where u_H^{FE} is the standard finite element approximation.

Note that, although the partition of unity method usually considers N^j to be the standard linear finite element basis functions, the generalized method allows combining the partition of unity method with the p-version of the finite element method (included in u_H^{FE}). Thus, two different finite element shape functions can be involved in the generalized method: the linear ones describing the partition of unity and the shape functions of degree p describing u_H^{FE}.

The application of the finite element generalized method using plane-wave functions for the two-dimensional Helmholtz equation with cartesian finite element meshes shows an improved computational efficiency, however, the pollution effect can not be totally removed. It is increasing with κ and decreasing for larger values of p. The authors mention some open problems such as: the characterization of the pollution effect or the extension of the theory for coarse meshes since the existing theory is only valid for sufficiently fine meshes.

1.3.6 Discontinuous methods

The discontinuous enrichment method (DEM) is a general approach for problems with sharp gradients and rapid oscillations. A complete description of the method and its application to Helmholtz and advection-diffusion problems is presented in Farhat, Harari and Franca (2001).

Farhat, Harari and Hetmaniuk (2003) present a discontinuous method for the solution of the Helmholtz equation in the mid-frequency regime. The approach proposed by the authors is based on the discontinuous enrichment method in which the standard polynomial field is enriched within each finite element by a non-conforming field that contains space solutions of the homogeneous partial differential equation to be solved. Thus, for the Helmholtz equation, the enrichment field is chosen as the superposition of plane waves. The method enforces a weak continuity of these plane waves across the element interfaces by suitable Lagrange multipliers.

The results obtained for two-dimensional problems discretized by uniform meshes reveal that the proposed discontinuous method enables the development of elements that are far more competitive than both the standard linear and the standard quadratic Galerkin elements for the discretization of Helmholtz problems.

Farhat, Wiedemann-Goiran and Tezaur (2004) extend this discontinuous method to irregular meshes and exterior Helmholtz problems, being able to consider practical acoustic scattering problems. The results of this approach for two-dimensional problems highlight the superior performance of the method over the standard finite element method.

Recently, interesting studies and developments in the context of acoustics governed by the Helmholtz equation have been developed by Gabard (2006), Tezaur and Farhat (2006) Grosu and Harari (2008). All the studies conclude that these methods are competitive in situations where the standard finite element method runs into difficulties.

1.3.7 Multi-scale methods

The multi-scale methods aim at reducing the dispersion by incorporating *a priori* knowledge about the dispersive behavior in the local approximation field similar to generalized methods. However, the multi-scale methods follow an additive approach rather than multiplicative approach.

Multi-scale methods decompose the solution into the two subproblems: the coarse-scale problem and the fine-scale problem. Several multi-scale methods have been proposed (Hughes 1995, Hughes, Feijoo, Mazzei and Quincy 1998).

Numerical experiments for multi-scale methods show that the same level of accuracy than the finite element method is achieved for frequencies which are three times higher. Oberai and Pinsky (1998) solve the fine-scale problem approximately by applying Green's functions. The derived multi-scale method shows a super convergent behavior in the one-dimensional problem. However, for the two-dimensional problem where the exact solution is a plane wave, the accuracy depends on the direction of propagation of the wave. This deficiency holds for all multi-scale methods based on a fine-scale solution, which vanishes on the element boundaries.

1.3.8 Variational theory of complex rays

The variational theory of complex rays (VTCR) proposed by Ladevèze and Arnaud (2000), Ladevèze, Arnaud, Rouch and Blanzé (2001) and Riou, Ladevèze and Rouch (2004), is a numerical method aimed at the prediction of mid-frequency vibrations. The method is able to yield numerical predictions with the same level of accuracy in the mid-frequency range as the finite element method, however with substantially less computational effort.

The features which characterize the method are: first, the use of a new variational formulation of the problem to be solved. The transmission conditions are incorporated in the variational formulation. Second, a two-scale approximation with a strong mechanical meaning is introduced: the solution is assumed to be well-described locally in the neighborhood of a point as the superposition of an infinite number of local vibration modes. These basic modes verify the laws of dynamics. All wave directions are taken into account and the unknowns are discretized amplitudes relative to particular wavelengths. The authors also suggest that only effective quantities are retained from the calculated discretized amplitudes, such as: elastic energy, kinetic energy, dissipation work, effective displacements, among others.

The method has been successfully applied to assemblies of homogeneous or heterogeneous substructures. Riou et al. (2004) extend the method to shells for medium-frequency vibrations, where the space of approximation is enriched by local solutions of the wave equation.

1.3.9 Trefftz methods

Trefftz methods are a classical approache to incorporate information in the approximation space. These methods can also be classified by the way the boundary conditions are enforced. There are three well known strategies: a collocation scheme, a least-squares formulation or a Galerkin approach. Furthermore, two large classes of Trefftz-elements exist based on the treatment of the continuity conditions between elements, namely the hybrid elements and the frameless elements. For instance, Pluymers, Van Hal, Vandepitte and Desmet (2007) classify the discontinuous enrichment method as an hybrid Trefftz method and the variational theory of complex

rays as a frameless Trefftz method.

The key issue in these methods is the definition of the so-called T-complete function sets. Several T-complete function sets have already been defined for solving steady-state acoustic problems. Although the theoretical convergence for these function sets has been proven, their practical convergence is disturbed, or even prevented, due to the ill-conditioning of the involved model matrices. These numerical problems may be circumvented by subdividing the considered continuum domain into small elemental subdomains. This has led to the development of the Trefftz-element approach, which allows the introduction of the Trefftz idea into a standard finite element scheme. That is, the internal field variables within the T-elements are approximated in terms of a suitably truncated non-conforming T-complete set of functions, satisfying the governing equations *a priori*, while the boundary conditions and inter-element continuity are enforced in an average integral sense.

Pluymers et al. (2007) present a detailed review on the existing numerical methods for the analysis of time-harmonic acoustics, with a specific focus on Trefftz-based methods.

1.4 Error estimation

Computational approximations of a given mathematical model always involve numerical errors. The assessment of such errors is crucial for the computations to be reliable, as well as a basis for adaptive control of the numerical process.

The first use of error estimates for adaptive remeshing strategies, in significant engineering problems, was in the work of Guerra (1977), but the paper of Babuška and Rheinboldt (1978) is often cited as the first work aimed at developing rigorous global error bounds for finite element approximations. A brief history of the subject is given in the book by Ainsworth and Oden (2000). Also the books by Verfurth (1996), Ladevèze and Oden (1998) and Babuška and Strouboulis (2001) provide a good overview of the techniques developed in the late nineties.

It can be argued that the vast majority of the published work on *a posteriori* error estimation deals with global estimates of the errors of finite element approximations of linear elliptic problems, and moreover, most estimates are usually energy-type

norms. For the Helmholtz equation these estimators have the natural tendency to underestimate the true error as the wave number increases. In the late 1990's, techniques for computing estimates of the errors committed in the approximation of some *quantities of interest* began to appear. Such quantities manifest themselves as functionals on the solutions of boundary- and initial-value problems. These estimates provide the basis of the so-called *goal-oriented adaptivity* wherein adaptive remeshing procedures are devised to control the error in these user-defined quantities of interest, also named after *outputs*.

This section is intended to provide a brief overview of the main error estimation techniques for numerical approximations of boundary value problems. In particular, special interest is placed in specific results or techniques concerning time-harmonic waves in interior regions modeled by the Helmholtz equation and approximated by the finite element method. The main objective is to describe existing *a priori* and *a posteriori* error estimation techniques which have been developed and applied to acoustic wave problems in the last years, both for global measures of the error and for the error assessing in quantities of interest.

1.4.1 *A priori* error estimation

A priori estimation of the errors arising in numerical simulations has long been an enterprise for numerical analysts. Such estimates give information on the convergence and stability of the finite element approximations and provide rough information on the asymptotic behavior of the errors of the calculations if the mesh parameters are appropriately set.

In the wave propagation problem modeled by Helmholtz equation an important *a priori* result refers to the dispersion error committed when using linear finite element approximations. Ihlenburg and Babuška (1995a) shows that the dispersion error, defined as the phase difference between the exact and numerical waves, can be approximated by

$$\kappa - \kappa_H \approx \frac{1}{24}\kappa^3 H^2 + \mathcal{O}(\kappa^5 H^4).$$

Equation (1.11) is another important result of *a priori* error estimation for acoustic problems that provides a bound on the $\mathcal{H}^1$-seminorm of the error. Similar *a priori*

estimates have been also derived for the $h-p$ version of the finite element method (Ihlenburg and Babuška 1997, Ihlenburg 1998, Ainsworth 2004).

1.4.2 *A posteriori* error estimation

A distinctive characteristic of *a priori* error estimation is that the error is estimated without employing the discrete solution u_H. The primary objective of these estimates is to derive rates of convergence with respect to the discretization parameters, h and p, to evaluate the performance of a given numerical method. It follows that *a priori* error estimates generally involve unknown constants (independent of h and p) which prevent them from providing useful information about the quantitative error of a particular solution u_H.

In contrast, *a posteriori* error estimation aims at developing quantitative methods in which the error $e = u - u_H$ is estimated using the solution u_H as data for the error estimation strategies. *A posteriori* error estimates are useful in two ways: first, to assess the accuracy of a given approximation u_H, and second, since they are the basis of adaptive strategies.

Initially, error estimation methods were confined to global estimates, which measure the error with respect to global norms computed over the whole computational domain. Although the error is measured using global norms, the resulting estimates are usually decomposable into local contributions, providing the necessary information for adaptivity. Theses estimates are usually classified into: *explicit residual methods*, *implicit residual methods* and *recovery-type methods*. Some developments and features of these techniques in the context of the Helmholtz equation are presented in the following. First, residual methods are shortly revised and then a brief overview of recovery-type estimates is given.

To set the notation, let u denote the solution of the problem (1.8) and u_H be its finite element approximation. The approximation error $e \in \mathcal{V}$ is the unique solution of the equation

$$a(e, v) = \ell(v) - a(u_H, v) = R^P(v) \quad \forall v \in \mathcal{V}, \tag{1.12}$$

where $R^P(v)$ is the weak residual associated to u_H. Furthermore, since u_H is a

Galerkin approximation, the error satisfies the *Galerkin orthogonality property*

$$a(e, v) = 0 \quad \forall v \in \mathcal{V}_H, \tag{1.13}$$

which is equivalent to say that the residual is orthogonal to $\mathcal{V}_H$, namely $R^P(v) = 0, \forall v \in \mathcal{V}_H$.

Residual methods aim at obtaining estimates, either for a global measure of the error or for a given quantity of interest, by using the information provided by the residual $R^P(\cdot)$. Depending on the treatment of this information, residual methods are classified into *explicit* and *implicit.* Explicit methods are those which do not require solving any auxiliary problems. They only involve direct computations using available data, in particular, they usually employ the strong residuals in the current approximation. In contrast, implicit methods involve the solution of local or global problems, using the residuals indirectly. They generally involve the solution of small linear systems of equations where the r.h.s of the problems involve local restrictions of the weak residual $R^P(\cdot)$.

Explicit residual methods

Irimie and Bouillard (2001) employ an explicit residual method to compute error estimates in the context of the Helmholtz equation. The conclusions of this investigation are that the quality of the error estimator deteriorates as the wave number increases and that it is incapable of detecting the pollution error.

Stewart and Hughes (1996), Stewart and Hughes (1997) and Stewart and Hughes (1997) develop explicit residual error estimators for the classical Galerkin and -Galerkin least-squares finite element methods, for the Helmholtz equation in exterior domains. The authors focus on the development of an *a posteriori* error estimator for the error distribution, and an *h*-adaptive strategy. The methodology for computing the error estimates is to determine the scaling constants appearing in the error estimator. Several measures are computed to assess the quality of the error estimator and results indicate that the error distributions are adequately captured. However, the quality of the global error estimates degrades as the wave number is increased.

Implicit residual methods

The main motivation in developing implicit residual methods is to be able to compute more accurate estimates, or even bounds, of the residual norm by avoiding introducing the unknown constants that are characteristics of explicit methods. Implicit residual methods require the solution of auxiliary problems, approximating the residual equation (1.12) satisfied by the error itself. These estimate are classified into *element*, *subdomain*, and *global residual methods*, depending on whether the local problems are posed over a single element, a small patch of elements, or in the whole computational domain.

Babuška, Ihlenburg, Strouboulis and Gangaraj (1997) presents a one-dimensional study of a Dirichlet element error estimator for the Helmholtz problem. That is, the estimates are computed solving local elementary problems with Dirichlet boundary conditions at the edges of the element (or nodes in the one-dimensional case). They show that, at high wave numbers, the error estimator actually approximates the difference between the finite element solution and the associated shifted function. That is, instead of approximating the exact error the estimate approximates the difference between the solution of a modified problem with wave number κ_H (the numerical wave number) and the finite element approximation.

Bouillard (1999) extends the element residual approach proposed by Ladevezè in the late 1990's (Ladevèze and Maunder 1996, Ladevèze and Rougeot 1997) to the Helmholtz problem. These estimates are also referred to error estimation in the constitutive law or equilibrated flux-splitting approach. These investigations concern vibro-acoustic problems and are limited to low values of the wave number where the pollution error is negligible. Various examples demonstrate that, in the case of linear or bilinear elements, the estimator provides asymptotic upper bounds on the error with effectivity indices closer to two.

In subdomain residual methods, the global residual problem for the error is decomposed in local problems posed over small patches of elements. Although some progress has been achieved since the first pioneer work of Babuška and Rheinoldt in 1978 (Carstensen and Funken 2000, Machiels, Maday and Patera 2000, Parés, Díez and Huerta 2006), these kind of estimates have not yet been used to calculate error estimates for the Helmholtz equation.

Recovery-type methods

Recovery-based error estimators were first suggested by Zienkiewicz and Zhu (1987) and improved later by the same authors in 1992. These methods follow the simple observation that piecewise continuous finite element solutions generally exhibit discontinuous gradients at the interface of the elements. If the exact solution to be sought is smooth enough, such jumps in the gradients of the numerical solution indicate that the numerical solution is erroneous. Several approaches have been proposed in the literature to compute these gradients (Zienkiewicz and Zhu 1992*b*, Ainsworth and Oden 2000).

Bouillard and Ihlenburg (1999) performed numerical experiments to test the quality of recovery or smoothening techniques on acoustic. The results show that the effectivity index of recovery-type methods converge to one as the discretization parameter tends to zero, meaning that the recovered smooth function gets closer and closer to the exact solution as the pollution error diminishes. However, the effectivity index clearly deteriorates when κ becomes large, i.e. when dispersion becomes too significant. They also show that the estimates are suitable to drive mesh adaptation for low wave numbers.

1.4.3 Error estimation in quantities of interest

A class of methods based on duality techniques which compute error estimates in terms of quantities of interest is described by various authors (Becker and Rannacher 1996, Paraschivoiu, Peraire and Patera 1997, Becker and Rannacher 2001, Oden and Prudhomme 2001). These strategies are also called goal-oriented adaptive methods strategies.

In goal-oriented error estimation, analysts specify the goal of their calculations by identifying a *quantity of interest*, where this quantity of interest or output is represented by a functional defined on the space of admissible solutions. Namely, the desired output of the simulation is $J(u)$ where $J(\cdot)$ is a linear or non-linear functional representing the quantity of interest. In this thesis, $J(u)$ will represent a general non-linear quantity of interest. However, most strategies are developed with respect to linear outputs. In this case, $\ell^{\mathcal{O}}(u)$ will be used to denote only linear

quantity of interest. It is worth noting that in the general case, the functional $\ell^{\mathcal{O}}(\cdot)$ will be obtained from $J(\cdot)$ using a linearization technique.

The standard approach to obtain error estimates in some quantity of interest defined by a linear functional is to obtain an error representation using an adjoint problem. The adjoint problem is similar to the direct one but with different *loads* (source term and/or boundary conditions). The error representation is an alternative expression for the error in the quantity of interest as *energy* products of the errors of the direct and adjoint problems.

In the following, the basis of *a posteriori* goal-oriented error estimation strategies is briefly summarized.

Let $\ell^{\mathcal{O}}(\cdot)$ be a linear functional representing the quantity of interest. That is, the goal of the numerical simulation is to evaluate $\ell^{\mathcal{O}}(u)$. The accuracy of the solution is then estimated in terms of the exact error $\ell^{\mathcal{O}}(e) = \ell^{\mathcal{O}}(u) - \ell^{\mathcal{O}}(u_H)$ or a reference counterpart $\ell^{\mathcal{O}}(e) \approx \ell^{\mathcal{O}}(u_h) - \ell^{\mathcal{O}}(u_H)$, where the reference solution u_h is associated with a much finer *over kill* discretization (for instance with $h \ll H$).

An adjoint problem is introduced associated with $\ell^{\mathcal{O}}(\cdot)$ reading: find $\psi \in \mathcal{V}$ such that

$$a(v, \psi) = \ell^{\mathcal{O}}(v) \;\; \forall v \in \mathcal{V}, \tag{1.14}$$

along with its finite element approximation ψ_H and its associated error $\varepsilon = \psi - \psi_H$. Using equation (1.14), the error in the quantity of interest is readily expressed as an inner product of the error in the direct problem and the adjoint solution or, using the Galerkin orthogonality property (1.13), as an inner product of the direct and adjoint errors. Namely,

$$\ell^{\mathcal{O}}(e) = a(e, \psi) = a(e, \psi - \psi_H) = a(e, \varepsilon) \tag{1.15}$$

Thus, if one can get approximations to e and ε properly behaving in terms of energy, then the error representation (1.15) allows obtaining a proper approximation of the error in the quantity of interest, $\ell^{\mathcal{O}}(e)$.

Moreover, using the definition of the primal residual, $R^P(\cdot)$, given in equation (1.12), an alternative representation for the error in the output follows:

$$\ell^{\mathcal{O}}(e) = a(e, \varepsilon) = R^P(\varepsilon). \tag{1.16}$$

Thus, an approximation to ε suffices to obtain estimates for $\ell^{\mathcal{O}}(e)$, if injected into the residual of the direct problem, as suggested in (Díez and Calderón 2007*a*). In the above mentioned reference effort is devoted to obtain a better approximation to the exact/reference solution (u/u_h or ψ/ψ_h) based on the numerical approximation (u_H or ψ_H) via some post-processing techniques (Zienkiewicz and Zhu 1992*a*, Zienkiewicz and Zhu 1992*b*, Zienkiewicz and Zhu 1992*c*, Wiberg, Zeng and Li 1992).

Its is important to highlight that most goal-oriented estimates are based on using similar technique to the ones proposed to obtain global measures of the error. These techniques provide approximations to e and ε that are then injected in one of the error representations for the quantity of interest.

Few contributions on goal-oriented error estimation for the Helmholtz equation have been published. Sarrate, Peraire and Patera (1999) extend the implicit error estimates based on the equilibrated residual method given in (Paraschivoiu et al. 1997) to interior Helmhotz equation problems. Asymptotic bounds for linear and non-linear quantities of interest are reported. The results confirm that the bounds are less sharp with increasing wave number. However, they do not mention whether the pollution error in the solutions is significant or not.

Walsh and Demkowicz (2003) give another approach to goal-oriented adaptation techniques for acoustic problems, where a technique for the modeling the external human auditory system by the boundary element method is presented.

In fact, not many works in goal-oriented error estimation and adaptation techniques for the wave propagation problem modeled by Helmholtz equation are present in the literature. The time-dependent wave equation is studied in (Bangerth and Rannacher 1999, Becker and Rannacher 2001). One extra difficulty for estimating the error in quantities of interest for transient wave problems is that the adjoint function is the solution of a reversed time-dependent problem that has to be integrated backwards in time. In this context Bangerth, Geiger and Rannacher (2010) have recently presented an overview of goal-oriented adaptivity for acoustic problems, in particular, for the elastic wave equation.

1.5 Overview

The thesis is organized in two parts: the exposition and the contributions of the thesis enclosed in form of published or accepted papers.

The exposition part is divided in 4 chapters: this first chapter is intended to provide an overview of numerical methods for the Helmholtz problem, placing special interest in new methods aiming at reducing the pollution effects, along with a state-of-art in error estimation. In chapter 2 an *a posteriori* error estimation technique to assess the dispersion error of standard and stabilized finite element approximations for the Helmholtz equation is proposed. Chapter 3 is concerned with goal-oriented error estimates and *h*-adaptivity. It presents the study and analysis of linear and non-linear outputs for the Helmholtz equation. Finally chapter 4 presents the main conclusions and future developments.

The three appended papers at the end of the thesis correspond to the references Steffens and Díez (2009), Steffens et al. (2010*a*) and Steffens et al. (2010*b*), respectively. Throughout the thesis these papers are cited using the corresponding reference.

Chapter 2

Assessment of the dispersion error for the Helmholtz equation

In this chapter an *a posteriori* estimator for the error in the wave number is presented in the context of finite element approximations of the Helmholtz equation for both standard and stabilized formulations. This chapter is a summary of the main ideas introduced in (Steffens and Díez 2009) and (Steffens et al. 2010*a*). The reader may find some discrepancies between the notation used in this chapter and the aforementioned references since a unified framework for assessing the dispersion error joining both works presented.

The chapter is structured as follows: section 2.1 introduces the acoustic model problem and the finite element method for both standard and Galerkin least-squares formulations. In section 2.2 the concepts of dispersion and pollution errors are reminded. Section 2.3 is devoted to introduce the *a posteriori* technique proposed to assess the error in the wave number. In section 2.4 the recovery technique based in a standard polynomial least-squares fitting and a new recovery strategy is introduced. The procedure builds up an inexpensive approximation of the exact solution, using standard post-processing techniques in error estimation analysis, from which the estimate of the error in the wave number is computed using a simple closed expression. Finally, in section 2.5 the estimation procedure is used in several numerical examples demonstrating the efficiency of the proposed technique both in academic and practical examples.

2.1 Model problem

Consider the acoustic problem (1.8) given in weak form as: find $u \in \mathcal{U}$ such that

$$a(\kappa; u, v) = \ell(\kappa; v) \quad \forall v \in \mathcal{V}. \tag{2.1}$$

Note that the notation adopted in this chapter marks the explicit dependence of κ on the sesquilinear form $a(\kappa; \cdot, \cdot)$ and on the antilinear functional $\ell(\kappa; \cdot)$. However these forms are the same as the ones described in equation (1.9). Although not standard, this is useful in the following to assess the error in the wave number.

It is worth noting that the sesquilinear form $a(\kappa; \cdot, \cdot)$ is not elliptic but it satisfies the inf-sup condition and the Gärding inequality. However, for large wave numbers κ the upper bound for the inf-sup condition is too crude (Ihlenburg 1998). Moreover, the inf-sup property is not carried over from $\mathcal{V}$ to a discrete subspace yielding to a loss of stability which produces spurious dispersion in the discrete approximations.

2.1.1 Galerkin finite element approximation

As described in section 1.3.1 the Galerkin approximation is obtained from a partition $\mathcal{T}_H$ of the domain Ω into nonoverlapping elements and by introducing the discrete spaces $\mathcal{U}_H \subset \mathcal{U}$ and $\mathcal{V}_H \subset \mathcal{V}$. The discrete finite element solution is then $u_H \in \mathcal{U}_H$ such that

$$a(\kappa; u_H, v) = \ell(\kappa; v) \quad \forall v \in \mathcal{V}_H. \tag{2.2}$$

In practice, low-order Galerkin approximations to the Helmholtz equation involving high wave numbers are corrupted by large dispersion or pollution errors due to the loss of stability of $a(\kappa; \cdot, \cdot)$. Moreover, it is widely known that the *rule of thumb* is not sufficient to obtain reliable results for large κ. This undermines the practical utility of the Galerkin finite element method since severe mesh refinement is needed for large wave numbers.

The performance of finite element computations at high wave numbers can be improved by using stabilization techniques. These techniques, which are extremely simple to implement, alleviate the dispersion effect of the finite element solution without requiring mesh refinement.

2.1.2 Galerkin least-squares finite element approximation

The idea behind stabilized finite element methods is to modify the variational form $a(\kappa;\cdot,\cdot)$ and, accordingly, the right hand side, in such a way that the new variational form is *unconditionally stable*. In particular, the additional stabilization terms of the Galerkin lest-squares method method are an element-by-element weighted least-squares formulation of the original differential equation.

Recall that, as introduced in section 1.3.2, the weak form of the Galerkin least-squares method associated with the partition $\mathcal{T}_H$ is: find $u \in \mathcal{U}$ such that

$$a(\kappa;u,v) + (\mathcal{L}u - f, \tau_H \mathcal{L}\bar{v})_{\widehat{\Omega}} = \ell(v) \quad \forall v \in \mathcal{V}, \tag{2.3}$$

where $\mathcal{L}u = -\boldsymbol{\Delta}u - \kappa^2 u$, $\widehat{\Omega} = \bigcup_{k=1}^{\mathrm{n_{el}}} \Omega_k$ denotes the union of element interiors of $\mathcal{T}_H$, $\mathrm{n_{el}}$ being the number of elements in the mesh and $(\cdot,\cdot)_{\widehat{\Omega}}$ is the reduced L^2 inner product, where integration is carried out only on the element interiors, that is, the singularities at inter-element boundaries are suppressed in the reduced inner product. Thus, the Galerkin least-squares formulation depends on the stabilization parameter τ_H which has to be properly defined to make the form on the l.h.s. unconditionally stable.

Note that the Galerkin least-squares method is consistent for any choice of τ_H, since the exact solution u verifies equation (2.3) for any choice of the stabilization parameter τ_H due to $\mathcal{L}u - f = 0$.

The Galerkin least-squares finite element approximation of u is $u_H \in \mathcal{U}_H$ such that

$$a_{\mathrm{GLS}}(\kappa,\tau_H;u_H,v) = \ell_{\mathrm{GLS}}(\kappa,\tau_H;v) \quad \forall v \in \mathcal{V}_H, \tag{2.4}$$

where

$$a_{\mathrm{GLS}}(\kappa,\tau;u,v) = a(\kappa;u,v) + (\tau\mathcal{L}u, \mathcal{L}\bar{v})_{\widehat{\Omega}},$$

and

$$\ell_{\mathrm{GLS}}(\kappa,\tau;v) = \ell(\kappa;v) + (\tau f, \mathcal{L}\bar{v})_{\widehat{\Omega}}.$$

Note that for the sake of simplicity, the same notation, u_H, for the Galerkin and Galerkin least-squares finite element approximations is used. A different notation for the Galerkin least-squares finite element approximation, for instance u_H^{GLS}, would be more precise. However, since the error estimation strategy is valid for any

approximation $u_H \in \mathcal{V}_H$ of u, there is no need to distinguish between u_H and u_H^{GLS} or any other approximation. Moreover, note that $\tau_H = 0$ results in the Galerkin approximation.

The stabilization parameter τ_H is usually determined by using discrete dispersion analysis with the aim of eliminating spurious dispersion of plane waves in a user-prescribed direction (θ). That is, the goal is that the Galerkin least-squares finite element approximation has no phase lag if the exact solution is a plane wave in the direction θ. Different definitions for the parameter τ_H depending on the underlying size and topology of the mesh may be found in the literature (Harari and Magoulès 2004, Harari and Nogueira 2002). The reader is also referred to (Steffens et al. 2010*a*) for different choice of the stabilization parameter.

Unfortunately, it is not possible in general to design a stabilization parameter τ_H that confers the ability of fully removing the dispersion error on the Galerkin least-squares method. The reason is twofold. First, a general signal consists of plane waves going in an infinite number of directions. Even if there are directionally prevalent components in this decomposition, they are not necessarily known *a priori*. Second, the parameter τ_H is derived for particular structured topology meshes. The optimal behavior obtained for some particular structured meshes is partially lost when general unstructured meshes are used.

2.1.3 Matrix form

The Galerkin or Galerkin least-squares finite element approximation u_H is expressed in terms of the finite element basis-functions as $u_H = \mathbf{N}\mathbf{u}_H$, see equation (1.10), where $\mathbf{u}_H$ is the vector containing the complex nodal values of u_H. In the case of linear finite elements ($p = 1$), $\mathcal{L}u_H$ reduces to $\mathcal{L}u_H = -\kappa^2 u_H$ in $\hat{\Omega}$, and the matrix form of (2.4) reads

$$\left(\mathbf{K}_H - \mathbf{C}_H - \kappa^2 \mathbf{M}_H^{\tau_H}\right)\mathbf{u}_H = \mathbf{f}_H^{\tau_H} + \mathbf{f}_H^{\text{N}}, \tag{2.5}$$

where $\mathbf{K}_H$, $\mathbf{C}_H$ and $\mathbf{M}_H^{\tau_H}$ are the so-called stiffness, damping and mass matrices defined by

$$\mathbf{K}_H = \int_\Omega (\nabla \mathbf{N})^{\mathsf{T}} (\nabla \mathbf{N}) d\Omega, \quad \mathbf{C}_H = \int_{\Gamma_{\text{R}}} m \mathbf{N}^{\mathsf{T}} \mathbf{N} d\Gamma,$$

and

$$\mathbf{M}_H^{\tau_H} = \sum_{k=1}^{\mathtt{n_{el}}} \int_{\Omega_k} (1 - \tau_H \kappa^2) \mathbf{N}^{\mathsf{T}} \mathbf{N} d\Omega.$$

The right-hand side vectors accounting for the source term and the Neumann boundary conditions are

$$\mathbf{f}_H^{\tau_H} = \sum_{k=1}^{\mathtt{n_{el}}} \int_{\Omega_k} (1 - \tau_H \kappa^2) \mathbf{N}^{\mathsf{T}} f \, d\Omega \quad \text{and} \quad \mathbf{f}_H^{\mathrm{N}} = \int_{\Gamma_{\mathrm{N}}} \mathbf{N}^{\mathsf{T}} g \, d\Gamma.$$

In the particular case where the stabilization parameter τ_H is constant in the elements of the mesh the mass matrix and the source vector can be rewritten as $\mathbf{M}_H^{\tau_H} = (1 - \tau_H \kappa^2)\mathbf{M}_H$ and $\mathbf{f}_H^{\tau_H} = (1 - \tau_H \kappa^2)\mathbf{f}_H$, where

$$\mathbf{M}_H = \int_{\Omega} \mathbf{N}^{\mathsf{T}} \mathbf{N} d\Omega \quad \text{and} \quad \mathbf{f}_H = \int_{\Omega} \mathbf{N}^{\mathsf{T}} \, d\Gamma,$$

are the standard mass matrix and unit vector force. Besides, recall that $\tau_H = 0$ results in the matrix form of the Galerkin finite element method (2.2).

2.2 Dispersion and pollution effects

As mentioned in chapter 1, Galerkin approximations of the Helmholtz equation at high frequencies show dispersion which pollutes the interpolation errors. The pollution effect, originating mainly from the dispersive behavior of the numerical wave, is global in nature because the error sources affect the solution in the whole domain, and not only where the resolution of the mesh is not sufficient to properly approximate the solution. Thus, opposed to the standard interpolation error, the pollution error cannot be removed by local refinement.

Recently, many attempts have been made in the mathematical and engineering literature to overcome this lack of robustness by various modifications of the classical finite element and the application of news methods. Numerical experiments show that in some situations the pollution effect can be reduced but, in two and more space dimensions it has been proved that it is impossible to eliminate. Moreover, quantitative results about the size of the pollution are very vague and a theoretical foundation is missing. In this thesis, a tool for obtaining quantitative measures of the dispersion error is given.

The error introduced in the numerical solution of wave problems has two different components: *interpolation error* and *pollution error*. The interpolation error is the classical error arising in elliptic problems and pertains to the ability of the discretization to properly approximate the solution. In the present work it is defined as

$$e^{\mathrm{int}} = u - u_H^{\mathrm{proj}} = u(\mathbf{x}) - \sum_{j=1}^{\mathtt{n_{np}}} N^j(\mathbf{x}) u(\mathbf{x}^j),$$

where u_H^{proj} is the approximation of u in $\mathcal{U}_H$ coinciding with u at the mesh nodes $\mathbf{x}^j$, $j = 1, 2, \ldots, \mathtt{n_{np}}$, $\mathtt{n_{np}}$ being the number of nodal points in the mesh. Thus, the pollution error is defined as:

$$e^{\mathrm{pol}} = u_H^{\mathrm{proj}} - u_H = \sum_{j=1}^{\mathtt{n_{np}}} N^j(\mathbf{x})(u(\mathbf{x}^j) - u_H^j).$$

In standard thermal and elasticity problems, the error in the finite element solution is equivalent to the interpolation error, and converges with the same rate. This error is local in nature because it may be reduced in a given zone by reducing the mesh size locally in this zone.

The *pollution* error, however, is especially relevant in the framework of Helmholtz problems due to the blowup of the inf-sup and continuity constants of the weak form when the wave number is large. In transient wave problems, pollution is associated with the variation of the numerical wave speed with the wavelength. This phenomenon results in the dispersion of the different components of the total wave.

In the steady Helmholtz problem, the word dispersion is also used and corresponds to the error in the numerical wave number κ_H, which is therefore identified with the pollution. In other words, the finite element error (FE error) is decomposed into two terms

$$\text{FE error } = u - u_H = e^{\mathrm{int}} + e^{\mathrm{pol}} = \text{ Interpolation error } + \text{Dispersion/pollution error},$$

which, in the case of wave problems, behave completely differently (see figure 2.1). It has been shown that the pollution term converges at a different rate, lower than the standard interpolation error.

The pollution error e^{pol} is related to the phase difference between the exact and finite element solutions, that is, difference between the wave number κ associated

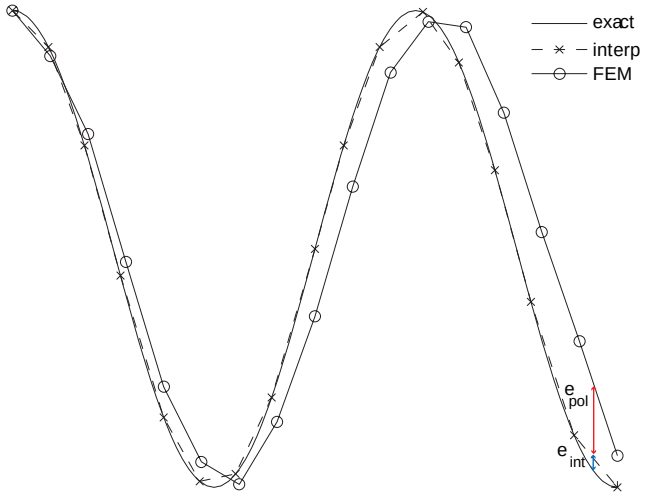

Figure 2.1: Illustration of the errors arising in the approximation of the Helmholtz equation. The exact solution (solid line, smooth) and best approximation (dashed line) coincide at the nodes, the finite element solution reproduces approximately the shape of the wave with a larger wavelength ($\kappa_H < \kappa$).

with u and the numerical wave number κ_H associated with u_H. Usually, the dispersion or pollution error is assessed by obtaining an approximation of the error in the wave number $\kappa - \kappa_H$ instead of trying to measure the pollution error e^{pol} in some predefined norm.

2.2.1 *A priori* error assessment

A priori error estimates assess the dispersion error by means of providing a closed formula of the numerical wave number κ_H. The key idea is to define an auxiliary solution $u_H^m \in \mathcal{U}$ having the same wave number as u_H and from which to recover the value of κ_H. Intuitively, $u_H^m \in \mathcal{U}$ is the best solution of the Helmholtz equation (2.1) associated with a wave number κ_H matching u_H at the nodes of the mesh, see figure 2.2.

The *a priori* error analysis is performed by studying a simple one-dimensional case. This analysis is recalled here because its basic rationale is useful in the following. Consider the one dimensional Helmholtz equation in $\Omega = (0, 1)$ with boundary conditions

$$u(0) = 1 \quad \text{and} \quad \frac{du}{d\mathbf{x}}(1) = i\kappa u(1).$$

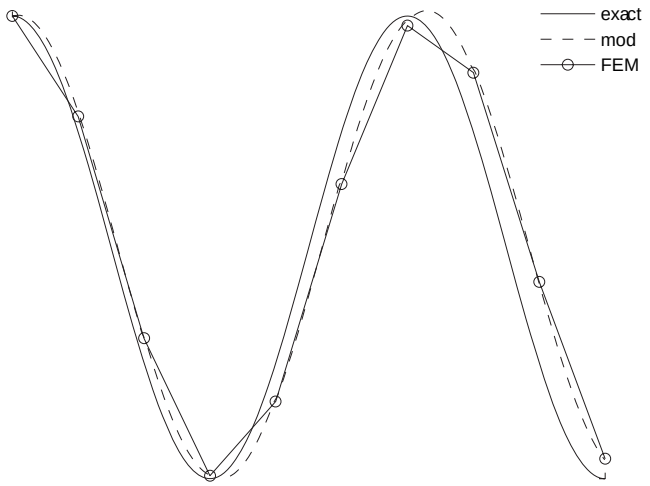

Figure 2.2: Illustration of the exact solution u, the approximate solution u_H and the auxiliary solution u_H^m coinciding with u_H at the nodes and sharing its wave number κ_H.

This simple problem admits the analytical solution $u(\mathbf{x}) = e^{i\kappa\mathbf{x}}$. Then, given a uniform finite element mesh and its associated finite element approximation u_H, it turns out that there is a wave number κ_H such that the solution of Helmholtz equation associated to κ_H, $u_H^m = e^{i\kappa_H x}$, exactly fulfils the equations of the Galerkin method (2.5) associated to the interior nodes. In other words, consider the patch of elements surrounding node $\mathbf{x}^j$, see figure 2.3. Let N^{j-1}, N^j and N^{j+1} be the linear shape functions corresponding to the nodes $\mathbf{x}^{j-1}$, $\mathbf{x}^j$ and $\mathbf{x}^{j+1}$, which are consecutive in the mesh and are the only ones involved in the equation for node $\mathbf{x}^j$. The discrete equation corresponding to node $\mathbf{x}^j$ reads

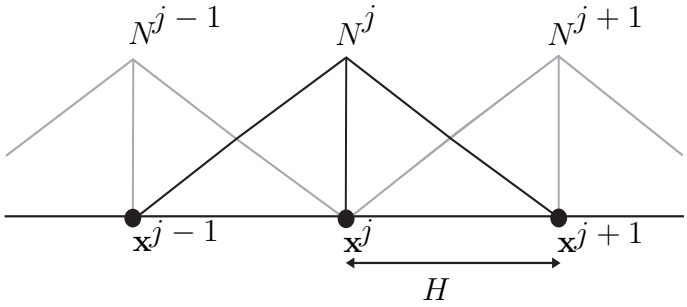

Figure 2.3: Nodes surrounding $\mathbf{x}_j$ in a one-dimensional linear finite element mesh and their corresponding shape functions.

$$Ru_H^{j-1} + 2Su_H^j + Ru_H^{j+1} = 0, \tag{2.6}$$

where the coefficients R and S are

$$R = -1 - \frac{1}{6}(\kappa H)^2 \text{ and } S = 1 - \frac{1}{3}(\kappa H)^2.$$

Recall that u_H^j stands for the nodal unknown at node $\mathbf{x}^j$. Noting that $\mathbf{x}^{j-1} = x^j - H$ and $\mathbf{x}^{j+1} = \mathbf{x}^j + H$ and imposing that the modified solution $u_H^m = e^{i\kappa_H \mathbf{x}}$ exactly fulfills the discrete equation (2.6) yields the following expression for the numerical wave number

$$\kappa_H = \frac{1}{H}\arccos\left(\frac{1-(\kappa H)^2/3}{1+(\kappa H)^2/6}\right) \approx \kappa - \frac{1}{24}\kappa^3 H^2 + \frac{3}{640}\kappa^5 H^4 + \mathcal{O}(\kappa^7 H^6),$$

see (Ihlenburg and Babuška 1995a).

The verification of the equations (2.6) associated to the interior nodes enforces that the auxiliary solution u_H^m shares the same wave number of u_H, although this does not guarantee that u_H^m matches exactly u_H at the nodes of the mesh, due to the influence of the Robin boundary conditions. However, the difference of u_H^m and u_H at the nodes of the mesh is nearly negligible. Thus, for this particular problem, a very good measure of the dispersion error can be computed as

$$\boxed{E = \kappa - \kappa_H \approx \frac{1}{24}\kappa^3 H^2 + \mathcal{O}(\kappa^5 H^4)} \tag{2.7}$$

2.3 *A posteriori* error estimation of the wave number

The standard approach to obtain an error estimate in some quantity of interest defined by a linear functional is to obtain an error representation using an adjoint problem. In the present case, the quantity of interest is the wave number κ, and, therefore, the goal is to assess the error in the wave number. The error assessment using an adjoint problem and the corresponding error representation is not applicable to the wave number quantity of interest. This is due to two reasons. First, there is no linear functional extracting the wave number of an arbitrary function u. Second, in this case, the value for κ is known for the exact solution u (it is an input data!), but not for the numerical solution u_H: κ is known but κ_H is unknown.

The strategy of the error estimate is reversed in this case. Instead of devoting effort to obtain a better approximation, as close as possible to the exact solution and then, compare it with the numerical result, here the effort has to be oriented to obtain the wave number of the approximate solution.

A new approach to *a posteriori* error estimation is introduced here, based on the ideas of the *a priori* analysis sketched in section 2.2.1. The first problem to face is to find a proper definition for the numerical wave number κ_H. The concept of defining κ_H based on the idea of fitting the numerical solution into a modified equation, implicitly used in *a priori* analysis, is extended so that it can be exploited in *a posteriori* error assessment setting.

Unfortunately, in general, it is not possible to determine $u_H^m \in \mathcal{U}$ verifying the weak form of problem (2.1) for a suitable wave number $\kappa_H \in \mathbb{R}$ and concurrently fulfilling the equations of the Galerkin method associated to the interior nodes. However a slight modification of this idea yields a proper definition for u_H^m. Specifically, $u_H^m \in \mathcal{U}$ and $\kappa_H \in \mathbb{R}$ are such that:

- $u_H^m \in \mathcal{U}$ coincides with u_H at the nodes of the mesh, that is

$$u_H^m(\mathbf{x}^j) = u_H(\mathbf{x}^j) \quad \text{for} \quad j = 1, 2, \ldots, \mathtt{n_{np}},$$

- for a given κ_H, $u_H^m \in \mathcal{U}$ is such that

$$a(\kappa_H; u_H^m, v) = \ell(\kappa_H; v) \quad \forall v \in \mathcal{V}_0, \tag{2.8}$$

  where

$$\mathcal{V}_0 = \{v \in \mathcal{V}, v(\mathbf{x}^j) = 0, j = 1, 2, \ldots, \mathtt{n_{np}}\}$$

- κ_H and u_H^m minimize the norm of the residual functional

$$\|R(\kappa_H, u_H^m; \cdot)\|_* = \max_{v \in \mathcal{H}_0^1 \setminus \{0\}} \frac{R(\kappa_H, u_H^m; v)}{\|v\|},$$

  where

$$R(\kappa_H, u_H^m; \cdot) = \ell(\kappa_H; \cdot) - a(\kappa_H; u_H^m, \cdot),$$

$$\mathcal{H}_0^1 = \{v \in \mathcal{H}^1(\Omega), v|_{\partial\Omega} = 0\},$$

  and $\|v\|$ is the $\mathcal{H}^1$ norm.

Note that the values of u_H^m on the boundary of Ω do not affect the norm of the residual $\|\cdot\|_*$. This definition is used to minimize the influence of the errors due to the boundary conditions (which are considered to be a part of the interpolation error and not of the dispersion error) in the assessment of the dispersion error. It is also important to note that the condition enforcing that u_H^m and u_H share the same phase lag, i.e., fulfilling of the equations of the Galerkin method associated to the interior nodes, is replaced by the more simple and equivalent condition of matching u_H at the nodes of the mesh.

In a compact form, κ_H and u_H^m are the solution of the following constrained optimization problem

$$
\begin{aligned}
(\kappa_H, u_H^m) \quad = \quad & \arg\min \ \|R(\kappa^m, u^m; \cdot)\|_* \\
& \kappa^m \in \mathbb{R} \\
& u^m \in \mathcal{U} \\
& \text{subject to} \quad a(\kappa^m; u^m, v) = \ell(\kappa^m; v) \quad \forall v \in \mathcal{V}_0 \\
& \qquad\qquad\quad\ \ u^m(\mathbf{x}^j) = u_H(\mathbf{x}^j),\ j = 1, 2, \ldots, \mathtt{n_{np}}.
\end{aligned}
$$

The relation between the finite element solution u_H and the modified solution u_H^m allows us to state that the numerical wave number associated with u_H, coincides with the wave number associated with the solution u_H^m. That is, the finite element solution u_H and u_H^m share the same phase lag and therefore the dispersion error associated to u_H is

$$\boxed{E = \kappa - \kappa_H}$$

It is worth noting that this definition of the numerical wave number through the modified solution u_H^m is not applicable as a practical error estimation strategy, since κ_H and u_H^m are even more difficult to compute than the exact solution u. Nevertheless, this rationale is used as a starting point to obtain a fully computable estimate for the dispersion error, by just introducing two simple modifications.

First, the finite dimensional reference spaces $\mathcal{U}_h$ and $\mathcal{V}_h$ much finer than $\mathcal{U}_H$ and $\mathcal{V}_H$ are introduced. These spaces yield to the following approximations of κ_H and

u_H^m

$$
\begin{aligned}
(\kappa_H[h], u_H^m[h]) \quad = \quad & \underset{\substack{\kappa^m \in \mathbb{R} \\ u^m \in \mathcal{U}_h}}{\arg\min} \ \|R(\kappa^m, u^m; \cdot)\|_{*,h} \\
& \text{subject to} \quad a(\kappa^m; u^m, v) = \ell(\kappa^m; v) \quad \forall v \in \mathcal{V}_h \cap \mathcal{V}_0 \\
& \qquad\qquad\ \ u^m(\mathbf{x}^j) = u_H(\mathbf{x}^j),\ j = 1, 2, \ldots, \mathtt{n}_{\mathrm{np}}
\end{aligned}
\tag{2.9}
$$

and

$$
\|R(\kappa_H[h], u_H^m[h]; \cdot)\|_{*,h} = \max_{\substack{v \in \mathcal{V}_h \setminus \{0\} \\ v|_{\partial\Omega} = 0}} \frac{R(\kappa_H[h], u_H^m[h]; v)}{\|v\|}.
$$

If the finite element mesh $\mathcal{V}_h$ is sufficiently fine, one expects that $u_H^m \approx u_H^m[h]$ and therefore $\kappa_H[h] \approx \kappa_H$. If the finite element mesh $\mathcal{V}_h$ is not fine enough a correction factor has to be applied to recover a good approximation of κ_H from $\kappa_H[h]$, that is, $\kappa_H[0] = c_f \kappa_H[h]$, where c_f is the correction factor based on a Richardson extrapolation technique, see (Steffens and Díez 2009).

Second, since the computation of $\kappa_H[h]$ and $u_H^m[h]$ is still unaffordable in practical applications another simplification is introduced. An approximation of $u_H^m[h]$ in $\mathcal{U}_h$, denoted by u^*, is obtained by post-processing u_H.

In general, the approximation u^* is not obtained solving equation (2.8) for some κ_H and thus the computation of κ_H is independent. Indeed, u^* does not verify

$$
a(\kappa_H[h]; u^*, v) = \ell(\kappa_H[h]; v) \quad \forall v \in \mathcal{V}_h \cap \mathcal{V}_0,
$$

and is therefore no longer linked with the computation of $\kappa_H[h]$. Once this approximation u^* is computed, the wave number $\kappa_H[h]$ is approximated by κ^* solution of

$$
\kappa^* \quad = \quad \underset{\kappa^m \in \mathbb{R}}{\arg\min} \, \|R(\kappa^m, u^*; \cdot)\|_{*,h}.
$$

It is worth noting that the norm of the residual $\|R(\kappa^m, u^*; \cdot)\|_{*,h}$ is a function depending only on the scalar variable κ^m and may be computed as

$$
\|R(\kappa^m, u^*; \cdot)\|_{*,h} = \sqrt{\mathbf{r}(\kappa^m, u^*)' \mathbf{r}(\kappa^m, u^*)},
$$

where

$$\begin{aligned}\mathbf{r}(\kappa^m, u^*) &= \mathbf{B}_0\Big(\Big(\mathbf{K}_h - \mathbf{C}_h - (\kappa^m)^2\mathbf{M}_h\Big)\mathbf{u}^* - \mathbf{f}_h - \mathbf{f}_h^{\mathrm{N}}\Big)\\ &= \mathbf{B}_0\Big(\Big(\mathbf{K}_h - (\kappa^m)^2\mathbf{M}_h\Big)\,\mathbf{u}^* - \mathbf{f}_h\Big),\end{aligned}$$

is the residual associated with the interior nodes of the fine h-mesh, the approximation u^* and the wave number κ^m. The symbol $'$ stands for the conjugated transpose, that is $v' \equiv \bar{v}^{\mathsf{T}}$, and $\mathbf{B}_0$ is a diagonal matrix on the h-mesh with ones in the positions associated with the interior nodes and zero elsewhere. That is, the matrix $\mathbf{B}_0$ sets the values of the residual at the boundary (either Dirichet, Neumann or Robin) to zero.

Thus, for a given value of $u^* \approx u_H^m[h]$, the wave number κ^* is the parameter of the modified problem that better accommodates u^*. In practice, κ^* is determined by minimizing the squared norm of the residual, namely

$$\kappa^* = \underset{\kappa^m\in\mathbb{R}}{\arg\min}\, \|R(\kappa^m, u^*; \cdot)\|_{*,h} = \underset{\kappa^m\in\mathbb{R}}{\arg\min}\, \sqrt{\mathbf{r}'\mathbf{r}} = \underset{\kappa^m\in\mathbb{R}}{\arg\min}\, \mathbf{r}'\mathbf{r}. \tag{2.10}$$

Note that given u^*, the squared residual norm $\mathbf{r}'\mathbf{r}$ is a fourth degree polynomial in κ^m and thus κ^* is computed explicitly. Indeed

$$\mathbf{r}(\kappa^m, u^*) = \mathbf{a}_0 + \mathbf{a}_2(\kappa^m)^2, \tag{2.11}$$

where

$$\mathbf{a}_0 = \mathbf{B}_0(\mathbf{K}_h\mathbf{u}^* - \mathbf{f}_h) \quad \text{and} \quad \mathbf{a}_2 = -\mathbf{B}_0\mathbf{M}_h\mathbf{u}^*.$$

Thus, the squared residual norm $\mathbf{r}'\mathbf{r}$ is a fourth degree polynomial in κ^m, namely

$$F(\kappa^m) = \mathbf{r}'\mathbf{r} = \mathbf{c}_0 + \mathbf{c}_2(\kappa^m)^2 + \mathbf{c}_4(\kappa^m)^4, \tag{2.12}$$

with the coefficients

$$\mathbf{c}_0 = \mathbf{a}_0'\mathbf{a}_0, \quad \mathbf{c}_2 = \mathbf{a}_0'\mathbf{a}_2 + \mathbf{a}_2'\mathbf{a}_0 \quad \text{and} \quad \mathbf{c}_4 = \mathbf{a}_2'\mathbf{a}_2.$$

It is worth noting that despite the vectors $\mathbf{a}_0$ and $\mathbf{a}_2$ are complex, the coefficients $\mathbf{c}_0, \mathbf{c}_2$ and $\mathbf{c}_4$ are real.

Thus, for a given value of u^*, the wave number κ^* minimizing the squared residual is explicitly computed by solving the cubic equation

$$\frac{dF}{d\kappa^m} = 2\mathbf{c}_2(\kappa^m) + 4\mathbf{c}_4(\kappa^m)^3 = 0.$$

The previous equation admits the trivial solution $\kappa^m = 0$ and two solutions $\kappa^m = \pm\sqrt{-\mathbf{c}_2/(2\mathbf{c}_4)}$. Since the wave number is a positive parameter, the numerical wave number is approximated by $\kappa^* = +\sqrt{-\mathbf{c}_2/(2\mathbf{c}_4)}$. Since $\mathbf{c}_4 \geq 0$, κ^* provides a proper estimate for κ as long as $\mathbf{c}_2 < 0$. In all the numerical tests that have been carried out, a negative value for $\mathbf{c}_2$ has been obtained. However, it is expected that positive values of $\mathbf{c}_2$ could appear for arbitrary choices of u^* not reproducing the main features of u_H. A positive $\mathbf{c}_2$ parameter would indicate that either u^* has not been properly chosen or that the numerical method has provided a really really poor approximation u_H.

In short, the approximation κ^* of the numerical wave number κ_H is assessed by first post-processing the finite element solution u_H to compute u^* and then setting $\kappa^* = \sqrt{-\mathbf{c}_2/(2\mathbf{c}_4)}$. The computable *a posteriori* error estimate for the wave number is then

$$\boxed{E^* = \kappa - \kappa^*}$$

Remark 2.3.1. The expression given in Steffens and Díez (2009) for the squared residual norm $\mathbf{r}'\mathbf{r}$ involves extra terms not appearing in equation (2.12). This is due the fact that in (2.12) the coefficients including the Robin boundary conditions are not presented due to the use of the non-boundary matrix $\mathbf{B}_0$. However, both formulations provide fairly similar results.

2.3.1 Assessment of the wave number for stabilized formulations

The dispersion error associated with a stabilized finite element approximation of u may be assessed using the same methodology detailed for the standard Galerkin approximation. Given the Galerkin least-squares finite element approximation u_H, a post-processing technique is used to compute an approximation u^* of the solution $u_H^m[h]$ and then the wave number κ_H is approximated by κ^*.

However, the use of stabilized formulations also for the fine mesh solutions in (2.9) allows to improve the quality of the estimates. Note that the accuracy of the estimate κ^* relies on two facts: first on the quality of the approximation u^* of $u_H^m[h]$, and second on the quality of the approximation $u_H^m[h]$ of u_H^m. The quality of u^* depends on the post-processing strategy which will be discussed in the following section. The quality of $u_H^m[h]$, on the other hand, depends on the size h of the reference mesh $\mathcal{V}_h$. In fact, it depends on the ratio of κ versus h since for large values of κ the reference mesh should be finer in order to get good approximations of u_H^m. Thus, for large wave numbers, the discrete approximation $u_H^m[h]$ will only be a good approximation of u_H^m if the reference mesh is taken remarkably fine.

A simple workaround which avoids dealing with fine reference meshes, is to stabilize the problem associated with $u_H^m[h]$. That is, for a given finite element approximation, either stabilized or not, the stabilized approximation $u_H^m[h;\tau_h]$ is the solution of

$$\begin{aligned}(\kappa_H[h;\tau_h], u_H^m[h;\tau_h]) \;=\; & \arg\min \;\; \|R_{\text{GLS}}(\kappa^m,\tau_h,u^m;\cdot)\|_{*,h} \\ & \kappa^m \in \mathbb{R} \\ & u^m \in \mathcal{U}_h \\ & \text{subject to} \\ & a_{\text{GLS}}(\kappa^m,\tau_h;u^m,v) = \ell_{\text{GLS}}(\kappa^m,\tau_h;v) \;\; \forall v \in \mathcal{V}_h \cap \mathcal{V}_0 \\ & \qquad u^m(\mathbf{x}^j) = u_H(\mathbf{x}^j),\; j = 1,2,\ldots,\mathtt{n}_{\mathtt{np}}\end{aligned} \tag{2.13}$$

where

$$R_{\text{GLS}}(\kappa^m,\tau_h,u^m;v) = \ell_{\text{GLS}}(\kappa^m,\tau_h;v) - a_{\text{GLS}}(\kappa^m,\tau_h;u^m,v).$$

This modification yields to the following strategy to assess the error in the numerical wave number:

1. compute u^* approximation of $u_H^m[h;\tau_h]$ by post-processing u_H

2. compute the approximation $\kappa^*[\tau_h]$ solution of

$$\kappa^*[\tau_h] = \underset{\kappa^m\in\mathbb{R}}{\arg\min}\, \|R_{\text{GLS}}(\kappa^m,\tau_h,u^*;\cdot)\|_{*,h}, \tag{2.14}$$

where the residual norm

$$\|R_{\text{GLS}}(\kappa^m, \tau_h, u^*; \cdot)\|_{*,h} = \mathbf{r}_{\text{GLS}}(\kappa^m, \tau_h, u^*)' \mathbf{r}_{\text{GLS}}(\kappa^m, \tau_h, u^*)$$

for

$$\mathbf{r}_{\text{GLS}}(\kappa^m, \tau_h, u^*) = \mathbf{B}_0 \Big(\Big(\mathbf{K}_h - (\kappa^m)^2 \mathbf{M}_h^{\tau_h} \Big) \mathbf{u}^* - \mathbf{f}_h^{\tau_h} \Big).$$

Note that the matrix $\mathbf{M}_h^{\tau_h}$ and the vector $\mathbf{f}_h^{\tau_h}$ depend explicitly on the wave number κ^m and also implicitly via the stabilization parameter τ_h. Therefore the dependency of $\mathbf{r}'_{\text{GLS}}\mathbf{r}_{\text{GLS}}$ with respect to the wave number κ^m is no longer a fourth order polynomial and the solution of (2.14) may not be computed explicitly in general.

In order to detail the computation of $\kappa^*[\tau_h]$ verifying (2.14) in a simple manner, the stabilization parameter τ_h is assumed constant on the elements of the fine mesh. In this case, $\kappa^*[\tau_h]$ is the solution of (2.14) where

$$\mathbf{r}_{\text{GLS}}(\kappa^m, \tau_h, u^*) = \mathbf{B}_0 \Big(\mathbf{K}_h \, \mathbf{u}^* - (\kappa^m)^2 \mathbf{M}_h \, \mathbf{u}^* + \tau_h (\kappa^m)^4 \mathbf{M}_h \, \mathbf{u}^* - \mathbf{f}_h + \tau_h (\kappa^m)^2 \mathbf{f}_h \Big)$$

and τ_h depends non-linearly on κ^m.

For instance, to minimize the dispersion error of a plane wave in the direction θ for structured regular quadrilateral meshes, Harari and Magoulès (2004) propose the use of

$$\tau_h(\kappa^m, \theta) = \frac{1}{(\kappa^m)^2} - \frac{6}{(\kappa^m)^4 h^2} \left(\frac{1 - \cos(\kappa^m h \cos\theta)}{2 + \cos(\kappa^m h \cos\theta)} + \frac{1 - \cos(\kappa^m h \sin\theta)}{2 + \cos(\kappa^m h \sin\theta)} \right).$$

Thus, the computation of $\kappa^*[\tau_h]$ requires solving a scalar root- finding problem. Three different options have been considered in the present work to approximate $\kappa^*[\tau_h]$:

Option 1: the first approach is to compute an approximation of $\kappa^*[\tau_h]$ using an algorithm to numerically approximate the minimum of

$$F(\kappa^m) = \mathbf{r}_{\text{GLS}}(\kappa^m, \tau_h, u^*)' \mathbf{r}_{\text{GLS}}(\kappa^m, \tau_h, u^*).$$

Namely, a root-finding method on the derivative of $F(\kappa^m)$ is used taking as initial guess $\kappa^m = \kappa$. This approximation is taken to represent the exact value $\kappa^*[\tau_h]$ since its accuracy can be controlled by the end-user through adjusting the tolerance of the root-finding method.

Option 2: the second approach assumes that τ_h does not vary considerably when varying the parameter κ^m. In this case, the dependency of the parameter τ_h with respect to κ^m is removed by setting the value of

$$\tau_h(\kappa^m) = \tau_h^\kappa,$$

where $\tau_h^\kappa = \tau_h(\kappa)$. This approximation of $\kappa^*[\tau_h]$ is denoted by $\kappa^*[\tau_h^\kappa]$. Note that τ_h^κ denotes the value of the parameter τ_h associated to the wave number κ. Doing this approximation, the residual $\mathbf{r}_{\text{GLS}}(\kappa^m, \tau_h, u^*)$ is approximated by a fourth order polynomial on κ^m

$$\mathbf{r}_{\text{GLS}}(\kappa^m, \tau_h, u^*) \approx \mathbf{a}_0 + \mathbf{a}_2(\kappa^m)^2 + \mathbf{a}_4(\kappa^m)^4,$$

for

$$\mathbf{a}_0 = \mathbf{B}_0(\mathbf{K}_h\mathbf{u}^* - \mathbf{f}_h), \quad \mathbf{a}_2 = \mathbf{B}_0(-\mathbf{M}_h\mathbf{u}^* + \tau_h^\kappa\mathbf{f}_h) \quad \text{and} \quad \mathbf{a}_4 = \tau_h^\kappa\mathbf{B}_0\mathbf{M}_h\mathbf{u}^*.$$

Note that the vectors $\mathbf{a}_2$ and $\mathbf{a}_4$, in this case, depend on the stabilization parameter τ_h^κ. Note also that if the stabilization parameter is set to zero, $\tau_h^\kappa = 0$, the expression for the residual given in (2.11) is recovered.

The minimization of the squared residual $F(\kappa^m)$ is then reduced to find the critical points of $F(\kappa^m)$, which is equivalent to find the solutions of

$$\frac{dF}{d\kappa^m} = 2\kappa^m\left(\mathbf{c}_2 + 2\mathbf{c}_4(\kappa^m)^2 + 3\mathbf{c}_6(\kappa^m)^4 + 4\mathbf{c}_8(\kappa^m)^6\right) = 0, \tag{2.15}$$

where

$$\mathbf{c}_2 = \mathbf{a}_0'\mathbf{a}_2 + \mathbf{a}_2'\mathbf{a}_0,\ \mathbf{c}_4 = \mathbf{a}_0'\mathbf{a}_4 + \mathbf{a}_2'\mathbf{a}_2 + \mathbf{a}_4'\mathbf{a}_0,\ \mathbf{c}_6 = \mathbf{a}_2'\mathbf{a}_4 + \mathbf{a}_4'\mathbf{a}_2,\ \mathbf{c}_8 = \mathbf{a}_4'\mathbf{a}_4.$$

Although equation (2.15) may have seven real solutions, $\kappa^*[\tau_h^\kappa]$ is defined to be the solution of (2.15) closer to κ. Thus, ruling out the trivial solution $\kappa^m = 0$, $\kappa^*[\tau_h^\kappa]$ is computed by first finding the roots of the bicubic polynomial appearing in equation (2.15), which is equivalent to find the three solutions $\hat{\kappa}$ of

$$\mathbf{c}_2 + 2\mathbf{c}_4\hat{\kappa} + 3\mathbf{c}_6\hat{\kappa}^2 + 4\mathbf{c}_8\hat{\kappa}^3 = 0,$$

and then set $\kappa^*[\tau_h^\kappa]$ to be the value of $\sqrt{\hat{\kappa}}$ nearer to κ. Thus, the assumption $\tau_h(\kappa^m) = \tau_h^\kappa$ yields a simple and explicit algorithm to approximate the exact value of $\kappa^*[\tau_h^\kappa]$.

As in the case of the non-stabilized approach, a negative result could be encountered for very crude approximation u^*. However, none of the considered numerical tests yield negative values for $\hat{\kappa}$.

Note also that the coefficients $\mathbf{c}_j$, for $j = 2, 4, 6, 8$ associated to the residual $\mathbf{r}_{\text{GLS}}$, depend on the stabilization parameter τ_h^κ which in turn depends on a user prescribed direction θ which will be denoted in the following by θ_h. In the case that u_H is computed using the standard Galerkin method, it is not natural to define a direction θ_h. However, information of the prevalent wave direction of the exact solution can be used if available. If u_H is computed using the Galerkin least-squares method with wave direction θ, the estimates may be computed using $\theta_h = \theta$ or again, if information of the exact solution is available, this parameter may be set to adjust the prevalent wave direction of the exact solution. The choice of this parameter will be further discussed in the numerical examples.

Option 3: finally, the third approach considers that the terms added by the Galerkin least-squares method are constant with respect to κ^m, that is, not only the parameter τ_h is set to τ_h^κ but also the $(\kappa^m)^2$ associated with the Galerkin least-squares method is set to κ^2. In this way, the residual is approximated by the quadratic function

$$\mathbf{r}_{\text{GLS}}(\kappa^m, \tau_h, u^*) \approx \mathbf{B}_0\Big(\mathbf{K}_h\,\mathbf{u}^* - (\kappa^m)^2\mathbf{M}_h\,\mathbf{u}^* + \tau_h^\kappa\kappa^2(\kappa^m)^2\mathbf{M}_h\,\mathbf{u}^* - \mathbf{f}_h + \tau_h^\kappa\kappa^2\mathbf{f}_h\Big),$$

that can be rewritten as

$$\mathbf{r}_{\text{GLS}}(\kappa^m, \tau_h, u^*) \approx \mathbf{a}_0 + \mathbf{a}_0(\kappa^m)^2,$$

where

$$\mathbf{a}_0 = \mathbf{B}_0(\mathbf{K}_h\,\mathbf{u}^* + (\tau_h^\kappa\kappa^2 - 1)\mathbf{f}_h) \quad \text{and} \quad \mathbf{a}_2 = \mathbf{B}_0((\tau_h^\kappa\kappa^2 - 1)\mathbf{M}_h\mathbf{u}^*).$$

Therefore, the minimization of the fourth order polynomial $F(\kappa^m)$ which allows to compute the approximation of $\kappa^*[\tau_h]$ is done as in equation (2.12)

with the only difference that here the vectors $\mathbf{a}_0$ and $\mathbf{a}_2$ contain an extra contribution coming from the stabilization terms.

2.4 Enhanced solution u^* by postprocessing of u_H

The methodology introduced in the previous section is only applicable as a practical error estimation strategy if the cost of computing u^* is low. Thus, as mentioned before, the error estimation procedure can not be based on solving problems in the complete finer reference mesh. It has also been noted that once the solution u^* is found, the corresponding wave number κ^* is fairly computed solving explicitly an equation as discussed previously.

The quality of the estimate κ^* depends on the quality of the approximation u^* of $u_H^m[h] \in \mathcal{U}_h$ or of $u_H^m[h;\tau_h]$, respectively. The idea proposed here is to build up an inexpensive approximation using a postprocessing technique standard in error estimation analysis (Wiberg et al. 1992, Díez and Calderón 2007*a*) and likely to have all its features. The post-processing technique starts from the finite element solution $u_H \in \mathcal{U}_H$ and computes an approximation u^* of $u_H^m[h]$ in $\mathcal{U}_h$.

The enhanced solution is produced locally, in patches of elements, centered in every element of the mesh. For each element of the H-mesh, Ω_k, the patch of elements surrounding Ω_k is considered and it is denoted by ω_k. In this patch, the values of $\mathbf{u}_H$ at the nodes of the H-mesh are used as input data and a polynomial is fitted using a constrained least squares technique, as illustrated in figure 2.4.

In particular, in a two dimensional setting, where $\mathbf{x} = (x, y)$ for a given polynomial degree q, a complex valued polynomial field

$$p(\mathbf{x}) = \sum_{n+l\leq q} p_{nl} x^n y^l$$

is determined from the following constrained least squares problem

$$\min_{p_{nl}\in\mathbb{C}} \sum_{\mathbf{x}^j\in\omega_k} \left|u_H^j - p(\mathbf{x}^j)\right|^2$$

$$\text{restricted to } \; p(\mathbf{x}^j) = u_H^j \;\; \text{for } \mathbf{x}^j \in \Omega_k,$$

where $|\cdot|$ denotes the modulus of a complex number.

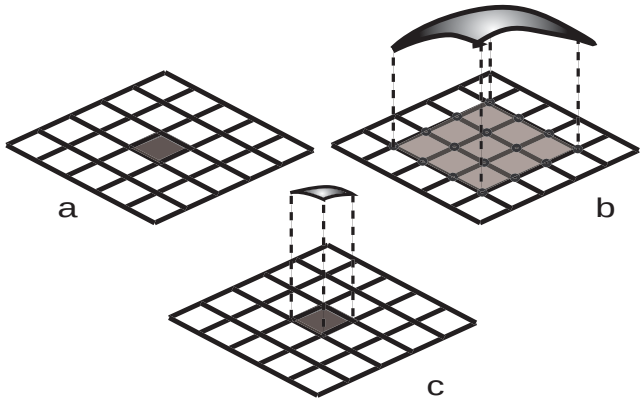

Figure 2.4: Element Ω_k of the H-mesh (darkened in plot a) is associated with a patch (shadowed in plot b). A polynomial is fitted using the values in the nodes in this patch ω_k using a least squares criterion (b). This polynomial is evaluated to obtain the nodal values of the enhanced function u^* in the nodes of the refined h-mesh in the element under consideration (c).

Once the polynomial is obtained in ω_k it is evaluated to find the nodal values of u^* in the nodes of the h-mesh lying inside the element Ω_k of the H-mesh. This approach allows recovering the curvatures of the solution coinciding with u_H at the nodes where it is computed.

This simple and straightforward strategy provides fairly good results. However, this approach does not use specific information about the differential operator or the exact solution. The use of analytical information on the natural solutions of the differential operator yields an alternative approach to compute u^*.

The approach to compute u^* also requires solving a local constrained least squares problem for each element Ω_k. However, instead of using a polynomial representation for $u^*|_{\omega_k}$ an exponential fitting is used. This is a natural choice because the exact solution of the two-dimensional homogeneous Helmholtz equation is an infinite sum of plane waves of the form $Ae^{i\mathbf{k}\cdot\mathbf{x}}$, where $\mathbf{k} = \kappa[\cos\theta, \sin\theta]$.

Thus, in each patch ω_k, u_H is approximated by an exponential field of the form

$$A(\mathbf{x})e^{ip(\mathbf{x})},$$

where $A(\mathbf{x})$ and $p(\mathbf{x})$ are polynomial fields representing the amplitude and wave direction, respectively. The fields $A(\mathbf{x})$ and $p(\mathbf{x})$ are determined by a constrained

least squares criterion and hence, they are taken as those minimizing

$$\begin{aligned}&\min \sum_{\mathbf{x}^j\in\omega_k}\left|u_H^j - A(\mathbf{x}^j)e^{ip(\mathbf{x}^j)}\right|^2\\ &\text{restricted to } \; A(\mathbf{x}^j)e^{ip(\mathbf{x}^j)} = u_H^j \;\text{ for } \mathbf{x}^j\in\Omega_k.\end{aligned}$$

Using a standard technique to linearize the exponential least squares fitting transforms the previous problem into an equivalent linear constrained least squares problem

$$\begin{aligned}&\min \sum_{\mathbf{x}^j\in\omega_k}\left|\ln(u_H^j) - \ln\left(A(\mathbf{x}^j)e^{ip(\mathbf{x}^j)}\right)\right|^2\\ &\text{restricted to } \; \ln\left(A(\mathbf{x}^j)e^{ip(\mathbf{x}^j)}\right) = \ln(u_H^j) \;\text{ for } \mathbf{x}^j\in\Omega_k.\end{aligned}$$

Indeed, let $u_H^j\in\mathbb{C}$ be represented in its exponential form

$$u_H(\mathbf{x}^j) = |u_H^j|e^{i\arg(u_H^j)},$$

where $|\cdot|$ and $\arg(\cdot)$ denote the modulus and argument of a complex number. Then, the restriction $\ln\left(A(\mathbf{x}^j)e^{ip(\mathbf{x}^j)}\right) = \ln(u_H^j)$ becomes

$$\ln\left(A(\mathbf{x}^j)\right) + ip(\mathbf{x}^j) = |u_H^j| + i\arg(u_H^j).$$

Thus, splitting the real and imaginary parts yield

$$\ln\left(A(\mathbf{x}^j)\right) = |u_H^j| \quad\text{and}\quad p(\mathbf{x}^j) = \arg(u_H^j).$$

Similarly, the objective function can be rewritten as:

$$\begin{aligned}&\sum_{\mathbf{x}^j\in\omega_k}\left|\ln(u_H^j) - \ln\left(A(\mathbf{x}^j)e^{ip(\mathbf{x}^j)}\right)\right|^2\\ &\qquad= \sum_{\mathbf{x}^j\in\omega_k}\left|\ln(|u_H^j|) + i\arg(u_H^j) - \ln\left(A(\mathbf{x}^j)\right) - ip(\mathbf{x}^j)\right|^2\\ &\qquad= \sum_{\mathbf{x}^j\in\omega_k}\left|\ln(|u_H^j|) - \ln\left(A(\mathbf{x}^j)\right) + i\left(\arg(u_H^j) - p(\mathbf{x}^j)\right)\right|^2\\ &\qquad= \sum_{\mathbf{x}^j\in\omega_k}\left(\ln(|u_H^j|) - \ln\left(A(\mathbf{x}^j)\right)\right)^2 + \sum_{\mathbf{x}^j\in\omega_k}\left(\arg(u_H^j) - p(\mathbf{x}^j)\right)^2.\end{aligned}$$

Thus, splitting the modulus and angle contributions, both in the objective function and in the constraint, yields a simple strategy to compute $\ln(A(\mathbf{x}))$ and $p(\mathbf{x})$ independently, namely:

$$\begin{aligned} &\min \sum_{\mathbf{x}^j \in \omega_k} \left|\ln(|u_H^j|) - \ln(A(\mathbf{x}^j))\right|^2 \\ &\text{restricted to } \ln(A(\mathbf{x}^j)) = \ln(|u_H^j|) \text{ for } \mathbf{x}^j \in \Omega_k, \end{aligned}$$

and

$$\begin{aligned} &\min \sum_{\mathbf{x}^j \in \omega_k} \left|\arg(u_H^j) - p(\mathbf{x}^j)\right|^2 \\ &\text{restricted to } p(\mathbf{x}^j) = \arg(u_H^j) \text{ for } \mathbf{x}^j \in \Omega_k, \end{aligned}$$

where a polynomial fitting of $\ln(A(\mathbf{x}))$ and $p(\mathbf{x})$ is considered.

The only intricate part of this strategy involves the input data, $\arg(u_H^j)$, of the least squares problem for $p(\mathbf{x})$. The non-unique arguments associated to the data u_H^j have to be carefully selected so that the polynomial fitting yields proper results.

In the following, a brief description of the main difficulties involved in the preprocessing of the input data, $\arg(u_H^j)$, and the adopted solution is presented.

Consider the simplest case where the finite element approximation is a plane wave traveling in a predefined direction θ, namely

$$u_H = Ae^{i(\kappa\cos\theta x + \kappa\sin\theta y)}.$$

In this case, it is clear that $|u_H^j| = A$. However, since the argument of a complex number it is a multi-valued function, the computation of $\arg(u_H^j)$ does not necessarily return $(\kappa\cos\theta x + \kappa\sin\theta y)$. That is, in general

$$\arg(u_H^j) = \Im\mathrm{m}(\ln(u_H^j)) \neq \kappa\cos\theta x^j + \kappa\sin\theta y^j$$

but

$$\arg(u_H^j) = \kappa\cos\theta x^j + \kappa\sin\theta y^j + 2\pi l$$

for a given number $l \in \mathbb{Z}$. Thus, although the least-square fitting problem should return the plane $p(\mathbf{x}) = \kappa\cos\theta x + \kappa\sin\theta y$, if the input data is not carefully preprocessed, the results are not the expected.

For this simple case, a workaround to this problem can be found by adding multiples of 2π to the input data in the patch ω_k, $\arg(u_H^j)$, so that its deviation from a plane is minimum.

However, the exact solution of the general homogeneous Helmholtz equation is not a simple plane wave, but it is general expressed as an infinite sum of plane waves traveling in different directions.

In the case that the solution is extremely complicated, without a predominant direction, the exponential fitting may fail to properly approximate the local behavior of the enhanced solution. Actually, the exponential recovery in these zones introduces unrealistic discontinuities.

Even if the exact solution has no prevalent directions, one can consider an exponential representation of the solution of the problem

$$u(\mathbf{x}) = \mathfrak{r}(\mathbf{x})e^{i\theta(\mathbf{x})},$$

where $\mathfrak{r}(\mathbf{x})$ and $\theta(\mathbf{x})$ are the real-valued functions providing the modulus and angle of u respectively.

In the cases where the solution does not have a prevalent direction two phenomena may appear: on one hand the angle distribution $\theta(\mathbf{x})$ may present discontinuities coinciding with areas where the modulus vanishes, and, on the other hand, the modulus distribution $\mathfrak{r}(\mathbf{x})$ may present a highly non-linear and non-smooth behavior in some regions.

To illustrate these phenomena, three different solutions are considered for the wave propagation problem in a unit square: $u_1(\mathbf{x}) = 2e^{i\kappa x}+e^{i\kappa y}$, $u_2(\mathbf{x}) = e^{i\kappa x}+e^{i\kappa y}$ and $u_3(\mathbf{x}) = e^{i\kappa x} + e^{i\kappa y} + e^{-i\kappa y}$. The modulus and angle distributions of the three solutions are shown in figure 2.6.

First, consider the solution $u_1(\mathbf{x}) = 2e^{i\kappa x} + e^{i\kappa y}$. Note that, in this case, the plane wave traveling in the x-direction, $e^{\kappa i x}$, prevails over the wave traveling in the y-direction, $e^{\kappa i y}$. As can be seen in figure 2.6, the standard representation of the angle distribution $\theta(\mathbf{x})$ is a discontinuous function, which can be easily post-processed to recover a continuous angle distribution. Moreover, the modulus does not present large variations over small regions. In this case, the exponential fitting provides accurate approximations of u.

The second example $u_2(\mathbf{x}) = e^{i\kappa x} + e^{i\kappa y}$, shows that if the solution is obtained combining two plane waves of the same amplitude, and thus it does not have any prevalent direction, angle discontinuities appear in some predefined straight lines. In this case, as can be see in figure 2.6, even if the fictitious discontinuities may

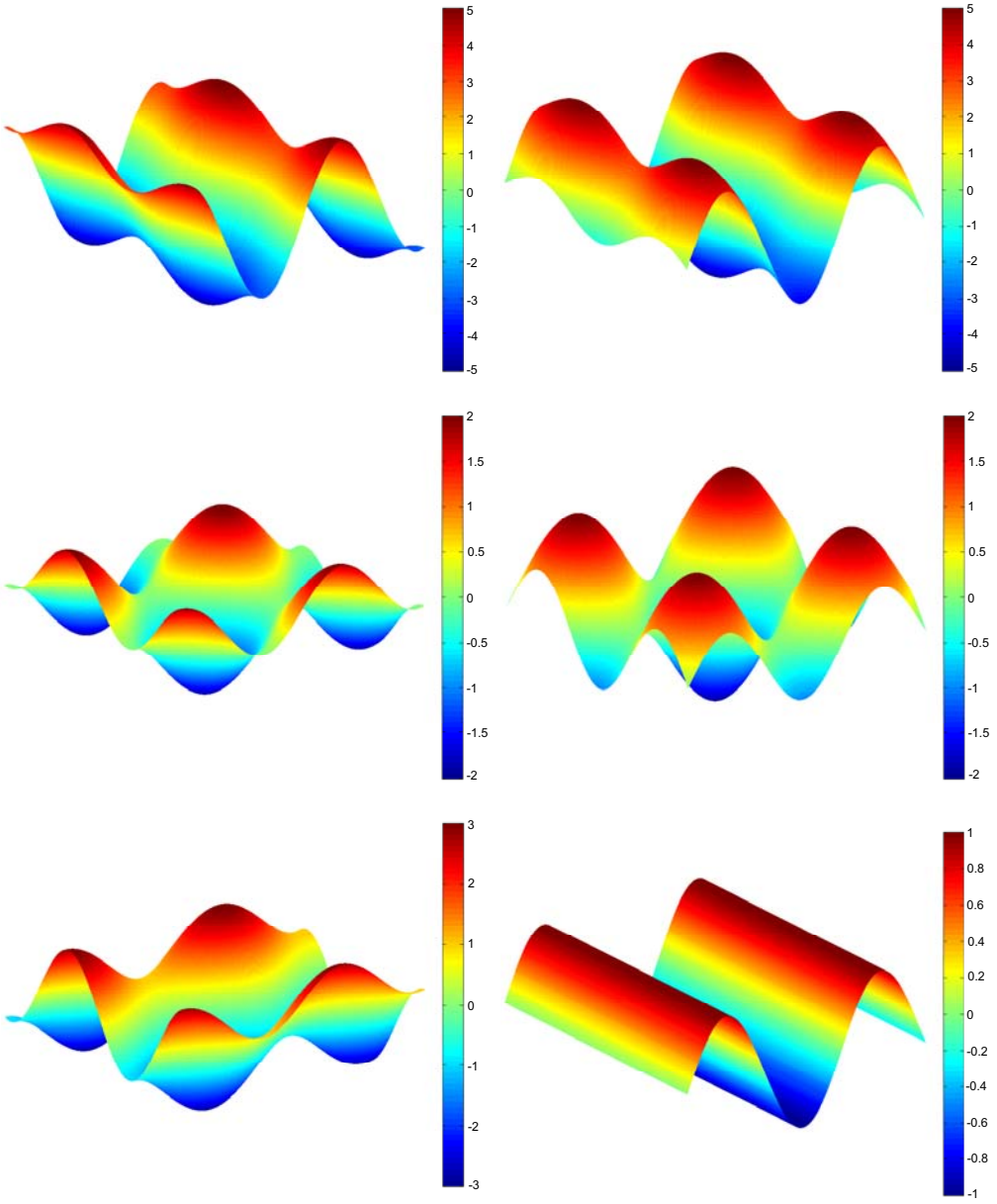

Figure 2.5: Real part (left) and imaginary part (right) for three solutions in the unit square. From top to bottom: $u_1 = 2e^{i\kappa x} + e^{i\kappa y}$, $u_2 = e^{i\kappa x} + e^{i\kappa y}$ and $u_3 = e^{i\kappa x} + e^{i\kappa y} + e^{-i\kappa y}$ for $\kappa = 9.7$.

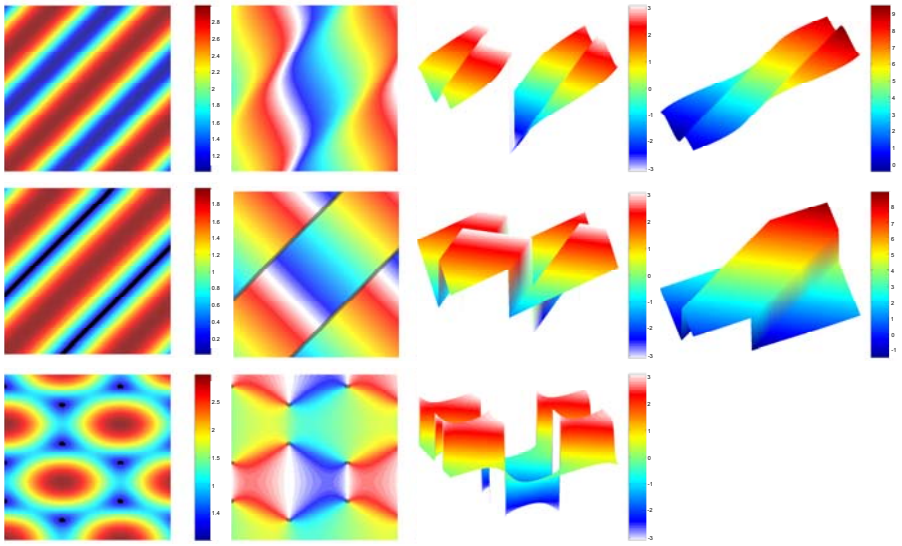

Figure 2.6: Behavior of the modulus and angle distributions, $\theta(\mathbf{x})$ and $r(\mathbf{x})$ respectively, for three simple solutions in the unit square. From top to bottom: u_1, u_2 and u_3. For each solution, the modulus distribution (left) and two views of the angle distributions (middle left, middle right) are shown. When possible, equivalent angle distributions only containing non-removable discontinuities – where the discontinuities associated to a 2π angle jump have been smoothed – are shown (right).

be removed bye pre-processing the initial data $\arg(u_H^j)$, the real discontinuities are poorly approximated using a polynomial least-squares technique. Note however, that after smoothing is applied, the elements surrounding the discontinuity may be clearly identified.

As the number of plane waves that comprise the solution u increases, see for instance the third example $u_3(\mathbf{x}) = e^{\kappa i x} + e^{\kappa i y} + e^{-\kappa i y}$, the modulus and angle distributions may present areas with a highly non-linear and nonsmooth behavior. Note that, although the angle distribution only presents point or removable discontinuities at nine points of the domain, obtaining a globally smooth angle distribution from the standard angle representation is not a trivial task.

The exponential fitting technique is aimed at finding a proper local polynomial representation for the modulus and angle distributions. Thus, in regions where either the angle is discontinuous or the modulus presents large oscillations, the exponential representation yields poor results.

In this work, a simple workaround is proposed: first, the smoothing technique

is applied to remove the fictitious discontinuities. The same smoothing technique identifies the elements near the angle discontinuities or near the regions where the modulus has a non-smooth behavior. Finally, the exponential fitting is applied only to the non-selected elements while a polynomial fitting is applied to the problematic elements.

2.5 Numerical examples

The presented strategy to assess the error in the wave number is illustrated in three numerical examples. Additional results and examples can be found in (Steffens and Díez 2009) and (Steffens et al. 2010*a*), see the enclosed papers at the end of the thesis.

First, the influence of the selection of the finite reference mesh and the different options to approximate the wave number are studied for the simple one-dimensional case. For the following examples -the plane wave in a square domain and the noise transmission inside a car cavity- the performance of the estimates of the dispersion error is shown both for Galerkin and Galerkin least-squares approximations. A study of the influence of the post-processing technique yielding u^* in the resulting effectivity is analyzed. Finally an analysis of the impact of the choice of the prescribed direction θ for stabilized formulations in the dispersion error is also presented.

The finite element approximations are computed using triangular and quadrilateral meshes of linear (resp. bilinear) elements, $p = 1$. Different definitions of the stabilization parameter τ_H are used to compute the Galerkin least-squares approximations depending on the underlying topology of the mesh. In particular, for structured and unstructured quadrilateral meshes the following definition of the parameter, designed to minimize the dispersion error of plane wave in the direction θ on cartesian meshes, is used (Harari and Magoulès 2004, Harari and Nogueira 2002):

$$\tau_H = \frac{1}{\kappa^2} - \frac{6}{\kappa^4 h^2}\left(\frac{1-\cos(\kappa h\cos\theta)}{2+\cos(\kappa h\cos\theta)} + \frac{1-\cos(\kappa h\sin\theta)}{2+\cos(\kappa h\sin\theta)}\right).$$

For triangular meshes, the definition derived for hexagonal meshes, namely,

$$\tau_H = \frac{1}{\kappa^2} - \frac{8}{\kappa^4 h^2}\frac{3 - f(\kappa h, \theta)}{3 + f(\kappa h, \theta)}$$

where $f(\kappa h, \theta) = \cos(\kappa h \cos\theta) + 2\cos(\kappa h \cos\theta/2)\cos(\sqrt{3}\kappa h \sin\theta/2)$ is used because it provides good results also for unstructured meshes.

For non-uniform meshes, the stabilization parameter is not constant over the whole mesh. In each element Ω_k a different stabilization parameter is used depending on its characteristic element size h_k. This characteristic element size is taken as the smallest side of the element both for quadrilateral and triangular meshes.

2.5.1 One-dimensional strip

The first example models a plane wave propagating in the x-direction in strip a rectangular $1 \times \sqrt{3}/8$ domain. The boundary conditions are specified in order to yield the exact solution $u(x, y) = e^{i\kappa x}$: Dirichlet on the left hand side, Robin on the right hand side and Neumann elsewhere. The performance of the Galerkin finite element solutions is studied for $\kappa = 8\pi$.

If the finite element mesh $\mathcal{V}_h$ is sufficiently fine, one expects that

$$u_H^m \approx u_H^m[h; \tau_h] \approx u_H^m[h]$$

and, therefore

$$\kappa_H \approx \kappa_H[h; \tau_h] \approx \kappa_H[h].$$

If the finite element mesh $\mathcal{V}_h$ is not fine enough, one should apply a correction factor to $\kappa_H[h]$ to account for the finite size h of the reference mesh and recover a good approximation of κ_H. This correction factor is not necessary for the estimate $\kappa_H[h; \tau_h]$. That is when the reference problem is also stabilized.

To analyze the influence of the selection of the finite element reference mesh, the different *a posteriori* estimates of the dispersion error are computed using a series of successively refined nested reference meshes. An initial uniform coarse mesh of 24×2 quadrilateral elements is used. The refinement is performed only in the x-direction and thus maintaining two rows of elements on all the reference meshes, due to the one-dimensional character of the solution.

The results are shown in the table 2.1. The first columns of the table show the truth or reference estimates of the dispersion error

$$E[h] = \kappa - \kappa_H[h] \quad \text{and} \quad E[h;\tau_h] = \kappa - \kappa_H[h;\tau_h],$$

where the numerical wave numbers $\kappa_H[h]$ and $\kappa_H[h;\tau_h]$ are computed solving the non-linear problems (2.9) and (2.13) respectively. The correction factor applied to $\kappa_H[h]$ is defined as

$$c_f = \frac{n_r^2}{(n_r^2-1)},$$

where $n_r = H/h$. Note that these reference estimates are computationally unaffordable in real applications, because they involve many resolutions of the problem in the reference mesh. They are computed here to see the effectivity of the proposed practical estimates. As can be seen, both the estimates $c_f E[h]$ and $E[h;\tau_h]$ assessing the dispersion error of the Galerkin approximation are in very good agreement with the a-priori estimate defined by equation (2.7), namely E^{pri}. It is worth noting that the estimate $E[h;\tau_h]$ yields very good results even for the case $h = H/2$ being less sensitive than $c_f E[h]$ to the choice of the reference mesh size.

The last columns in the table 2.1, correspond to the practical estimates obtained from the recovered solution u^*. In this case u^* is computed using the exponential fitting. Four different estimates are computed. The first one is the estimate, $E^* = \kappa - \kappa^*$, associated with the assessed wave number obtained from equation (2.10) and enhanced by its multiplicative factor. The other three options correspond to the three approximations of $\kappa^*[\tau_h]$ detailed in section 2.3.1. It is worth nothing that all estimates produce similar and sharp approximations to the dispersion error for all the values of the reference mesh size h.

As expected, the reference estimates provide almost exact values for the dispersion error, fully coinciding with the *a priori* estimate. There is an equivalence between the effect of correcting the estimate with factor c_f or considering a stabilized reference problem.

Following these results, in the remainder of the numerical examples, the parameter h is set to $h = H/4$ and the Option 2 of the stabilized formulation is set to approximate the wave number $\kappa^*[h]$, which provides a really good result. Note that Option 1 y 2 provide practically identical results at a very different cost: Option 1

				Galerkin	$E^{\text{pri}} = 1.02211$		
h	$E[h]$	$c_f E[h]$	$E[h;\tau_h]$	$c_f E^*$	Option 1 $E^*[\tau_h]$	Option 2 $E^*[\tau_h^\kappa]$	Option 3
$H/2$	0.76790	1.02387	1.02211	1.01428	1.01469	1.01486	1.03682
$H/4$	0.95869	1.02261	1.02211	1.01428	1.01469	1.01486	1.03682
$H/8$	1.00627	1.02224	1.02211	1.01227	1.01232	1.01232	1.01368
$H/16$	1.01815	1.02214	1.02211	1.01214	1.01215	1.01215	1.01249
$H/32$	1.02112	1.02212	1.02211	1.01210	1.01210	1.01210	1.01218
$H/64$	1.02186	1.02211	1.02211	1.01208	1.01208	1.01208	1.01210

Table 2.1: Example 1: Assessment of the dispersion error for a uniform coarse quadrilateral mesh (24×2 elements) an successively refined reference meshes for the Galerkin approximations of the solution. The reference error estimates (left) are computed using the fully non-linear solution yielding to $E[h]$ and $E[h;\tau_h]$. The exponential post-processed solution (right) u^* obtained from u_H and then different options are used to recover the wave number κ^* associated to u^* only for the Galerkin approximation.

involves the solution of a one-dimensional non-linear problem while the estimate for Option 2 is computed from a simple closed-formula. Hence, in the following the notation E^* is used to denote the estimate $E^*[\tau_h^\kappa]$ (both for the Galerkin and Galerkin least-squares methods). Finally, the estimate E^* is compared with the reference estimate $E[h;\tau_h]$ which is considered as the one providing the *most accurate-but not computable* approximation of the dispersion error, and it is denoted by E.

2.5.2 Plane wave in a square domain

The second considered example is the unit square $\Omega =]0,1[\times]0,1[$ with inhomogeneous Robin boundary conditions specified on all the boundaries of the square so that the exact solution is $u = e^{i\kappa(\cos\alpha x + \sin\alpha y)}$. That is, a plane wave propagating in the direction of angle α, as illustrated in figure 2.7. The model parameters are $\kappa = 8$ and $\alpha = \pi/8$ and the analytical solution associated with these parameters is depicted in figure 2.7.

The performance of the estimates is studied for three different structured uniform quadrilateral meshes (8×8, 16×16 and 32×32 elements). In order to estimate the dispersion error associated with the Galerkin approximation, the stabi-

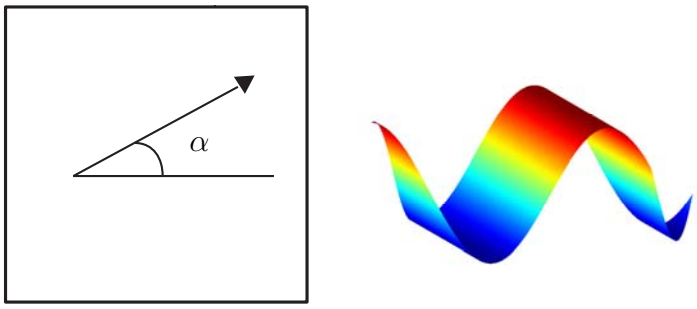

Figure 2.7: Example 2: Problem setup (left) and solution for $\alpha = \pi/8$ (right).

lization parameters involved in the computation of $E = E[h; \tau_h]$ and $E^* = E^*[\tau_h^\kappa]$ are computed using the predefined direction $\theta_h = \alpha = \pi/8$.

The results of the dispersion error for Galerkin approximations are shown in table 2.2, where $I^{\text{eff}}_{\text{pol}} = E^*_{\text{pol}}/E$ and $I^{\text{eff}}_{\text{exp}} = E^*_{\text{exp}}/E$ is the effectivity index of the estimates with respect to the reference value E and E^*_{pol} and E^*_{exp} are the estimates obtained from $u^a st$ using the polynomial or exponential least-squares recovery respectively. It is clear that the exponential fitting captures more precisely the shape of the solution and thus provides better estimates to the dispersion error yielding very good effectivity indexes near to one.

	Galerkin				
$\mathtt{n}_{\text{np}}$	E	E^*_{pol}	E^*_{exp}	$I^{\text{eff}}_{\text{pol}}$	$I^{\text{eff}}_{\text{exp}}$
81	0.24912	0.41670	0.23725	1.6727	0.9524
289	0.06330	0.09033	0.06328	1.4271	0.9998
1089	0.01563	0.01943	0.01593	1.2434	1.0197

Table 2.2: Example 2: Assessment of the dispersion error of the Galerkin method for uniformly refined structured quadrilateral meshes.

The same study is done for the Galerkin least-squares approximations of the problem using the same meshes. Although the exact solution is a plane wave, since the cartesian meshes are not aligned with the wave direction $\alpha = \pi/8$, none of the possible choices for stabilization direction θ yields a nodally exact solution. Table 2.3 shows the dispersion error of the Galerkin least-squares method for three different stabilization parameters $\theta = 0$, $\theta = \pi/8$ and $\theta = \pi/4$. In all the computations the error estimates are performed using the same value of θ for the reference

$h-$mesh. The error estimates E^*_{exp} are properly approximating the reference error E in all cases. The Galerkin least-squares method substantially reduces de dispersion error even for the non-optimal parameters $\theta = 0$ and $\theta = \pi/4$. For $\theta = \pi/8$ the dispersion error is so small that the resulting effectivity is not as sharp as for the choices producing longer errors.

	GLS/FE					
	$\theta = 0$		$\theta = \pi/8$		$\theta = \pi/4$	
$\mathtt{n}_{\text{np}}$	E	E^*_{exp}	E	E^*_{exp}	E	E^*_{exp}
81	-7.45·10^{-2}	-7.17·10^{-2}	6.82·10^{-4}	3.40·10^{-4}	7.71·10^{-2}	7.34·10^{-2}
289	-1.99·10^{-2}	-1.93·10^{-2}	-4.43·10^{-4}	3.80·10^{-5}	1.91·10^{-2}	1.95·10^{-2}
1089	-5.02·10^{-3}	-4.87·10^{-3}	-1.84·10^{-4}	1.68·10^{-6}	4.66·10^{-3}	4.88·10^{-3}

Table 2.3: Example 2: Assessment of the dispersion error of the Galerkin least-squares method for uniformly refined structured quadrilateral meshes. The Galerkin least-squares approximations are computed using different stabilization directions θ.

Figure 2.8 graphically displays the information shown in the tables in tables 2.2 and 2.3. As can be seen, the estimates depicted on the left of the figure are in very good agreement with the reference mesh computations, depicted on the right of the figure. As mentioned before, the Galerkin least-squares method always performs better than the Galerkin method but there is a qualitative leap of accuracy when the optimal parameter $\theta = \pi/8$ is used.

Figure 2.9 shows the influence of the stabilization direction θ used to compute the Galerkin least-squares finite element approximation in the dispersion error. The study is done varying θ in the range $[0, \pi/2]$. As expected, the optimal performance is reached when the wave direction of the Galerkin least-squares method coincides with the angle of the exact solution, $\theta = \alpha = \pi/8$. In any case, if no information of the exact solution is at hand and thus, an arbitrary choice of θ is considered, the Galerkin least-squares method provides an important reduction of the dispersion error when compared to the Galerkin approximation: the estimated dispersion error is reduced from $E^*_{\text{exp}} = 0.06328$ to $E^*_{\text{exp}} \approx 0.02$ in the worst case.

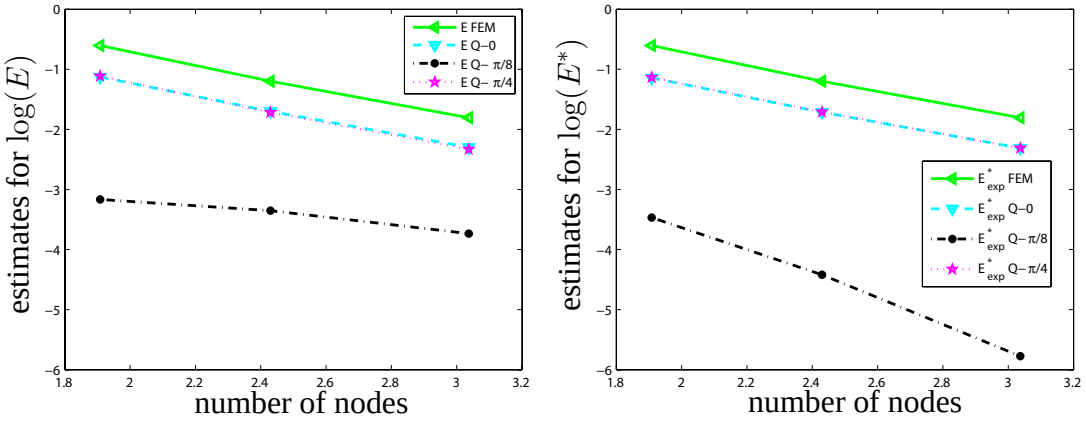

Figure 2.8: Example 2: Performance Galerkin w.r.t. Galerkin least-squares of a plane wave oriented horizontally with $\alpha = \pi/8$ and with different Galerkin least-squares stabilization parameters for solution in the reference mesh (left) and exponential solution (right).

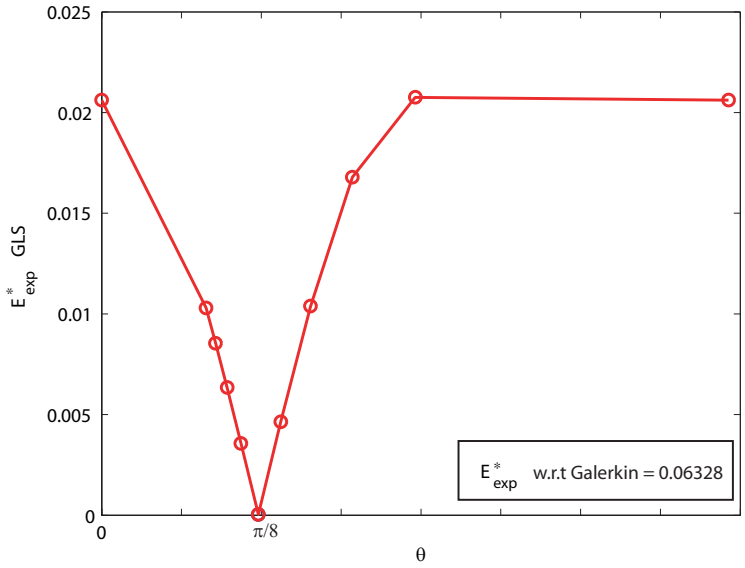

Figure 2.9: Example 2: Influence of the selection of the stabilization angle θ in the dispersion error of the Galerkin least-squares approximation for the mesh with 269 degrees of freedom. The estimates are computed both using $\theta = \alpha$.

2.5.3 Two-dimensional acoustic car cavity

The noise transmission inside the interior of passenger cars is considered as a practical application. A two-dimensional section of the cabin of a car which is excited by vibrations of the front panel and damped by Robin boundary conditions is studied. Moreover, this example is frequently used as a benchmark problem in error assessment for interior acoustic problems (Bouillard and Ihlenburg 1999, Suleau et al. 2000, Harari and Magoulès 2004).

The geometry of the cabin is shown in figure 2.10. The size of the domain is characterized by the maximum horizontal and vertical lengths, $L_x = 2.7\,m$ and $L_y = 1.1\,m$, respectively. The source term is $f = 0$, and, as mentioned in chapter 1, for interior acoustic wave propagation problems, the Neumann and Robin boundary conditions are of the form $g = -i\rho c\kappa v_n$ and $mu = -i\rho c\kappa A_n u$. In this case the material parameters are $c = 340\,m/s$ standing for the speed of sound of the medium and $\rho = 1.225\,kg/m^3$ standing for the mass density. The vibrating front panel is excited with a unit normal velocity $v_n = 1\,m/s$ whereas the roof is considered to be an absorbent panel with associated admittance $A_n = 1/2000\,m.(Pa.s)^{-1}$. The rest of the boundary is assumed to be perfectly reflecting and thus $v_n = 0\,m/s$. Finally, a wave number of $\kappa \approx 9.7$, equivalent to a frequency of $525\,Hz$, has been considered in the computations.

The dispersion effect along a specific line L is depicted on the right of the figure 2.10. The two curves correspond to the finite element approximations obtained using a coarse and finer computational meshes. Note that, compared with the finer mesh, the dispersion error in the coarse mesh is significant.

In this problem, the exponential fitting yields bad estimates, worse than the standard polynomial fitting. As mentioned in section (2.4), this is due to the fact that the solution is extremely complex, without a predominant direction. At many points of the domain, the solution can be expressed as a different sum of diverse plane waves. Thus, the exponential fitting fails, in the vicinity of these points, to properly approximate the local behavior of the enhanced solution.

In the previous examples, the solutions were either a single plane wave traveling in a predefined direction or had a prevalent plane wave direction, although the prevalent wave direction may vary from different zones of the domain (see also the

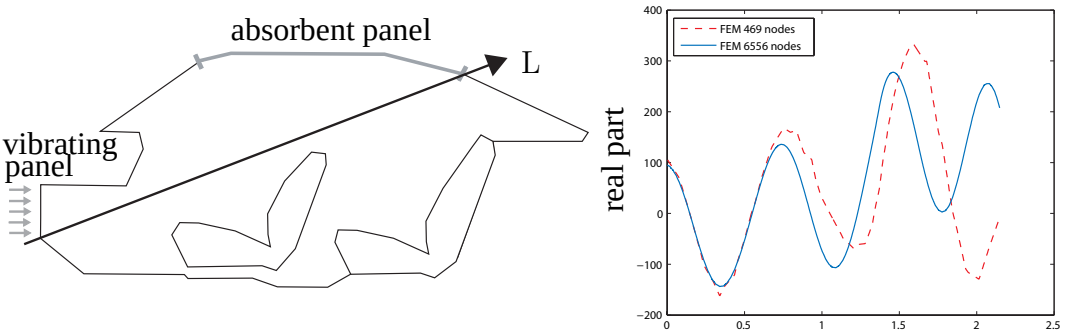

Figure 2.10: Example 3: Description of the two-dimensional section of the cabin of a car and its associated boundary conditions (left) and dispersion effect for the real part of an approximated solution for 525 Hz (right).

scattered solution from submarine obstacle in Steffens et al. (2010*a*)). The sound transmission inside a car cabin is a more complex phenomenon and the solution does not present clear prevalent directions but is a combination of different plane waves with similar amplitudes, see figure 2.11.

Figure 2.12 shows the behavior of the modulus and angle distribution associated to the acoustic pressure inside the car cabin. As can bee seen, its not easy to clearly identify the regions where the angle distribution is discontinuous.

Therefore, in this example we identify the elements near the angle discontinuities or near the regions where the modulus has a non-smooth behavior, and in these problematic elements a polynomial fitting is applied while the exponential fitting is applied only to the non-selected elements. The estimates obtained with this combined approach are denoted in the following by $\widehat{E}^{*}_{\text{exp}}$.

Estimates of the dispersion error for the Galerkin approximations of the solution are computed for two different triangular meshes of 568 and 2122 nodes respectively. The results are shown in table 2.4. As can be seen, both the polynomial and the combined estimates provide fairly good approximations to the reference value E. However, using an exponential representation, where possible, allows obtaining effectivities closer to one.

Figure 2.13 shows the elements that have been selected in the combined approach to apply the polynomial smoothing technique instead of the exponential one. Note that these regions are in good agreement with those highlighted in figure 2.12.

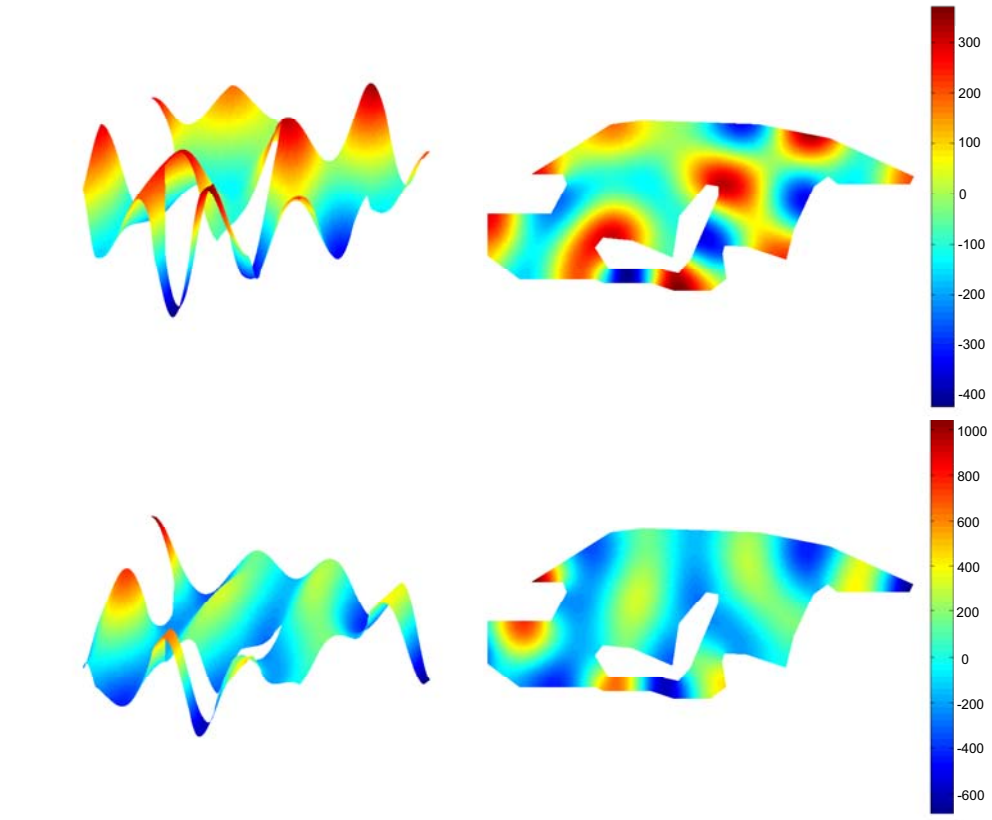

Figure 2.11: Example 3: Solution of the noise transmission problem inside the cabin of a car obtained with an overkill mesh of 20160 nodes: real part of u (top) and imaginary part of u (bottom).

Figure 2.12: Example 3: Modulus (left) and angle (middle and right) distribution of the acoustic pressure inside the car cabin. The areas where the modulus is nearly zero are highlighted in the plot in the middle to see the areas where the angle distribution may present discontinuities.

	Galerkin				
$\mathtt{n}_{\mathrm{np}}$	E	E^*_{pol}	$\widehat{E}^*_{\mathrm{exp}}$	$I^{\mathrm{eff}}_{\mathrm{pol}}$	$I^{\mathrm{eff}}_{\mathrm{exp}}$
568	0.15001	0.08231	0.12960	0.5486	0.8639
1092	0.07506	0.06694	0.07389	0.8918	0.9845

Table 2.4: Example 3: Assessment of the dispersion error of the Galerkin method for unstructured triangular meshes.

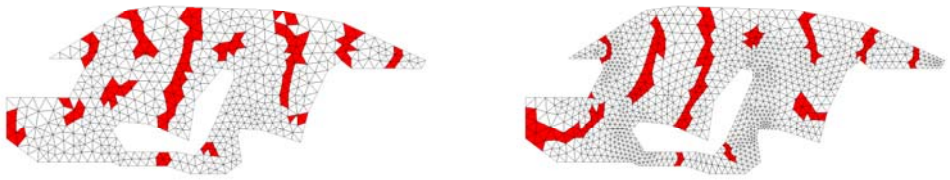

Figure 2.13: Example 3: Two unstructured triangular mesh where the red elements corresponding to solution fitting polynomial.

The reduction in the dispersion error obtained by using stabilization techniques is shown in table 2.5. This table also shows the influence of the selection of the stabilization parameter. As can be seen, the results of the Galerkin least-squares approximations with the three stabilization parameters are nearly identical for the two meshes, and provide significant improvement over the Galerkin method.

2.6 Summary

An error assessment technique for the numerical wave number κ_H of the Helmholtz problem has been proposed, both for standard Galerkin and stabilized formulations.

The proposed strategy requires obtaining an inexpensive approximation of the modified problem, using post-processing techniques. Thus, the associated numerical wave number is readily recovered using a closed expression. The standard poly-

		GLS/FE		
stabilization direction	$\mathtt{n}_{\mathtt{np}}$	E	$I^{\text{eff}}_{\text{pol}}$	$I^{\text{eff}}_{\text{exp}}$
$\theta = 0$	568	0.03792	0.6052	0.9396
	1092	0.00577	1.1304	1.1157
$\theta = \pi/12$	568	0.03808	0.5990	0.9409
	1092	0.00583	1.1279	1.1155
$\theta = \pi/6$	568	0.03824	0.5999	0.9417
	1092	0.00589	1.1255	1.1128

Table 2.5: Example 3: Assessment of the dispersion error of the Galerkin least-squares method for an unstructured triangular mesh. The Galerkin least-squares approximations are shown for different stabilization directions θ.

nomial least squares techniques is replaced by an exponential fitting yielding much sharper results in most applications. However, both the error estimates computed using a polynomial and exponential fitting provide reasonable approximations of the true errors.

Amongst the different possibilities to approximate the wave number, both the correction factor and the second option - which assumes that the stabilization parameter does not vary considerably with respect to numerical wave number - yield fairly good results. The estimates obtained produce similar and sharp approximations to the dispersion error.

The numerical examples demonstrate that the proposed methodology is able to assess the dispersion error for both Galerkin and Galerkin least-squares formulations. The estimates clearly detected that the Galerkin least-squares method considerably reduces the dispersion error.

The sensitivity of the selection of the stabilization parameter for the Galerkin least-squares method has been studied, concluding that the change in the orientation of the stabilization parameter has a significant effect on academic problems. It has, however, little effect in non-academic problems or when considering non-structured meshes.

Chapter 3

Goal-oriented error estimation and *h*-adaptivity

This chapter introduces a new goal-oriented adaptive strategy based on the post-processing techniques introduced in the previous chapter. A simple but very effective post-process of the finite element approximations of the direct and the adjoint problems, see section 1.4.3, allow computing competitive estimates for linear and non-linear quantities of interest. Thus, the error estimation proposed herein would fall into the category of recovery-type explicit *a posteriori* error estimation techniques.

This chapter is a summary of the ideas introduced in (Steffens et al. 2010*b*) and is structured as follows: section 3.1 presents a general framework for assessing the error in general linear and non-linear quantities of interest. Different representations for the linear contribution to the output are introduced in section 3.2. Section 3.3 is devoted to obtain error estimates for general outputs using the different error representations given in section 3.2. The adaptive strategy is introduced in the section 3.4, where local indicators and several strategies of refinement are defined. Finally, in section 3.5 the proposed procedure for goal-oriented adaptivity is analyzed in some numerical examples. The relation between the different error representations and the dispersion error of the direct and adjoint problems is also investigated.

3.1 Error assessment for quantities of interest

Consider a general acoustic problem given in weak form as: find $u \in \mathcal{U}$ such that

$$a(u, v) = \ell(v) \quad \forall v \in \mathcal{V}.$$

and denote by u_H its finite element approximation.

A posteriori error estimation techniques aim at assessing the error committed in the approximation of u, $e = u - u_H$, where $e \in \mathcal{V}$ is the solution of the primal residual problem

$$a(e, v) = \ell(v) - a(u_H, v) = R^P(v) \quad \forall v \in \mathcal{V}, \tag{3.1}$$

$R^P(\cdot)$ standing for the weak residual associated to the finite element approximation u_H.

In acoustic problems, since the Helmholtz equation is not elliptic, the form $||v||^2 = a(v, v)$ does not define a squared norm. Therefore, there is no natural energy norm to measure the error. Additionally, assessing the error measured in some functional norm is not sufficient for many applications. In practice, the finite element user is interested in specific magnitudes extracted from the global solution by some post-process. These magnitudes are referred as quantities of interest or functional outputs. Goal-oriented error assessment strategies aim at estimating the error committed in these quantities and possibly providing bounds for it.

The quantities of interest considered in this work are non-linear functional outputs of the solution, $J(u)$, and the aim is to assess the error committed when approximating these quantities using the finite element approximation. Specifically, the goal is to assess and control the quantity

$$J(u) - J(u_H).$$

For the purposes of this thesis, it is convenient to make the linear, quadratic and higher order terms contributions of $J(u)$ more explicit. To this end, $J(u)$ is expanded introducing the Gateaux first and second derivatives of $J(\cdot)$ at u_H, namely

$$J(u_H + v) = J(u_H) + \ell^{\mathcal{O}}(v) + \mathcal{Q}(v, v) + \mathcal{W}(v), \tag{3.2}$$

where $\ell^{\mathcal{O}}(v) = [D_v J](u_H) \cdot (v)$ and $2\mathcal{Q}(v_1, v_2) = [D_v^2 J](u_H) \cdot (v_1, v_2)$, see (Sarrate et al. 1999, Maday, Patera and Peraire 1999). Note that $\ell^{\mathcal{O}} : \mathcal{H}^1(\Omega) \to \mathbb{C}$ and $\mathcal{Q} : \mathcal{H}^1(\Omega) \times \mathcal{H}^1(\Omega) \to \mathbb{C}$ are the linear and bilinear contributions of $J(\cdot)$, respectively, and that the functional $\mathcal{W}$ contains the higher order terms. In the case of a linear output, notice that $\mathcal{Q} = \mathcal{W} = 0$.

Using this decomposition and taking into account that $u = u_H + e$, the error in the quantity of interest may be rewritten as

$$J(u) - J(u_H) = J(u_H + e) - J(u_H) = \ell^{\mathcal{O}}(e) + \mathcal{Q}(e, e) + \mathcal{W}(e). \tag{3.3}$$

Thus, it is clear that in order to estimate the error in the quantity of interest, it is sufficient to estimate the linear, quadratic and higher-order terms separately, $\ell^{\mathcal{O}}(e)$, $\mathcal{Q}(e, e)$ and $\mathcal{W}(e)$ respectively.

We assume that $\mathcal{Q}$ and $\mathcal{W}$ are L^2-continuous. Thus, for all v, $|\mathcal{Q}(v)| \leq c_1 \|v\|_0^2$ and $|\mathcal{Q}(v)| \leq c_2 \|v\|_0^3$, where $\|\cdot\|_0$ denotes the L^2-norm. Consequently, $\mathcal{Q}(e, e)$ and $\mathcal{W}(e)$, converge as $\mathcal{O}(H^4)$ and $\mathcal{O}(H^6)$ respectively, whereas the linear term $\ell^{\mathcal{O}}(e)$ converges quadratically. Therefore, for sufficiently small H the linear term provides a good inside to the error in the output since the other terms are negligible.

In this work, three different engineering outputs are considered. The first output is the integral of the solution over a subdomain $\Omega^{\mathcal{O}} \subset \Omega$

$$J_1(u) = \int_{\Omega^{\mathcal{O}}} u \, d\Omega.$$

Since the output depends linearly on u, $J_1(v) = \ell_1^{\mathcal{O}}(v)$ and $\mathcal{Q}_1(v, v) = \mathcal{W}_1(v) = 0$ in (3.2). Note that eventually $\Omega^{\mathcal{O}}$ can be Ω to compute an average of the solution over the whole domain.

The second output is the average of the squared modulus of the solution over a boundary strip $\Gamma^{\mathcal{O}} \subset \Gamma_{\mathrm{N}} \cup \Gamma_{\mathrm{R}}$

$$J_2(u) = \frac{1}{l_{\Gamma^{\mathcal{O}}}} \int_{\Gamma^{\mathcal{O}}} u\bar{u} \, d\Gamma,$$

where $l_{\Gamma^{\mathcal{O}}}$ is the length of the boundary strip. Since this output depends quadratically on u, $\mathcal{W}_2(v) = 0$ and the linear and quadratic contributions are

$$\ell_2^{\mathcal{O}}(v) = \frac{1}{l_{\Gamma^{\mathcal{O}}}} \int_{\Gamma^{\mathcal{O}}} (u_H \bar{v} + \bar{u}_H v) \, d\Gamma, \quad \mathcal{Q}_2(v, v) = J_2(v). \tag{3.4}$$

Indeed, appealing to (3.2)

$$\begin{aligned} J_2(u_H+v) &= \frac{1}{l_{\Gamma^{\mathcal{O}}}}\int_{\Gamma^{\mathcal{O}}}(u_H+v)(\overline{u_H+v})\,d\Gamma \\ &= \frac{1}{l_{\Gamma^{\mathcal{O}}}}\int_{\Gamma^{\mathcal{O}}}\left(u_H\bar{u}_H+u_H\overline{v}+v\bar{u}_H+v\overline{v}\right)\,d\Gamma \\ &= J_2(u_H)+\frac{1}{l_{\Gamma^{\mathcal{O}}}}\int_{\Gamma^{\mathcal{O}}}(u_H\bar{v}+\bar{u}_Hv)\,d\Gamma+J_2(v). \end{aligned}$$

The third output is the normalized squared L^2-norm of the solution over a region $\Omega^{\mathcal{O}}$

$$J_3(u)=\frac{1}{A_{\Omega^{\mathcal{O}}}}\int_{\Omega^{\mathcal{O}}}u\bar{u}\,d\Omega,$$

where $A_{\Omega^{\mathcal{O}}}$ stands for the area of the subdomain $\Omega^{\mathcal{O}}$. Again, since the output is quadratic, $\mathcal{W}_3(v)=0$ and

$$\ell_3^{\mathcal{O}}(v)=\frac{1}{A_{\Omega^{\mathcal{O}}}}\int_{\Omega^{\mathcal{O}}}(u_H\bar{v}+\bar{u}_Hv)\,d\Omega,\quad \mathcal{Q}_3(v,v)=J_3(v). \tag{3.5}$$

The derivation is analogous to the one provided for $J_2(\cdot)$ except for the integrals being placed over a subdomain of Ω instead of its boundary.

Note that, the second and third outputs $J_2(u)$ and $J_3(u)$ are real quantities since they only involve the squared modulus of the solution. In particular, all the involved functionals, are real functions of a single complex variable, that is, for instance $\ell_2^{\mathcal{O}}:\mathbb{C}\to\mathbb{R}$.

The following sections are devoted to describe the error assessment techniques to estimate the linear and higher order contributions of $J(u)-J(u_H)$ and to provide local error estimators able to effectively drive the adaptive procedures.

3.2 Error representation of a linearized output

This section presents alternative representations for the linear contribution to the error in the output $\ell^{\mathcal{O}}(e)$. This alternative representations do not directly yield computable expressions for the estimates of the output because they depend on the exact errors on the primal and adjoint problems. However, estimates may be easily recovered using existing strategies providing approximations for the errors, as described in section 3.3.

The quantities of interest considered here are such that their linear part is expressed as

$$\ell^{\mathcal{O}}(v) = \int_{\Omega} f^{\mathcal{O}} v \, d\Omega + \int_{\Gamma_{\mathrm{N}}} g^{\mathcal{O}} v \, d\Gamma, \tag{3.6}$$

where $f^{\mathcal{O}}$ and $g^{\mathcal{O}}$ are given functions characterizing the linearized quantity of interest. Note that $\ell^{\mathcal{O}}(v)$ has the same structure as $\ell(v)$, see equation (1.9), excepting the conjugate in its argument. Thus, $\ell^{\mathcal{O}}$ is a linear functional while ℓ is an antilinear functional.

Most existing techniques to estimate the error in a quantity of interest introduce an alternative representation for $\ell^{\mathcal{O}}(e)$. In practice, different error representations are used to properly estimate $\ell^{\mathcal{O}}(e)$. These error representations require introducing an auxiliary problem, denoted as *adjoint* or *dual* problem which reads: find $\psi \in \mathcal{V}$ such that

$$a(v, \psi) = \ell^{\mathcal{O}}(v) \quad \forall v \in \mathcal{V}, \tag{3.7}$$

which is equivalent to determine the adjoint solution ψ verifying the Helmholtz problem

$$-\Delta\psi - \kappa^2\psi = \bar{f}^{\mathcal{O}} \qquad \text{in}\Omega, \tag{3.8a}$$

$$\psi = 0 \qquad \text{on } \Gamma_{\mathrm{D}}, \tag{3.8b}$$

$$\boldsymbol{\nabla}\psi \cdot \mathbf{n} = \bar{g}^{\mathcal{O}} \qquad \text{on } \Gamma_{\mathrm{N}}, \tag{3.8c}$$

$$\boldsymbol{\nabla}\psi \cdot \mathbf{n} = \overline{m}\psi \qquad \text{on } \Gamma_{\mathrm{R}}. \tag{3.8d}$$

In order to assess the error in the quantity of interest the adjoint solution ψ is approximated numerically by $\psi_H \in \mathcal{V}_H$ such that

$$a(v, \psi_H) = \ell^{\mathcal{O}}(v) \quad \forall v \in \mathcal{V}_H,$$

introducing the adjoint error $\varepsilon = \psi - \psi_H$ solution of the adjoint residual problem

$$a(v, \varepsilon) = \ell^{\mathcal{O}}(v) - a(v, \psi_H) = R^D(v) \quad \forall v \in \mathcal{V}_H, \tag{3.9}$$

where $R^D(\cdot)$ is the weak adjoint residual associated with ψ_H.

The adjoint problem is introduced such that the following error representation holds:

$$\ell^{\mathcal{O}}(e) = a(e, \psi) = a(e, \varepsilon)$$

where the Galerkin orthogonality of the adjoint approximation ψ_H is used in the last equality. In turn, this error representation allows assessing the error in terms of the residuals of the direct and adjoint problems, namely

$$\ell^{\mathcal{O}}(e) = a(e,\varepsilon) = R^P(\varepsilon) = R^D(e). \tag{3.10}$$

These representations are obtained substituting $v = \varepsilon$ in (3.1) and $v = e$ in (3.9) respectively.

It is worth noting that for general non-linear quantity of interest $J(u)$, its first Gateux derivative which provides the functional $\ell^{\mathcal{O}}(v)$ is not necessarily of the form of (3.6). Indeed, a close look on the linear contributions to the quantities $J_2(v)$ and $J_3(v)$ given in the previous section, equations (3.4) and (3.5), reveals that even for simple outputs $\ell^{\mathcal{O}}(v)$ can not be written as in (3.6).

The proposed strategy is valid for general functionals $\ell^{\mathcal{O}}(v)$. However, if the functional $\ell^{\mathcal{O}}(v)$ is not in the form of (3.6), the adjoint problem is no longer the solution of the strong Helmholtz problem given in (3.8). Depending on the form of $\ell^{\mathcal{O}}(v)$, r.h.s. of equation (3.7), the adjoint problem might have no physical meaning. In many practical applications a simple workaround to overcome this limitation cause adopted.

To be specific, consider the quantity of interest $J_2(u)$ with the associated linear contribution

$$\ell_2^{\mathcal{O}}(v) = \frac{1}{l_{\Gamma^{\mathcal{O}}}} \int_{\Gamma^{\mathcal{O}}} (u_H \bar{v} + \bar{u}_H v)\, d\Gamma, \quad \mathcal{Q}_2(v,v) = J_2(v).$$

Note that, $\ell_2^{\mathcal{O}}(v)$ is a real number coinciding with

$$\ell_2^{\mathcal{O}}(v) = 2\Re\mathrm{e}\left(\frac{1}{l_{\Gamma^{\mathcal{O}}}} \int_{\Gamma^{\mathcal{O}}} \bar{u}_H v\, d\Gamma\right).$$

The adjoint problem is then defined with respect to the auxiliary linear functional $\int_{\Gamma^{\mathcal{O}}} \bar{u}_H v\, d\Gamma / l_{\Gamma^{\mathcal{O}}}$ which corresponds to $f^{\mathcal{O}} = 0$ and zero elsewhere and $g^{\mathcal{O}} = \bar{u}_H / l_{\Gamma^{\mathcal{O}}}$ on $\Gamma^{\mathcal{O}} \cap \Gamma_{\mathrm{N}}$ and zero elsewhere in equation (3.6). The original linear functional and all the required estimates are recovered from this auxiliary functional taking the real part and multiplying by a factor two.

The same approach is used for $\ell_3^{\mathcal{O}}(v)$. Recall that

$$\ell_3^{\mathcal{O}}(v) = \frac{1}{A_{\Omega^{\mathcal{O}}}} \int_{\Omega^{\mathcal{O}}} (u_H \bar{v} + \bar{u}_H v)\, d\Omega, \quad \mathcal{Q}_3(v,v) = J_3(v).$$

Then, the adjoint problem is defined with respect to the modified functional $\int_{\Omega^{\mathcal{O}}} \bar{u}_H v \, d\Omega / A_{\Omega^{\mathcal{O}}}$, for which the data entering in (3.6) are $g^{\mathcal{O}} = 0$ and $f^{\mathcal{O}} = \bar{u}_H / A_{\Omega^{\mathcal{O}}}$ in $\Omega^{\mathcal{O}}$ and $f^{\mathcal{O}} = 0$ elsewhere.

3.3 Error estimates for linear and non-linear outputs

A posteriori assessment of quantities of interest relies on obtaining a good approximation of $J(u) - J(u_H)$. This translates in finding a new enhanced solution u^*, based on the information at hand, that is u_H, and such that u^* approximates the actual solution u much better than u_H. Thus, a computable error estimate is readily obtained

$$e \approx e^* = u^* - u_H$$

yielding also the corresponding estimate for the quantity of interest

$$J(u) - J(u_H) \approx \ell^{\mathcal{O}}(e^*) + \mathcal{Q}(e^*, e^*) + \mathcal{W}(e^*). \tag{3.11}$$

This approximation of the error in the quantity of interest is obtained from equation (3.3) substituting the actual error e by its approximation e^*.

The key issue in any error estimation technique is to produce a properly enhanced solution u^*, or in some cases obtaining an enhanced approximation of the gradient of the solution $q^* \approx \nabla u$ suffices. The strategies producing the enhanced solution u^*, or q^* respectively, are classified into two categories: recovery type estimators and implicit residual type estimators. Recovery techniques, based on the ideas of Zienkiewicz and Zhu (Zienkiewicz and Zhu 1987, Zienkiewicz and Zhu 1992*a*, Díez, Rodenas and Zienkiewicz 2007), are often preferred by practitioners because they are robust and simple to use. On the other hand, *a posteriori* implicit residual-type estimators have a sounder mathematical basis and produce estimates that are upper or lower bounds of the error (Ainsworth and Oden 2000, Ladevèze and Leguillon 1983, Díez, Parés and Huerta 2003, Parés et al. 2006).

At first glance on could think that, once the enhanced solutions u^* are obtained either using recovery or residual-type error estimators, estimates for the error in the quantity of interest may be directly obtained using equation (3.11). However, as mentioned in section 3.2, this representation does not provide sound results. This

is because inserting the enhanced error e^* in the functionals $\ell^{\mathcal{O}}(\cdot)$, $\mathcal{Q}(\cdot,\cdot)$ and $\mathcal{W}(\cdot)$ may not yield accurate results even when the enhanced approximation u^* provides a reasonable approximation of u in terms of energy. In practice, since the most-contributing term to the error in the quantity of interest is the linear term, alternative representations are used for this term, as the ones described in section 3.2, whereas no additional effort is done in the higher-order terms.

The linear term $\ell^{\mathcal{O}}(e)$ may be assessed by any of the following strategies:

1. Compute the primal enhanced solution u^* to obtain $e^* = u^* - u_H$ and evaluate $\ell^{\mathcal{O}}(e^*)$ (not used in practice).

2. Compute the primal enhanced solution u^* to obtain e^* and evaluate $R^D(e^*)$.

3. Compute the adjoint enhanced solution ψ^* to obtain $\varepsilon^* = \psi^* - \psi_H$ and evaluate $R^P(\varepsilon^*)$.

4. Compute both the primal and enhanced errors e^* and ε^* and evaluate $a(e^*, \varepsilon^*)$.

Here, the postprocessing strategies presented in section 2.4 are used to recover the enhanced solutions u^* and ψ^* from u_H and ψ_H respectively. Thus, $u^* \in \mathcal{U}_h$ and $\psi^* \in \mathcal{V}_h$, where $\mathcal{U}_h$ and $\mathcal{V}_h$ are the discrete functional spaces associated to the finer reference mesh, $\mathcal{U}_H \subset \mathcal{U}_h \subset \mathcal{U}$ and $\mathcal{V}_H \subset \mathcal{V}_h \subset \mathcal{V}$.

As mentioned before, for sufficiently refined meshes, the error in the quantity of interest is controlled by the linear term, since the quadratic and higher-order contributions converge faster to zero. For this, the proposed approach is to make use of the available estimate e^* to obtain a simple and inexpensive estimate of the non-linear contributions. Namely, the quadratic and higher-order contributions to the error in the output, $\mathcal{Q}(e,e)$ and $\mathcal{W}(e)$ respectively, are assessed using the reconstruction of the primal error e^* used to assess the linear part of the error, namely

$$\mathcal{Q}(e,e) \approx \mathcal{Q}(e^*,e^*) \quad \text{and} \quad \mathcal{W}(e) \approx \mathcal{W}(e^*).$$

3.4 Local indicators and adaptivity criteria

Adaptive mesh refinement is nowadays an essential tool to obtain high-fidelity simulations at the lesser cost. The main ingredients of the proposed adaptive procedure

are: the *h-refinement*, that is, the new meshes are obtained by subdividing the elements of the mesh; *optimal indicators*, the refinement is organized with the aim of achieving equal error in each element of new mesh; *iterative process*, the target in each step of refinement is to reduce the global error until the calculated error drops below the tolerance specified by the user. Figure 3.1 displays the flow diagram of an adaptive procedure.

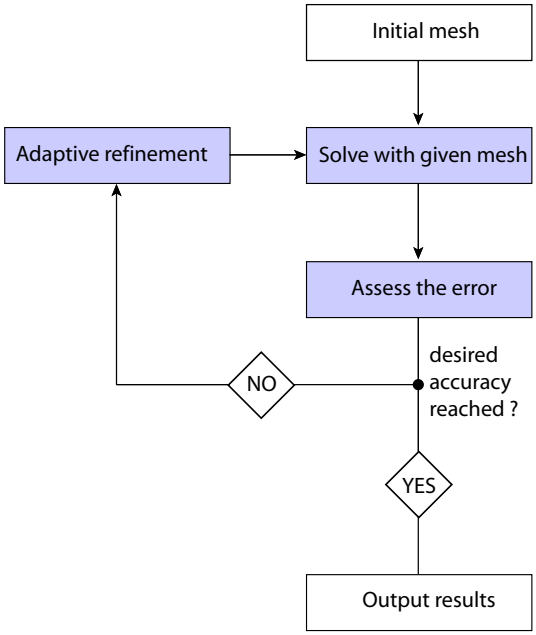

Figure 3.1: Flow diagram of an adaptive algorithm

The adaptive procedure requires obtaining local error indicators allowing to decide the elements to be marked for refinement – those with larger contribution to the total error. In order to determine the contribution of every element to the total error spatial error distributions of the estimates are derived decomposing the global estimates into a sum of local contributions in each element of the mesh induced by $\mathcal{U}_H$.

The estimates for the error in the quantity of interest are of the form

$$J(u) - J(u_H) \approx \ell^{\mathcal{O}}(e^*) + \mathcal{Q}(e^*, e^*) + \mathcal{W}(e^*),$$

where the linear term $\ell^{\mathcal{O}}(e^*)$ is replaced by either $a(e^*, \varepsilon^*)$, $R^P(\varepsilon^*)$ or $R^D(e^*)$, depending on the selected representation of the linear term. Since the linear term

is the driving term of the error in the quantity of interest, in this work, the adaptive procedure is chosen to be driven by $\ell^{\mathcal{O}}(e^*)$. That is, the global estimate for the linear term $\ell^{\mathcal{O}}(e)$ is decomposed into a sum of local contributions in each element. These local quantities are used to design the adaptive procedure.

The natural restriction to every element Ω_k of the integral forms $a(\cdot,\cdot)$, $\ell(\cdot)$ and $\ell^{\mathcal{O}}(\cdot)$ yield the elementary contributions denoted by $a_k(\cdot,\cdot)$, $\ell_k(\cdot)$ and $\ell_k^{\mathcal{O}}(\cdot)$ such that

$$a(u,v)=\sum_{k=1}^{\mathrm{n_{el}}} a_k(u,v),\quad \ell(v)=\sum_{k=1}^{\mathrm{n_{el}}} \ell_k(v),\quad \ell^{\mathcal{O}}(v)=\sum_{k=1}^{\mathrm{n_{el}}} \ell_k^{\mathcal{O}}(v).$$

Similarly, the primal and adjoint residuals are decomposed as

$$R^P(v)=\sum_{k=1}^{\mathrm{n_{el}}} R_k^P(v),\qquad R^D(v)=\sum_{k=1}^{\mathrm{n_{el}}} R_k^D(v),$$

where $R_k^P(\cdot)=\ell_k(\cdot)-a_k(u_H,\cdot)$ and $R_k^D(\cdot)=\ell_k^{\mathcal{O}}(\cdot)-a_k(\cdot,\psi_H)$.

Hence, the error representations for the linear contribution of the error in the quantity of interest given in equation (3.10) are associated to the elementary error distributions

$$\ell^{\mathcal{O}}(e)=\sum_{k=1}^{\mathrm{n_{el}}} \ell_k^{\mathcal{O}}(e)=\sum_{k=1}^{\mathrm{n_{el}}} a_k(e,\varepsilon)=\sum_{k=1}^{\mathrm{n_{el}}} R_k^P(\varepsilon)=\sum_{k=1}^{\mathrm{n_{el}}} R_k^D(e).$$

It is worth mentioning that, while the global error quantities are equal in all the representations, the local quantities $\ell_k^{\mathcal{O}}(e)$, $a_k(e,\varepsilon)$, $R_k^P(\varepsilon)$ and $R_k^D(e)$ represent different elementary contributions to the error and, besides, they are not necessarily positive nor even real numbers.

From the four possible representations of the linear contribution of the error $\ell^{\mathcal{O}}(e)$, in this work only the two expressions involving the primal and adjoint residuals are used, thus yielding the global estimates

$$\eta^{\varepsilon}=R^P(\varepsilon^*)\quad\text{and}\quad \eta^{e}=R^D(e^*),$$

and its associated local error indicators $\eta_k^{\varepsilon}=R_k^P(\varepsilon^*)$ and $\eta_k^{e}=R_k^D(e^*)$, such that

$$\eta^{\varepsilon}=\sum_{k=1}^{\mathrm{n_{el}}}\eta_k^{\varepsilon}\quad\text{and}\quad \eta^{e}=\sum_{k=1}^{\mathrm{n_{el}}}\eta_k^{e}.$$

It is worth noting that the local elemental contributions η_k^ε and η_k^e are the natural decomposition of the estimates η^ε and η^e to the elements. However, the computation of the local contributions η_k^ε and η_k^e requires the computation of local integral forms. This can be done either by storing the elemental contributions to the system matrices and vectors or by recomputing these contributions in an elementary loop. A cheaper and more natural to implement alternative is to decompose the estimates η^ε and η^e into nodal contributions. This is because it uses the finite element nature of the estimates η^ε and η^e.

In practice, the estimates e^* and ε^* are computed in a finer reference mesh associated with the space $\mathcal{V}_h$, namely $e^* = \sum_j e_j^* N^{h,j}$ and $\varepsilon^* = \sum_j \varepsilon_j^* N^{h,j}$, where $N^{h,j}$ are the shape functions associated with the nodes of the reference mesh, $\mathbf{x}^{h,j}$. Thus, a natural decomposition of the estimates η^ε and η^e into nodal contributions on the reference mesh holds

$$\eta^\varepsilon = \sum_j \varepsilon_j^* R^P(N^{h,j}) = \sum_j \eta^\varepsilon_{\mathbf{x}^{h,j}} \quad \text{and} \quad \eta^e = \sum_j e_j^* R^D(N^{h,j}) = \sum_j \eta^e_{\mathbf{x}^{h,j}}.$$

Note that $\eta^\varepsilon_{\mathbf{x}^{h,j}}$ and $\eta^e_{\mathbf{x}^{h,j}}$ are readily computed multiplying the j-th components of the finite element vectors associated to ε^* and $R^P(\cdot)$ and e^* and $R^D(\cdot)$ respectively. Then, the local elemental contributions associated to the element Ω_k of the coarse mesh are computed from a weighted average of the local nodal contributions $\eta^\varepsilon_{\mathbf{x}^{h,j}}$ and $\eta^e_{\mathbf{x}^{h,j}}$ associated to the nodes $\mathbf{x}^{h,j}$ belonging to Ω_k. To be specific

$$\eta^\varepsilon = \sum_j \eta^\varepsilon_{\mathbf{x}^{h,j}} = \sum_{k=1}^{\mathrm{n_{el}}} \sum_{\mathbf{x}^{h,j}\in\Omega_k} \sigma^{h,j} \eta^\varepsilon_{\mathbf{x}^{h,j}} = \sum_{k=1}^{\mathrm{n_{el}}} \hat{\eta}_k^\varepsilon, \tag{3.12}$$

and

$$\eta^e = \sum_j \eta^e_{\mathbf{x}^{h,j}} = \sum_{k=1}^{\mathrm{n_{el}}} \sum_{\mathbf{x}^{h,j}\in\Omega_k} \sigma^{h,j} \eta^e_{\mathbf{x}^{h,j}} = \sum_{k=1}^{\mathrm{n_{el}}} \hat{\eta}_k^e, \tag{3.13}$$

where $\sigma^{h,j}$ is the inverse of the number of elements in the coarse mesh to which a particular node $\mathbf{x}^{h,j}$ belongs. For a detailed description, see (Díez and Calderón 2007*b*).

A simple adaptive strategy is employed, using the local indicators η_k^ε or η_k^e (or $\hat{\eta}_k^\varepsilon$ and $\hat{\eta}_k^e$ respectively) produced during the calculation of the estimate for the output, to drive the non-linear output to a prescribed precision. That is, the algorithm ends

if

$$\sum_{k=1}^{\mathrm{n_{el}}} \eta_k^{\circledast} + \mathcal{Q}(e^*, e^*) + \mathcal{W}(e^*) < \Delta_{tol},$$

where $\eta_k^{\circledast}$ stands for any of the following local contributions η_k^{ε}, η_k^{e}, $\hat{\eta}_k^{\varepsilon}$ or $\hat{\eta}_k^{e}$, Δ_{tol} is a user-prescribed desired final accuracy. At each level of refinement, the elements marked for refinement are those with larger values of the local linear contribution $\eta_k^{\circledast}$.

In acoustic problems, the local contributions are not necessarily positive and in fact, in contrast to what occurs in thermal or elasticity problems, they can be complex numbers. To select the elements with larger local contributions, the modulus of the values $\eta_k^{\circledast}$ is considered, and the elements selected to be refined are the ones verifying

$$|\eta_k^{\circledast}| \geq \frac{\sum_{k=1}^{\mathrm{n_{el}}} |\eta_k^{\circledast}|}{\mathrm{n_{el}}}. \tag{3.14}$$

Note that this marking algorithm aims at obtaining elements with equal local error contribution. However, this is not equivalent to obtaining a uniform spatial error distribution, since the elements with larger area are penalized. In order to obtain a uniform spatial error distribution, the local contributions are weighted by the element area yielding the following marking criterion: the elements to be subdivided are the ones verifying

$$\frac{|\eta_k^{\circledast}|}{\mathrm{A}_k} \geq \frac{\sum_{k=1}^{\mathrm{n_{el}}} |\eta_k^{\circledast}|}{\mathrm{A}_\Omega}, \tag{3.15}$$

where A_k is the area of the element Ω_k and A_Ω is the area of the whole domain Ω. Note that expressions (3.14) and (3.15) are equivalent in uniform meshes where all the elements have the same area since in this case $\mathrm{A}_k = \mathrm{A}_\Omega/\mathrm{n_{el}}$ is constant.

Other alternative of remeshing criterions can be implemented to refine the elements at each step of the adaptive refinement algorithm. In (Steffens et al. 2010*b*), the two previous strategies are compared with the following alternatives:

- at each step, a fix percentage of the elements are refined, those with larger contributions $|\eta_k^{\circledast}|$ or to $|\eta_k^{\circledast}|/A_k$.

- the smallest number of elements such that the sum of the contributions $|\eta_k^{\circledast}|$

toward the global error $\sum_{k=1}^{\mathrm{n_{el}}}|\eta_k^{\circledast}|$ from these elements exceeds a fix percentage of the value.

- all elements on which the local error estimate $|\eta_k^{\circledast}|$ exceeds a fixed percentage of the largest local error estimate are refined at each step.

3.5 Numerical examples

The performance of the goal-oriented estimates and error indicators described above is illustrated in two numerical examples. Additional results can be found in Steffens et al. (2010*b*) the following acoustic problems: noise transmission in an expansion chamber and in a cabin car cavity.

In the examples, when reporting the numerical results, $\eta^{\varepsilon}_{\text{pol}} = R^P(\varepsilon^*_{\text{pol}})$, $\eta^{\varepsilon}_{\text{exp}} = R^P(\varepsilon^*_{\text{exp}})$, $\eta^{e}_{\text{pol}} = R^D(e^*_{\text{pol}})$ and $\eta^{e}_{\text{exp}} = R^D(e^*_{\text{exp}})$ denote the estimates of the linear contribution to the error in the quantity of interest $\eta = \ell^{\mathcal{O}}(e)$ obtained by using the post-processing strategy described in section. Recall that the subindeces exp and pol indicate the polynomial and exponential fitting, respectively.

In order to see how well the estimators perform, the value of the true error $J(u) - J(u_H)$ or $\ell^{\mathcal{O}}(e)$ are required, but the analytical solutions of the considered problems are not available. An accurate value for the true error is obtained by making use of a sufficiently accurate approximation u_h of u in a finer reference mesh, that is, the estimates are compared with the reference values $J(u_h) - J(u_H)$ and $\eta_h = \ell^{\mathcal{O}}(e_h)$ respectively. Note that this reference value can also be recovered from a faithful representation of the adjoint problem ψ_h since $\eta_h = \ell^{\mathcal{O}}(e_h) = R^P(\psi_h) = R^P(\varepsilon_h)$.

In the examples, the approximations u^* and ψ^* used to recover the estimates of the errors $e^* = u^* - u_H$ and $\varepsilon^* = \psi^* - \psi_H$ and its corresponding estimates for the output $\eta^e = R^D(e^*)$ and $\eta^{\varepsilon} = R^P(\varepsilon^*)$, are also computed using the same reference mesh. Noting that $\eta_h = R^D(e_h) = R^P(\varepsilon_h)$ reveals that the quality of the estimates depends on the quality of the approximations $e^* \approx e_h$ and $\varepsilon^* \approx \varepsilon_h$.

The accuracy of the approximations is closely related to the pollution or dispersion error. Since the approximations u^* and ψ^* are constructed using a constrained least-squares technique, the estimates for the error e^* and ε^* vanish at the nodes of

the coarse mesh, yielding crude approximations if the solutions presents large dispersion errors. The influence of the dispersion error in the estimates for the quantity of interest is analyzed using the estimates for the dispersion error introduced in chapter 2. These estimates are denoted by E^e and E^ε for the primal and adjoint problems respectively.

3.5.1 Scattering from a obstacle in a square domain

The first example is the scattering of a plane wave by a rigid obstacle introduced in (Sarrate et al. 1999). The incident wave travels in the negative y-direction inside a square domain which contains a rigid body, see figure 3.2.

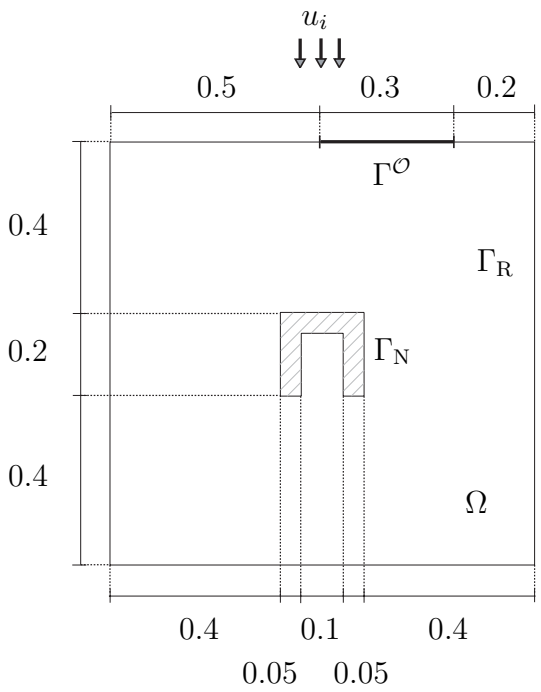

Figure 3.2: Example 1: Description of the geometry and boundary conditions for the plane wave scattering by a rigid body.

Recall that the solution of the scattering problem is composed of a prescribed incident wave and a reflected wave, namely $u = u_{\mathrm{r}} + u_{\mathrm{i}}$. The incident wave is characterized by its wave number $\kappa = \pi$ and the angle of incidence $\alpha = \pi/2$. To reproduce the scattering nature of the problem, no essential boundary conditions are imposed and it is assumed that there are no sources in the domain and that the rigid

obstacle is perfectly reflecting, that is, $\boldsymbol{\nabla} u_{\mathrm{r}} \cdot \mathbf{n} = -\boldsymbol{\nabla} u_{\mathrm{i}} \cdot \mathbf{n}$ on Γ_{N}. On the exterior boundary, Robin absorbing boundary conditions are applied. Thus, the reflected wave u_{r} is the solution of the Helmholtz equation for $f = 0$ and where the data are $g = -\boldsymbol{\nabla} u_{\mathrm{i}} \cdot \mathbf{n}$ and $m = -i\kappa$.

For this problem, the quantity of interest is the average of the reflected solution over the whole domain, that is $J_1(u_{\mathrm{r}})$ for $\Omega^{\mathcal{O}} = \Omega$, which is a linear quantity of interest. The behavior of the estimates for this quantity is first analyzed for a uniform mesh refinement in a series of unstructured triangular meshes. Three triangular meshes are considered, starting from an initial mesh of 636 nodes and obtaining the subsequent meshes by refining each triangle into four new ones.

The finite element approximations for both the primal and adjoint solutions, computed at the final mesh of the uniform refinement procedure of 9825 nodes, are shown in figure 3.3.

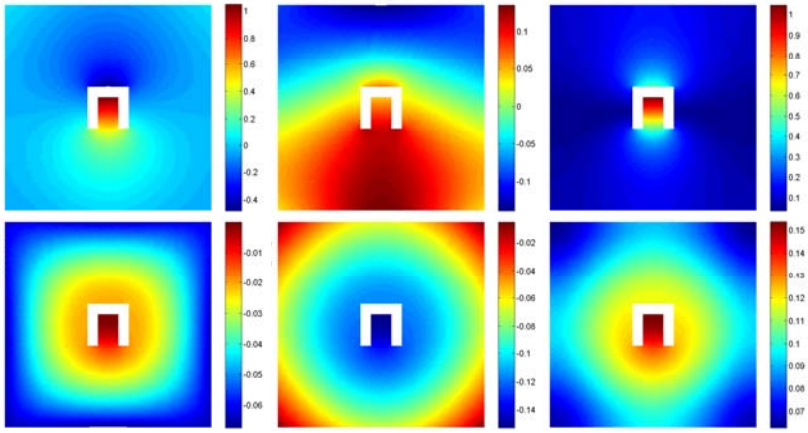

Figure 3.3: Example 1: Real part, imaginary part and modulus of the primal solution (top) and of the adjoint solution (bottom) associated to the quantity of interest $J_1(u_{\mathrm{r}})$, for $\kappa = \pi$ computed using the Galerkin method and a mesh of 9852 nodes.

Figure 3.4 shows the local elementary contributions to the error in the quantity of interest for the initial mesh of 636 nodes. Both the local contributions of the reference values η_h^{ε} and η_h^{e} and its estimates computed using the representations given by equations (3.12) and (3.13) are shown. The estimates are obtained using the polynomial and the exponential fitting. Note that even though the global error

quantities η_h^ε and η_h^e are equal, they represent different elementary contributions to the error. The spatial distribution of the estimates is in good agreement with the reference ones: they properly detect the elements with larger contributions to the error even though the obtained elemental contributions underestimate its reference value.

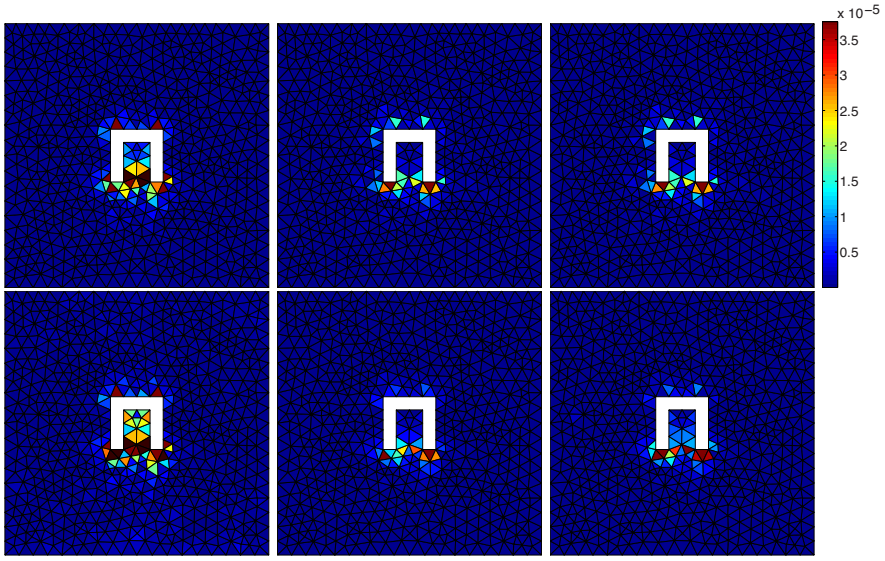

Figure 3.4: Example 1: Local maps of the error in the linear quantity of interest $J_1(u_\mathrm{r})$. The distributions on the top are obtained using the representation η^ε, that is, η_h^ε (left), $\eta_{\mathrm{pol}}^\varepsilon$ (middle) and $\eta_{\mathrm{exp}}^\varepsilon$ (right) are shown. The distributions on the bottom correspond to η^e, that is, η_h^e (left), η_{pol}^e (middle) and η_{exp}^e (right) are shown.

The convergence of the estimates is shown in figure 3.5. Two refinement strategies are implemented: first, the meshes are uniformly refined whereby each triangle is subdivided into four subtriangles at each step and second, the meshes are adaptively refined using the criterion given in equation (3.15).

The singular nature of the solution yields an order of convergence for the uniform mesh refinement of $\mathcal{O}(H^{4/3})$ for the quantity of interest, which is equivalent to $\mathcal{O}((\mathtt{n}_{\mathrm{np}})^{2/3})$ where $\mathtt{n}_{\mathrm{np}}$ denotes the number of nodes of the mesh, instead of the standard convergence rate of $\mathcal{O}(H^4)$ obtained for regular solutions. As expected, the use of an adaptive refinement strategy leads to a faster reduction of the error in the quantity of interest than if a uniform refinement is used.

It can be seen that, in this example, all the estimates provide similar results

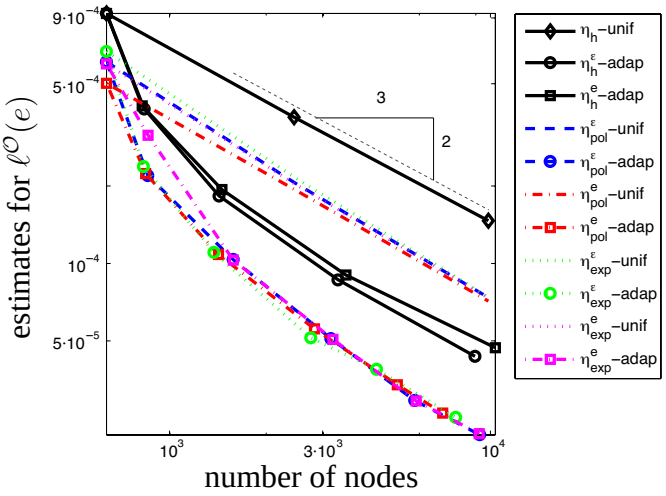

Figure 3.5: Example 1: Performance of the estimators for the error in the quantity of interest $J_1(u_\mathrm{r})$ with a uniform and an adaptive refinement strategies. The estimates are compared with the reference values.

providing an underestimation of the reference values. For comparison, the adaptive algorithm guided by the reference errors η_h^e and η_h^ε are also run. Comparing the convergence curves obtained for these two local indicators and the ones produced by the estimates, it can be seen that the estimates perform optimally since they lead to even slightly better convergence ratios than the reference errors.

The first and final adapted meshes produced by the local indicator associated to $\eta_{\mathrm{exp}}^{\varepsilon} = R^P(\varepsilon_{\mathrm{exp}}^*)$ subdividing at each remeshing step the elements satisfying the criterion given by equation (3.15) are shown in figure 3.6, along with a intermediate mesh of the adaptive procedure. The meshes obtained using the other local error indicators are virtually identical and are therefore not shown.

Since the quantity of interest is the non-weighted average of the solution over the whole domain, the meshes are refined in the areas where the primal solution presents larger errors, that is, at the neighborhood of the obstacle where the singularities occur.

Additional results for this example can be found in Steffens et al. (2010*b*) including the influence of the dispersion error in the estimates for the quantities of interest and the behavior of the estimates for the non-linear quantity of interest $J_2(u_\mathrm{r})$, that is, the average of the squared modulus of the reflected solution over the

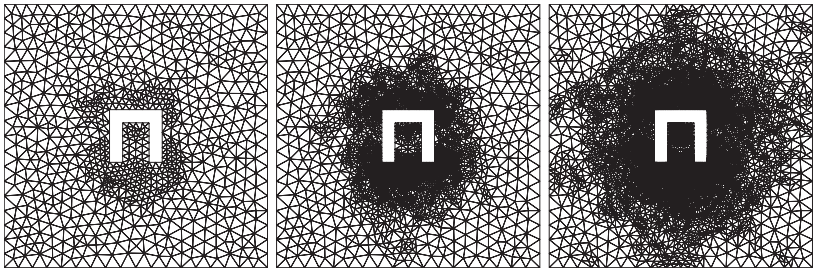

Figure 3.6: Example 1: First, intermediate and final adapted meshes obtained using the local error indicators provided by the estimate $\eta^{\varepsilon}_{\text{exp}}$ with 857, 3229 and 13852 nodes respectively, for the quantity of interest $J_1(u_{\text{r}})$.

boundary strip $\Gamma^{\mathcal{O}}$ depicted in figure 3.2.

3.5.2 Radar wave problem

This example involves the scattering from an acoustically hard obstacle. In this case the obstacle is composed of three ellipses, see figure 3.7. Two different computational domain containing the ellipses are considered: rectangular domain of dimensions 30×20 and a circular domain with radius $\text{r} = 25$.

This problem was developed as a benchmark problem for the *Industrial and Academic Database Workshop* held in Finland in March 2010. In particular, the rectangular geometry was develop to study the inverse problem of recovering a target pressure on the surface of the two small ellipses. The objective of the inverse problems was to recover the position of the small ellipses. Although the original goal was to study the full inverse problem, the performance of different methods was also studied for smaller involved subproblems. In particular, interest was placed in studying the behavior of adaptive algorithms for the computation of the acoustic field either in global norms or in specific quantities of interest.

Here, this benchmark test is used to analyze the proposed adaptive refinement strategy. Although the most relevant quantity of interest for this problem is the scattering cross section, here an initial not-so-ambitious goal has been considered: obtaining the average of squared modulus of the scattered solution on $\Gamma^{\mathcal{O}}$ and $\Omega^{\mathcal{O}}$ respectively. For a proper definition of the problem see: *http://jucri.jyu.fi/?q=testcase/5*.

Consider the scattering problem of computing the reflected wave u_{r} solution of

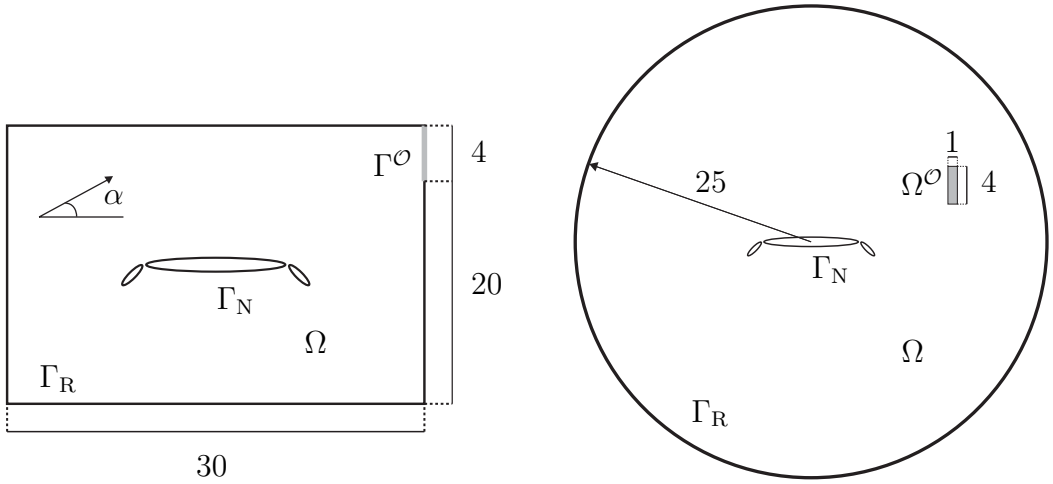

Figure 3.7: Example 2: Description of the geometry and boundary conditions for the plane wave scattering by tree rigid ellipses where the exterior boundary is described by a rectangular form (left) and a circular one (right).

the Helmholtz equation with $f = 0$. Neumman boundary conditions are applied on the boundary of the obstacle, $\boldsymbol{\nabla} u_{\mathrm{r}} \cdot \mathbf{n} = -\boldsymbol{\nabla} u_{\mathrm{i}} \cdot \mathbf{n}$, and first order Bayliss-Gunzberger-Turkel (BGT) non-reflecting boundary conditions are applied to the fictitious boundary

$$\boldsymbol{\nabla} u_{\mathrm{r}} \cdot \mathbf{n} = m u_{\mathrm{r}} = -i\kappa u_{\mathrm{r}} + \frac{\zeta}{2} u_{\mathrm{r}}, \tag{3.16}$$

where ζ is the curvature of the surface of the scatterer. For the case of a rectangular exterior boundary $\zeta = 0$, and equation (3.16) reduces to a standard Robin condition, which is equivalent to a zero-order BGT-0 condition. It is known that a BGT-0 boundary is not very accurate in practical implementations (Ihlenburg 1998). For the circular exterior boundary of radius r, the curvature is given by $\zeta = 1/\mathrm{r}$. Thus, the circular domain approximation is expected to yield smaller errors due to the approximation of the boundary conditions.

As mentioned before, the simplified problem of predicting the noise (an eventually reducing it) in a specific area of the domain is considered. For this, the aim is placed in measuring the modulus of the reflected solution. Specifically, for the example with the rectangular boundary, the output of interest is the average of the squared modulus of the solution over the boundary strip $\Gamma^{\mathcal{O}}$ shown on the left of the figure 3.7, namely $J_2(u_{\mathrm{r}})$. For the example with circular boundary, the quantity of interest is the normalized L^2-norm of the squared modulus of the solution over

the subdomain $\Omega^{\mathcal{O}}$ shown on the right of the figure 3.7, namely $J_3(u_{\rm r})$. Note that, for simplicity of computation in the circular region, instead of considering a strip inside the domain, a subdomain $\Omega^{\mathcal{O}}$ is used. In this case, $\Omega^{\mathcal{O}}$ is obtained from $\Gamma^{\mathcal{O}}$ by expanding the strip to a width of $1m$.

Figures 3.8 and 3.9 show the Galerkin approximations of the primal and adjoint problems both for the rectangular and circular geometries for two wave numbers $\kappa = \pi/4$ and $\kappa = \pi$, respectively. As expected, both approximations provide similar results for the acoustic field surrounding the obstacles.

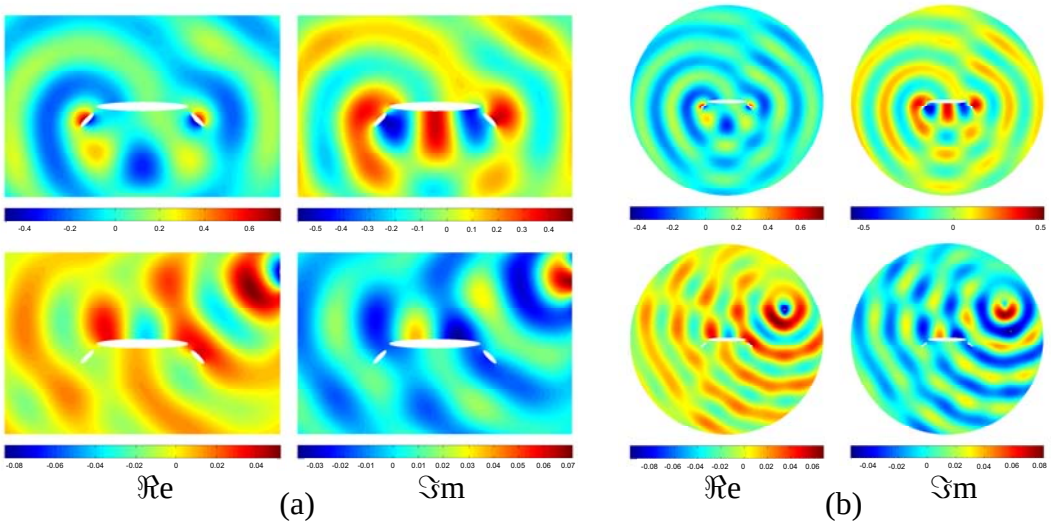

Figure 3.8: Example 2: Galerkin finite element approximation of the primal problem (top) and of the adjoint solution (bottom) for the waver number $\kappa = \pi/4$ and for the meshes of 16212 and 26584 nodes, corresponding to the problems with rectangular (a) and circular (b) exterior boundaries, respectively.

First, the error in the linear contribution $\ell_3^{\mathcal{O}}(u_{\rm r})$ is analyzed for a uniform mesh refinement in a series of unstructured meshes for both wave numbers. Table 3.1 shows the values of the reference relative errors, $\rho_h = \ell_3^{\mathcal{O}}(e_h)/\ell_3^{\mathcal{O}}(u_H)$, and its corresponding estimates $\rho^{\varepsilon}_{\rm exp} = \eta^{\varepsilon}_{\rm exp}/\ell_3^{\mathcal{O}}(u_H)$ and $\rho^{e}_{\rm exp} = \eta^{e}_{\rm exp}/\ell_3^{\mathcal{O}}(u_H)$ along with the estimates for the relative dispersion error $\rho^{E^{\varepsilon}}_{\rm exp} = E^{\varepsilon}_{\rm exp}/\kappa$ and $\rho^{E^{e}}_{\rm exp} = E^{e}_{\rm exp}/\kappa$. Note that while the errors are larger for $\kappa = \pi$ the estimates behave similarly providing similar relative errors. Since the dispersion error is an important source of error for this problem, the dispersion error is closely associated to the behavior of the representations η^{ε} and η^{e}. Indeed, representation using the recovered adjoint error

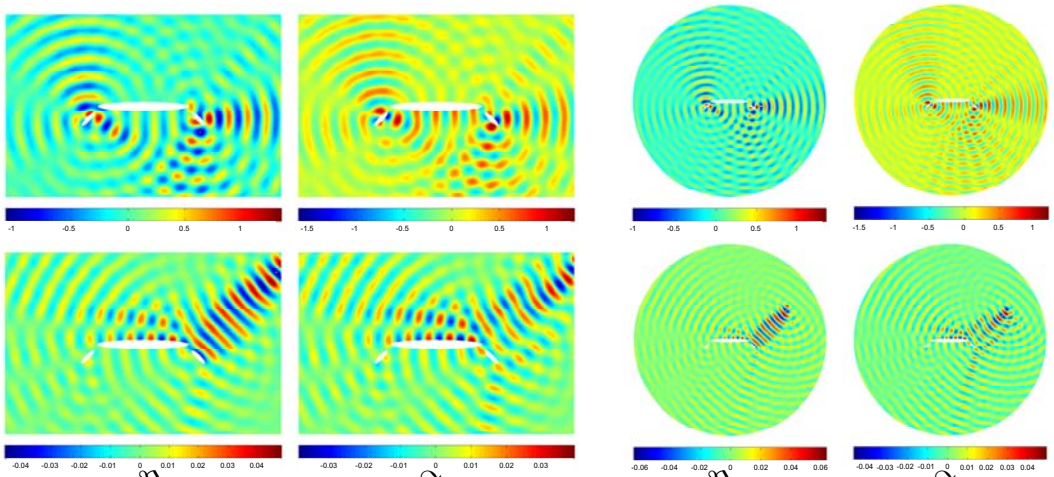

Figure 3.9: Example 2: Galerkin finite element approximation of the primal problem (top) and of the adjoint solution (bottom) for the waver number $\kappa = \pi$ and for the meshes of 16212 and 26584 nodes, correspondent to the problems with rectangular (a) and circular (b) exterior boundaries, respectively.

ε^* is slightly better than the representation using the recovered primal error e^*. Thus, the dispersion error can be used to choose the error representation from which to obtain the approximation for the output.

Note also that increasing the value of κ does not involve a deterioration of the estimates. In fact, in this example, the effectivity indices improve. Indeed, looking at the representation η^{ε}, the effectivity index $\rho^e_{\text{exp}}/\rho_h$ is decreasing from 0.58 to 0.40 in the in the first mesh, and from 0.89 to 0.81 in the final mesh.

It is worth noting that a similar behavior is obtained for the problem with rectangular boundary and the quantity of interest $J_2(u_{\text{r}})$.

Table 3.2 shows the estimates obtained for the quantity of interest $J_2(u_{\text{r}})$ for the parameter $\kappa = \pi/4$ using three uniformly refined meshes for the rectangular geometry. In order to illustrate the influence of the different terms contributing to the error in the quantity of interest, the linear and quadratic contributions are shown separately. As can be seen, the linear term provides a very good inside to the total error since the quadratic term converges rapidly to zero. In this example, for all the meshes, the dispersion error is smaller for the adjoint problem which causes the representation η^{ε} to be more accurate than η^e.

$\kappa = \pi/4$

$\mathtt{n}_{\mathrm{np}}$	ρ_h	$\rho^{\varepsilon}_{\mathrm{exp}}$	ρ^{e}_{exp}	$\rho^{E^\varepsilon}_{\mathrm{exp}}$	$\rho^{E^e}_{\mathrm{exp}}$
1711	0.1006	0.0590	0.0472	0.0429	0.0468
6713	0.0690	0.0353	0.0305	0.0124	0.0131
26584	0.0279	0.0248	0.0233	0.0030	0.0031

$\kappa = \pi$

$\mathtt{n}_{\mathrm{np}}$	ρ_h	$\rho^{\varepsilon}_{\mathrm{exp}}$	ρ^{e}_{exp}	$\rho^{E^\varepsilon}_{\mathrm{exp}}$	$\rho^{E^e}_{\mathrm{exp}}$
1711	0.8873	0.3563	0.3430	0.1101	0.1906
6713	0.7341	0.2753	0.2699	0.0994	0.1002
26584	0.1313	0.1067	0.0780	0.0431	0.0504

Table 3.1: Example 2: Estimates for the error in the linear term $\ell_3^{\mathcal{O}}(e_h)$ relative to $\ell_3^{\mathcal{O}}(u_H)$ and relative dispersion error for the primal and adjoint problem for a uniformly refined set of meshes.

The convergence of the estimates for a uniform and an adaptive procedure using the strategy given in equation (3.15) are shown in figure 3.10. Note that the adaptive refinement leads to a faster reduction of the error and it can be seen that the local indicators associated to the estimates behave properly since the convergence curves of the estimates are in good agreement with the reference ones. For $\kappa = \pi/4$, the curve associated to the reference estimate η_h and a uniform refinement has a convergence of $\mathcal{O}(\mathtt{n}_{\mathrm{np}})^{2/3}$. However, for the estimates $\eta^{\varepsilon}_{\mathrm{exp}}$ and η^{e}_{exp}, there is a short range where the solution is in a preasymptotic stage (Ihlenburg 1998). Note that as the wave number κ grows, for instance $\kappa = \pi$, the preasymptotic range is increased due to dispersion errors.

Figure 3.11 shows the local elementary contributions of $\eta^{\varepsilon}_{\mathrm{exp}}$ to the error in the quantity of interest in the initial mesh of the problem for both wave numbers and the rectangular geometry. Also, the intermediate and the final meshes produced by the adaptive procedure associated to this estimate are shown in figure 3.12. Note that the adaptive procedure refines the neighborhood of the obstacle but also refines around the boundary strip, where the solution is evaluated to compute the quantity of interest.

Finally, figure 3.13 shows the elements marked to be refined for the problem with circular boundary in the first step, in on intermediate mesh and the final mesh produced by the adaptive procedure associated to the estimate $\eta^{\varepsilon}_{\mathrm{exp}}$ for the wave

	number of nodes		
	1065	4123	16212
$J(u_h)$	3.3862e-2	4.2634e-2	4.7342e-2
$J(u_H)$	2.4265e-2	3.7859e-2	4.5476e-2
$J(u_H) + \eta^\varepsilon + \mathcal{Q}(e^*, e^*)$	2.6712e-2	3.9939e-2	4.6638e-2
$J(u_H) + \eta^e + \mathcal{Q}(e^*, e^*)$	2.6622e-2	3.9867e-2	4.6588e-2
η^ε	2.4350e-3	2.0785e-3	1.1621e-3
η^e	2.3456e-3	2.0068e-3	1.1117e-3
$\mathcal{Q}(e^*, e^*)$	1.2002e-5	1.2984e-6	1.0155e-7
E^ε	5.9456e-3	1.4779e-3	3.5560e-4
E^e	8.7771e-3	3.9217e-3	1.5675e-3

Table 3.2: Example 2: Estimates for the non-linear quantity of interest $J_2(u_{\mathrm{r}})$ for $\kappa = \pi/4$ and for the its error, including the linear and and quadratic contributions to the quantity of interest and the dispersion errors for the primal and adjoint problems.

number $\kappa = \pi/4$.

It can be seen that the regions refined in the both geometries are very similar. However, since the circular domain is slightly bigger, in this case the adaptive procedure has to refine areas not included in the rectangular domain.

3.6 Summary

In this chapter a simple strategy for guiding goal-oriented adaptive procedures has been presented, based on the post-processing techniques introduced in chapter 2. Two different representations for the error in the quantities of interest have been studied which provide similar results. It has been shown that the accuracy of these representations, which involve the post-processing of either the primal or adjoint finite element approximations, is related to the dispersion error of its corresponding problems.

The adaptive procedure is valid both for linear and non-linear quantities of interest. However it has been shown that the linear part of the quantity of interest is the leading term, since the higher order contributions converge faster to zero.

The performance of the adaptive procedure is tested in comparison with uniform refinements of the computational mesh. As expected, the adaptive refinement leads

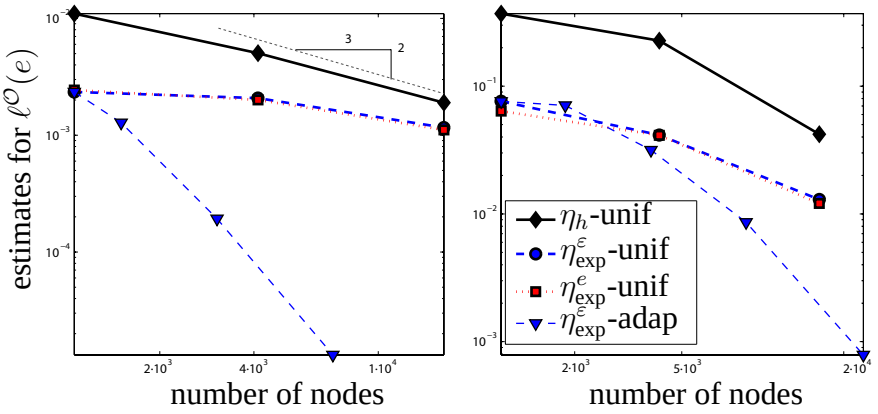

Figure 3.10: Example 2: Convergence of the relative error for the quantity of interest $J_2(u_{\mathrm{r}})$ for $\kappa = \pi/4$ (left) and $\kappa = \pi$ (right), respectively for uniform and adaptive processes in the reference solution compared with the enhanced solutions.

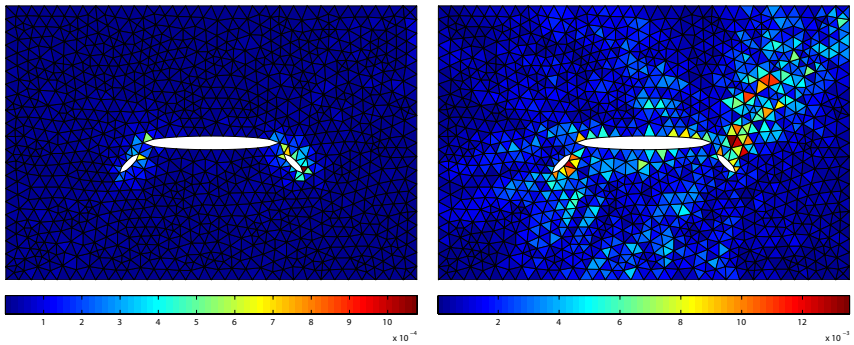

Figure 3.11: Example 2: Local maps of the error in the linear term contribution to the quantity of interest $J_2(u_{\mathrm{r}})$ using the representation $\eta^{\varepsilon}_{\text{exp}}$ for $\kappa = \pi/4$ (left) and $\kappa = \pi$ (right).

to a faster reduction of the error.

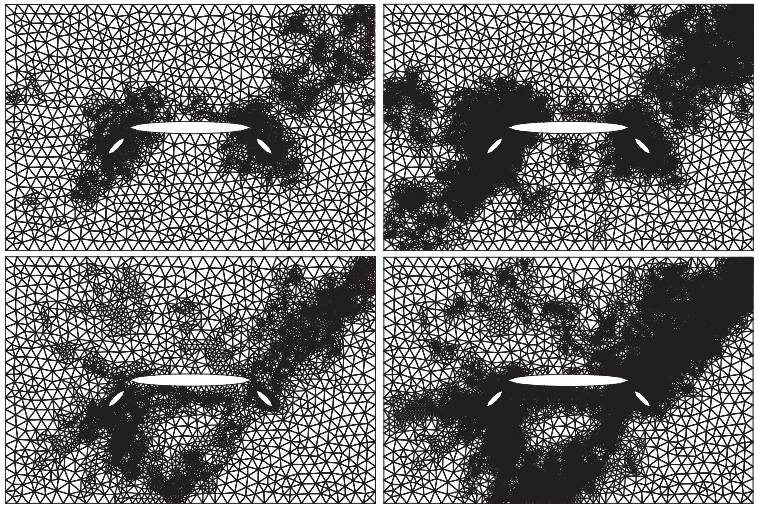

Figure 3.12: Example 2: Intermediate and final adapted meshes for the rectangular exterior boundary. For $\kappa = \pi/4$ (top) with 3050 and 17916 nodes and for $\kappa = \pi$ (bottom) with 3842 and 23635 nodes.

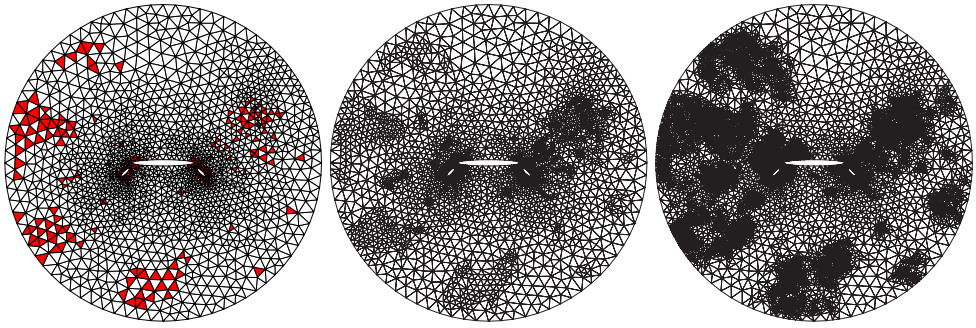

Figure 3.13: Example 2: Elements to be refined in the first step highlighted for the strategy proposed (left) and the intermediate (middle) and final (right) adapted meshes with 2790 and 14207 nodes for the circular exterior boundary with $\kappa = \pi/4$.

Chapter 4

Conclusions

This chapter summarizes the main achievements and conclusions and also provides some ideas for future research.

The main contributions of this work are summarized in three items, all addressed to obtaining error estimates for outputs of interest for wave propagation problems described by the Helmholtz equation.

The first contribution is a simple strategy to assess the error in the wave number of the Helmholtz problem, both for standard Galerkin and stabilized formulations. The introduced strategy is based on the determination of the numerical wave number that better accommodates the numerical solution. Compared to other goal-oriented error estimation strategies, the approach proposed in this work is innovative because it adopts a new paradigm. A distinctive feature of this method is that the error estimation procedure is devoted to obtain the numerical wave number of the approximate solution instead of the exact one, which is data for the problem. An enhanced approximation is obtained from the finite element solution using a simple local least-squares technique. Once the enhanced solution is obtained, the associated numerical wave number is readily recovered using a simple closed expression.

It is worth highlight that the behavior of the estimates obtained for the dispersion error reaffirm that using stabilized approximations substantially improves the performance of finite element computations of time-harmonic acoustics at high wave numbers. Unfortunately, the dispersion error for the Helmholtz equation can not be totally avoided by using stabilized formulations, as confirmed by the new *a posteriori* error technique. Moreover, the error estimates provide reasonable ap-

proximations of the reference errors, in agreement also with the measured values of the dispersion error in the simple cases where they can be evaluated. In practical application the results match the expected distributions and converge at the predicted rates.

Second, a new improved recovery technique is developed to take advantage of the nature of the solutions of wave problems. The strategy proposed to assess the dispersion error requires obtaining an inexpensive approximation of a modified problem, using post-processing techniques. The standard polynomial least-squares technique is replaced by an new exponential fitting, yielding much sharper results in most applications. However, both the error estimates computed using the polynomial and the exponential fitting provide reasonable approximations of the true errors. Besides, a simple combination of both, polynomial and exponential fitting, is proposed for the cases where the solution is extremely complicated and the exponential fitting fails to recover a proper approximation in some regions of the domain.

Finally, a new goal-oriented adaptive strategy is proposed. This strategy is based on the post-processing techniques discussed above. The proposed procedure is valid both for linear and non-linear quantities of interest. However it has been shown that the linear contribution to the quantity of interest is the leading term. Two different representations to recover the error in the quantity of interest are studied, both providing similar results. It has been shown that the accuracy of these representations, which involve the post-processing of either the primal or adjoint finite element approximations, is related to the dispersion error of its corresponding problems. Moreover, the performance of the adaptive procedure compared with an uniform refinement leads to a faster reduction of the error. The proposed error estimation procedure properly identifies the areas most contributing to the error in the quantity of interest and consequently the adaptive procedure yields adapted meshes which provide accurate results.

4.1 Future developments

The work carried out in this thesis leaves some open research lines that will be studied in the near future. We suggest the following lines:

- First, some applications have been considered in goal-oriented error estimation and adaptive techniques for the wave propagation problem modeled by Helmholtz equation. However, it would be interesting to analyze the behavior of the estimates for more types of quantities of interest in order to confirm its accuracy and also to reaffirm whether the method is sensitive to the dispersion error for high wave numbers. It would be also interesting to study the described goal-oriented mesh adaptivity technique in real-life problems.

- Second, a goal-oriented mesh adaptive procedure has been derived in the context of the standard Galerkin method. This technique could be extended to able to assess stabilized formulations.

- Third, as discussed in this thesis, the lack of precision in most simulations of the Helmholtz equation is mainly due to the dispersion error. In this work a precise analysis of the dispersion error arising in standard and stabilized finite element methods is given. However, as described in the chapter 1, there are many alternatives to alleviate the dispersion appearing in the simulations. An extension of the *a posteriori* error estimate for the dispersion error proposed in this thesis to these methods would provide a general framework for comparing the performance of the different methods.

- Fourth, it would be interesting to extend the error estimation and adaptivity procedures developed in this thesis to the Berkhoff equation, since a goal-oriented adaptive strategy based on post-processing techniques can be easily applied to this problem. It is worth noting that in this case the error assessment in the wave number becomes more complex because the wave number is not constant over the whole domain since it depends on the depth. Thus, it is not possible to obtain a global estimate for the error in the wave number but it has to be estimated locally and maps of the dispersion error have to be build.

- Finally, since the Berkhoff equation can be seen as a Helmholtz equation with non-constant coefficients. Thus more general problem could also be studied. It would be interesting to propose alternative methods aiming at reducing the dispersion error in this context. Some very preliminary results have been obtained in this respect.

Bibliography

Ainsworth, M. (2004), 'Discrete dispersion relation for hp-version finite element approximation at high wave number', *SIAM J. Numer. Anal.* **42**(2), 553–575.

Ainsworth, M. and Oden, J. T. (2000), *A posteriori error estimation in finite element analysis*, Pure and Applied Mathematics (New York), Wiley-Interscience [John Wiley & Sons], New York.

Babuška, I., Ihlenburg, F., Strouboulis, T. and Gangaraj, K. (1997), 'A posterori error estimation for finite element solutions of Helmholtz Part I: The quality of locar indicators and estimators', *Internat. J. Numer. Methods Engrg.* **40**, 3443–3462.

Babuška, I. and Melenk, J. M. (1997), 'The partition of unity method', *Internat. J. Numer. Methods Engrg.* **40**, 727–758.

Babuška, I. and Sauter, S. A. (2000), 'Is the pollution effect of the FEM avoidable for the Helmholtz equation considering high wavenumber?', *SIAM Rev.* **42**(3), 451–484.

Babuška, I. and Strouboulis, T. (2001), *The Finite Element Method and its Reliability*, Applied Mathematical Sciences, University Press, Oxford.

Babuška, I. and Rheinboldt, C. (1978), 'A-posteriori error estimates for the finite element method', *Internat. J. Numer. Methods Engrg.* **12**(10), 1597–1615.

Bangerth, W., Geiger, M. and Rannacher, R. (2010), 'Adaptive Galerkin finite element methods for the wave equation', *Comput. Methods Appl. Mech. Engrg.* **10**, 3–48.

Bangerth, W. and Rannacher, R. (1999), 'Finite element approximation of the acoustic wave equation: Error control and mesh refinement', *East-West J. Numer. Math.* **7**(4), 263–282.

Becker, R. and Rannacher, R. (1996), 'A feedback approach to error control in finite elements methods: Basic analysis and examples', *East-West J. Numer. Math.* **4**, 237–264.

Becker, R. and Rannacher, R. (2001), 'An optimal control approach to a posteriori error estimation in finite element methods', *Acta Numer.* **19**, 1–102.

Belytschko, T., Krongauz, Y., Organ, D., Fleming, M. and Krysl, P. (1996), 'Meshless methods: An overview and recent developments', *Comput. Methods Appl. Mech. Engrg.* **139**(1-4), 3–47.

Belytschko, T., Lu, Y. Y. and Gu, L. (1994), 'Element-free Galerkin methods', *Internat. J. Numer. Methods Engrg.* **37**(2), 229–256.

Berkhoff, J. C., Booy, N. and Radderc, A. C. (1982), 'Verification of numerical wave propagation models for simple harmonic linear water waves', *Coastal Engrg.* **6**(3), 255–279.

Bouillard, P. (1999), 'Admissible fields and error estimation for acoustic FEA with low wave numbers', *Comput. Struct.* **73**(1-5), 227–237.

Bouillard, P., Almeida, J. P. M., Decouvreur, V. and Mertens, T. (2008), 'Some challenges in computational vibro-acoustics: verification, validation and medium frequencies', *Comput. Mech.* **42**(2), 317–326.

Bouillard, P. and Ihlenburg, F. (1999), 'Error estimation and adaptivity for the finite element method in acoustics: 2D and 3D applications', *Comput. Methods Appl. Mech. Engrg.* **176**(1), 147–163.

Bouillard, P., Lacroix, V. and De Bel, E. (2004), 'A wave-oriented meshless formulation for acoustical and vibro-acoustical applications', *Wave Motion* **39**, 295–305.

Bouillard, P. and Suleau, S. (1998), 'Element-Free Galerkin solutions for Helmholtz problems: formulation and numerical assessment of the pollution effect', *Comput. Methods Appl. Mech. Engrg.* **162**, 317–335.

Carstensen, C. and Funken, S. (2000), 'Fully reliable localized error control in the FEM', *SIAM J. Numer. Anal.* **21**(4), 1465–1484.

Díez, P. and Calderón, G. (2007*a*), 'Goal-oriented error estimation for transient parabolic problems', *Comput. Mech.* **39**.

Díez, P. and Calderón, G. (2007*b*), 'Remeshing criteria and proper error representations for goal oriented h-adaptivity', *Comput. Methods Appl. Mech. Engrg.* **196**(4-6), 719–733.

Díez, P., Parés, N. and Huerta, A. (2003), 'Recovering lower bounds of the error by postprocessing implicit residual a posteriori error estimates', *Internat. J. Numer. Methods Engrg.* **56**(10), 1465–1488.

Díez, P., Rodenas, J. and Zienkiewicz, O. (2007), 'Equilibrated patch recovery error estimates: simple and accurate upper bounds of the error', *Internat. J. Numer. Methods Engrg.* **69**(10), 2075–2098.

Djellouli, R., Farhat, C., Macedo, A. and Tezaur, R. (2000), 'Finite element solution of two-dimensional acoustic scattering problems using arbitrarily shaped convex artificial boundaries', *J. Comput. Acoust.* **8**(1), 81–99.

Donea, J. and Huerta, A. (2003), *Finite Element Methods for Flow Problems*, John Wiley & Sons, Chichester.

Farhat, C., Harari, I. and Franca, L. P. (2001), 'The discontinuous enrichment method', *Comput. Methods Appl. Mech. Engrg.* **190**, 6455–6479.

Farhat, C., Harari, I. and Hetmaniuk, U. (2003), 'A discontinuous Galerkin method with Lagrange multipliers for the solution of Helmholtz problems in the mid-frequency range', *Comput. Methods Appl. Mech. Engrg.* **192**, 1389–1419.

Farhat, C., Wiedemann-Goiran, P. and Tezaur, R. (2004), 'A discontinuous Galerkin method with plane waves and Lagrange multipliers for the solution of short wave exterior Helmholtz problems on unstructured meshes', *Wave Motion* **39**, 307–317.

Gabard, G. (2006), 'Discontinuous Galerkin methods with plane waves for the displacement-based acoustic equation', *Internat. J. Numer. Methods Engrg.* **66**, 549–569.

Grosu, E. and Harari, I. (2008), 'Studies of the discontinuous enrichment method for two-dimensional acoustics', *Finite Elem. Anal. Des.* **44**, 272–287.

Guerra, F. (1977), Finite element analysis for the adaptive method of rezoning, PhD thesis, The University of Texas at Austin.

Harari, I. (1997), 'Reducing spurious dispersion, anisotropy and reflection in finite element analysis of time-harmonic acoustics', *Comput. Methods Appl. Mech. Engrg.* **140**, 39–58.

Harari, I. (2006), 'A survey of finite element methods for time-harmonic acoustics', *Comput. Methods Appl. Mech. Engrg.* **195**, 1594–1607.

Harari, I. and Avraham, D. (1997), 'High-order finite element methods for acoustic problems', *J. Comput. Acoust.* **5**(1), 33–51.

Harari, I. and Djellouli, R. (2004), 'Analytical study of the effect of wave number on the performance of local absorbing boundary conditions for acoustic scattering', *Appl. Numer. Math.* **50**, 15–47.

Harari, I. and Hughes, T. (1992), 'Galerkin/least-squares finite element methods for the reduced wave equation with nonreflecting boundary conditions in unbounded domains', *Comput. Methods Appl. Mech. Engrg.* **98**(3), 411–454.

Harari, I. and Magoulès, F. (2004), 'Numerical investigations of stabilized finite element computations for acoustics', *Wave Motion* **39**, 339–349.

Harari, I. and Nogueira, C. L. (2002), 'Reducing dispersion of linear triangular elements for the Helmholtz equation', *J. Engrg. Mech.* **128**(3), 351–358.

Hughes, T. J. R. (1995), 'Multiscale phenomena: Green's functions, dirichlet-to-neumann formulation, subgrid scale models, bubbles and the origins of stabilized methods', *Comput. Methods Appl. Mech. Engrg.* **127**, 387–401.

Hughes, T. J. R. and Brooks, A. N. (1979), 'A multi-dimensional upwind scheme with no crosswind diffusion', *Finite Element Methods for Convection Dominated Flows (Collection of Papers Pres at Winter Ann. Meeting Amer. Soc. Mech. Engrs(ASME), New York)* **34**, 19–35.

Hughes, T. J. R., Feijoo, G. R., Mazzei, L. and Quincy, J.-B. (1998), 'The variational multiscale method - a paradigm for computational mechanics', *Comput. Methods Appl. Mech. Engrg.* **166**, 3–24.

Hughes, T. J. R., Franca, L. P. and Hulbert, G. (1989), 'A new finite element formulation for computational fluid dynamics', *Comput. Methods Appl. Mech. Engrg.* **73**, 173–189.

Ihlenburg, F. (1998), *Finite Element Analysis of Acoustic Scattering*, Vol. 132 of *Applied Mathematical Sciences*, Springer-Verlarg, New York.

Ihlenburg, F. and Babuška, I. (1995a), 'Dispersion analysis and error estimation of Galerkin fininite element methods for the Helmholtz equation', *Internat. J. Numer. Methods Engrg.* **38**, 3745–3774.

Ihlenburg, F. and Babuška, I. (1995b), 'Finite element solution of the Helmholtz equation with high wave number. Part 1: The hp-version of the FEM', *Comput. Math. Appl.* **38**, 9–37.

Ihlenburg, F. and Babuška, I. (1997), 'Finite element solution of the Helmholtz equation with high wave number. Part 2: The hp-version of the FEM', *SIAM J. Numer. Anal.* **34**(1), 315–358.

Irimie, S. and Bouillard, P. (2001), 'A residual a posteriori error estimator for the finite element solution of the Helmholtz equation', *Comput. Methods Appl. Mech. Engrg.* **190**(31), 4027–4042.

Lacroix, V., Bouillard, P. and Villon, P. (2003), 'An iterative defectcorrection type meshless method for acoustics', *Internat. J. Numer. Methods Engrg.* **57**(15), 2131–2146.

Ladevèze, P. and Arnaud, L. (2000), 'A new computational method for structural vibrations in the medium-frequency range', *Comput. Assist. Mech. Engrg. Sc.* **7**, 219–226.

Ladevèze, P., Arnaud, L., Rouch, P. and Blanzé (2001), 'The variational theory of complex rays for the calculation of mediumfrequency vibrations', *Engrg. Comput.* **18**(1/2), 193–214.

Ladevèze, P. and Leguillon, D. (1983), 'Error estimate procedure in the finite element method and applications', *SIAM J. Numer. Anal.* **20**(3), 485–509.

Ladevèze, P. and Maunder, E. A. W. (1996), 'A general method for recovering equilibrating element tractions', *Comput. Methods Appl. Mech. Engrg.* **137**(3), 111–151.

Ladevèze, P. and Oden, J. T. (1998), *Advances in Adaptive Computational Methods in Mechanics,*, Studies in Applied Mechanics, Elsevier, Amsterdam.

Ladevèze, P. and Rougeot, P. (1997), 'New advances on a posteriori error on constitutive relation in FE analysis', *Comput. Methods Appl. Mech. Engrg.* **150**(3), 239–249.

Machiels, L., Maday, Y. and Patera, A. T. (2000), 'A "flux-free" nodal neumann subproblem approach to output bounds for partial differential equations', *C. R. Acad. Sci. Paris Ser. I Math.* **330**(3), 249–254.

Maday, Y., Patera, A. T. and Peraire, J. (1999), 'A general formulation for a posteriori bounds for output functionals of partial differential equations; application to the eigenvalue problem', *C. R. Acad. Sci. Paris - Anal. Numér.* **328**(1), 823–828.

Oberai, A. A. and Pinsky, P. M. (1998), 'A multiscale finite element method for the Helmholtz equation', *Comput. Methods Appl. Mech. Engrg.* **154**, 281–297.

Oden, J. and Prudhomme, S. (2001), 'Goal-oriented error estimation and adaptivity for the finite element method', *Comput. Math. Appl.* **41**(5-6), 735–756.

Paraschivoiu, M., Peraire, J. and Patera, A. T. (1997), 'A posteriori finite element bounds for linear-functional outputs of elliptic partial differential equations', *Comput. Methods Appl. Mech. Engrg.* **150**, 289–312.

Parés, N., Díez, P. and Huerta, A. (2006), 'Subdomain-based flux-free a posteriori error estimators', *Comput. Methods Appl. Mech. Engrg.* **195**(4-6), 297–323.

Pluymers, B., Van Hal, B., Vandepitte, D. and Desmet, W. (2007), 'Trefftz-based methods for time-harmonic acoustics', *Arch. Comput. Methods Engrg.* **33**, 343–381.

Riou, H., Ladevèze, P. and Rouch, P. (2004), 'Extension of the variational theory of complex rays to shells for medium-frequency vibrations', *J. Sound Vibration* **272**, 341–360.

Sarrate, J., Peraire, J. and Patera, A. T. (1999), 'A posteriori finite element error bounds for non-linear outputs of the Helmholtz equation', *Internat. J. Numer. Methods Engrg.* **31**(1), 17–36.

Steffens, L. M. and Díez, P. (2009), 'A simple strategy to assess the error in the numerical wave number of the finite element solution of the Helmholtz equation', *Comput. Methods Appl. Mech. Engrg.* **198**, 1389–1400.

Steffens, L. M., Parés, N. and Díez, P. (2010*a*), 'Estimation of the dispersion error in the numerical wave number of standard and stabilized finite element approximations of the Helmholtz equation', *Internat. J. Numer. Methods Engrg.* **Accepted for publication**.

Steffens, L. M., Parés, N. and Díez, P. (2010*b*), 'Goal oriented h-adaptivity for the Helmholtz equation: error estimates, local indicators and refinement strategies', *Comput. Mech.* **Submitted for publication**.

Stewart, J. R. and Hughes, T. (1996), 'Explicit residual-based a posteriori error estimation for finite element discretizations of the Helmholtz equation: computation of the constant and new measures of error estimator quality', *Comput. Methods Appl. Mech. Engrg.* **131**(3-4), 335–363.

Stewart, J. R. and Hughes, T. (1997), 'An a posteriori error estimator and hp-adaptive strategy for finite element discretizations of the Helmholtz equation in exterior domains', *Finite Elem. Anal. Des.* **25**, 1–26.

Strouboulis, T., Babuška, I. and Hidajat, R. (2006), 'The generalized finite element method for Helmholtz equation theory, computation, and open problems', *Comput. Methods Appl. Mech. Engrg.* **195**, 4711–4731.

Strouboulis, T. and Hidajat, R. (2006), 'Partition of unity method for Helmholtz equation: q-convergence for plane-wave and wave-band local bases', *Appl. Math.* **51**(2), 181–204.

Suleau, S. and Bouillard, P. (2000), 'One dimensional dispersion analysis for the element-free Galerkin method for the Helmholtz equation', *Internat. J. Numer. Methods Engrg.* **47**, 1169–1188.

Suleau, S., Deraemaeker, A. and Bouillard, P. (2000), 'Dispersion and pollution of meshless solutions for the Helmholtz equation', *Comput. Methods Appl. Mech. Engrg.* **190**, 639–657.

Tezaur, R. and Farhat, C. (2006), 'Three-dimensional discontinuous Galerkin elements with plane waves and Lagrange multipliers for the solution of mid-frequency Helmholtz problems', *Internat. J. Numer. Methods Engrg.* **66**, 796–815.

Thompson, L. L. and Pinsky, P. (1994), 'Complex wavenumber fourier analysis of the p-version finite element method', *Comput. Methods Appl. Mech. Engrg.* **13**, 255–275.

Thompson, L. L. and Pinsky, P. (1995), 'A Galerkin least squares finite element method for the twodimensional Helmholtz equation', *Internat. J. Numer. Methods Engrg.* **38**, 371–398.

Verfurth, R. (1996), *A Review of A Posteriori Error Estimation and Adaptive Mesh-refinement Techniques*, Applied Mathematical Sciences, Wiley-Teubner, Stuttgart.

Walsh, T. and Demkowicz, T. (2003), 'hp boundary element modeling of the external human auditory system - Goal oriented adaptivity with multiple load vectors', *Comput. Methods Appl. Mech. Engrg.* **192**(1-2), 125–146.

Wiberg, N.-E., Zeng, L. and Li, X. (1992), 'Error estimation and adaptivity in elastodynamics', *Comput. Methods Appl. Mech. Engrg.* **101**, 369–395.

Zienkiewicz, O. C. and Zhu, J. (1987), 'A simple error estimator and adaptive procedure for practical engineering analysis', *Internat. J. Numer. Methods Engrg.* **24**, 337–357.

Zienkiewicz, O. and Zhu, J. (1992*a*), 'The superconvergent patch recovery (SPR) and adaptive finite element refinement', *Comput. Methods Appl. Mech. Engrg.* **101**, 207–224.

Zienkiewicz, O. and Zhu, J. (1992*b*), 'The superconvergent patch recovery (SPR) and *a posteriori* error estimates. Part 1: The recovery technique', *Internat. J. Numer. Methods Engrg.* **33**, 1331–1364.

Zienkiewicz, O. and Zhu, J. (1992*c*), 'The superconvergent patch recovery (SPR) and *a posteriori* error estimates. Part 2: Error estimates and adaptivity', *Internat. J. Numer. Methods Engrg.* **33**, 1365–1382.

A simple strategy to assess the error in the numerical wave number of the finite element solution of the Helmholtz equation

Steffens L. M. and Díez P.

Computer Methods in Applied Mechanics and Engineering

198, 1389-1400, 2009

Comput. Methods Appl. Mech. Engrg. 198 (2009) 1389–1400

Contents lists available at ScienceDirect

Comput. Methods Appl. Mech. Engrg.

journal homepage: www.elsevier.com/locate/cma

A simple strategy to assess the error in the numerical wave number of the finite element solution of the Helmholtz equation ☆

Lindaura Maria Steffens, Pedro Díez *

Laboratori de Càlcul Numèric, Departament de Matemàtica Aplicada III, E.T.S. Ingenieros de Caminos, Universitat Politècnica de Catalunya, Mòdul C2, Jordi Girona 1-3, Barcelona E-08034, Spain

ARTICLE INFO

Article history:
Received 15 July 2008
Received in revised form 27 November 2008
Accepted 5 December 2008
Available online 30 December 2008

Keywords:
Wave problems
Helmholtz equation
Error estimation of wave number
Dispersion/pollution error
Goal oriented adaptivity
Global/local estimates

ABSTRACT

The standard approach for goal oriented error estimation and adaptivity uses an error representation via an adjoint problem, based on the linear functional output representing the quantity of interest. For the assessment of the error in the approximation of the wave number for the Helmholtz problem (also referred to as dispersion or pollution error), this strategy cannot be applied. This is because there is no linear extractor producing the wave number from the solution of the acoustic problem. Moreover, in this context, the error assessment paradigm is reverted in the sense that the exact value of the wave number, κ, is known (it is part of the problem data) and the effort produced in the error assessment technique aims at obtaining the numerical wave number, κ_H, as a postprocess of the numerical solution, u_H. The strategy introduced in this paper is based on the ideas used in the a priori analysis. A modified equation corresponding to a modified wave number κ_m is introduced. Then, the value of κ_m such that the modified problem better accommodates the numerical solution u_H is taken as the estimate of the numerical wave number κ_H. Thus, both global and local versions of the error estimator are proposed. The obtained estimates of the dispersion error match the a priori predicted dispersion error and, in academical examples, the actual values of the error in the wave number.

1. Introduction

The numerical simulation of acoustic problems requires an accurate answer to properly predict their performance. In the low frequency range domain the finite element method (FEM) is a standard tool for solving the acoustic equations. In the medium and high frequency ranges the end-user should be concerned by the errors associated with the numerical discretization. In practice, two components of the error are clearly identified in this framework: interpolation error and pollution error. The classical interpolation error decays with the mesh size as predicted by standard a priori error estimates. The behavior of the pollution error is more complex: the convergence rate predicted by the a priori estimates depends on the range where the mesh size lies (relative to the wavelength) [1].

In practice, the end-user of a finite element acoustic computation is concerned with the accuracy of the solution in terms of the dispersion, the error committed in the evaluation of the wave number, κ. Paradoxically, this is not because the value of κ is a quantity of interest that has to be evaluated accurately. In fact, the exact value of κ is known a priori as part of the problem data. The overall quality of the numerical solution is however associated with the error in the approximation of κ.

The standard approach for goal oriented error estimation and adaptivity is based on the representation of the error in a quantity of interest obtained using an adjoint problem [14,17]. The solution of the adjoint problem is also denoted extractor and the corresponding error representation combines the extractor and the original solution. Thus, the error assessment for the quantity of interest is reduced to assess the error in energy norm of this auxiliary problem. This strategy cannot be used when the quantity to be assessed is the wave number. This is because there is not a proper extractor associated with this quantity, κ. Moreover, as already noted, the exact value of κ is a priori known. This reverts the final goal of the error assessment technique. The target of the error estimation strategies is in standard cases to find a better approximation than the one provided by the numerical solution, u_H, and then compare them. In the present situation, this is somehow reverted to find the actual approximation of the quantity of interest provided by u_H, say κ_H, and to compare it with the exact value κ. Summarizing, assessing the error in κ requires a complete different paradigm. The quality of the solution is assessed via the approximation of a

☆ Partially supported by Ministerio de Educación y Ciencia, Grants DPI2007-62395 and BIA2007-66965; Programme Alßan, the European Union Programme of High Level Scholarships for Latin America, scholarship no. E06D100641BR.

* Corresponding author. Tel.: +34 934017240; fax: +34 934011825.
E-mail addresses: lindaura.steffens@upc.edu (L.M. Steffens), pedro.diez@upc.edu (P. Díez).
URL: http://www-lacan.upc.edu (P. Díez).

0045-7825/$ - see front matter © 2009 Elsevier B.V. All rights reserved.
doi:10.1016/j.cma.2008.12.005

quantity which is exactly known. The numerical wave number κ_H is unknown and has to be evaluated.

The first problem to face is to find a proper definition for κ_H. Heuristically, the *wavelength* of the approximate solution is the distance of two consecutive local maxima (or minima). Although this represents a precise definition for 1D waves, it cannot be easily generalized to higher dimensions. Moreover, it cannot be converted into an explicit functional output of the numerical solution. One definition for κ_H is implicitly used in a priori analysis, based on the idea of fitting the numerical solution into a modified equation. Here, this concept is extended such that it can be exploited in a posteriori error assessment setting.

Namely, this paper introduces a technique to assess the value of κ_H based on finding the wave number of a modified problem which better accommodates the numerical solution u_H. This approach is inspired by the a priori estimates developed in [12].

The idea is also extended to find a local indicator of the error in the wavelength. This local quantity is assumed to measure the ability of the local discretization (in a given portion of the domain) to properly capture the wavelength. The possible use of this information to adapt the mesh and reduce the overall error is beyond the scope of this paper but is part of the work in progress.

The remainder of the paper is structured as follows. Section 2 introduces the notation presenting the problem to be solved, the finite element formulation and the concepts of dispersion and pollution effect in this type of problem. The basic lines of the a priori analysis performed in [12] are briefly sketched in Section 3. Then, Section 4 is devoted to introduce the a posteriori technique proposed to assess the error in the wave number. A local version of the estimate providing a spatial error distribution for adaptive purposes is introduced in Section 5. Finally, Section 6 contains numerical examples showing the good behavior of the proposed technique both in academic and practical examples.

2. Problem statement

2.1. Acoustic modeling: the Helmholtz equation

The presentation and notation introduced by Ihlenburg [11] is followed in the remainder of this section.

The transient acoustic problem consists in obtaining the unknown pressure field $P(\mathbf{x},t)$, taking values for $\mathbf{x} \in \Omega \subset \mathbb{R}^d$ (d being the dimension in space, $d = 1, 2$ or 3). The field $P(\mathbf{x},t)$ is the solution of the following partial differential equation:

$$\Delta P = \frac{1}{c^2}\frac{\partial^2 P}{\partial t^2}, \tag{1}$$

where c is the speed of sound in the medium.

The pressure time dependency is eliminated assuming a harmonic behavior and selecting an angular frequency ω, namely

$$P(\mathbf{x},t) = u(\mathbf{x})\exp(i\omega t), \tag{2}$$

where $u(\mathbf{x})$ is the complex spatial distribution of the acoustic pressure and i the imaginary unit. Substituting (2) into (1), the wave equation reduces to the Helmholtz equation:

$$\Delta u + \kappa^2 u = 0, \tag{3}$$

where $\kappa := \omega/c$ stands for the wave number.

The physical pressure is the real part of the complex unknown u. The velocity $\mathbf{v}$ is proportional to the gradient of pressure:

$$\nabla u = -i\rho c\kappa \mathbf{v}, \tag{4}$$

where ρ is the density of the fluid.

A complete definition of the Boundary Value Problem to be solved requires adding to Eq. (3) a proper set of boundary conditions. For interior acoustic problems, three types of boundary conditions are considered: Dirichlet, Neumann and Robin (or mixed).

The Dirichlet boundary conditions prescribe values of the pressure on part of the boundary, say $\Gamma_D \subset \partial\Omega$, where u is prescribed to be equal to a given value $\bar{u}$, that is

$$u = \bar{u} \quad \text{on } \Gamma_D. \tag{5}$$

On the Neumann part of the boundary $\Gamma_N \subset \partial\Omega$ the normal component of the velocity $\mathbf{v}$ is prescribed to be equal to $\bar{v}_n$, namely

$$\frac{\partial u}{\partial \mathbf{n}} = -i\rho c\kappa \bar{v}_n \quad \text{on } \Gamma_N. \tag{6}$$

The prescribed value $\bar{v}_n$ corresponds to the normal velocity of a vibrating wall producing the sound that propagates within the medium.

Finally, on the Robin part of the boundary $\Gamma_R \subset \partial\Omega$ the velocity is imposed to be proportional to the pressure, that is

$$\frac{\partial u}{\partial \mathbf{n}} = -i\rho c\kappa A_n u \quad \text{on } \Gamma_R, \tag{7}$$

where the coefficient A_n is the admittance and represents the structural damping. This type of boundary conditions is associated with absorbing walls. For $A_n = 0$ it coincides with the homogeneous Neumann boundary condition, standing for a perfectly reflecting panel. For particular case of plane waves, the value $A_n = 1/\rho c$ describes a fully absorbent panel.

In order to get a well posed Boundary Value Problem, the three parts of the boundary must cover the whole boundary, that is $\partial\Omega = \overline{\Gamma_D \bigcup \Gamma_N \bigcup \Gamma_R}$.

The weak form of the Boundary Value Problem defined by Eqs. (3), (5)–(7) is readily expressed in its weak form using the corresponding natural functional spaces. The space for the trial functions is $U = \{u \in H^1(\Omega), u|_{\Gamma_D} = \bar{u}\}$ while the space for the test functions is $V = \{v \in H^1(\Omega), v|_{\Gamma_D} = 0\}$, $H^1(\Omega)$ being the standard Hilbert space of square integrable functions with square integrable first derivatives.

Thus, the weak form of the problem reads: find $u \in U$ such that

$$a(u,v) = l(v) \quad \forall v \in V, \tag{8}$$

where the bilinear and linear forms are defined as follows:

$$a(u,v) := \int_\Omega \nabla u \cdot \nabla \tilde{v}\, d\Omega - \int_\Omega \kappa^2 u\tilde{v}\, d\Omega + \int_{\Gamma_R} i\rho c\kappa A_n u\tilde{v}\, d\Gamma \quad \text{and}$$

$$l(v) := -\int_{\Gamma_N} i\rho c\kappa \bar{v}_n \tilde{v}\, d\Gamma$$

and the symbol $\tilde{\cdot}$ denotes the complex conjugate.

2.2. Finite element approximation

The discrete counterparts of U and V are the finite element spaces $U_H \subset U$ and $V_H \subset V$ associated with a mesh of characteristic element size H. Thus, the discrete finite element solution is the function $u_H \in U_H$ such that

$$a(u_H, v_H) = l(v_H) \quad \forall v_H \in V_H. \tag{9}$$

The finite element solution u_H is expressed in terms of the basis-functions N_j spanning U_H:

$$u_H = \sum_{j=1}^{n} N_j u_j = \mathbf{N}\mathbf{u}_H, \tag{10}$$

where u_j, for $j = 1,2,\ldots,n$, are the complex nodal values, $\mathbf{N} = [N_1, N_2, \ldots, N_n]$ and $\mathbf{u}_H^T = [u_1, u_2, \ldots, u_n]$.

The matrix form of (9) reads

$$(\mathbf{K}_H + i\rho c\kappa A_n \mathbf{C}_H - k^2 \mathbf{M}_H)\mathbf{u}_H = -i\rho c\kappa \mathbf{f}_H, \tag{11}$$

where $\mathbf{K}_H$, $\mathbf{C}_H$ and $\mathbf{M}_H$ are the so-called stiffness, damping and mass matrices defined by

$$\mathbf{K}_H := \int_\Omega (\nabla \mathbf{N})^\mathrm{T} (\nabla \mathbf{N}) d\Omega, \quad \mathbf{C}_H := \int_{\Gamma_R} \mathbf{N}^\mathrm{T} \mathbf{N} d\Gamma \quad \text{and}$$

$$\mathbf{M}_H := \int_\Omega \mathbf{N}^\mathrm{T} \mathbf{N} d\Omega.$$

Note that the damping matrix $\mathbf{C}_H$ accounts for the Robin boundary conditions while the right-hand side term vector $\mathbf{f}_H$ given by

$$\mathbf{f}_H := \int_{\Gamma_N} \mathbf{N}^\mathrm{T} \bar{v}_n d\Gamma$$

includes the effect of Neumann boundary conditions.

2.3. Dispersion and pollution effects

The error introduced in the numerical solution of wave problems has two different components: *interpolation error* and *pollution error*. The interpolation error is the classical error arising in elliptic problems and pertains to the ability of the discretization to properly approximate the solution. The interpolation error is obtained by simply using the exact values of u at the mesh nodes $\mathbf{x}_j$, $j = 1, 2, \ldots, n$:

$$\text{Interpolation error} = u(\mathbf{x}) - \sum_{j=1}^{n} N_j(\mathbf{x}) u(\mathbf{x}_j).$$

In standard thermal and elasticity problems (i.e. problems for which the bilinear form $a(u, v)$ in (8) is symmetric as positive-definite, that is, induces an inner product), the error in the finite element solution is equivalent to the interpolation error, and converges with the same rate. This error is local in nature because it may be reduced in a given zone by reducing the mesh size locally in this zone.

In wave problems, in particular in the solution of the Helmholtz equation, a new error component has to be considered which is referred to as *pollution* error. This error component is especially relevant in the framework of Helmholtz problems due to the blowup of the inf–sup and continuity constants of the weak form when the wave number is large (i.e. the inf–sup constant tends to zero and the continuity constant tends to ∞ as κ tends to ∞). In transient wave problems, pollution is associated with the variation of the numerical wave speed with the wavelength. This phenomenon results in the dispersion of the different components of the total wave. In the steady Helmholtz problem, the word dispersion is also used and corresponds to the error in the numerical wave number, κ_H, and it is therefore identified with the pollution. In other words, the FE error is decomposed into two terms which, in the case of wave problems, behave completely differently:

$$\begin{aligned} \text{FE error} &= u(\mathbf{x}) - \sum_{j=1}^{n} N_j(\mathbf{x}) u_j \\ &= \text{Interpolation error} + \underbrace{\textstyle\sum_{j=1}^{n} N_j(\mathbf{x})(u(\mathbf{x}_j) - u_j)}_{\text{dispersion/pollution}}. \end{aligned}$$

This is illustrated in Fig. 1. The second term in this estimate characterizes the pollution error and is denoted by e_{pol}. This error component is related to the phase difference between the exact and FE solutions, that is the dispersion.

Much attention has been paid to the a priori analysis of the pollution/dispersion error, see for instance [4,12,13]. As shown in Section 3, the pollution term converges at a different rate, lower than the standard interpolation error. The pollution effect may be suppressed only in 1D problems, as noted in [2,3]. In higher dimensions, pollution affects every numerical scheme and cannot be avoided [4].

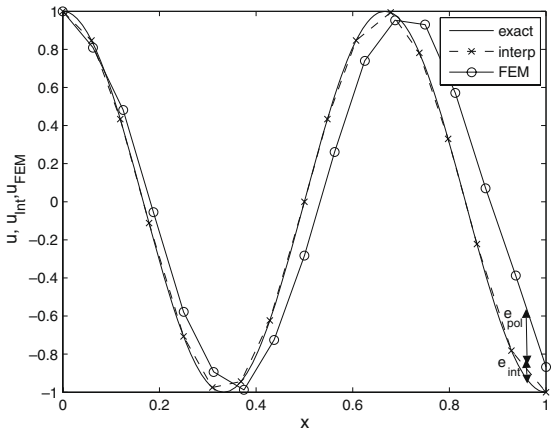

Fig. 1. Illustration of the errors arising in the approximation of the Helmholtz equation. The exact solution (solid line, smooth) and interpolant (dashed line) coincide at the nodes, the FEM solution reproduces approximately the shape of the wave with a larger wavelength ($\kappa_H < \kappa$).

3. A priori error assessment

The a priori error analysis is performed studying a simple 1D case [12]. This analysis is recalled here because its basic rationale is useful in the following. The analysis is based on considering a modified problem and identifying the parameter of the modified problem that better accommodates the FE solution.

3.1. Modified problem

A modified Helmholtz equation is introduced as

$$\Delta u_m + \kappa_m^2 u_m = 0. \tag{12}$$

Note that in the 1D case, this reduces to

$$\frac{d^2 u_m}{dx^2} + \kappa_m^2 u_m = 0. \tag{13}$$

Therefore, in 1D case, supposing that $\Omega = (0,1)$, the solution $e^{i\kappa_m x}$ is obtained from the characteristic solutions by selecting the following boundary conditions: $u_m(0) = 1$ and $u_m'(1) = i\kappa u(1)$.

The a priori analysis aims at determining the value of κ_m that better accommodates the numerical solution of the Helmholtz equation. This value κ_m is identified with the discrete wave number and it is denoted by κ_H^{pri} (the superscript pri stands for *a priori*) (see Fig. 2).

To this end, the patch of elements surrounding node $\mathbf{x}_j$ in a 1D mesh is considered, see Fig. 3. Let N_{j-1}, N_j and N_{j+1} be the linear shape functions corresponding to the nodes $\mathbf{x}_{j-1}$, $\mathbf{x}_j$ and $\mathbf{x}_{j+1}$, which are consecutive in the mesh and are the only ones involved in the equation for node $\mathbf{x}_j$. The discrete equation corresponding to node $\mathbf{x}_j$ reads

$$R u_{j-1} + 2S u_j + R u_{j+1} = 0, \tag{14}$$

the coefficients R and S being defined as

$$R := -1 - \frac{1}{6}(\kappa H)^2 \quad \text{and} \quad S := 1 - \frac{1}{3}(\kappa H)^2$$

and u_j the nodal unknown at node $\mathbf{x}_j$. Noting that $\mathbf{x}_{j-1} = \mathbf{x}_j - H$ and $\mathbf{x}_{j+1} = \mathbf{x}_j + H$, using $u_m(\mathbf{x}) = e^{i\kappa_m \mathbf{x}}$ and replacing κ_m by κ_H^{pri} in the dis-

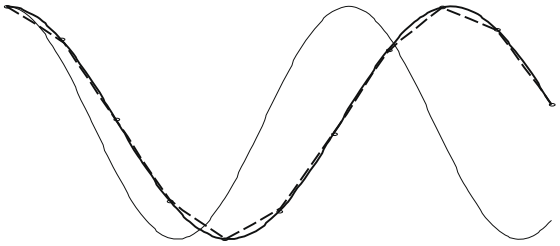

Fig. 2. Illustration for the 1D case of the exact solution u (solid thinner line), the approximate solution u_H (dashed line) and the solution of the modified problem u_m (thicker solid line) for $\kappa_m = \kappa_H^{\text{pri}}$, coinciding with u_H at the nodes.

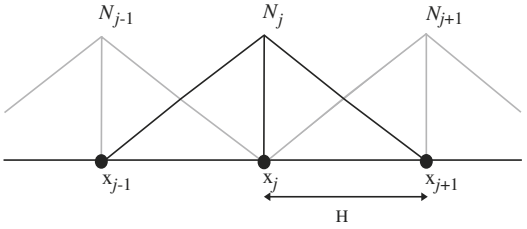

Fig. 3. Nodes surrounding $\mathbf{x}_j$ in a 1D linear FEM mesh and their corresponding shape functions.

crete equation (14) yields the following expression (see [12] for details):

$$\kappa_H^{\text{pri}} H \approx \kappa H - \frac{1}{24}(\kappa H)^3 + O((\kappa H)^5). \tag{15}$$

Consequently, the following a priori estimate for the dispersion error is defines as

$$E^{\text{pri}} := \kappa - \kappa_H^{\text{pri}} \approx \frac{\kappa^3 H^2}{24}. \tag{16}$$

Next section introduces an a posteriori error estimation technique that is inspired by the derivation of the above a priori estimate.

4. A posteriori error estimation of the wave number

The standard approach to obtain an error estimate in some Quantity of Interest (QoI) defined by a linear functional is to obtain an error representation using an adjoint problem. The adjoint problem for linear problems is similar to the direct one but with different *loads* (source term and/or boundary conditions). The error representation is an expression of the error in the QoI as an *energy* product of the errors of the direct and adjoint problems [1].

Recall however that the aim is here to assess the error in the wave number κ, which is the current QoI. The error assessment using an adjoint problem and the corresponding error representation is not applicable for the wave number QoI. This is due to two reasons. First, there is no linear functional extracting the wave number (or the wavelength) of an arbitrary function u. Second, in this case the value for κ is known for the exact solution u (it is an input data!) but not for the numerical solution $u_H : \kappa$ is known but κ_H is unknown. The strategy of the error estimate is reversed in this case. Instead of devoting effort to obtain a better approximation, as close as possible to the exact solution and then, compare it with the numerical result, here the effort has to be oriented to obtain the wave number of the approximate solution.

A new approach to a posteriori error estimation is introduced here, based on the ideas of the a priori analysis sketched in Section 3.

4.1. Direct and inverse solution of a computable modified equation

Recall that, in the a priori analysis, a modified problem is introduced into which the numerical solution can be somehow injected. The same idea is used here in an a posteriori setup. To do that, a computable modified problem has to be defined on a computable basis as it is standard in error estimation procedures [9,15]. To this effect, the exact modified problem is replaced by a reference one, associated with a finer mesh of characteristic element size $h < H$. Thus, the solution of the modified problem is a nodal value vector $\mathbf{u}_m$ (in the finer h-mesh) such that

$$[\mathbf{K}_h + i\rho c A_n \kappa_m \mathbf{C}_h - \kappa_m^2 \mathbf{M}_h]\mathbf{u}_m = -i\rho c \kappa_m \mathbf{f}_h. \tag{17}$$

Note that this can also be solved as an inverse problem by considering the solution $\mathbf{u}_m$ as input. Then, for the given $\mathbf{u}_m$ the inverse problem is finding κ_m such that $\mathbf{u}_m$ is the solution of (17). This is performed minimizing the residual norm.

For a given $\mathbf{u}_m$, the residual is defined as a function of the wave number κ_m, that is

$$\begin{aligned}\mathbf{r}(\kappa_m; u_m) &:= [\mathbf{K}_h + i\rho c A_n \kappa_m \mathbf{C}_h - \kappa_m^2 \mathbf{M}_h]\mathbf{u}_m + i\rho c \kappa_m \mathbf{f}_h \\ &= \mathbf{a}_0 + \mathbf{a}_1 \kappa_m + \mathbf{a}_2 \kappa_m^2,\end{aligned} \tag{18}$$

where

$$\mathbf{a}_0 = \mathbf{K}_h \mathbf{u}_m, \quad \mathbf{a}_1 = i\rho c (A_n \mathbf{C}_h \mathbf{u}_m + \mathbf{f}_h) \quad \text{and} \quad \mathbf{a}_2 = -\mathbf{M}_h \mathbf{u}_m.$$

Note that given $\mathbf{u}_m$, the squared residual norm $\mathbf{r}'\mathbf{r}$ (the symbol $'$ stands for the conjugated transpose, that is $v' \equiv \bar{v}^{\mathrm{T}}$) is a fourth degree polynomial in κ_m, namely

$$F(\kappa_m; u_m) = \mathbf{r}'\mathbf{r} = c_0 + c_1 \kappa_m + c_2 \kappa_m^2 + c_3 \kappa_m^3 + c_4 \kappa_m^4, \tag{19}$$

where

$$c_0 = \mathbf{a}_0'\mathbf{a}_0, \quad c_1 = \mathbf{a}_0'\mathbf{a}_1 + \mathbf{a}_1'\mathbf{a}_0, \quad c_2 = \mathbf{a}_0'\mathbf{a}_2 + \mathbf{a}_2'\mathbf{a}_0 + \mathbf{a}_1'\mathbf{a}_1,$$
$$c_3 = \mathbf{a}_1'\mathbf{a}_2 + \mathbf{a}_2'\mathbf{a}_1 \quad \text{and} \quad c_4 = \mathbf{a}_2'\mathbf{a}_2.$$

Thus, for a given value of $\mathbf{u}_m$, the wave number κ_m minimizing the squared residual $F(\kappa_m; u_m)$ is explicitly found by solving the cubic equation

$$\frac{dF}{d\kappa_m} = c_1 + 2c_2 \kappa_m + 3c_3 \kappa_m^2 + 4c_4 \kappa_m^3 = 0. \tag{20}$$

Note that despite the fact that vectors $\mathbf{a}_i$, for $i = 0,1,2$ are complex, coefficients c_i, for $i = 0,1,2,3,4$, are real and there is at least one real root of (20). In the case the three roots are real, two of the roots are associated with local minima because F is a nonnegative function. The root selected is the one providing the absolute minimum provided it is not negative: in all the examples it coincides with the root closer to the exact value κ.

In the next section, this idea is used to assess the numerical wave number κ_H associated with the numerical solution u_H. This is performed selecting $\mathbf{u}_m$ properly representing the solution u_H.

4.2. A new paradigm in a posteriori error assessment: best fitting of the modified equation

As previously announced, the goal of this section is to select $u_m \approx u_H$, and then define κ_H as the parameter of the modified problem that better accommodates u_m, namely

$$\kappa_H := \arg\min_{\kappa_m} F(\kappa_m; u_m). \tag{21}$$

Note that the function u_m is in fact described by the vector of nodal values $\mathbf{u}_m$ representing it in the reference h-mesh.

Thus, an a posteriori error estimate for the wave number can be readily computed

$$E = \kappa - \kappa_H. \tag{22}$$

The question is now how to select a proper $\mathbf{u}_m$ approximating u_H.

The idea is to imitate the derivation of the a priori estimate described in Section 3. Recall that κ_H was selected as the value of κ_m such that u_m was coinciding with u_H at the nodes P_j, $j = 1, 2, \ldots, n_H$, of the H-mesh. In the 1D model problem selected in Section 3, the solution u_m is explicitly found as a function of κ_m and therefore κ_H (in its a priori version, κ_H^{pri}) is readily obtained.

A similar procedure is proposed here in the context of the discrete modified problem (17) defined in the h-mesh. Now, for a given value of κ_m, the solution u_m of the modified problem is subjected to an additional constraint imposing that u_m coincides with u_H at the nodes of the coarse H-mesh, that is at P_j, $j = 1, 2, \ldots, n_H$.

That is, for a given value of κ_m, the constrained modified problem reads

$$\begin{aligned}&[\mathbf{K}_h + i\rho c A_n \kappa_m \mathbf{C}_h - \kappa_m^2 \mathbf{M}_h]\mathbf{u}_m \\ &\quad = -i\rho c \kappa_m \mathbf{f}_h \text{enforcing the additional constraint } u_m|_{P_j} = u_H|_{P_j}.\end{aligned} \tag{23}$$

The additional constraints are simply enforced using the Lagrange multipliers technique. The resulting solution u_m is expressed in the h-mesh. The residual $\mathbf{r}$ associated with the solution u_m is defined as in (18) and it depends explicitly on u_m through the coefficients c_j, $j = 0, \ldots, 4$, and the vectors $\mathbf{a}_j$, $j = 0, 1, 2$. Note that $\mathbf{r}$ is not null because the additional constraints induce unbalanced reaction terms.

Thus, function F is defined and computed exactly as in (19). The only difference is that now u_m is not given a priori but is a function of κ_m obtained by solving (23). Thus, F depends only on κ_m but in a more complex way and, consequently, F is not anymore a polynomial in κ_m. The numerical wave number κ_H is defined to be the value of κ_m minimizing F. This value results from solving an optimization problem and the minimum is attained for the value κ_H corresponding to the solution of (23) denoted as $\mathbf{u}_m^{\text{opt}}$. Once κ_H is available, the corresponding estimate is readily computed: $E = \kappa - \kappa_H$.

Note that for a given $\mathbf{u}_m^{\text{opt}}$, ignoring the value of κ_m, one could compute the corresponding vectors and coefficients and derive the value of κ_m solving the cubic equation (20). The result of this procedure is denoted as $\kappa_H^{\min}$ and the corresponding error estimate is $E^{\min} = \kappa - \kappa_H^{\min}$.

The computation of $\mathbf{u}_m^{\text{opt}}$ and κ_H is computationally unaffordable in a practical application. The optimization problem requires solving many times problem (23), which in every occasion results in a large system of equations in the reference mesh. Consequently, this can only be performed for academic examples. On the other hand, once $\mathbf{u}_m^{\text{opt}}$ is obtained, the computation of $\kappa_H^{\min}$ is explicit and does not require solving any system of equations.

It is observed in all the test cases that the values of κ_H and $\kappa_H^{\min}$ are practically identical. That is, once the function $\mathbf{u}_m^{\text{opt}}$ is found, the corresponding wave number is exactly computed solving explicitly the cubic equation (20).

In any case, both κ_H and $\kappa_H^{\min}$ behave well in the sense that they match the a priori estimates described in Section 3 and the measured values of κ_H in the cases where such a measure is feasible.

Following this idea, the dispersion error is isolated of interpolation error because the shape of the modified solution in the interior of the elements of the coarse H-mesh is recovered as the solution of the constrained modified equation (23).

Remark 1. In order to obtain a computable estimate, the definition of κ_H introduced above depends on the selected reference mesh of characteristic size h. For the sake if simplicity, the dependence of κ_H with h is omitted in the notation. A notation explicitly stating the dependence of h, for instance $\kappa_{H;h}$, would be more accurate. The definition is however consistent in the sense that for h tending to zero, the limit value $\kappa_{H;0}$ is actually the solution of a continuous problem that can be stated as follows.

The continuous counterpart of (23), that is the constrained modified equation, reads: find $u_m \in \mathscr{H}^1(\Omega)$ such that $u_m = u_H$ at the nodes of the H-mesh (that is $u_m|_{P_j} = u_H|_{P_j}$ for $j = 1, 2, \ldots, n_H$) and fulfilling

$$a_m(\kappa_m; u_m, v) = l_m(\kappa_m; v)$$

for all $v \in \mathscr{H}^1(\Omega)$ such that $v|_{P_j} = 0$ for $j = 1, 2, \ldots, n_H$, where

$$a_m(\kappa_m; u, v) := \int_\Omega \nabla u \cdot \nabla \tilde{v}\, d\Omega - \int_\Omega \kappa_m^2 u \tilde{v}\, d\Omega + \int_{\Gamma_R} i\rho c \kappa_m A_n u \tilde{v}\, d\Gamma$$

$$\text{and} \quad l_m(\kappa_m; v) := -\int_{\Gamma_N} i\rho c \kappa_m \bar{v}_n \tilde{v}\, d\Gamma.$$

Thus, κ_H is selected as the value of κ_m minimizing the residual of the non-constrained problem. Let us introduce the residual as

$$R(\kappa_m; u_m; v) := l_m(\kappa_m; v) - a_m(\kappa_m; u_m, v)$$

for any v in $\mathscr{H}^1(\Omega)$. Note that the value of $R(\kappa_m; u_m; v)$ is only equal to zero if $v|_{P_j} = 0$ for $j = 1, 2, \ldots, n_H$. For v functions taking non-zero values at nodes, the residual is not null. The scalar measure of the residual $R(\cdot)$ is introduced as

$$F(\kappa_m; u_m) := \max_{v \in \mathscr{H}^1(\Omega)\setminus\{0\}} \frac{R(\kappa_m; u_m; v)}{\|v\|}.$$

Thus, the value of κ_H is retrieved as the value of κ_m minimizing F, as indicated in Eq. (21) (the expression is valid both for the reference h-solution and the continuous case).

Note that in the case that it exists a value of κ_m such that the solution of the non-constrained problem coincides with u_H at the nodes P_j, this value of κ_m is precisely κ_H because for this value and the corresponding u_m, F vanishes.

The definition of a practical error estimate following this rationale requires introducing a proper approximation to $\mathbf{u}_m^{\text{opt}}$, resulting from a computationally affordable procedure.

4.3. Interpolation of u_H in the h-mesh

The first and obvious choice is to set u_m as the interpolant of u_H in the h-mesh, $[u_H]_h$. Since in practice the finer h-mesh is nested in the coarser H-mesh, $[u_H]_h$ is an exact representation of u_H.

For this choice the vector of nodal values $\mathbf{u}_m$ is readily obtained: at the nodes of the coarse mesh P_i, for $i = 1, 2, \ldots, n_H$, u_m and u_H coincide. At the rest of the nodes of the h-mesh, the nodal value is obtained by simple interpolation in the element of the coarse H-mesh where the node is located.

Once $\mathbf{u}_m$ is computed the corresponding value of κ_H^{int} is calculated analytically solving the cubic equation (20). Recall that the coefficients c_1, c_2, c_3 and c_4 depend on the choice for $\mathbf{u}_m$. As previously said, in the case the three roots are real the one selected is the absolute minimum of F which in all the test cases coincides with the closest root to κ. Once the value of the numerical wave number κ_H^{int} is assessed, the corresponding error estimate follows:

$$E^{\text{int}} = \kappa - \kappa_H^{\text{int}}. \tag{24}$$

As it is shown in the examples presented in Section 6, the approximations to κ_H provided with this methodology are not as good as expected when compared with the measured numerical wave number (this measurement can be performed in very simple test examples) or with the a priori estimates. The estimates obtained using this strategy are not as sharp as desired, with effectivity indices between 70% and 90% in the simpler example. However, with the methods proposed below, the effectivity index from 86% to 100%.

This behavior is explained using the following rationale: the interpolated function $[u_H]_h$ is not a *natural* solution of a modified equation (17). The function $[u_H]_h$ is piecewise linear in the elements of the coarse H-mesh and no solution of (17) would fulfill this type of constraint. A typical solution of (17) is smoother, without the slope discontinuities concentrated in the nodes P_i, for $i = 1, 2, \ldots, n_H$, of the coarse H-mesh. In other words, we cannot expect to find a value of κ_m properly accommodating $[u_H]_h$ in (17).

Moreover, in the a priori analysis sketched in Section 3 only the nodal values of the numerical solution are used to recover the numerical wave number κ_H. No information about the value of u_H inside the elements enters the analysis. This makes complete sense because only the dispersion/pollution part of the error is to be assessed. Including the information inside the elements would result in assessing also the interpolation error.

Consequently, in the value of κ_H^{int} assessed with the a posteriori strategy described here (using $u_m = [u_H]_h$), the effects of both the dispersion error (error in κ) and the interpolation error are taken into account together. Next section is devoted to introducing a new strategy allowing to assess the dispersion error separately.

4.4. Enhanced solution $u^\star$ by postprocessing of u_H

The methodology introduced in Section 4.2 is not applicable as a practical error estimation strategy. The error estimation procedure cannot be based on solving problems in the complete finer reference mesh. It has been noted also that once the function $\mathbf{u}_m^{\text{opt}}$ is found, the corresponding wave number is fairly computed solving explicitly the cubic equation (20). The idea proposed here is to build up an inexpensive approximation of $\mathbf{u}_m^{\text{opt}}$ using a postprocessing technique standard in error estimation analysis [19,8] and likely having all its features. This approximation is expressed as a nodal vector in the finer h-mesh and it is denoted by $\mathbf{u}^\star$. Once $\mathbf{u}^\star$ is obtained from $\mathbf{u}_H$, the corresponding wave number $\kappa_H^\star$ is readily computed solving the cubic equation (20) and hence $E^\star = \kappa - \kappa_H^\star$.

The enhanced solution is produced locally, in patches of elements, centered in every element of the mesh. The values of $\mathbf{u}_H$ at the nodes of the H-mesh are used as the input data and a polynomial is fitted using a least squares technique. The degree of the polynomial fitted is larger than the degree of the finite elements used to compute u_H. For every element Ω_n, $n = 1, \ldots, n_{\text{el}}$, of the H-mesh, the patch of elements surrounding Ω_n is considered. The polynomial fitting the values of u_H in the nodes of the patch is computed. Once the polynomial is obtained it is evaluated to find the nodal values of $u^\star$ in the nodes of the h-mesh lying in element Ω_n of the H-mesh. This is illustrated in Fig. 4. This approach allows to recover the natural curvatures of the solution coinciding with u_H at the nodes where it is computed. Calderón and Díez [6] describes the details of the least squares fitting strategy.

As it is shown in the numerical tests, this strategy provides a fair and inexpensive approximation $\mathbf{u}^\star$ of the optimal solution $\mathbf{u}_m^{\text{opt}}$ of the constrained modified problem (23), which is computationally unaffordable. The corresponding numerical wave number assessment and error estimate, $\kappa_H^\star$ and $E^\star$, perform well, similarly as the computationally unaffordable estimates κ_H and $\kappa_H^{\min}$.

The reference mesh in which $\mathbf{u}^\star$ is supported is described above as generated by h-refinement. Obviously, the p-refined analogous strategy is readily defined by just using a higher order H-mesh and by using the locally fitted polynomial to compute the nodal values of $u^\star$ in the p-refined discretization. As it is shown in the examples, the results produced by the p-refined solution are not as good. This is probably due to the loss of accuracy observed in parts of the frequency spectrum when using standard p-refinement, as suggested by Hughes and co-workers [7,10].

4.5. Correction factor introduced to account for the finite size h of the reference mesh

The estimates introduced in the previous section rely on a reference discretization of mesh size h which supposedly provides a more accurate solution than the computed H-approximation. In practice, h is far from being infinitesimal and it is taken as a subdivision of H, namely $h = H/n_r$ with relatively small values of n_r (in the examples $n_r = 2$) in order to lower the computational cost of the estimate.

Thus, in practice, the values of the assessed error are with respect to the numerical wave number corresponding to the h-mesh, κ_h. The different values of E obtained in the previous sections are approximations to $\kappa_h - \kappa_H$ and not to $\kappa - \kappa_H$ as it could be expected.

Here, a correction factor is introduced to account for this fact, based on a Richardson-like extrapolation strategy [16].

The a priori estimate (16), described in Section 3, is assumed to hold for both the H-mesh and the h-mesh, that is

$$\kappa - \kappa_h \approx \frac{\kappa^3 h^2}{24} \quad \text{and} \quad \kappa - \kappa_H \approx \frac{\kappa^3 H^2}{24}.$$

It follows that

$$\kappa_h - \kappa_H = \frac{\kappa^3}{24}(H^2 - h^2)$$

and using $h = H/n_r$ yields

$$\kappa_h - \kappa_H = \frac{\kappa^3 H^2}{24}\left(1 - \frac{1}{n_r^2}\right).$$

That is

$$\kappa - \kappa_H = \frac{n_r^2}{(n_r^2 - 1)}(\kappa_h - \kappa_H). \tag{25}$$

Thus, the factor $n_r^2/(n_r^2 - 1)$ (4/3 for $n_r = 2$) is used to correct the estimates which are, in principle, assessing the error with respect to κ_h. Using above correction, we are now able to estimate the error with respect to κ.

5. Local version

As previously said, once the recovered function $\mathbf{u}^\star$ is obtained, the estimate $E^\star$ is easily computed. Moreover, a local version of the estimator giving local values of the wave number and, hence, of the error is also straightforward. The goal is to approximate the value of the numerical wave number associated with the element Ω_n, $n = 1, \ldots, n_{\text{el}}$, of the H-mesh. Let us denote this value by κ_H^n. The idea is simply to minimize the local version of the squared residual (19) corresponding to a patch of elements around Ω_n. This approach is simple to implement and computationally inexpensive.

In order to obtain enough information and to properly recover κ_H^n, the patch of elements around Ω_n must be of size larger than a wavelength. This often requires using patches of more than one layer of elements around Ω_n. Fig. 5 illustrates both, the simplest case of a patch including just the first layer of elements around Ω_n and a second patch including two layers of elements, corresponding to a larger wave number.

Thus, the local version of the residual corresponding to patch n is

$$\mathbf{r}^n(\kappa^n) = \mathbf{a}_0^n + \mathbf{a}_1^n \kappa^n + \mathbf{a}_2^n (\kappa^n)^2, \tag{26}$$

where $\mathbf{r}^n$ is a function of κ^n and $\mathbf{a}_0^n$, $\mathbf{a}_1^n$ and $\mathbf{a}_2^n$ are defined as in Section 4, using $\mathbf{u}^\star$ as the modified function.

Then, the approximation for the local wave number κ_H^n is determined minimizing the squared local residual:

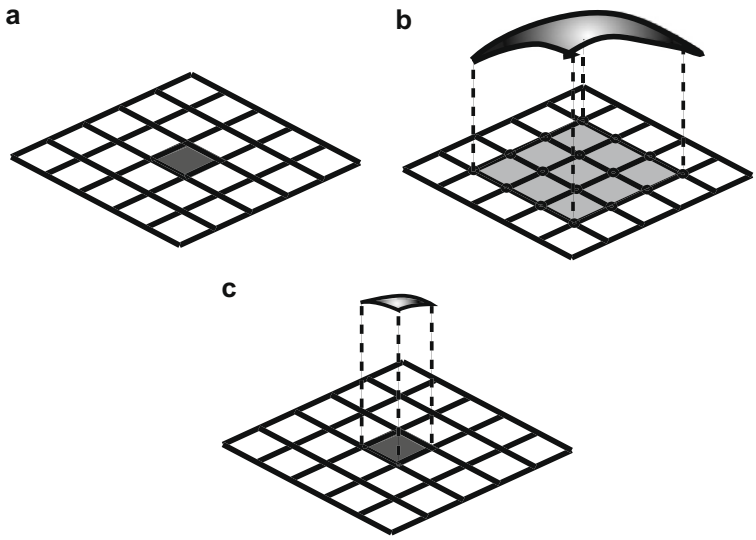

Fig. 4. Every element of the H-mesh (darkened in plot a) is associated with a patch (shadowed in plot b). A polynomial is fitted to the values in the nodes in this patch using a least squares criterion (b). This polynomial is evaluated to obtain the nodal values of the enhanced function $u^\star$ in the nodes of the refined h-mesh in the element under consideration (c).

$$\kappa_H^n := \arg\min_{\kappa^n}(\mathbf{r}^{n'}\mathbf{r}^n). \tag{27}$$

Recall that solving this minimization problem is a purely explicit calculation because it only requires finding the roots of (20).

6. Numerical examples

The strategy to assess the error in the wave number presented in the previous sections is validated in three numerical examples.

6.1. Example 1: 1D strip

The first example is a 1D problem solved in a rectangular domain as illustrated in Fig. 6. This simple case allows testing the performance of the estimates provided by comparing them with the actual values that, in this case, can be easily measured.

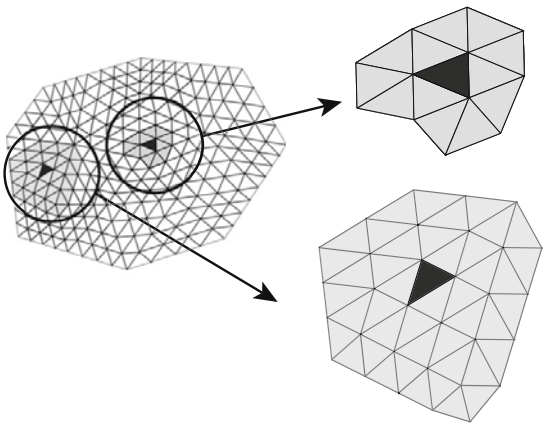

Fig. 5. Every element of the mesh (darkened) generates a patch of all the elements in contact with it (shadowed in gray). Two different patches are shown corresponding to required sizes associated with different wavelengths.

Eq. (3) is solved in the rectangular domain shown in Fig. 6, with $\rho c = 1$, $A_n = -1$ and $\kappa = 8\pi$ (such that the wavelength is 1/4 and therefore the solution has four complete waves in the domain of length $L = 1$).

Dirichlet boundary condition is imposed on the left side of the boundary, Eq. (5) with $\bar{u} = 1$, while Robin boundary condition (denoted also as ficticious boundary condition) is enforced on the right lateral side. The boundary condition on the upper and lower horizontal boundaries are assumed to be Neumann homogeneous to keep the 1D character of the solution.

The solution $u(x,y)$ of the problem is independent of y and its analytical expression is

$$u(x,y) = \cos(\kappa x) + i\sin(\kappa x).$$

This solution obviously fulfills (3), with Dirichlet boundary conditions (5) and Robin boundary conditions (7), respectively

$$u(0,y) = 1 \quad \text{at } x = 0,$$
$$\frac{\partial u}{\partial x}(1,y) = i\kappa u(1) \quad \text{at } x = 1.$$

Having at hand the analytical expression for $u(x,y)$ allows computing a direct measure of the error in the wave number or, conversely, in the wavelength. Let u_H^L be the average value of the real part of the numerical solution at $x = L$ (for uniform quadrilateral meshes all the

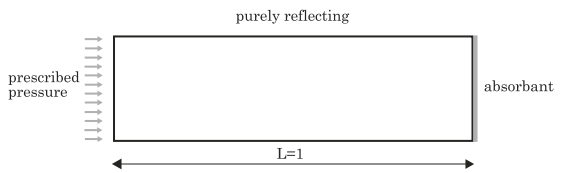

Fig. 6. Example 1. 1D strip: problem setup.

nodal values are equal on this line). Then the error in wavelength is denoted by $\Delta\lambda$ and satisfies

$$u(x = L - \Delta\lambda) = u_H^L \tag{28}$$

taking the real part of above equation, we obtain

$$\cos(\kappa(L - \Delta\lambda)) = \mathrm{Re}(u_H^L) \Rightarrow \Delta\lambda = -\frac{\arccos(u_H^L)}{\kappa} + L. \tag{29}$$

The wavelength error $\Delta\lambda$ is equally distributed among the n periods present in the domain, where $n = L/\lambda$ and $\lambda = 2\pi/\kappa$. Thus the measure of numerical wavelength is $\lambda_H = \lambda + \Delta\lambda/n$ and, consequently

$$\kappa_H^{\mathrm{meas}} = \frac{2\pi}{\lambda_H}. \tag{30}$$

Thus, the resulting a posteriori measure of the dispersion is

$$E^{\mathrm{meas}} = \kappa - \frac{2\pi}{\left(\lambda + \frac{\Delta\lambda}{n}\right)}, \tag{31}$$

where $\Delta\lambda$ is given by (29).

The problem is numerically approximated using quadrilateral meshes (4-noded bilinear elements), starting from a coarse mesh of 24×2 elements (in the x-direction $H = 1/24$, i.e. 6 elements per wavelength. The corresponding approximation is depicted in Fig. 7).

The error estimates described in the previous sections are computed using a refinement factor $n_r = 2$ in order to reduce the computational cost.

The numerical results are summarized in Tables 1–3. Each row in the tables corresponds to a different mesh. Due to the 1D character of the problem the meshes are only refined in the x-direction. The consecutive meshes have two rows of elements. The size of the element in the x-direction is therefore $H = 2/n_{\mathrm{el}}$. The different value for κ_H are displayed in Table 1, that is $\kappa_H^{\mathrm{pri}}, \kappa_H^{\mathrm{meas}}, \kappa_H^{\mathrm{int}}, \ldots, \kappa_H^{\star}$ corresponding to the notation introduced above. Table 2 shows the corresponding error estimates and the effectivity indices with respect to the measured value, namely

$$\theta^{\square} = \frac{E^{\square}}{E^{\mathrm{meas}}}. \tag{32}$$

Table 3 is analogous to Table 2 but for a p-refined reference discretization, where the correction factor introduced in Section 4.5 cannot be applied.

The analysis of the results of Tables 1–3 reveals that the estimate E and E^{min} are yielding very good approximations of the actual error E^{meas}. Recall however that these two quantities are not computationally affordable in a practical context and have been produced only as an academic illustration of the presented paradigm. The two practical estimates E^{int} and $E^{\star}$ are also showing a good behavior, especially if the reference mesh is build up using h-refinement (Table 2). When using p-refinement (Table 3), the effectivity is degraded probably due to the effect suggested at the end of Section 4.4. It is worth noting that the estimate $E^{\star}$ is, as expected, sharper than E^{int}.

The convergence of the dispersion error when reducing H is shown in Fig. 8. Note that the horizontal axis in these plots corresponds to $\log \mathrm{dof}$ which is equal to $-\log H$ up to an additive constant. The plot on the top describes the convergence behavior for the estimates taking as a reference solution an h-refined one. The second plot is the analogous with a p-refined reference solution. The results demonstrate that all the proposed estimates converge at the due rate, compared with the a priori and the measured dispersion errors. Moreover, the h-refined reference mesh estimates yields sharper results than the p-refined ones in all the tests.

Finally, the spatial error distribution corresponding to the local (elementary) contributions to the dispersion error as described in Section 5 is displayed in Fig. 9. The second plot corresponds to a variant of the problem where the Dirichlet boundary conditions

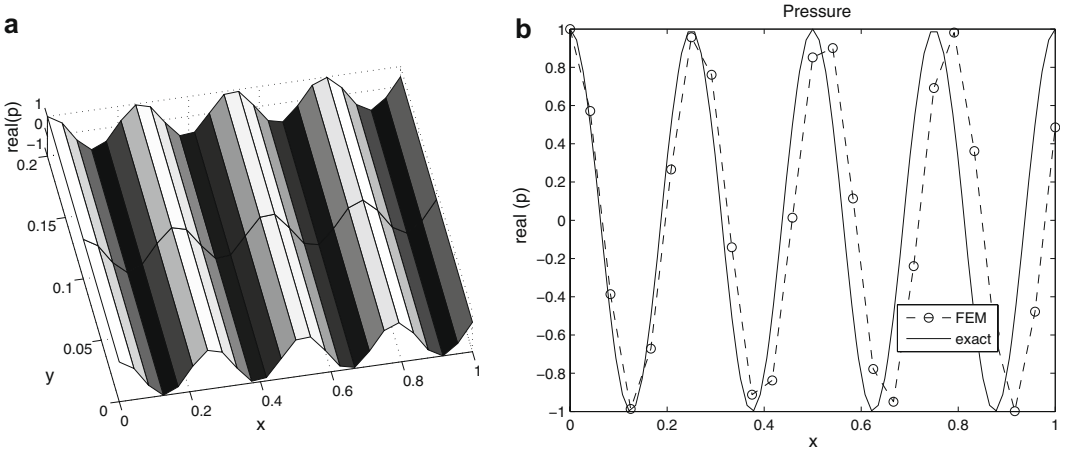

Fig. 7. Distribution pressure (a) and dispersion effect (b) for wave number $\kappa = 8\pi$ in a structured quadrilateral mesh.

Table 1
Example 1: Degrees of freedom dof; number elements n_{el}; interval of mesh H and wave numbers κ_H.

dof	n_{el}	H	κ_H^{pri}	κ_H^{meas}	κ_H^{int}	κ_H	κ_H^{min}	$\kappa_H^{\star}$
75	48	1/24	23.9844	24.1126	24.4287	24.3595	24.3622	24.3643
99	64	1/32	24.4868	24.5196	24.6672	24.6795	24.6788	24.6989
123	80	1/40	24.7193	24.7315	24.7980	24.8295	24.8346	24.8610
147	96	1/48	24.8456	24.8513	24.8773	24.9195	24.9233	24.9497

Table 2
Example 1: Values of the relative dispersion error (%) a priori, measured and for the case h-refined solution with the respective effectivity indices.

dof	E^{pri}	E^{meas}	E^{int}	θ^{int}	E	θ	$E^{\min}$	$\theta^{\min}$	$E^{\star}$	$\theta^{\star_h}$
75	4.569	4.059	3.734	0.92	4.102	1.01	4.089	1.00	4.077	1.00
99	2.570	2.439	2.469	1.01	2.405	0.98	2.408	0.98	2.301	0.94
123	1.644	1.596	1.774	1.11	1.609	1.08	1.582	0.99	1.442	0.90
147	1.142	1.119	1.354	1.21	1.131	1.01	1.111	0.99	0.971	0.87

Table 3
Example 1: Values of wave numbers and relative dispersion error (%) correspondent to solution p-refined and the respective effectivity indices.

dof	κ_H	E	θ	$\kappa_H^{\min}$	$E^{\min}$	$\theta^{\min}$	$\kappa_H^{\star}$	$E^{\star}$	$\theta^{\star}$
75	24.0995	4.111	1.01	24.1088	4.074	1.00	23.4682	6.623	1.63
99	24.5295	2.400	0.98	24.5311	2.394	0.98	24.1255	4.007	1.64
123	24.7295	1.605	1.00	24.7324	1.593	0.99	24.4709	2.633	1.65
147	24.8495	1.127	1.00	24.8514	1.119	0.99	24.6703	1.839	1.64

at the left side are replaced by Neumann type boundary condition. It is worth noting that the local contributions to the dispersion error are, as expected, sensitive to the selected boundary conditions.

6.2. Example 2: 2D acoustic problem in L-shaped domain

The second example has a full 2D character. The L-shaped domain shown in Fig. 10 is considered. The size of the domain is set by the values $L_1 = 0.8$ m and $L_2 = 0.2$ m. Most of the domain boundary is of Neumann type, homogeneous everywhere on the boundary except on the top left edge where the velocity is prescribed to be $\bar{v}_n = 1$ m/s (this corresponds to a vibrating panel, see Fig. 10). Moreover, the bottom side is an absorbent material, corresponding to a Robin boundary condition (7) with $A_n = 1/\rho c$ m/Pa s.

The wave number is $\kappa = 8\pi$, as in the previous example. The solution computed with a coarse mesh is displayed in Fig. 11.

The estimates $E, E^{\min}$ and $E^{\star}$ are computed for three series of refined meshes; structured quadrilaterals, structured triangles and unstructured triangles. The results are displayed in Tables 4–6, respectively. The practical error estimate $E^{\star}$ produces values that are reasonable approximations of the more accurate but computationally unaffordable estimates E and $E^{\min}$.

The convergence of the different series of refined meshes is shown in Fig. 12. Note that in this 2D case the relation between the number of degrees of freedom (dof) and H is different, dof is proportional to $1/H^2$, i.e. $\log \text{dof}$ is equal to $-2\log H$ up to an additive constant.

One can observe in the plots of Fig. 12 that the estimate $E^{\star}$ is behaving similarly to the reference estimates E and $E^{\min}$.

The slope of the curves given by E and $E^{\min}$ is (approximately) equal to 1 as predicted by the a priori estimate and the slopes associated with $E^{\star}$ are 0.96, 0.71 (discrepancy due to a bad result in the first coarse approximation in the series of structured triangular

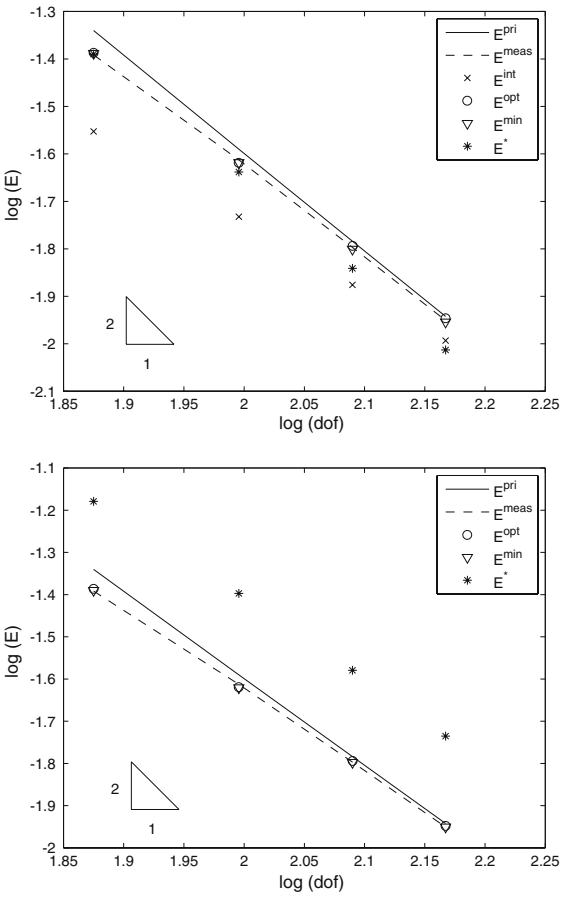

Fig. 8. Example 1: Convergence of the error for the h-refined reference mesh (top) and the p-refined reference mesh (bottom).

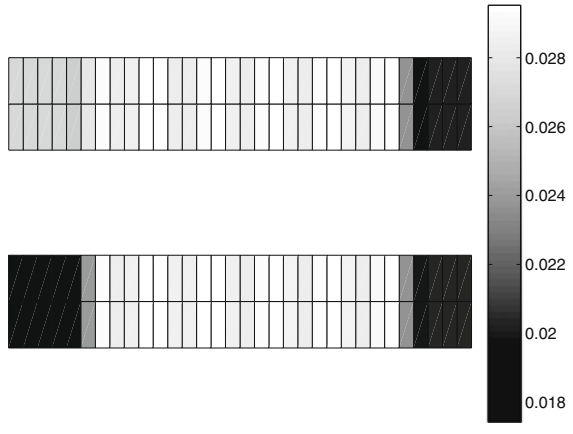

Fig. 9. Example 1: Spatial error distribution of the error for the problem for stated in Fig. 6 (top) and for a variant with Neumann boundary condition of the left side (bottom).

Table 4
Example 2: Results corresponding to structured quadrilateral meshes.

dof	n_{el}	κ_H	E	κ_H^{min}	E^{min}	$\kappa_H^\star$	$E^\star$
57	36	22.9895	8.528	21.8287	13.146	22.7910	9.317
185	144	24.0795	4.191	24.1039	4.093	24.1424	3.940
657	576	24.8395	1.167	24.8507	1.122	24.9077	0.895

Table 5
Example 2: Results corresponding to structured triangular meshes.

dof	n_{el}	κ_H	E	κ_H^{min}	E^{min}	$\kappa_H^\star$	$E^\star$
57	72	22.6195	10.000	22.5721	10.189	23.9924	4.537
185	288	24.1895	3.753	24.2237	3.617	24.3199	3.234
657	1152	24.8495	1.127	24.8734	1.032	24.9306	0.804

Table 6
Example 2: Results corresponding to unstructured triangular meshes.

dof	n_{el}	κ_H	E	κ_H^{min}	E^{min}	$\kappa_H^\star$	$E^\star$
81	120	22.6195	10.000	22.7151	9.619	23.6310	5.975
281	480	24.3095	3.276	24.3470	3.126	24.5641	2.262
1041	1920	24.9095	0.889	24.9193	0.849	25.0092	0.492

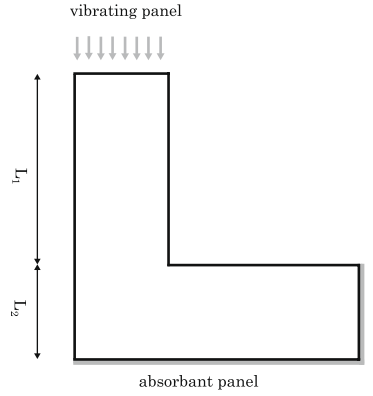

Fig. 10. Example 2: 2D L-shaped domain and boundary conditions.

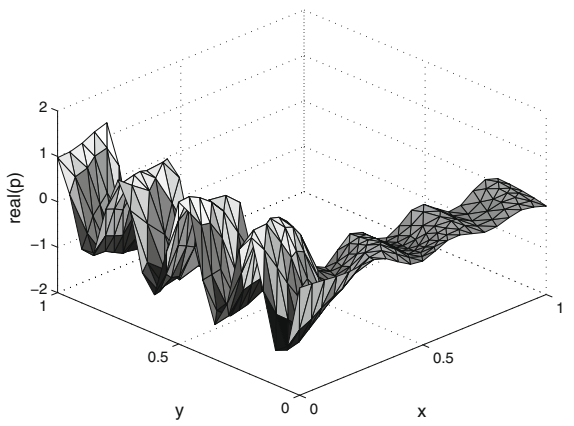

Fig. 11. Example 2: Real part of the acoustic pressure computed with an unstructured triangular mesh of 281 dof and 480 elements.

meshes) and 0.98 for the different mesh typologies. Fig. 13 shows the spatial error distribution for the second mesh of each of the

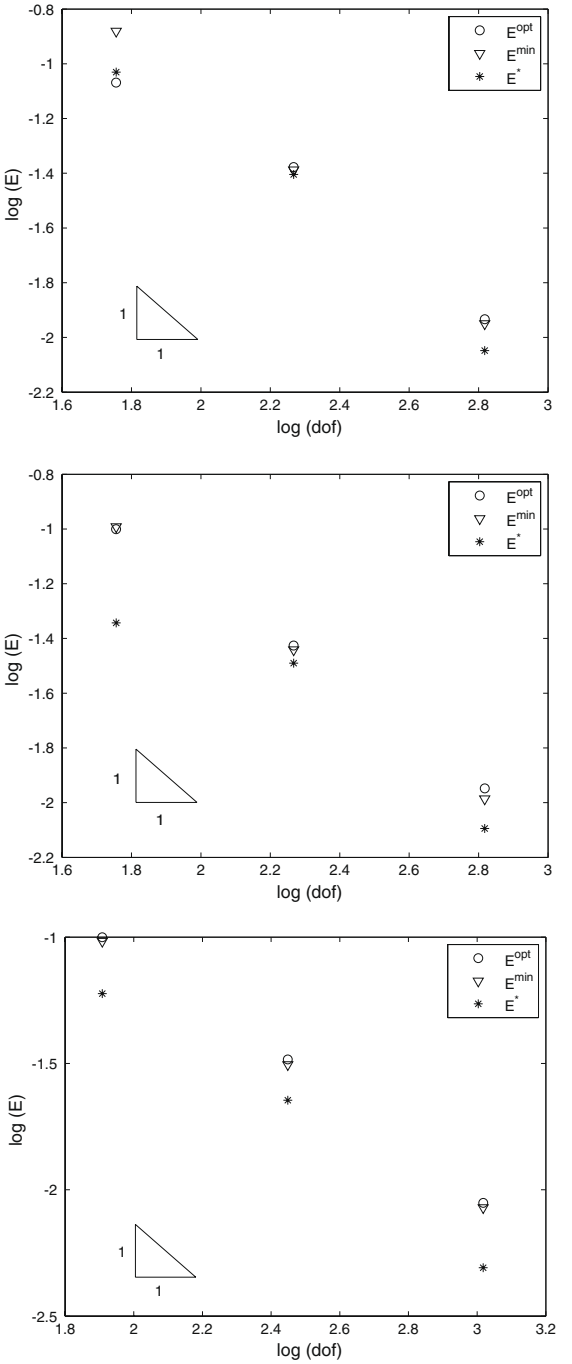

Fig. 12. Example 2: Convergence of the error in the structured quadrilateral (top), structured triangular (center) and unstructured triangular (bottom) series of meshes.

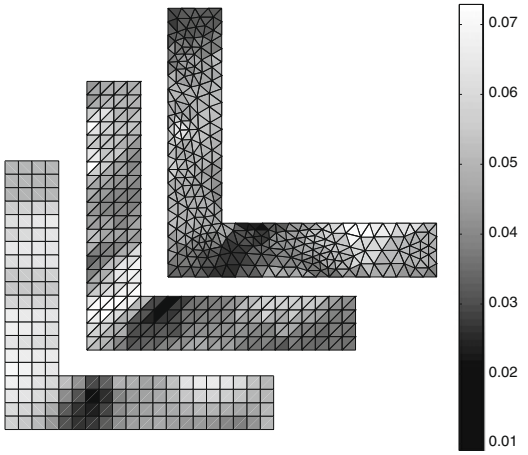

Fig. 13. Example 2: Spatial error distribution for the problem defined in Fig. 10 in structured quadrilateral and triangular and unstructured triangular meshes.

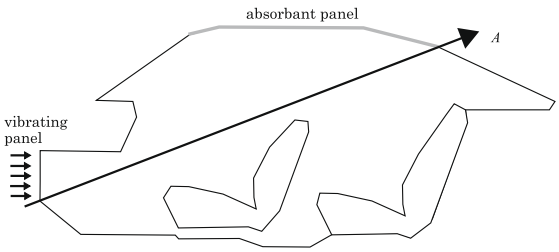

Fig. 14. Example 3: Description of boundary conditions for the car cavity.

refinement series (meshes with 144 structured quadrilaterals, 288 structured triangles and 480 unstructured triangles).

6.3. Example 3: 2D acoustic car cavity

Noise transmission inside the interior of passenger cars is considered as a practical application. This example has been frequently used as a benchmark in error assessment for interior acoustics [5,18].

The size of the domain is characterized by the maximum horizontal and vertical lengths, $L_x = 2.7$ m and $L_y = 1.1$ m, respectively. The values of the material parameters are $\rho = 1.225$ kg/m^3 (density) and $c = 340$ m/s (speed of sound). Fig. 14 describes the geometry of the domain and the boundary conditions: a unit normal velocity $\bar{v}_n = 1$ m/s is imposed on the left vertical side. The roof is considered to be an absorbent panel with $A_n = \frac{1}{2000}$ m/Pa s and the rest of the boundary is assumed to be perfectly reflecting ($\bar{v}_n = 0$).

The wave number of the incoming vibrations $\kappa = 9.7$ corresponds to a frequency of 525 Hz. Fig. 15 shows the distribution of the real part of the pressure and the pressure distribution along of the line A displayed in Fig. 14. The two curves correspond to a coarse and a finer computational meshes. Note that, compared with the finer mesh, the dispersion error in the coarse mesh is important.

The strategy to asses the dispersion error introduced in this paper is used in a series of uniformly refined FE meshes. The results are shown in Table 7 and Fig. 16. The estimate $E^\star$ is showing again

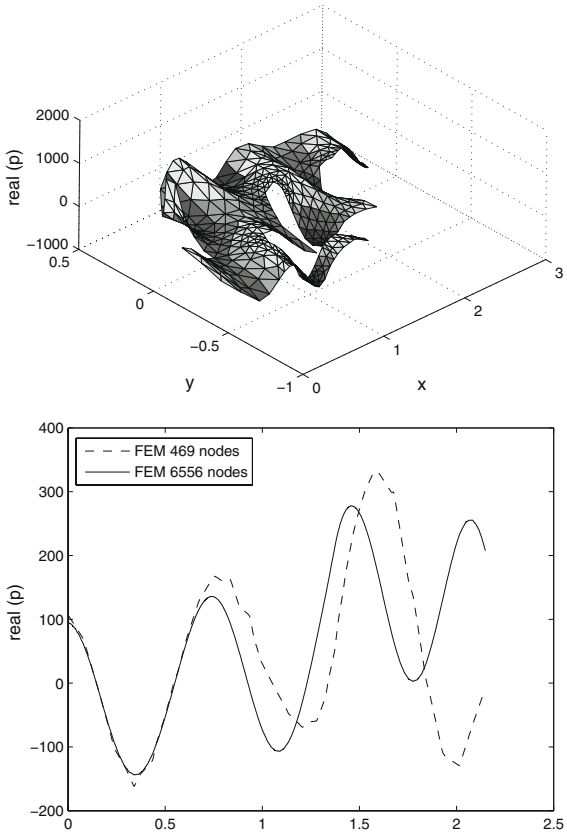

Fig. 15. Example 3: Solution of the pressure field (top) and dispersion effect (bottom) for 525 Hz.

Table 7
Example 3: Results corresponding to $\kappa = 9.7$, dispersion error in a uniformly refined series of meshes.

dof	n_{el}	κ_H	E	κ_H^{min}	E^{min}	$\kappa_H^\star$	$E^\star$
137	195	9.0618	6.598	9.0831	6.378	8.5908	11.452
469	780	9.5318	1.754	9.5363	1.708	9.5203	1.872
1718	3120	9.6518	0.517	9.6507	0.529	9.6534	0.501

a good performance, fairly approximating the academic estimates E and E^{min} and converging at the proper rate (the slope of the line is approximately 1.2). Finally, the error map is displayed in Fig. 17 and the larger contributions to the error are located at the expected zones.

An additional numerical experiment is performed for the same problem as described above but for a larger frequency of 1100 Hz, that is a wave number $\kappa = 20.3280$. The results obtained are displayed in Table 8. The quality of the estimates is also fair for this larger frequency. A good agreement is observed between the reference value E and the estimates E^{min} and $E^\star$.

7. Concluding remarks

The strategy introduced is based on the determination of the numerical wave number κ_H as the wave number of a modified problem that better accommodates the numerical solution u_H.

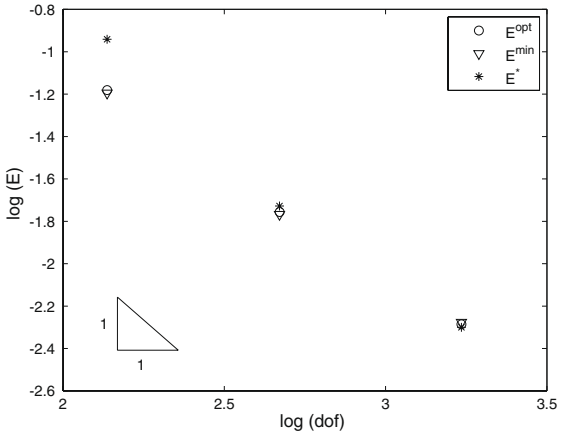

Fig. 16. Example 3: Convergence of the error.

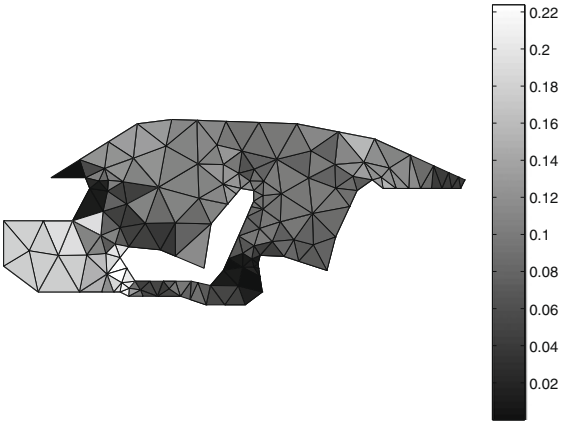

Fig. 17. Example 3: Map of the error for the car cavity problem in an mesh unstructured triangular of 137 dof.

Table 8
Example 3: Results corresponding to $\kappa = 20.328$, dispersion error in a uniformly refined series of meshes.

dof	n_{el}	κ_H	E	κ_H^{min}	E^{min}	$\kappa_H^{\star}$	$E^{\star}$
469	780	18.7052	7.983	18.8382	7.328	18.8105	7.465
1718	3120	19.9152	2.031	19.9200	2.007	19.8178	2.509

The modified problem is defined on a reference refined discretization because the resolution has to be increased to properly describe the oscillatory nature of the solution. Compared to other goal oriented error estimation strategies, the approach proposed here is innovative because it adopts a new paradigm. The computational effort in the error estimation procedure is devoted to obtain the wave number of the approximate solution κ_H instead of the exact one, κ, which is known as a problem data. The error estimator provides reasonable approximations of the actual errors, in agreement also with the measured valued of the dispersion error in the simple cases where they can be evaluated. In the practical cases the results match the expected distributions and converge at the predicted rates.

References

[1] M. Ainsworth, J.T. Oden, A Posteriori Error Estimation in Finite Element Analysis, John Wiley & Sons, Chichester, 2000.
[2] I. Babuska, F. Ihlenburg, E.T. Paik, S.A. Sauter, A generalized finite element method for solving the Helmholtz equation in two dimensions with minimal pollution, Comput. Methods Appl. Mech. Engrg. 128 (1995) 325–359.
[3] I. Babuska, J.M. Melenk, The partition of unity method, Int. J. Numer. Methods Engrg. 40 (1997) 727–758.
[4] I. Babuska, S.A. Sauter, Is the pollution effect of the FEM avoidable for the Helmholtz equation considering high wavenumber?, SIAM Rev 42 (3) (2000) 451–484.
[5] P. Bouillard, F. Ihlenburg, Error estimation and adaptivity for the finite element method in acoustics: 2d and 3d applications, Comput. Methods Appl. Mech. Engrg. 176 (1) (1999) 147–163.
[6] G. Calderón, P. Díez, Análisis de diferentes estimadores de error de postproceso para adaptatividad orientada al resultado, Rev. Int. Mét. Num. Cálc. Dis. Ing. 22 (2) (2006) 193–213.
[7] J.A. Cottrell, A. Reali, Y. Bazilevs, T.J.R. Hughes, Isogeometric analysis of structural vibrations, Comput. Methods Appl. Mech. Engrg. 195 (41–43) (2006) 5257–5296.
[8] P. Díez, G. Calderón, Goal-oriented error estimation for transient parabolic problems, Comput. Mech. 39 (5) (2007) 631–646.
[9] P. Díez, J.J. Egozcue, A. Huerta, A posteriori error estimation for standard finite element analysis, Comput. Methods Appl. Mech. Engrg. 163 (1998) 141–157.
[10] T.J.R. Hughes, A. Reali, G. Sangalli, Duality and unified analysis of discrete approximations in structural dynamics and wave propagation: Comparison of *p*-method finite elements with *k*-method NURBS, Comput. Methods Appl. Mech. Engrg. 197 (49–50) (2008) 4104–4124.
[11] F. Ihlenburg, Finite Element Analysis of Acoustic Scattering, Applied Mathematical Sciences, vol. 132, Springer-Verlag, New York, 1998.
[12] F. Ihlenburg, I. Babuska, Dispersion analysis and error estimation of Galerkin finite element methods for the Helmoholtz equation, Int. J. Numer. Methods Engrg. 38 (1995) 3745–3774.
[13] F. Ihlenburg, I. Babuska, Finite element solution of the Helmholtz equation with high wave number: Part 1. The *hp*-version of the FEM, Comput. Math. Appl. 38 (1995) 9–37.
[14] J.T. Oden, S. Prudhomme, Goal-oriented error estimation and adaptivity for the finite element method, Comput. Math. Appl. 41 (5–6) (2001) 735–756.
[15] N. Parés, P. Díez, A. Huerta, Subdomain-based flux-free a posteriori error estimators, Comput. Methods Appl. Mech. Engrg. 195 (4–6) (2006) 297–323.
[16] L.F. Richardson, The approximate arithmetical solution by finite differences of physical problems, Trans. Roy. Soc. London, A 210 (1910) 307–357.
[17] J. Sarrate, J. Peraire, A.T. Patera, A posteriori finite element error bounds for non-linear outputs of the Helmholtz equation, Int. J. Numer. Methods Fluid 31 (1) (1999) 17–36.
[18] S. Suleau, A. Deraemaeker, P. Bouillard, Dispersion and pollution of meshless solutions for the Helmholtz equation, Comput. Methods Appl. Mech. Engrg. 190 (2000) 639–657.
[19] N.-E. Wiberg, L.F. Zeng, X.D. Li, Error estimation and adaptivity in elastodynamics, Comput. Methods Appl. Mech. Engrg. 101 (1992) 369–395.

Estimation of the dispersion error in the numerical wave number of standard and stabilized finite element approximations of the Helmhotz equation

Steffens, L. M., Parés N., and Díez P.

International Journal for Numerical Methods in Engineering

Accepted for publication, 2010

INTERNATIONAL JOURNAL FOR NUMERICAL METHODS IN ENGINEERING
Int. J. Numer. Meth. Engng 2009; **00**:1 *Prepared using* nmeauth.cls *[Version: 2000/01/19 v2.0]*

Estimation of the dispersion error in the numerical wave number of standard and stabilized finite element approximations of the Helmholtz equation

Lindaura Maria Steffens, Núria Parés and Pedro Díez*

Laboratori de Càlcul Numèric (LaCàN)
Universitat Politècnica de Catalunya, Barcelona, Spain
C2 Campus Nord UPC, E-08034 Barcelona

SUMMARY

An estimator for the error in the wave number is presented in the context of finite element approximations of the Helmholtz equation. The proposed estimate is an extension of the ideas introduced in [28]. In the previous work, the error assessment technique was developed for standard Galerkin approximations. Here, the methodology is extended to deal also with stabilized approximations of the Helmholtz equation. Thus, the accuracy of the stabilized solutions is analyzed, including also their sensitivity to the stabilization parameters depending on the mesh topology. The procedure builds up an inexpensive approximation of the exact solution, using post-processing techniques standard in error estimation analysis, from which the estimate of the error in the wave number is computed using a simple closed expression. The recovery technique used in [28] is based in a polynomial least squares fitting. Here a new recovery strategy is introduced, using exponential (in a complex setup, trigonometric) local approximations respecting the nature of the solution of the wave problem.

KEY WORDS: Wave problems; Helmholtz equation; A posteriori error estimation; Error estimation of wave number; Dispersion/pollution error; Stabilized methods.

1. INTRODUCTION

Acoustic wave propagation phenomena are often modeled using the Helmholtz equation, assuming a harmonic character of the solution. Thus, time-dependent acoustic pressure is represented as $p(\mathbf{x}, t) = u(\mathbf{x})e^{i\omega t}$ for a given angular frequency ω, and the unknown $u(\mathbf{x})$ is the spatial distribution of the pressure. Function $u(\mathbf{x})$ is the solution of the Helmholtz equation, with an associated wave number $\kappa = \omega/c$, c being the speed of sound [22].

*Correspondence to: pedro.diez@upc.edu (P. Díez)), URL: http://www-lacan.upc.edu, Tel: +34934017240, Fax: +34 934011825
†Partially supported by Ministerio de Educación y Ciencia, Grants DPI2007-62395 and BIA2007-66965; Programme Alβan, the European Union Programme of High Level Scholarships for Latin America, scholarship no. E06D100641BR.

Contract/grant sponsor: Publishing Arts Research Council; contract/grant number: 98–1846389

Received **
Revised **

Galerkin approximations of the Helmholtz equation are affected by dispersion (or pollution) errors, that may be important especially if the wave number is large with respect to the mesh size. The pollution error, as opposed to the standard interpolation error, is global in nature because the error sources affect (pollute) the solution everywhere in the domain, and not only where the resolution of the mesh is not sufficient to properly approximate the solution. Thus, the pollution error cannot be removed by local refinement, even if the quantity to be assessed is defined locally.

The effect of the pollution or dispersion error has been extensively addressed in the literature [23, 24, 2, 22, 16, 6, 1] and a priori estimates for the dispersion error are available. Also, a posteriori error estimates assessing the accuracy of the Finite Element approximations of the Helmholtz equation either in global norms or in certain quantities of interest have been proposed [26, 25, 8, 9, 27, 4, 3, 29, 30]. However, the issue of measuring the dispersion error of the approximations of the Helmholtz equation using a posteriori error estimates was first addressed in [28].

The wave number corresponding to the approximate solution is different than the exact one. The corresponding error is directly related with the dispersion error and it is, according to practitioners, a good measure in order to assess the overall quality of the numerical solution. The problem of assessing the error in the wave number is addressed in [28] for standard finite element (Galerkin) approximations. The proposed error estimation strategy is paradoxical in the sense that, in the error to be assessed, the obvious information is the exact value κ and all the efforts are devoted to compute the value of the wave number corresponding to the approximate solution. Note that in the usual error estimation business the situation is the opposite: the approximate value is available and the exact value has to be estimated.

In practice, standard Galerkin methods are not competitive for high wave numbers because controlling the pollution effect requires using extremely fine meshes. Numerous approaches alleviating this deficiency have been proposed based on modifications of the classical Galerkin approximation [2, 5, 15, 18]. The Galerkin/Least-squares method is one of the most popular techniques. It provides a significant reduction in the dispersion error with an extremely simple implementation using only standard resources available in finite element codes [17].

Stabilized formulations allow eliminating the pollution effect for one-dimensional problems. In two dimensions, the pollution effect is reduced substantially but it cannot be completely eliminated [6]. Thus, also when using stabilized formulations, the end-user of a finite element acoustic computation is concerned with the accuracy of the solution in terms of the dispersion. In this work, an extension of [28] is proposed allowing to assess the dispersion error when the approximate solution is computed either using the standard Galerkin method or the GLS method.

The assessment of the dispersion error aims at obtaining a good estimate of the value of the *numerical wave number*, corresponding to the approximate solution. Here the definition of the numerical wave number provided in [28], based on the idea of fitting the numerical solution into a modified equation, is adopted. This strategy requires obtaining an inexpensive approximation of the solution of the modified problem using post-processing techniques. Here, a new recovery technique is introduced, using exponential functions rather than polynomials, to take advantage of the nature of the solutions of wave propagation problems.

The remainder of the paper is structured as follows. Section 2 introduces the notation and the description of the problem to be solved along with the standard and stabilized Galerkin formulations. Section 3 describes the main ideas of the paper. First, the basics of the dispersion error assessment are reviewed. Then, the extension to stabilized formulations is described. Finally, the standard polynomial recovery is recalled and the novel exponential post-processing technique is introduced. Section 4 contains four numerical examples demonstrating the efficiency of the proposed technique both in academic and practical examples.

2. PROBLEM STATEMENT

2.1. Acoustic modeling: the Helmholtz equation

The acoustic pressure $u(\mathbf{x})$ is a complex function taking values in the spatial domain $\Omega \subset \mathbb{R}^d$ (being $d = 1$, 2 or 3). The function u is determined as the solution of the Helmholtz equation

$$-\Delta u - \kappa^2 u = f \quad \text{in } \Omega, \tag{1}$$

which is stated for a given wave number κ as the Fourier transform of the transient wave equation. Equation (1) has to be complemented with proper boundary conditions on $\partial\Omega$. For interior problems, three types of boundary conditions are considered: Dirichlet, Neumann and Robin (or mixed). Thus, the boundary $\partial\Omega$ is partitioned into three disjoint sets Γ_{D}, Γ_{N} and Γ_{R} such that $\partial\Omega = \overline{\Gamma_{\mathrm{D}} \cup \Gamma_{\mathrm{N}} \cup \Gamma_{\mathrm{R}}}$ and its associated boundary conditions are

$$u = \bar{u} \qquad \text{on } \Gamma_{\mathrm{D}}, \tag{2a}$$

$$\boldsymbol{\nabla} u \cdot \mathbf{n} = g \qquad \text{on } \Gamma_{\mathrm{N}}, \tag{2b}$$

$$\boldsymbol{\nabla} u \cdot \mathbf{n} = \mathcal{M} u \qquad \text{on } \Gamma_{\mathrm{R}}, \tag{2c}$$

where $\mathbf{n}$ is the outward normal to Ω and $\bar{u}$, f, g and $\mathcal{M}$ are the prescribed data, which are assumed to be sufficiently smooth.

Remark 1. *For interior acoustic wave propagation problems $g = -i\rho c\kappa\bar{v}_n$ and $\mathcal{M}u = -i\rho c\kappa A_n u$, where c is the speed of sound in the medium, ρ is the mass density, $\bar{v}_n$ corresponds to the normal velocity of a vibrating wall producing the sound that propagates within the medium and the coefficient A_n is the admittance and represents the structural damping. For exterior problems, reduced to fictitious domains, $\mathcal{M}$ is a linear operator called the Dirichlet-to-Neumann (DtN) map relating Dirichlet data to the outward normal derivative of the solution on the fictitious boundary Γ_{R}. It is worth noting that in general the data g and $\mathcal{M}$ depend on the wave number κ. A notation explicitly stating the dependence of κ, for instance $g(\kappa)$ and $\mathcal{M}(\kappa)$, would be more accurate but for the sake of simplicity this dependence is omitted in the notation.*

The boundary value problem defined by equations (1) and (2) is readily expressed in its weak form introducing the solution and test spaces $\mathcal{U} := \{u \in \mathcal{H}^1(\Omega), u|_{\Gamma_{\mathrm{D}}} = \bar{u}\}$ and $\mathcal{V} := \{v \in \mathcal{H}^1(\Omega), v|_{\Gamma_{\mathrm{D}}} = 0\}$. Here $\mathcal{H}^1(\Omega)$ is the standard Sobolev space of complex-valued square integrable functions with square integrable first derivatives. The weak form of the problem then reads: find $u \in \mathcal{U}$ such that

$$a(\kappa; u, v) = l(\kappa; v) \quad \forall v \in \mathcal{V}, \tag{3}$$

where

$$a(\kappa; u, v) := \int_\Omega \nabla u \cdot \nabla \tilde{v}\, d\Omega - \int_\Omega \kappa^2 u \tilde{v}\, d\Omega - \int_{\Gamma_{\mathrm{R}}} \mathcal{M} u \tilde{v}\, d\Gamma,$$

$$l(\kappa; v) := \int_\Omega f \tilde{v}\, d\Omega + \int_{\Gamma_{\mathrm{N}}} g \tilde{v}\, d\Gamma,$$

the symbol $\tilde{\cdot}$ denotes the complex conjugate, $a(\kappa; \cdot, \cdot)$ is a sesquilinear form and $l(\kappa; \cdot)$ is an antilinear functional depending on κ through the Neumann boundary conditions g. The notation adopted marks the explicit dependence of κ on the forms $a(\kappa; \cdot, \cdot)$ and $l(\kappa; \cdot)$. Although not standard, this is useful in the following to assess the error in the wave number. It is worth noting that the sesquilinear form

$a(\kappa;\cdot,\cdot)$ is not elliptic but it satisfies the inf-sup condition and the Gärding inequality. However, for large wave numbers κ, the upper bound for the inf-sup condition is too crude [22]. Moreover, the inf-sup property is not carried over from $\mathcal{V}$ to a discrete subspace yielding to a loss of stability which produces spurious dispersion in the discrete approximations.

2.2. Galerkin finite element approximation

The Galerkin approximation is obtained from a partition $\mathcal{T}_H$ of the domain Ω into nonoverlapping elements and introducing the discrete spaces $\mathcal{U}_H \subset \mathcal{U}$ and $\mathcal{V}_H \subset \mathcal{V}$ associated with the parameters of the discretization, namely the characteristic element size H, and the degree of the polynomial approximation inside the elements p. The discrete finite element solution is then $u_H \in \mathcal{U}_H$ such that

$$a(\kappa; u_H, v) = l(\kappa; v) \quad \forall v \in \mathcal{V}_H. \tag{4}$$

In practice, low-order Galerkin approximations to the Helmholtz equation involving high wave numbers are corrupted by large dispersion or pollution errors due to the loss of stability of $a(\kappa;\cdot,\cdot)$. The wave number κ characterizes the oscillatory behavior of the exact solution: the larger the value of κ, the stronger the oscillations. Hence the *rule of thumb* is used in computations: each wavelength is resolved by a certain fixed number of elements. For linear elements, the rule of thumb is stated as $\kappa H = \text{constant} < 1$. However, it is widely known that this rule is not sufficient to obtain reliable results for large κ. The dispersion error, which is related to the phase lag of the FE-solution, can only be controlled when $\kappa^2 H/p$ is small. This undermines the practical utility of the Galerkin finite element method since severe mesh refinement is needed for large wave numbers. The performance of finite element computations at high wave numbers can be improved by using stabilization techniques. These techniques, which are extremely simple to implement, alleviate the dispersion effect of the finite element solution without requiring mesh refinement.

2.3. Galerkin/Least-squares finite element approximation

Stabilized finite element methods were originally developed for fluid problems [14]. The first upwind type stabilized methods [20] subsequently gave rise to consistent stabilization techniques – ensuring that the exact solution u is also a solution of the weak stabilized problem. Among these techniques, the Galerkin/Least-squares method (GLS) has been successfully applied both to fluids and to the Helmholtz equation [21, 19].

The idea behind stabilized finite element methods is to modify the variational form $a(\kappa;\cdot,\cdot)$ (and, accordingly, the right hand side) in such a way that the new variational form is *unconditionally stable*. In particular, the weak form of consistent stabilized methods is obtained from (3) by adding extra terms over the element interiors which are a function of the residual of the differential equation to ensure consistency. For instance, the additional stabilization terms of the GLS method are an element-by-element weighted least-squares formulation of the original differential equation.

The weak form of the GLS method associated with the partition $\mathcal{T}_H$ is: find $u \in \mathcal{U}$ such that

$$a(\kappa; u, v) + (\mathcal{L}u - f, \tau_H \mathcal{L}\tilde{v})_{\widehat{\Omega}} = l(v) \quad \forall v \in \mathcal{V}, \tag{5}$$

where $\mathcal{L}u = -\Delta u - \kappa^2 u$ is the indefinite Helmholtz operator, $\widehat{\Omega} = \bigcup_{n=1}^{n_{\text{el}}} \Omega_n$ denotes the union of element interiors of $\mathcal{T}_H$, n_{el} being the number of elements of $\mathcal{T}_H$, and $(\cdot,\cdot)_{\widehat{\Omega}}$ is the reduced L^2 inner product, where integration is carried out only on the element interiors (i.e., the singularities at interelement boundaries are suppressed in the reduced inner product). Note that the GLS formulation

depends on the stabilization parameter τ_H which has to be properly defined to make the form on the l.h.s. unconditionally stable.

Remark 2. *The exact solution u verifies equation* (5) *for any choice of the stabilization parameter τ_H since $\mathcal{L}u - f = 0$. That is, the GLS method is consistent for any choice of τ_H.*

The GLS finite element approximation of u is $u_H \in \mathcal{U}_H$ such that

$$a_{\rm GLS}(\kappa, \tau_H; u_H, v) = l_{\rm GLS}(\kappa, \tau_H; v) \quad \forall v \in \mathcal{V}_H. \tag{6}$$

where

$$a_{\rm GLS}(\kappa, \tau; u, v) := a(\kappa; u, v) + (\tau \mathcal{L}u, \mathcal{L}\tilde{v})_{\widehat{\Omega}}, \tag{7}$$

and

$$l_{\rm GLS}(\kappa, \tau; v) := l(\kappa; v) + (\tau f, \mathcal{L}\tilde{v})_{\widehat{\Omega}}. \tag{8}$$

Note that for the sake of simplicity, the same notation, u_H, for the Galerkin and GLS finite element approximations has been used. A different notation for the GLS/FE approximation, for instance $u_H^{\rm GLS}$, would be more precise. However, since the error estimation strategy is valid for any approximation $u_H \in \mathcal{V}_H$ of u, there is no need to distinguish between u_H and $u_H^{\rm GLS}$ or any other approximation. Moreover, note that $\tau_H = 0$ results in the Galerkin approximation.

The stabilization parameter τ_H is usually determined using discrete dispersion analyses with the aim of eliminating spurious dispersion of plane waves in a user-prescribed direction (θ). That is, the goal is that the GLS/FE approximation has no phase lag if the exact solution is a plane wave in the direction θ. Different definitions for the parameter τ_H depending on the underlying size and topology of the mesh may be found in the literature [18, 19] .

Unfortunately, it is not possible in general to design a stabilization parameter τ_H that confers the ability of fully removing the dispersion error on the GLS method. The reason is twofold. First, a general signal consists of plane waves going in an infinite number of directions. Even if there are directionally prevalent components in this decomposition, they are not necessarily known a priori. Moreover it is not clear if the GLS method improves the approximations of solutions that are not dominant in the preferred direction. Second, the parameter τ_H is derived for particular structured topology meshes. The optimal behavior obtained for some particular structured meshes (which are of limited use in real-life applications) is partially lost when general unstructured meshes are used.

2.4. Matrix form

The Galerkin or GLS finite element approximation u_H is expressed in terms of the basis-functions $\{N^j\}_{j=1\ldots n_{\rm np}}$ spanning $\mathcal{U}_H$, namely

$$u_H = \sum_{j=1}^{n_{\rm np}} N^j u_H^j = \mathbf{N}\mathbf{u}_H, \tag{9}$$

where $n_{\rm np}$ is the number of nodes in the mesh, u_H^j is the complex nodal value associated with the mesh node $\mathbf{x}^j$, $\mathbf{N} = [N^1, N^2, \ldots, N^{n_{\rm np}}]$ and $\mathbf{u}_H^{\rm T} = [u_H^1, u_H^2, \ldots, u_H^{n_{\rm np}}]$.

In the case of linear finite element elements ($p = 1$), $\mathcal{L}u_H$ reduces to $\mathcal{L}u_H = -\kappa^2 u_H$ in $\hat{\Omega}$, and the matrix form of (7) reads

$$(\mathbf{K}_H - \mathbf{C}_H - \kappa^2 \mathbf{M}_H^{\tau_H})\mathbf{u}_H = \mathbf{f}_H^{\tau_H} + \mathbf{f}_H^{\rm N}, \tag{10}$$

where $\mathbf{K}_H$, $\mathbf{C}_H$ and $\mathbf{M}_H^{\tau_H}$ are the so-called stiffness, damping and mass matrices respectively

$$\mathbf{K}_H := \int_\Omega (\nabla \mathbf{N})^\mathsf{T} (\nabla \mathbf{N}) d\Omega,\ \mathbf{C}_H := \int_{\Gamma_\mathrm{R}} \mathcal{M} \mathbf{N}^\mathsf{T} \mathbf{N} d\Gamma,\ \mathbf{M}_H^{\tau_H} := \sum_{n=1}^{n_\mathrm{el}} \int_{\Omega_n} (1 - \tau_H \kappa^2) \mathbf{N}^\mathsf{T} \mathbf{N} d\Omega,$$

and the right-hand side vectors accounting for the source term and the Neumann boundary conditions are

$$\mathbf{f}_H^{\tau_H} := \sum_{n=1}^{n_\mathrm{el}} \int_{\Omega_n} (1 - \tau_H \kappa^2) \mathbf{N}^\mathsf{T} f \, d\Omega \quad \text{and} \quad \mathbf{f}_H^\mathrm{N} := \int_{\Gamma_\mathrm{N}} \mathbf{N}^\mathsf{T} g \, d\Gamma.$$

In the particular case where the stabilization parameter τ_H is constant in the elements of the mesh, $\mathbf{M}_H^{\tau_H} = (1 - \tau_H \kappa^2) \mathbf{M}_H$ and $\mathbf{f}_H^{\tau_H} = (1 - \tau_H \kappa^2) \mathbf{f}_H$, where

$$\mathbf{M}_H := \int_\Omega \mathbf{N}^\mathsf{T} \mathbf{N} d\Omega \quad \text{and} \quad \mathbf{f}_H := \int_\Omega \mathbf{N}^\mathsf{T} f \, d\Gamma, \tag{11}$$

are the standard (non-weighted) mass matrix and vector force. Besides, recall that $\tau_H = 0$ results in the matrix form of the Galerkin finite element method (4).

3. A POSTERIORI ERROR ESTIMATION OF THE WAVE NUMBER

3.1. Basics of error estimation of the wave number for the Galerkin method

It is well known that the error introduced in the numerical solution of wave problems has two different components: *interpolation error* and *pollution error*. The interpolation error is the classical error arising in elliptic problems and pertains to the ability of the discretization to properly approximate the solution,

$$e^\mathrm{int} := u - u_H^\mathrm{int} = u(\mathbf{x}) - \sum_{j=1}^{n_\mathrm{np}} N^j(\mathbf{x}) u(\mathbf{x}^j),$$

where u_H^int is the approximation of u in $\mathcal{U}_H$ coinciding with u at the mesh nodes $\mathbf{x}^j$, $j = 1, 2, \ldots, n_\mathrm{np}$. Thus, the pollution error is defined as:

$$e^\mathrm{pol} := u_H^\mathrm{int} - u_H = \sum_{j=1}^{n_\mathrm{np}} N^j(\mathbf{x}) (u(\mathbf{x}^j) - u_H^j).$$

In standard thermal and elasticity problems, the error in the finite element solution is equivalent to the interpolation error, and converges with the same rate. This error is local in nature because it may be reduced in a given zone by reducing the mesh size locally in this zone.

The *pollution* error, however, is especially relevant in the framework of Helmholtz problems due to the blowup of the inf-sup and continuity constants of the weak form when the wave number is large (i.e. the inf-sup constant tends to zero and the continuity constant tends to ∞ as κ tends to ∞). In transient wave problems, pollution is associated with the variation of the numerical wave speed with the wavelength. This phenomenon results in the dispersion of the different components of the total wave. In the steady Helmholtz problem, the word dispersion is also used and corresponds to the error in the numerical wave number κ_H, which is therefore identified with the pollution. In other words, the FE error is decomposed into two terms

$$\text{FE error } = u - u_H = e^\mathrm{int} + e^\mathrm{pol} = \text{ Interpolation error } + \text{ Dispersion/pollution error},$$

which, in the case of wave problems, behave completely differently (see figure 1). It has been shown that the pollution term converges at a different rate, lower than the standard interpolation error.

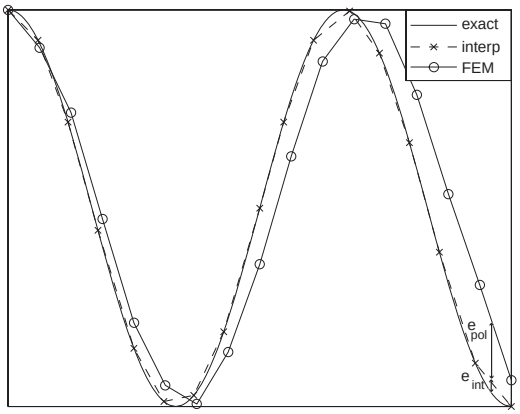

Figure 1. Illustration of the errors arising in the approximation of the Helmholtz equation. The exact solution (solid line, smooth) and interpolant (dashed line) coincide at the nodes, the FEM solution reproduces approximately the shape of the wave with a larger wavelength ($\kappa_H < \kappa$).

The pollution error e^{pol} is related to the phase difference between the exact and FE solutions, that is, the difference between the wave number κ associated with u and the numerical wave number κ_H associated with u_H. Usually, the dispersion or pollution error is assessed by obtaining an approximation of the error in the wave number $\kappa - \kappa_H$ instead of trying to measure the pollution error e^{pol} in some predefined norm.

A priori error estimates assess the dispersion error by means of providing a closed formula of the numerical wave number κ_H. Recently, a new approach to a-posteriori estimate the dispersion error, thus using the information given by u_H, has been developed [28].

The key idea is to define an auxiliary solution $u_H^m \in \mathcal{U}$ having the same wave number as u_H and from which to recover the value of κ_H. Intuitively, $u_H^m \in \mathcal{U}$ is the best solution of the Helmholtz equation (3) associated with a wave number κ_H matching u_H at the nodes of the mesh, see figure 2.

To fix the ideas, consider the one dimensional Helmholtz equation in $\Omega = (0,1)$ with boundary conditions $u(0) = 1$ and $u'(1) = i\kappa u(1)$. This simple problem admits the analytical solution $u(x) = e^{i\kappa x}$. Then, given a uniform finite element mesh and its associated FE approximation u_H, it turns out that it exists a wave number κ_H such that the solution of equation (3) associated to κ_H, $u_H^m = e^{i\kappa_H x}$, exactly fulfills the equations of the Galerkin method (10) associated to the interior nodes. This wave number is

$$\kappa_H = \frac{1}{H}\arccos\left(\frac{1-(\kappa H)^2/3}{1+(\kappa H)^2/6}\right) \approx \kappa - \frac{1}{24}\kappa^3 H^2 + \frac{3}{640}\kappa^5 H^4 + \mathcal{O}(\kappa^7 H^6), \tag{12}$$

see [23]. The verification of the equations (10) associated to the interior nodes enforces that the auxiliary solution u_H^m shares the same wave number than u_H, although this does not guarantee that u_H^m matches exactly u_H at the nodes of the mesh, due to the influence of the Robin boundary conditions.

However, the difference of u_H^m and u_H at the nodes of the mesh is nearly negligible. Thus, for this particular problem, a very good measure of the dispersion error can be computed as

$$E = \kappa - \kappa_H \approx \frac{1}{24}\kappa^3 H^2 + \mathcal{O}(\kappa^5 H^4). \tag{13}$$

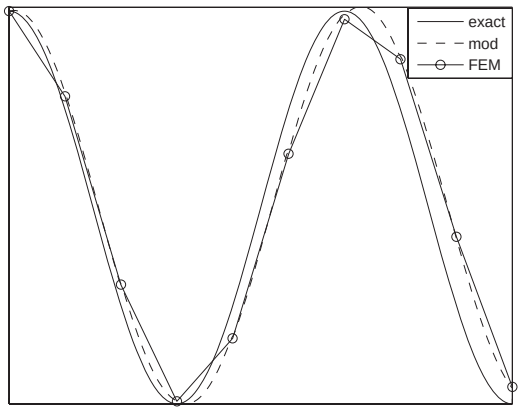

Figure 2. Illustration of the exact solution u, the approximate solution u_H and the auxiliary solution u_H^m coinciding with u_H at the nodes and sharing its wave number κ_H.

Unfortunately, in general, it is not possible to determine $u_H^m \in \mathcal{U}$ verifying (3) for a suitable wave number $\kappa_H \in \mathbb{R}$ and concurrently fulfilling the equations of the Galerkin method associated to the interior nodes. However a slight modification of this idea yields a proper definition for u_H^m. Specifically, $u_H^m \in \mathcal{U}$ and $\kappa_H \in \mathbb{R}$ are such that:

- $u_H^m \in \mathcal{U}$ coincides with u_H at the nodes of the mesh (that is $u_H^m(\mathbf{x}^j) = u_H(\mathbf{x}^j)$ for $j = 1, 2, \ldots, n_{\text{np}}$)
- for a given κ_H, $u_H^m \in \mathcal{U}$ is such that

$$a(\kappa_H; u_H^m, v) = l(\kappa_H; v) \quad \forall v \in \mathcal{V}_0, \tag{14}$$

  where

$$\mathcal{V}_0 := \{v \in \mathcal{V}, v(\mathbf{x}^j) = 0, j = 1, 2, \ldots, n_{\text{np}}\}$$

- κ_H and u_H^m minimize the norm of the residual functional

$$\|R(\kappa_H, u_H^m; \cdot)\|_* := \max_{v \in \mathcal{H}_0^1 \setminus \{0\}} \frac{R(\kappa_H, u_H^m; v)}{\|v\|},$$

  where $R(\kappa_H, u_H^m; \cdot) := l(\kappa_H; \cdot) - a(\kappa_H; u_H^m, \cdot)$, $\mathcal{H}_0^1 := \{v \in \mathcal{H}^1(\Omega), v|_{\partial\Omega} = 0\}$ and $\|v\|$ is the $\mathcal{H}^1$ norm.

Note that the values of u_H^m on the boundary of Ω do not affect the norm of the residual $\|\cdot\|_*$. This definition is used to minimize the influence of the errors due to the boundary conditions (which are

considered to be a part of the interpolation error and not of the dispersion error) in the assessment of the dispersion error. Also note that, the condition enforcing that u_H^m and u_H share the same phase lag, i.e. fulfilling of the equations of the Galerkin method associated to the interior nodes, is replaced by the more simple and equivalent condition of matching u_H at the nodes of the mesh.

In a compact form, κ_H and u_H^m are the solution of the following constrained optimization problem

$$\begin{aligned}(\kappa_H, u_H^m) \quad = \quad & \underset{\substack{\kappa^m \in \mathbb{R} \\ u^m \in \mathcal{U}}}{\arg\min} \ \|R(\kappa^m, u^m; \cdot)\|_* \\ & \text{subject to} \quad a(\kappa^m; u^m, v) = l(\kappa^m; v) \quad \forall v \in \mathcal{V}_0 \\ & \qquad\qquad\ \ u^m(\mathbf{x}^j) = u_H(\mathbf{x}^j),\ j = 1, 2, \ldots, n_{\text{np}}.\end{aligned} \tag{15}$$

The relation between the finite element solution u_H and the modified solution u_H^m allows to state that the numerical wave number associated with u_H, coincides with the wave number associated with the solution u_H^m. That is, the finite element solution u_H and u_H^m share the same phase lag and therefore the dispersion error associated to u_H is $E = \kappa - \kappa_H$.

It is worth noting that the definition of the numerical wave number through the modified solution u_H^m is not applicable as a practical error estimation strategy, since κ_H and u_H^m are even more difficult to compute than the exact solution u. Nevertheless, this rationale is used as a starting point to obtain a fully computable estimate for the dispersion error, by just introducing two simple modifications.

3.2. Practical a posteriori explicit error estimate for the wave number

First, the finite dimensional reference spaces $\mathcal{U}_h$ and $\mathcal{V}_h$ much finer than $\mathcal{U}_H$ and $\mathcal{V}_H$ are introduced. These spaces yield to the following approximations of κ_H and u_H^m

$$\begin{aligned}(\kappa_H[h], u_H^m[h]) \quad = \quad & \underset{\substack{\kappa^m \in \mathbb{R} \\ u^m \in \mathcal{U}_h}}{\arg\min} \ \|R(\kappa^m, u^m; \cdot)\|_{*,h} \\ & \text{subject to} \quad a(\kappa^m; u^m, v) = l(\kappa^m; v) \quad \forall v \in \mathcal{V}_h \cap \mathcal{V}_0 \\ & \qquad\qquad\ \ u^m(\mathbf{x}^j) = u_H(\mathbf{x}^j),\ j = 1, 2, \ldots, n_{\text{np}}\end{aligned} \tag{16}$$

and

$$\|R(\kappa_H[h], u_H^m[h]; \cdot)\|_{*,h} := \max_{\substack{v \in \mathcal{V}_h \setminus \{0\} \\ v|_{\partial\Omega} = 0}} \frac{R(\kappa_H[h], u_H^m[h]; v)}{\|v\|}.$$

If the finite element mesh $\mathcal{V}_h$ is sufficiently fine, one expects that $u_H^m \approx u_H^m[h]$ and therefore $\kappa_H[h] \approx \kappa_H$. If the finite element mesh $\mathcal{V}_h$ is not fine enough, as mentioned in [28] a correction factor has to be applied to recover a good approximation of κ_H from $\kappa_H[h]$, i.e., $\kappa_H[0] = c_f \kappa_H[h]$, where c_f is the correction factor based on a Richardson extrapolation technique.

Second, since the computation of $\kappa_H[h]$ and $u_H^m[h]$ is still unaffordable in practical applications another simplification is introduced. An approximation of $u_H^m[h]$ in $\mathcal{U}_h$, denoted by u^*, is obtained by post-processing u_H. In general, the approximation u^* is not obtained solving equation (14) for some κ_H and thus the computation of κ_H is independent. Indeed u^* does not verify

$$a(\kappa_H[h]; u^*, v) = l(\kappa_H[h]; v) \quad \forall v \in \mathcal{V}_h \cap \mathcal{V}_0,$$

and is therefore no longer linked with the computation of $\kappa_H[h]$. Once this approximation u^* is computed, the wave number $\kappa_H[h]$ is approximated by κ^* solution of

$$\kappa^* \quad = \quad \underset{\kappa^m \in \mathbb{R}}{\arg\min} \|R(\kappa^m, u^*; \cdot)\|_{*,h}.$$

It is worth noting that the norm of the residual $\|R(\kappa^m, u^*; \cdot)\|_{*,h}$ is a function depending only on the scalar variable κ^m and may be computed as

$$\|R(\kappa^m, u^*; \cdot)\|_{*,h} = \sqrt{\mathbf{r}(\kappa^m, u^*)' \mathbf{r}(\kappa^m, u^*)},$$

where

$$\begin{aligned} \mathbf{r}(\kappa^m, u^*) &:= \mathbf{B}_0 \Big((\mathbf{K}_h - \mathbf{C}_h - (\kappa^m)^2 \mathbf{M}_h) \mathbf{u}^* - \mathbf{f}_h - \mathbf{f}_h^{\mathrm{N}} \Big) \\ &= \mathbf{B}_0 \Big((\mathbf{K}_h - (\kappa^m)^2 \mathbf{M}_h)\, \mathbf{u}^* - \mathbf{f}_h \Big), \end{aligned} \tag{17}$$

is the residual associated with the interior nodes of the fine h-mesh, the approximation u^* and the wave number κ^m. The symbol $'$ stands for the conjugated transpose, that is $v' \equiv \tilde{v}^{\mathsf{T}}$, and $\mathbf{B}_0$ is a diagonal matrix on the h-mesh with ones in the positions associated with the interior nodes and zero elsewhere. That is, the matrix $\mathbf{B}_0$ sets the values of the residual at the boundary (either Dirichlet, Neumann or Robin) to zero.

Thus, for a given value of $u^* \approx u_H^m[h]$, the wave number κ^* is the parameter of the modified problem that better accommodates u^*. In practice, κ^* is determined minimizing the squared norm of the residual, namely

$$\kappa^* = \arg\min_{\kappa^m \in \mathbb{R}} \|R(\kappa^m, u^*; \cdot)\|_{*,h} = \arg\min_{\kappa^m \in \mathbb{R}} \sqrt{\mathbf{r}'\mathbf{r}} = \arg\min_{\kappa^m \in \mathbb{R}} \mathbf{r}'\mathbf{r}. \tag{18}$$

Note that given $\mathbf{u}^*$, the squared residual norm $\mathbf{r}'\mathbf{r}$ is a fourth degree polynomial in κ^m and thus κ^* is computed explicitly, see [28] for the computational details.

In short, the approximation κ^* of the numerical wave number κ_H is assessed by first post-processing the finite element solution u_H to compute u^* and then explicitly solving equation (18). The computable a posteriori error estimate for the wave number is then

$$E^* = \kappa - \kappa^*. \tag{19}$$

3.3. Assessment of the wave number for stabilized formulations

The dispersion error associated with a stabilized finite element approximation of u may be assessed using the same methodology detailed for the standard Galerkin approximation. Given the GLS/FE approximation u_H, a post-processing technique is used to compute an approximation u^* of the solution $u_H^m[h]$ of (16). Then, the wave number κ_H is approximated by κ^* solution of (18).

However, the use of stabilized formulations also for the fine mesh solutions in (16) allows to improve the quality of the estimates. Note that the accuracy of the estimate κ^* relies on two facts: first on the quality of the approximation u^* of $u_H^m[h]$, and second on the quality of the approximation $u_H^m[h]$ of u_H^m. The quality of u^* depends on the post-processing strategy which will be discussed in the following section. The quality of $u_H^m[h]$, on the other hand, depends on the size h of the reference mesh $\mathcal{V}_h$. In fact, it depends on the ratio of κ versus h since for large values of κ the reference mesh should be finer in order to get good approximations of u_H^m. Thus, for large wave numbers, the discrete approximation $u_H^m[h]$ will only be a good approximation of u_H^m if the reference mesh is taken remarkably fine.

A simple workaround which avoids dealing with fine reference meshes is to stabilize the problem associated to $u_H^m[h]$. That is, for a given finite element approximation (either stabilized or not), the

stabilized approximation $u_H^m[h,\tau_h]$ is the solution of

$$\begin{array}{rcll}(\kappa_H[h,\tau_h], u_H^m[h,\tau_h]) & = & \underset{\substack{\kappa^m \in \mathbb{R} \\ u^m \in \mathcal{U}_h}}{\arg\min} & \|R_{\mathrm{GLS}}(\kappa^m, \tau_h, u^m; \cdot)\|_{*,h} \\ & & \text{subject to} & a_{\mathrm{GLS}}(\kappa^m, \tau_h; u^m, v) = l_{\mathrm{GLS}}(\kappa^m, \tau_h; v) \quad \forall v \in \mathcal{V}_h \cap \mathcal{V}_0 \\ & & & u^m(\mathbf{x}^j) = u_H(\mathbf{x}^j),\ j = 1, 2, \ldots, n_{\mathrm{np}}\end{array} \tag{20}$$

where

$$R_{\mathrm{GLS}}(\kappa^m, \tau_h, u^m; v) := l_{\mathrm{GLS}}(\kappa^m, \tau_h; v) - a_{\mathrm{GLS}}(\kappa^m, \tau_h; u^m, v).$$

This modification yields to the following strategy to assess the error in the numerical wave number:

1. compute u^* approximation of $u_H^m[h,\tau_h]$ by post-processing u_H
2. compute the approximation $\kappa^*[\tau_h]$ solution of

$$\kappa^*[\tau_h] = \underset{\kappa^m \in \mathbb{R}}{\arg\min} \|R_{\mathrm{GLS}}(\kappa^m, \tau_h, u^*; \cdot)\|_{*,h} = \underset{\kappa^m \in \mathbb{R}}{\arg\min}\, \mathbf{r}_{\mathrm{GLS}}(\kappa^m)' \mathbf{r}_{\mathrm{GLS}}(\kappa^m), \tag{21}$$

where

$$\mathbf{r}_{\mathrm{GLS}}(\kappa^m) := \mathbf{B}_0 \Big((\mathbf{K}_h - (\kappa^m)^2 \mathbf{M}_h^{\tau_h})\, \mathbf{u}^* - \mathbf{f}_h^{\tau_h} \Big). \tag{22}$$

The explicit dependence of the vector $\mathbf{r}_{\mathrm{GLS}}$ on τ_h and u^*, $\mathbf{r}_{\mathrm{GLS}}(\kappa^m, \tau_h, u^*)$, is omitted for simplicity of presentation. Note that the matrix $\mathbf{M}_h^{\tau_h}$ and the vector $\mathbf{f}_h^{\tau_h}$ depend explicitly on the wave number κ^m and also implicitly via the stabilization parameter τ_h. Therefore the dependency of $\mathbf{r}'_{\mathrm{GLS}}\mathbf{r}_{\mathrm{GLS}}$ with respect to the wave number κ^m is no longer a fourth order polynomial and the solution of (21) may not be computed explicitly in general.

3.4. Computation of the wave number $\kappa^*[\tau_h]$

In order to detail the computation of $\kappa^*[\tau_h]$ verifying (21) in a simple manner, the stabilization parameter τ_h is assumed constant on the elements of the fine mesh. In this case, $\kappa^*[\tau_h]$ is the solution of (21) where

$$\mathbf{r}_{\mathrm{GLS}}(\kappa^m) := \mathbf{B}_0 \Big(\mathbf{K}_h\, \mathbf{u}^* - (\kappa^m)^2 \mathbf{M}_h\, \mathbf{u}^* + \tau_h (\kappa^m)^4 \mathbf{M}_h\, \mathbf{u}^* - \mathbf{f}_h + \tau_h (\kappa^m)^2 \mathbf{f}_h \Big), \tag{23}$$

and τ_h depends nonlinearly on κ^m. For instance, to minimize the phase lag on the x-direction for a structured regular quadrilateral mesh, [18] proposes the use of

$$\tau_h(\kappa^m) = \frac{1}{(\kappa^m)^2} - \frac{6}{(\kappa^m)^4 h^2} \frac{1 - \cos(\kappa^m h)}{2 + \cos(\kappa^m h)}.$$

Thus, the computation of $\kappa^*[\tau_h]$ requires solving a scalar root-finding problem.

Three different options have been considered in the present work to approximate $\kappa^*[\tau_h]$. The first approach is to compute an approximation of $\kappa^*[\tau_h]$ using an algorithm to numerically approximate the minimum of $F(\kappa^m) := \mathbf{r}_{\mathrm{GLS}}(\kappa^m)' \mathbf{r}_{\mathrm{GLS}}(\kappa^m)$. Namely, a root-finding method on the derivative of $F(\kappa^m)$ is used taking as initial guess $\kappa^m = \kappa$. This approximation is taken to represent the exact value $\kappa^*[\tau_h]$ since its accuracy can be controlled by the end-user through adjusting the tolerance of the root-finding method.

The second approach assumes that τ_h does not vary considerably when varying the parameter κ^m. In this case, the dependency of the parameter τ_h with respect to κ^m is removed by setting the value of

$\tau_h(\kappa^m) = \tau_h^\kappa$, where $\tau_h^\kappa := \tau_h(\kappa)$, and the approximation of $\kappa^*[\tau_h]$ is denoted by $\kappa^*[\tau_h^\kappa]$. Note that τ_h^κ denotes the value of the parameter τ_h associated to the wave number κ. Doing this approximation, the residual $\mathbf{r}_{\rm GLS}(\kappa^m)$ is approximated by a fourth order polynomial on κ^m

$$\mathbf{r}_{\rm GLS}(\kappa^m) \approx \mathbf{a}_0 + \mathbf{a}_2(\kappa^m)^2 + \mathbf{a}_4(\kappa^m)^4, \tag{24}$$

for $\mathbf{a}_0 = \mathbf{B}_0(\mathbf{K}_h\mathbf{u}^* - \mathbf{f}_h)$, $\mathbf{a}_2 = \mathbf{B}_0(-\mathbf{M}_h\mathbf{u}^* + \tau_h^\kappa\mathbf{f}_h)$ and $\mathbf{a}_4 = \tau_h^\kappa\mathbf{B}_0\mathbf{M}_h\mathbf{u}^*$. The minimization of the squared residual $F(\kappa^m)$ is then reduced to find the critical points of $F(\kappa^m)$ which is equivalent to find the solutions of

$$\frac{dF}{d\kappa^m} = 2\kappa^m\left(\mathbf{c}_0 + 2\mathbf{c}_2(\kappa^m)^2 + 3\mathbf{c}_4(\kappa^m)^4 + 4\mathbf{c}_6(\kappa^m)^6\right) = 0, \tag{25}$$

where $\mathbf{c}_0 = \mathbf{a}_0'\mathbf{a}_2 + \mathbf{a}_2'\mathbf{a}_0$, $\mathbf{c}_2 = \mathbf{a}_0'\mathbf{a}_4 + \mathbf{a}_2'\mathbf{a}_2 + \mathbf{a}_4'\mathbf{a}_0$, $\mathbf{c}_4 = \mathbf{a}_2'\mathbf{a}_4 + \mathbf{a}_4'\mathbf{a}_2$, $\mathbf{c}_6 = \mathbf{a}_4'\mathbf{a}_4$. Although equation (25) may have seven real solutions, $\kappa^*[\tau_h^\kappa]$ is defined to be the solution of (25) closer to κ. Thus, ruling out the trivial solution $\kappa^m = 0$, $\kappa^*[\tau_h^\kappa]$ is computed by first finding the roots of the bicubic polynomial appearing in equation (25), which is equivalent to find the three solutions $\bar\kappa$ of

$$\mathbf{c}_0 + 2\mathbf{c}_2\bar\kappa + 3\mathbf{c}_4\bar\kappa^2 + 4\mathbf{c}_6\bar\kappa^3 = 0,$$

and then set $\kappa^*[\tau_h^\kappa]$ to be the value of $\sqrt{\bar\kappa}$ nearer to κ, see [28] for the computational details. Thus, the assumption $\tau_h(\kappa^m) = \tau_h^\kappa$ yields to a simple and explicit algorithm to approximate the exact value of $\kappa^*[\tau_h^\kappa]$.

Finally, the third approach directly applies the strategy presented in [28] by considering that the terms added by the GLS method are constant with respect to κ^m, that is, not only the parameter τ_h is set to τ_h^κ but also the $(\kappa^m)^2$ associated with the GLS method is set to κ^2. In this way, the residual is approximated by the quadratic function

$$\mathbf{r}_{\rm GLS}(\kappa^m) \approx \mathbf{B}_0\Big(\mathbf{K}_h\,\mathbf{u}^* - (\kappa^m)^2\mathbf{M}_h\,\mathbf{u}^* + \tau_h^\kappa\kappa^2(\kappa^m)^2\mathbf{M}_h\,\mathbf{u}^* - \mathbf{f}_h + \tau_h^\kappa\kappa^2\mathbf{f}_h\Big),$$

and the minimization of the fourth order polynomial $F(\kappa^m)$ which allows to compute the approximation of $\kappa^*[\tau_h]$ is done by using the technique detailed in [28].

As will be seen in the numerical examples, the second option yields a fairly good approximation of the exact solution of the one-dimensional non-linear optimization problem (21). The practical and straightforward algorithm to estimate the dispersion error using this second option is summarized in the box shown in figure 3.

Remark 3. *Note that the second step of the previous procedure requires to compute the coefficients* $\mathbf{c}_0$, $\mathbf{c}_2$, $\mathbf{c}_4$ *and* $\mathbf{c}_6$ *associated to the residual* $\mathbf{r}_{\rm GLS}$. *These coefficients depend on the stabilization parameter* τ_h^κ *which in turn depends on a user prescribed direction* θ *which will be denoted in the following by* θ_h. *In the case that* u_H *is computed using the standard Galerkin method, it is not natural to define a direction* θ_h. *However, information of the prevalent wave direction of the exact solution can be used if available. If* u_H *is computed using the GLS method with wave direction* θ, *the estimates may be computed using* $\theta_h = \theta$ *or again, if information of the exact solution is available, this parameter may be set to adjust the prevalent wave direction of the exact solution. The choice of this parameter will be further discussed in the numerical examples.*

3.5. Enhanced solution u^* by post-processing u_H

The quality of the estimate κ^* depends on the quality of the approximation u^* of $u_H^m[h] \in \mathcal{U}_h$ (respectively $u_H^m[h,\tau_h]$). The idea proposed here is to build up an inexpensive approximation using

0.- Compute a finite element approximation u_H of the Helmholtz problem (either using the Galerkin method or a stabilized method).
1.- Compute an approximation u^* by post-processing u_H (see section 3.5).
2.- Compute the real coefficients $\mathbf{c}_0 = \mathbf{a}_0'\mathbf{a}_2 + \mathbf{a}_2'\mathbf{a}_0$, $\mathbf{c}_2 = \mathbf{a}_0'\mathbf{a}_4 + \mathbf{a}_2'\mathbf{a}_2 + \mathbf{a}_4'\mathbf{a}_0$, $\mathbf{c}_4 = \mathbf{a}_2'\mathbf{a}_4 + \mathbf{a}_4'\mathbf{a}_2$, $\mathbf{c}_6 = \mathbf{a}_4'\mathbf{a}_4$ where

$$\mathbf{a}_0 = \mathbf{B}_0(\mathbf{K}_h\mathbf{u}^* - \mathbf{f}_h), \quad \mathbf{a}_2 = \mathbf{B}_0(-\mathbf{M}_h\mathbf{u}^* + \tau_h^\kappa \mathbf{f}_h) \quad \text{and} \quad \mathbf{a}_4 = \tau_h^\kappa \mathbf{B}_0\mathbf{M}_h\mathbf{u}^*.$$

3.- Compute the roots of the polynomial

$$\mathbf{c}_0 + 2\mathbf{c}_2\bar{\kappa} + 3\mathbf{c}_4\bar{\kappa}^2 + 4\mathbf{c}_6\bar{\kappa}^3.$$

4.- Set $\kappa^*[\tau_h^\kappa]$ to be the value of $\sqrt{\bar{\kappa}}$ nearer to κ and compute the a posteriori error estimate for the wave number as

$$E^*[\tau_h^\kappa] = \kappa - \kappa^*[\tau_h^\kappa].$$

Figure 3. Practical and straightforward algorithm to estimate the dispersion error

a postprocessing technique standard in error estimation analysis [32, 12] and likely having all its features. The post-processing technique starts from the finite element solution $u_H \in \mathcal{U}_H$ and computes an approximation u^* of $u_H^m[h]$ in $\mathcal{U}_h$.

Reference [28] presents a procedure to compute u^* following the work by Calderón and Díez [11]. For each element of the H-mesh, Ω_n, the patch of elements surrounding Ω_n is considered and its denoted by ω_n. In this patch, the values of $\mathbf{u}_H$ at the nodes of the H-mesh are used as input data and a polynomial is fitted using a constrained least squares technique. That is, in a two dimensional setting, for a given polynomial degree q, a complex valued polynomial field

$$p(\mathbf{x}) = \sum_{k+l\leq q} p_{kl} x^k y^l$$

is determined from the following constrained least squares problem

$$\min_{p_{kl}\in\mathbb{C}} \sum_{\mathbf{x}^j\in\omega_n} \left| u_H^j - p(\mathbf{x}^j) \right|^2$$
$$\text{restricted to } \; p(\mathbf{x}^j) = u_H^j \;\; \text{for } \mathbf{x}^j \in \Omega_n,$$

where $|\cdot|$ denotes the modulus of a complex number. Note that the real and imaginary parts of $p(\mathbf{x})$ can be computed separately. The real part of $p(\mathbf{x})$ (and analogously its imaginary part) may be found solving the real-valued constrained optimization

$$\min_{\Re(p_{kl})\in\mathbb{R}} \sum_{\mathbf{x}^j\in\omega_n} \left| \Re(u_H^j) - \Re(p(\mathbf{x}^j)) \right|^2$$
$$\text{restricted to } \; \Re(p(\mathbf{x}^j)) = \Re(u_H^j) \;\; \text{for } \mathbf{x}^j \in \Omega_n.$$

Once the polynomial is obtained in ω_n it is evaluated to find the nodal values of $u^\star$ in the nodes of the h-mesh lying in element Ω_n of the H-mesh. This approach allows recovering the curvatures of the solution coinciding with u_H at the nodes where it is computed.

This simple and straightforward strategy provides fairly good results. However, this approach does not use specific information about the differential operator or the exact solution. The use of analytical

information on the natural solutions of the differential operator yields an alternative approach to compute u^*.

The approach to compute u^* also requires solving a local constrained least squares problem for each element Ω_n. Instead of using a polynomial representation for $u^*|_{\omega_n}$ an exponential fitting is used. This is a natural choice because the exact solution of the 2D homogeneous Helmholtz equation is an infinite sum of plane waves of the form $Ae^{i\mathbf{k}\cdot\mathbf{x}}$, where $\mathbf{k} = \kappa[\cos(\theta), \sin(\theta)]$.

Thus, in each patch ω_n, u_H is approximated by an exponential field of the form

$$A(\mathbf{x})e^{ip(\mathbf{x})},$$

where $A(\mathbf{x})$ and $p(\mathbf{x})$ are polynomial fields representing the amplitude and wave direction. The fields $A(\mathbf{x})$ and $p(\mathbf{x})$ are determined by a constrained least squares criterion and hence, they are taken as those minimizing

$$\begin{aligned} &\min \sum_{\mathbf{x}^j \in \omega_n} \left| u_H^j - A(\mathbf{x}^j)e^{ip(\mathbf{x}^j)} \right|^2 \\ &\text{restricted to } \; A(\mathbf{x}^j)e^{ip(\mathbf{x}^j)} = u_H^j \;\; \text{for } \mathbf{x}^j \in \Omega_n. \end{aligned}$$

Using a standard technique to linearize the exponential least squares fitting transforms the previous problem into an equivalent linear constrained least squares problem

$$\begin{aligned} &\min \sum_{\mathbf{x}^j \in \omega_n} \left| \ln(u_H^j) - \ln\left(A(\mathbf{x}^j)e^{ip(\mathbf{x}^j)} \right) \right|^2 \\ &\text{restricted to } \; \ln\left(A(\mathbf{x}^j)e^{ip(\mathbf{x}^j)} \right) = \ln(u_H^j) \;\; \text{for } \mathbf{x}^j \in \Omega_n. \end{aligned}$$

Splitting the real and imaginary part of the previous problem yields a simple strategy to compute $\ln(A(\mathbf{x}))$ and $p(\mathbf{x})$ independently using a restricted least squares fitting, namely:

$$\begin{aligned} &\min \sum_{\mathbf{x}^j \in \omega_n} \left| \ln(|u_H^j|) - \ln(A(\mathbf{x}^j)) \right|^2 \\ &\text{restricted to } \; \ln(A(\mathbf{x}^j)) = \ln(|u_H^j|) \;\; \text{for } \mathbf{x}^j \in \Omega_n, \end{aligned}$$

and

$$\begin{aligned} &\min \sum_{\mathbf{x}^j \in \omega_n} \left| \arg(u_H^j) - p(\mathbf{x}^j) \right|^2 \\ &\text{restricted to } \; p(\mathbf{x}^j) = \arg(u_H^j) \;\; \text{for } \mathbf{x}^j \in \Omega_n, \end{aligned}$$

where $\arg(\cdot)$ denotes the argument of a complex number and a polynomial fitting of $\ln(A(\mathbf{x}))$ and $p(\mathbf{x})$ is considered.

The only intricate part of this strategy involves the input data, $\arg(u_H^j)$, of the least squares problem for $p(\mathbf{x})$. The non-unique arguments associated to the data u_H^j have to be carefully selected so that the polynomial fitting yields proper results.

4. NUMERICAL EXAMPLES

The strategy to assess the error in the wave number presented in the previous sections is validated in four numerical examples. The performance of the estimates of the dispersion error is shown both for

Galerkin and GLS approximations. Moreover, the influence of the post-processing technique yielding u^* in the resulting effectivity is also discussed.

The finite element approximations are computed using triangular and quadrilateral meshes of linear (resp. bilinear) elements, $p = 1$. Different definitions of the stabilization parameter τ_H are used to compute the GLS approximations depending on the underlying topology of the mesh. In particular, for structured and unstructured quadrilateral meshes the following definition of the parameter, designed to minimize the dispersion error of plane wave in the direction θ on cartesian meshes, is used [18, 19]:

$$\tau_H = \frac{1}{\kappa^2}\left(1 - \frac{6}{(\kappa h)^2}\left(\frac{1-\cos(\kappa h\cos\theta)}{2+\cos(\kappa h\cos\theta)} + \frac{1-\cos(\kappa h\sin\theta)}{2+\cos(\kappa h\sin\theta)}\right)\right).$$

For triangular meshes, the definition derived for hexagonal meshes, namely,

$$\tau_H = \frac{1}{\kappa^2}\left(1 - \frac{8}{(\kappa h)^2}\frac{3-f(\kappa h,\theta)}{3+f(\kappa h,\theta)}\right), \tag{26}$$

where $f(\kappa h,\theta) = \cos(\kappa h\cos\theta) + 2\cos(\kappa h\cos\theta/2)\cos(\sqrt{3}\kappa h\sin\theta/2)$ is used because it provides good results also for unstructured meshes.

For non-uniform meshes, the stabilization parameter is not constant over the whole mesh. In each element Ω_n a different stabilization parameter is used depending on its characteristic element size h_n. This characteristic element size is taken as the smallest side of the element both for quadrilateral and triangular meshes.

As mentioned in section 2.3 the parameter τ_H depends on a user-prescribed direction θ. The influence of the selection of this direction in the reduction of the dispersion error is studied in the following examples.

4.1. Example 1: 1D strip

The first example models a plane wave propagating in the x-direction in a two dimensional rectangular domain, with length $L = 1$ and width $V = \sqrt{3}/8$, see figure 4. The boundary conditions are specified in order to yield the exact solution $u(x,y) = e^{i\kappa x}$: Dirichlet on the left hand side, Robin on the right hand side and Neumann homogeneous on the upper and lower sides to maintain the one-dimensional character of the solution. That is, the data entering in equation (2) are $\bar{u} = 1$ on $x = 0$, $\mathcal{M}u = i\kappa u$ on $x = 1$ and $g = 0$ on $y = 0$ and $y = \sqrt{3}/8$. The performance of the Galerkin and GLS finite element solutions is studied for $\kappa = 8\pi$. Due to the 1D character of the problem, the stabilization angle used in all the GLS computations (both for the coarse and fine meshes) is set to 0, that is, $\theta = \theta_h = 0$. Note that the solution of the problem is independent of the width of the domain V and the value $\sqrt{3}/8$ has been selected in order to accommodate an hexagonal triangular mesh.

First the influence of the selection of the finite reference mesh associated to $\mathcal{V}_h$ is studied. If the finite element mesh $\mathcal{V}_h$ is sufficiently fine, one expects that $u_H^m \approx u_H^m[h,\tau_h] \approx u_H^m[h]$ and therefore $\kappa_H \approx \kappa_H[h,\tau_h] \approx \kappa_H[h]$. If the finite element mesh $\mathcal{V}_h$ is not fine enough, one should apply a correction factor to $\kappa_H[h]$ to account for the finite size h of the reference mesh and recover a good approximation of κ_H, see [28]. This correction factor is not necessary for the estimate $\kappa_H[h,\tau_h]$. That is when the reference problem is also stabilized.

A uniform coarse mesh of 24×2 quadrilateral elements is used both for the Galerkin and the GLS method. The dispersion error associated with the Galerkin approximation can be assessed using the a-priori estimate of the wave number given by (12)

$$E^{\mathrm{pri}} = \kappa - \kappa^{\mathrm{pri}} = \kappa - \frac{1}{H}\arccos\left(\frac{1-(\kappa H)^2/3}{1+(\kappa H)^2/6}\right),$$

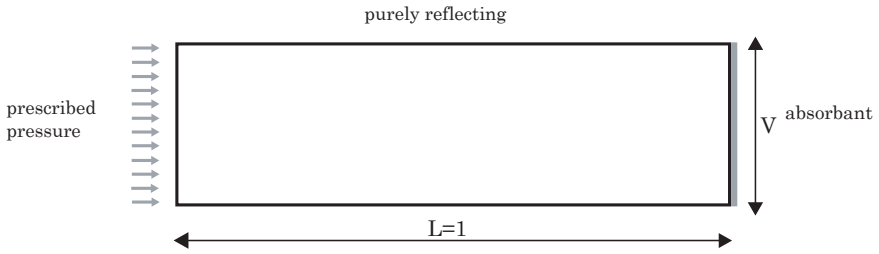

Figure 4. Example 1; 1D strip: problem setup.

which in this case is taken as the actual error in the wave number due to the one dimensional character of the solution (up to the pollution errors introduced by the Robin boundary conditions). Note that the GLS solution is, for this particular mesh and problem, dispersion free. Thus, the Robin boundary conditions are the unique perturbation producing errors in the approximations of κ.

The different a posteriori estimates of the dispersion error are computed using a series of successively nested reference meshes, both triangular and quadrilateral. For the quadrilateral meshes, refinement is performed only in the x-direction and thus maintaining two rows of elements on all the reference meshes, due to the one-dimensional character of the solution: for $h = H/2$ each quadrilateral in the coarse mesh is divided into two new ones yielding a mesh of 48×2 elements, for $h = H/4$, each quadrilateral element is divided into 4 new ones yielding a mesh of 96×2 elements...

The first columns of the table I show the truth estimates of the dispersion error $E[h] := \kappa - \kappa_H[h]$ and $E[h, \tau_h] := \kappa - \kappa_H[h, \tau_h]$ where the numerical wave numbers $\kappa_H[h]$ and $\kappa_H[h, \tau_h]$ are computed solving the nonlinear problems (16) and (20) respectively, and $c_f = n_r^2/(n_r^2 - 1)$ stands for the correction factor applied to $\kappa_H[h]$ where $n_r = H/h$. Note that these truth estimates are computationally unaffordable in real applications, because they involve many resolutions of the problem in the reference mesh. They are computed in academic problems to see the effectivity of the proposed practical estimates. As can be seen, both the estimates $c_f E[h]$ and $E[h, \tau_h]$ assessing the dispersion error of the Galerkin approximation are in very good agreement with the a-priori estimate. It is worth noting that the estimate $E[h, \tau_h]$ yields very good results even for the case $h = H/2$ being less sensitive than $c_f E[h]$ to the choice of the reference mesh size.

The last columns in table I, correspond to the practical estimates obtained from the recovered solution u^*. In this case u^* is computed using the exponential fitting. Four different estimates are computed. The first one is the estimate proposed by [28], $E^* := \kappa - \kappa^*$, associated to the assessed wave number obtained from (18) and enhanced by its multiplicative factor. The other three options correspond to the three approximations of $\kappa^*[\tau_h]$ detailed in section 3.3. Recall that Option 1 results from numerically solving the non-linear one dimensional problem and, since this approximation only depends on an end-user relative tolerance set to 10^{-12}, it is assumed to be exact, that is $E^*[\tau_h] := \kappa - \kappa^*[\tau_h]$. Option 2 is associated with $\kappa^*[\tau_h^\kappa]$ yielding the estimate $E^*[\tau_h^\kappa] := \kappa - \kappa^*[\tau_h^\kappa]$, and Option 3 is the most crude approximation of $\kappa^*[\tau_h]$ since it considers that all the terms in the residual associated to the GLS formulation are constant with respect to the wave number. It is worth nothing that all estimates produce similar and sharp approximations to the dispersion error for all the values of the reference mesh size h.

As expected, the truth estimates provide almost exact values for the dispersion error, fully coinciding with the a priori estimate. The effect of correcting the estimate with factor c_f or considering a stabilized

	Galerkin				$E^{\text{pri}} = 1.02211$		
h	$E[h]$	$c_f E[h]$	$E[h,\tau_h]$	$c_f E^*$	Option 1 $E^*[\tau_h]$	Option 2 $E^*[\tau_h^\kappa]$	Option 3
$H/2$	0.76790	1.02387	1.02211	1.01428	1.01469	1.01486	1.03682
$H/4$	0.95869	1.02261	1.02211	1.01428	1.01469	1.01486	1.03682
$H/8$	1.00627	1.02224	1.02211	1.01227	1.01232	1.01232	1.01368
$H/16$	1.01815	1.02214	1.02211	1.01214	1.01215	1.01215	1.01249
$H/32$	1.02112	1.02212	1.02211	1.01210	1.01210	1.01210	1.01218
$H/64$	1.02186	1.02211	1.02211	1.01208	1.01208	1.01208	1.01210

Table I. Example 1: Assessment of the dispersion error for a uniform coarse quadrilateral mesh (24×2 elements) an successively refined reference meshes for the Galerkin approximations of the solution. The truth error estimates (left) are computed using the fully nonlinear solution yielding to $E[h]$ and $E[h,\tau_h]$. The exponential post-processed solution (right) u^* obtained from u_H and then different options are used to recover the wave number κ^* associated to u^* only for the Galerkin approximation.

reference problem are equivalent.

Following these results, in the remainder of the numerical examples, the parameter h is set to $h = H/4$ (refining only in the x-direction for this example and uniformly refining the elements in the following examples) and the wave number is approximated using Option 2 which provides really good approximations. Hence, in the following the notation E^* is used to denote the estimate $E^*[\tau_h^\kappa]$ (both for the Galerkin and GLS method). A subindex is added to the notation E^* to specify the type of recovery used to compute u^*, namely E^*_{pol} ans E^*_{exp} for the polynomial and exponential fittings respectively. Finally, the estimate E^* is compared with the truth estimate $E[h,\tau_h]$ which is considered as the one providing the *most accurate-but not computable* approximation of the dispersion error, and it is denoted by E.

Table II and figures 5 and 6 present the estimates corresponding to a sequence of uniformly refined meshes. Two series of meshes are used: one of structured quadrilaterals and one of triangular elements following an hexagonal pattern. The two fitting strategies (polynomial and exponential) are compared.

Note that the dispersion error associated with the GLS solution is almost negligible for the truth estimates. The Robin boundary conditions are the unique perturbation producing errors in the approximations of κ for the practical estimates.

Figure 5 shows the convergence of the estimates for the dispersion error of the Galerkin approximation using cartesian quadrilateral meshes. The convergence rate of all the estimates is 2 in the number of points of the mesh, matching the a priori expected convergence rate for the dispersion error, since, for a fix value of κ, $E = \kappa - \kappa_H = \mathcal{O}(H^2)$ which is equivalent to $\mathcal{O}((n_{\text{np}})^2)$ since the elements are not refined in the y-direction, see equation (13). However it can be observed that the exponential fitting provides estimates which are in better agreement with the a-priori or reference estimates.

Finally, figure 6 shows the convergence of the bounds for both the Galerkin and GLS approximations using either quadrilateral or hexagonal triangular meshes. The reduction of the dispersion error using the stabilized GLS formulation becomes apparent both for quadrilateral and hexagonal meshes. This important reduction is due to the fact that the stabilization parameters that have been used are particularly designed to eliminate the spurious dispersion of the exact solution $e^{\,i\kappa x}$ for the particular

	Galerkin				GLS/FE		
n_{np}	E^{pri}	E	E^*_{pol}	E^*_{exp}	E	E^*_{pol}	E^*_{exp}
75	1.02211	1.02211	1.23174	1.01293	$-4.1\cdot10^{-8}$	0.23026	-0.00626
99	0.60404	0.60404	0.71868	0.59251	$-5.1\cdot10^{-8}$	0.12522	-0.00134
123	0.39584	0.39584	0.46304	0.38942	$5.1\cdot10^{-8}$	0.07167	-0.00035
147	0.27851	0.27851	0.32051	0.27525	$4.1\cdot10^{-8}$	0.04401	-0.00011
	Galerkin				GLS/FE		
n_{np}	E^{pri}	E	E^*_{pol}	E^*_{exp}	E	E^*_{pol}	E^*_{exp}
172	0.79686	0.79782	0.58502	0.78168	$2.6\cdot10^{-8}$	-0.22714	-0.00542
293	0.47022	0.46319	0.36999	0.45619	$2.9\cdot10^{-8}$	-0.09656	-0.00229
446	0.30565	0.30074	0.25304	0.29794	$5.4\cdot10^{-8}$	-0.04915	-0.00116
631	0.21365	0.21040	0.18306	0.20935	$3.6\cdot10^{-8}$	-0.02829	-0.00066

Table II. Example 1: Convergence of the estimates of the dispersion error through a uniform mesh refinement using cartesian quadrilateral meshes (top) and hexagonal triangular meshes (bottom).

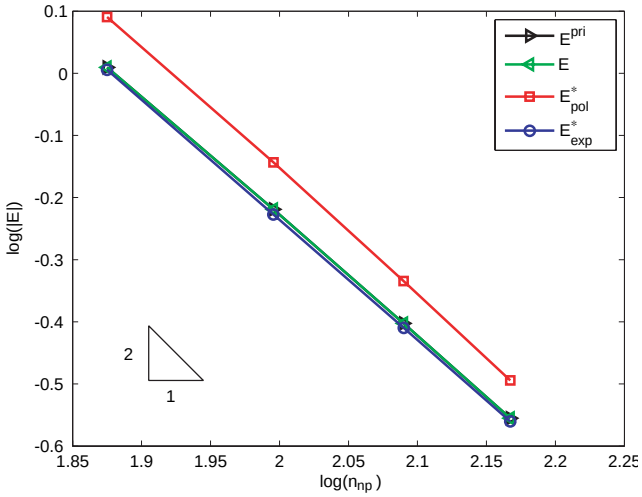

Figure 5. Example 1: Convergence of the estimates of the dispersion error of the Galerkin approximations through a uniform mesh refinement using cartesian quadrilateral meshes.

quadrilateral and hexagonal meshes at hand. It is also clear that the exponential fitting, in this example, captures more precisely the shape of the solution and thus yields better estimates for the dispersion error.

Although extremely simple, this example demonstrates that the proposed methodology is able to assess the dispersion error in both for Galerkin and GLS formulations. The estimate clearly detects that GLS method reduces the dispersion. As it is shown in the next examples, the same tools are also useful in more involved situations.

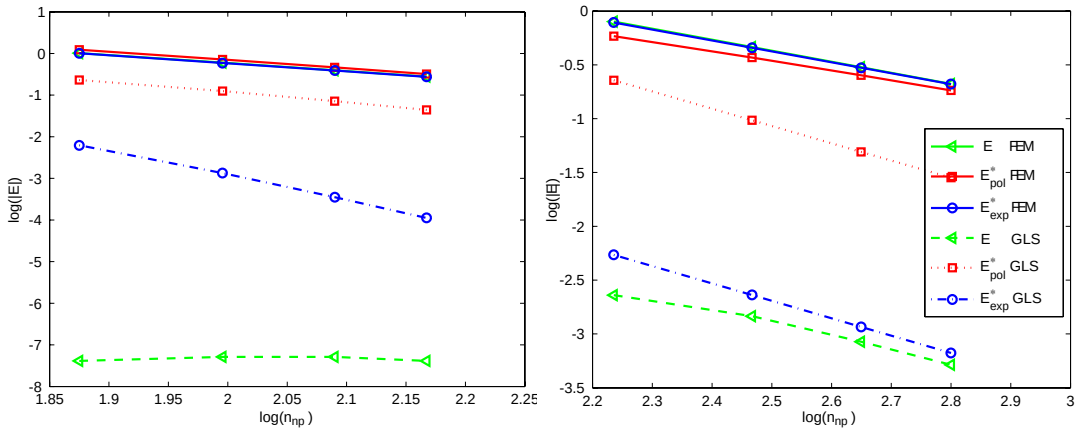

Figure 6. Example 1: Convergence of the dispersion error both for the Galerkin and GLS approximations in a series of uniformly refined meshes: quadrilateral meshes (left) and hexagonal triangular meshes (right).

4.2. Example 2: Plane Wave in Square Domain

We consider the unit square $\Omega =]0,1[\times]0,1[$ with inhomogeneous Robin boundary conditions specified on all the boundaries of the square so that the exact solution is $u = e^{i\kappa(\cos\alpha x + \sin\alpha y)}$. That is, the solution is a plane wave propagating in the direction of angle α, as illustrated in figure 7. The model parameters are $\kappa = 8$ and $\alpha = \pi/8$ and the analytical solution associated with these parameters is depicted in figure 7.

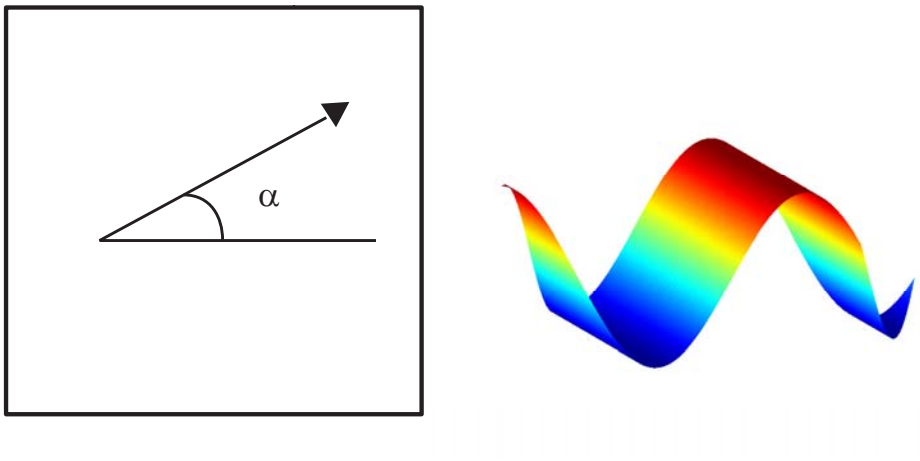

Figure 7. Example 2: Problem setup (left) and solution for $\alpha = \pi/8$ (right).

The performance of the estimates is studied for three different structured uniform quadrilateral meshes (8×8, 16×16 and 32×32 elements). In order to estimate the dispersion error associated with the Galerkin approximation, the stabilization parameters involved in the computation of $E := E[h, \tau_h]$ and $E^* := E^*[\tau_h^\kappa]$ in equations (20) and (24) are computed using the predefined direction $\theta_h = \alpha = \pi/8$.

The results are shown in table III where $\eta^*_{\rm pol} := E^*_{\rm pol}/E$ and $\eta^*_{\rm exp} := E^*_{\rm exp}/E$ is the effectivity index of the estimates with respect to the reference value E (truth estimates). Again, the exponential fitting provides better estimates to the dispersion error yielding very good effectivity indices near to one. The rate of convergence of the estimates with respect to the number of nodes in the mesh is 1, matching the a priori expected convergence rate for the dispersion error, since $E = \kappa - \kappa_H = \mathcal{O}(H^2)$ which, in this case, is equivalent to $\mathcal{O}(n_{\rm np})$ because the uniform refinement is done in both the x and y directions.

	Galerkin				
$n_{\rm np}$	E	$E^*_{\rm pol}$	$E^*_{\rm exp}$	$\eta^*_{\rm pol}$	$\eta^*_{\rm exp}$
81	0.24912	0.41670	0.23725	1.6727	0.9524
289	0.06330	0.09033	0.06328	1.4271	0.9998
1089	0.01563	0.01943	0.01593	1.2434	1.0197

Table III. Example 2: Assessment of the dispersion error of the Galerkin method for uniformly refined structured quadrilateral meshes.

The same study is done for the GLS approximations of the problem using the same meshes. Although the exact solution is a plane wave, since the cartesian meshes are not aligned with the wave direction $\alpha = \pi/8$, none of the possible choices for the stabilization direction θ yields a nodally exact solution. Table IV shows the dispersion error of the GLS method for three different stabilization parameters $\theta = 0$, $\theta = \pi/8$ and $\theta = \pi/4$. In all the computations the error estimates are performed using the same value of θ for the reference $h-$mesh, that is $\theta_h = \theta$. The GLS method substantially reduces de dispersion error even for the non-optimal parameters $\theta = 0$ and $\theta = \pi/4$. The error estimate $E^*_{\rm exp}$ are properly approximating the truth error E in the all cases. For $\theta = \pi/8$ the dispersion error so small that the resulting effectivity is not as sharp as for the choices producing longer errors.

	GLS/FE					
	$\theta = 0$		$\theta = \pi/8$		$\theta = \pi/4$	
$n_{\rm np}$	E	$E^*_{\rm exp}$	E	$E^*_{\rm exp}$	E	$E^*_{\rm exp}$
81	-7.45·10^{-2}	-7.17·10^{-2}	6.82·10^{-4}	3.40·10^{-4}	7.71·10^{-2}	7.34·10^{-2}
289	-1.99·10^{-2}	-1.93·10^{-2}	-4.43·10^{-4}	3.80·10^{-5}	1.91·10^{-2}	1.95·10^{-2}
1089	-5.02·10^{-3}	-4.87·10^{-3}	-1.84·10^{-4}	1.68·10^{-6}	4.66·10^{-3}	4.88·10^{-3}

Table IV. Example 2: Assessment of the dispersion error of the GLS method for uniformly refined structured quadrilateral meshes. The GLS approximations are computed using different stabilization directions θ.

Figure 8 graphically displays the information shown in the tables in tables III and IV. As can be seen, the estimates (depicted on the right of the figure) are in very good agreement with the reference mesh computations (depicted on the left of the figure). As mentioned before, the GLS method always performs better than the Galerkin method but there is a qualitative leap of accuracy when the optimal parameter $\theta = \pi/8$ is used.

Finally, figure 9 shows the influence of the stabilization direction θ used to compute the GLS finite element approximation in the dispersion error. The study is done varying θ in the range $[0, \pi/2]$. As expected, the optimal performance is reached when the wave direction of the GLS method coincides with the angle of the exact solution, $\theta = \alpha = \pi/8$. In any case, if no information of the exact solution is at hand and thus, an arbitrary choice of θ is considered, the GLS method provides an important reduction of the dispersion error when compared to the Galerkin approximation: the

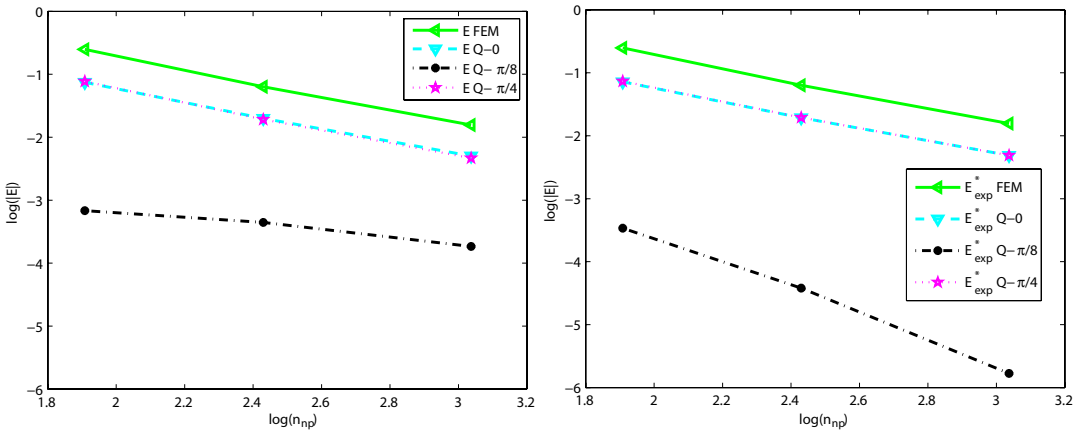

Figure 8. Example 2: Performance of the estimates of the dispersion error for the Galerkin method and the GLS method for a plane wave associated with $\alpha = \pi/8$ using a reference mesh (left) and the exponential fitting (right). The GLS approximations are computed using different stabilization parameters.

estimated dispersion error is reduced from $E^*_{\rm exp} = 0.06328$ to $E^*_{\rm exp} \approx 0.02$ in the worst case.

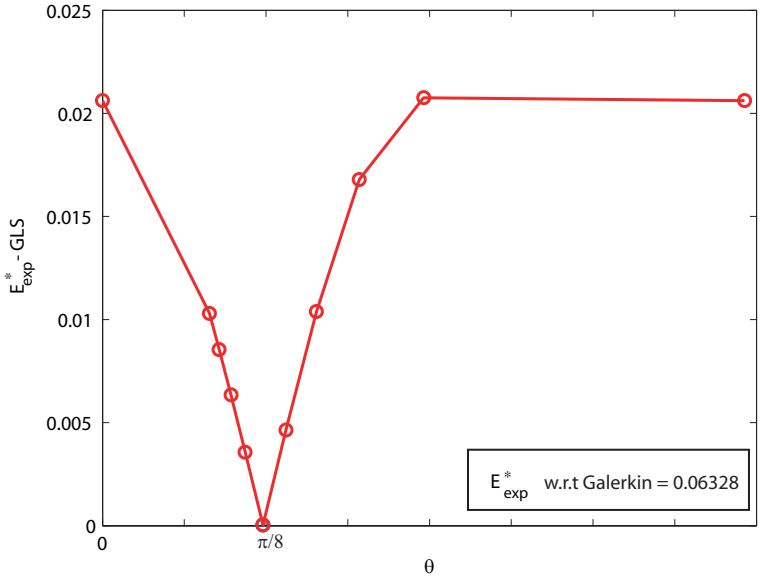

Figure 9. Example 2: Influence of the selection of the stabilization angle θ in the dispersion error of the GLS approximation for the mesh with 269 nodes. The estimates are computed both using $\theta = \alpha$.

4.3. Example 3: Scattering from Submarine-Shaped Obstacle

The acoustic scattering from an acoustically hard obstacle is studied. The geometry is a submarine-like object parametrized by the distances $l = 3, L = 60$ and $D = 6$, see figure 10. The incident wave

is characterized by its wave number $\kappa = \pi/3$ and an angle of incidence $\alpha = 5\pi/4$. The original problem is an unbounded Helmholtz problem which is reduced to an interior problem over a bounded computational domain with a circular boundary of radius $R = 36$. In the fictitious boundary, second-order Bayliss-Gunzberger-Turkel (BGT) [7, 13] absorbing boundary conditions are applied.

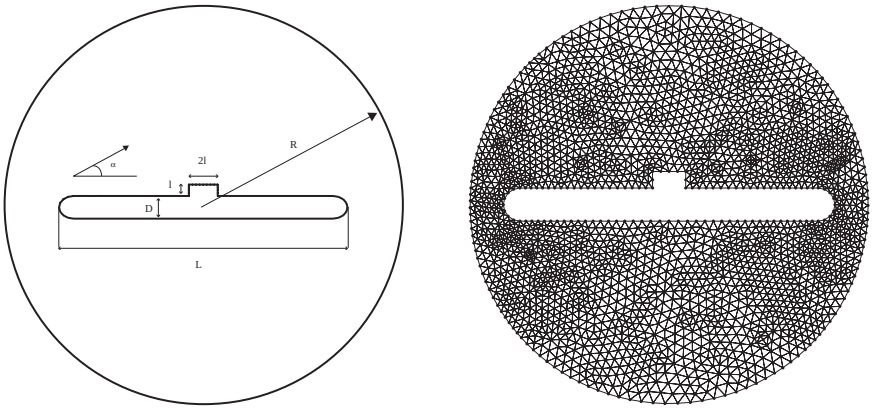

Figure 10. Example 3: Geometry of the fictitious bounded domain to study the scattering from a submarine-shaped obstacle problem (top) and a mesh of 2567 nodes (bottom).

The solution of the acoustic scattering problem is decomposed into $u = u_r + u_i$, where u_r and u_i are the so-called reflected and incident waves respectively. For a given wave number κ and incident wave direction α, the incident wave is $u_i = e^{i\kappa(\cos\alpha x + \sin\alpha y)}$, and the reflected wave u_r is the solution of the Helmholtz equation (1) with $f = 0$ (because $-\Delta u_i - \kappa u_i = 0$). Neumann boundary conditions are applied on the boundary of the obstacle

$$\boldsymbol{\nabla} u_r \cdot \mathbf{n} = -\boldsymbol{\nabla} u_i \cdot \mathbf{n},$$

($g = 0$ in (2b)), and first order Bayliss-Gunzberger-Turkel (BGT) non-reflecting boundary conditions are applied to the fictitious boundary

$$\boldsymbol{\nabla} u_r \cdot \mathbf{n} = \mathcal{M} u_r = -i\kappa u_r + \frac{\zeta}{2} u_r$$

in (2c). Here, ζ is the curvature of the surface of the scatterer, which for the particular case of a circular boundary of radius R is $\zeta = 1/R$.

In this example, the dispersion error committed in the approximation of the reflected solution u_r is studied. The total approximated scattered field u is computed from u_r adding the known incident field u_i. Figures 11 and 12 show the approximations obtained using the Galerkin method with a triangular mesh of 10026 nodes.

The behavior of the estimates of the dispersion error is analyzed for different unstructured triangular meshes both for the Galerkin and SUPG approximations of the reflected solution u_r. The triangular meshes are obtained from the initial mesh (see figure 10) using a uniform refinement, that is, a new mesh is obtained from a previous mesh by refining each triangle into 4 new triangles.

Table V shows the results associated to the Galerkin approximation. In this case, the stabilization parameters involved in the computation of the truth estimate E and the practical estimate E^* are computed using the predefined direction $\theta_h = \alpha = 5\pi/4$. Both the estimates obtained using

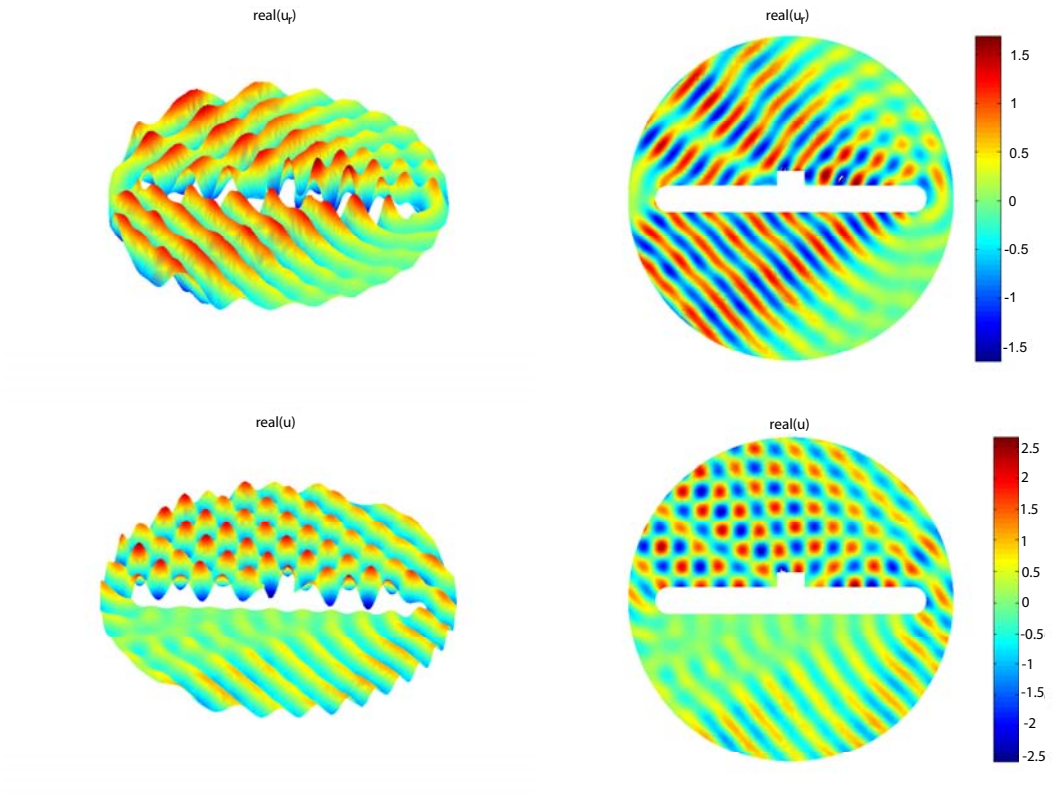

Figure 11. Example 3: Real part of the approximated solutions of the scattering problem for $\alpha = 5\pi/4$ and $\kappa L = 62.83$: scattered wave (top) and total wave (bottom). Approximations computed using the Galerkin method and a mesh of 10026 nodes.

a polynomial and an exponential fitting provide fairly good approximations to the truth value E. However, the exponential approach provides better effectivities, closer to one. Moreover the expected rate of convergence of the estimates of the dispersion error is obtained in all the cases.

	Galerkin				
$n_{\rm np}$	E	$E^*_{\rm pol}$	$E^*_{\rm exp}$	$\eta^*_{\rm pol}$	$\eta^*_{\rm exp}$
2567	0.69064	0.55271	0.67186	0.8003	0.9728
10026	0.19509	0.15604	0.20538	0.7998	1.0527
39620	0.04829	0.02959	0.05003	0.6128	1.0360

Table V. Example 3: Assessment of the dispersion error committed by the Galerkin method for uniformly refined unstructured triangular meshes.

Table VI shows the results obtained by the GLS approximations. Three different stabilized approximations are computed associated with the stabilization directions $\theta = 0$, $\theta = \pi/12$ and $\theta = \pi/6$. The corresponding estimates are computed using the same values of θ in the reference mesh, $\theta_h = \theta$.

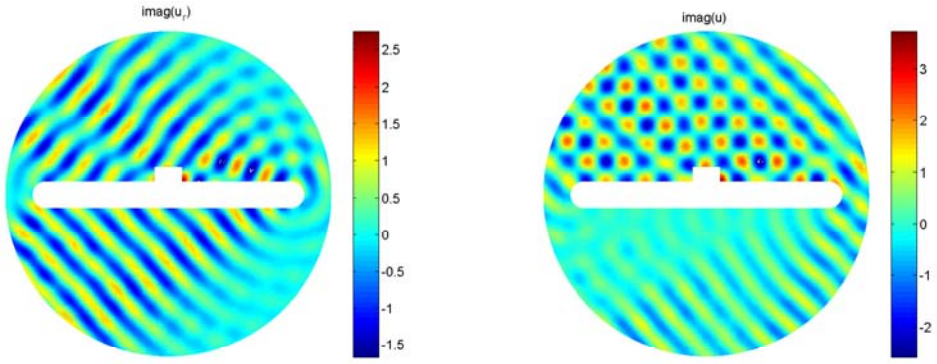

Figure 12. Example 3: Imaginary part of the approximated solutions of the scattering problem for $\alpha = 5\pi/4$ and $\kappa L = 62.83$ computed using the Galerkin method and a mesh of 10026 nodes: scattered wave (left) and total wave (right).

	GLS/FE					
	$\theta = 0$		$\theta = \pi/12$		$\theta = \pi/6$	
n_{np}	E^*_{pol}	E^*_{exp}	E^*_{pol}	E^*_{exp}	E^*_{pol}	E^*_{exp}
2567	$1.31{\cdot}10^{-2}$	$4.357{\cdot}10^{-3}$	$1.37{\cdot}10^{-2}$	$4.89{\cdot}10^{-3}$	$1.42{\cdot}10^{-2}$	$5.42{\cdot}10^{-3}$
10026	$4.77{\cdot}10^{-3}$	$1.771{\cdot}10^{-3}$	$4.80{\cdot}10^{-3}$	$1.79{\cdot}10^{-3}$	$4.83{\cdot}10^{-3}$	$1.81{\cdot}10^{-3}$
39620	$2.84{\cdot}10^{-3}$	$1.866{\cdot}10^{-4}$	$2.85{\cdot}10^{-3}$	$1.89{\cdot}10^{-4}$	$2.85{\cdot}10^{-3}$	$1.89{\cdot}10^{-4}$

Table VI. Example 3: Assessment of the dispersion error of the GLS method for uniformly refined unstructured triangular meshes. The GLS approximations are shown for different stabilization directions θ.

As expected, the use of stabilized formulations reduces considerably the dispersion error. In this case, the three tested stabilization directions provide similar results. Moreover, the exponential fitting which provides really good estimates for the Galerkin solution, yields really low estimates of the dispersion error of the stabilized approximations indicating that, in this example, the dispersion error is nearly negligible when using a GLS approach.

4.4. Example 4: 2D acoustic car cavity

This example studies the noise transmission inside a two-dimensional section of the cabin of a car which is excited by vibrations of the front panel and damped by Robin boundary conditions. This example is frequently used as a benchmark problem in error assessment for interior acoustic problems [10, 31, 18]. The geometry of the cabin is shown in figure 13. The size of the domain is characterized by the maximum horizontal and vertical lengths, $L_x = 2.7\,m$ and $L_y = 1.1\,m$, respectively. The source term entering in equation (1) is $f = 0$, and as mentioned in Remark 1, for interior acoustic wave propagation problems, the Neumann and Robin boundary conditions entering in equation (2) are of the form $g = -i\rho c\kappa\bar{v}_n$ and $\mathcal{M}u = -i\rho c\kappa A_n u$, where in this case the material parameters are $c = 340\,m/s$ standing for the speed of sound of the medium and $\rho = 1.225\,kg/m^3$ standing for the mass density. The vibrating front panel is excited with a unit normal velocity $\bar{v}_n = 1\,m/s$ whereas the roof is considered to be an absorbent panel with associated admittance $A_n = 1/2000\,m.(Pa.s)^{-1}$.

The rest of the boundary is assumed to be perfectly reflecting and thus $\bar{v}_n = 0\,m/s$. Finally, a wave

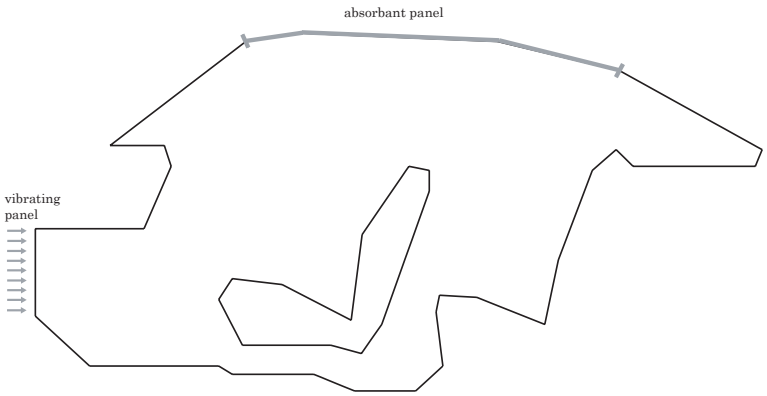

Figure 13. Example 4: Description of the two-dimensional section of the cabin of a car and its associated boundary conditions.

number of $\kappa \approx 9.7$ has been considered in the computations (equivalent to a frequency of $525\,Hz$).

In this problem, the exponential fitting presented above yields bad estimates, worse than the standard polynomial fitting. This is due to the fact that the solution is extremely complex, without a predominant direction. At many points of the domain, the solution can be expressed as a sum of several plane waves with similar amplitudes. Thus, the exponential fitting fails to properly approximate the local behavior of the modified solution in the vicinity of these points. Actually, the exponential recovery in these zones introduces unrealistic discontinuities resulting in bad estimates. In the following, this phenomenon is described in detail, as well as the proposed remedy.

It is well known that the exact solution of the 2D homogeneous Helmholtz equation can be expressed as an infinite sum of plane waves traveling in different directions. In the previous examples, the solutions were either a single plane wave traveling in a predefined direction (see examples 1 and 2) or had a prevalent plane wave direction, although the prevalent wave direction may vary from different zones of the domain (see the scattered solution of example 3). The sound transmission inside a car cabin is a more complex phenomenon and the solution does not present clear prevalent directions but is a combination of different plane waves with similar amplitudes (see figure 14).

Even if the exact solution has no prevalent directions, one can consider an exponential representation of the exact solution of the problem

$$u(\mathbf{x}) = r(\mathbf{x})e^{i\theta(\mathbf{x})},$$

where $r(\mathbf{x})$ and $\theta(\mathbf{x})$ are the real-valued functions providing the modulus and angle of u respectively. In the cases where the solution does not have a prevalent direction two phenomena may appear: on one hand the angle distribution $\theta(\mathbf{x})$ may present discontinuities coinciding with areas where the modulus vanishes, and, on the other hand, the modulus distribution $r(\mathbf{x})$ may present a highly non-linear and non-smooth behavior in some regions.

To illustrate these phenomena, the modulus and angle distributions of three simple solutions are shown in figure 15. First, the solution $u = 2e^{\kappa i x} + e^{\kappa i y}$ is considered. Note that, in this case, the plane wave traveling in the x-direction, $e^{\kappa i x}$, prevails over the wave traveling in the y-direction, $e^{\kappa i y}$. As can be seen in figure 15, the standard representation of the angle distribution $\theta(\mathbf{x})$ is a discontinuous function, which can be easily post-processed to recover a continuous angle distribution. Moreover,

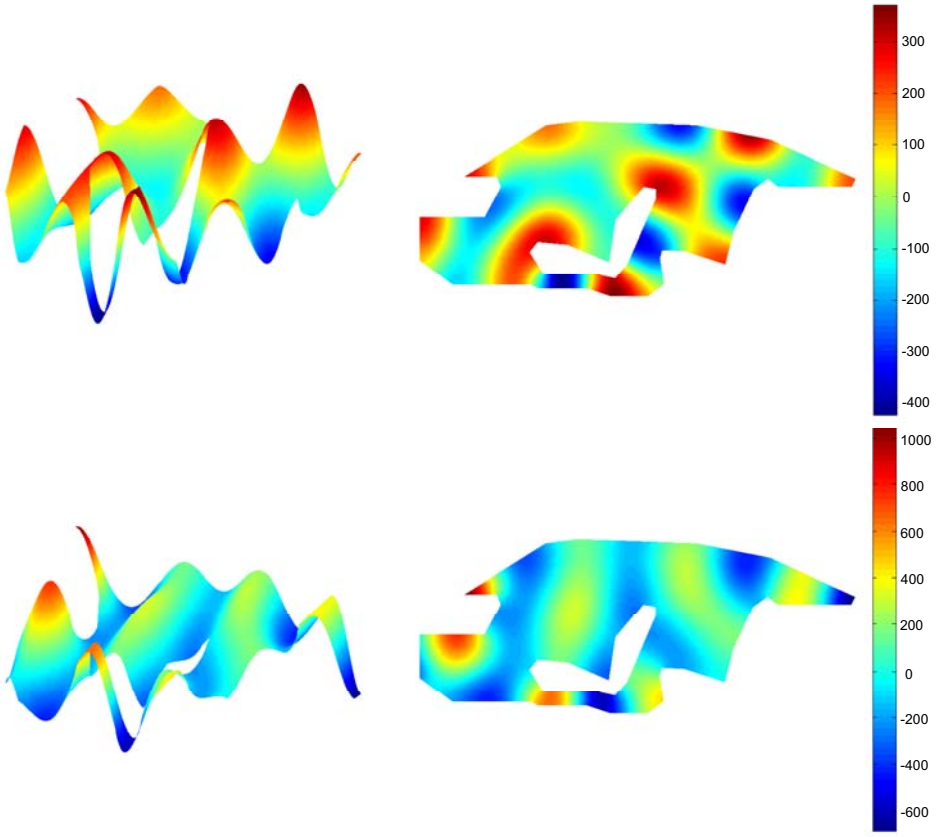

Figure 14. Example 4: Solution of the noise transmission problem inside the cabin of a car obtained with an overkill mesh of 20160 nodes: real part of u (top) and imaginary part of u (bottom).

the modulus does not present large variations over small regions. In this case, the exponential fitting described in section 3.5 provides accurate approximations of u. The second example, $u = e^{\kappa ix} + e^{\kappa iy}$, shows that if the solution is obtained combining two plane waves of the same amplitude, and thus it does not have any prevalent direction, angle discontinuities appear in some predefined straight lines. As the number of plane waves that comprise the solution u increases, see for instance the third example $u = e^{\kappa ix} + e^{\kappa iy} + e^{-\kappa iy}$, the modulus and angle distributions may present areas with a highly non-linear and non-smooth behavior. Note that, although the angle distribution only presents point or removable discontinuities at nine points of the domain, obtaining a globally smooth angle distribution from the standard angle representation is not a trivial task. Figure 16 shows, the behavior of the modulus and angle distribution associated to the acoustic pressure inside the car cabin. As can bee seen, its not easy to clearly identify the regions where the angle distribution is discontinuous.

The exponential fitting technique is based on finding a proper local polynomial representation for the modulus and angle distributions. Thus, in regions where either the angle is discontinuous or the modulus presents large oscillations, the exponential representation yields poor results. In this work,

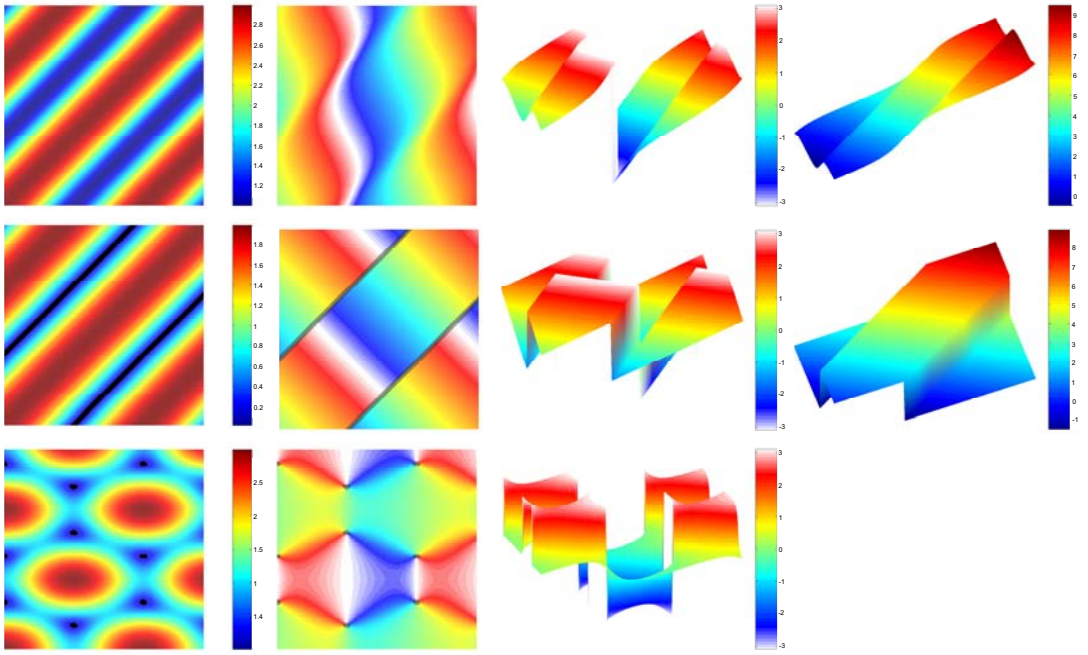

Figure 15. Example 4: Behavior of the modulus and angle distributions, $\theta(\mathbf{x})$ and $r(\mathbf{x})$ respectively, for three simple solutions in the unit square. From top to bottom: $u = 2e^{\kappa ix} + e^{\kappa iy}$, $u = e^{\kappa ix} + e^{\kappa iy}$ and $u = e^{\kappa ix} + e^{\kappa iy} + e^{-\kappa iy}$ for $\kappa = 9.7$. For each solution, the modulus distribution (left) and two views of the angle distributions (middle left, middle right) are shown. When possible, equivalent angle distributions only containing non-removable discontinuities – where the discontinuities associated to a 2π angle jump have been smoothed – are shown (right).

Figure 16. Example 4: Modulus (left) and angle (middle and right) distribution of the acoustic pressure inside the car cabin. The areas where the modulus is nearly zero are highlighted in the plot in the middle to see the areas where the angle distribution may present discontinuities.

a simple workaround is proposed: first, the smoothing technique identifies the elements near the angle discontinuities or near the regions where the modulus has a non-smooth behavior. Then, the exponential fitting is applied only to the non-selected elements while a polynomial fitting is applied

to the problematic elements. The estimates obtained with this combined approach are denoted in the following by $\widehat{E}^*_{\rm exp}$.

Estimates of the dispersion error for the Galerkin approximations of the solution are computed for two different triangular meshes of 568 and 2122 nodes respectively. The results are shown in table VII. As can be seen, both the polynomial and the combined estimates provide fairly good approximations to the truth value E. However, using an exponential representation, where possible, allows obtaining effectivities closer to one.

	Galerkin				
$n_{\rm np}$	E	$E^*_{\rm pol}$	$\widehat{E}^*_{\rm exp}$	$\eta^*_{\rm pol}$	$\eta^*_{\rm exp}$
568	0.15001	0.08231	0.12960	0.5486	0.8639
1092	0.07506	0.06694	0.07389	0.8918	0.9845

Table VII. Example 4: Assessment of the dispersion error of the Galerkin method for unstructured triangular meshes.

Figure 17 shows the elements that have been selected in the combined approach to apply the polynomial smoothing technique instead of the exponential one. Note that these regions are in good agreement with those highlighted in figure 16.

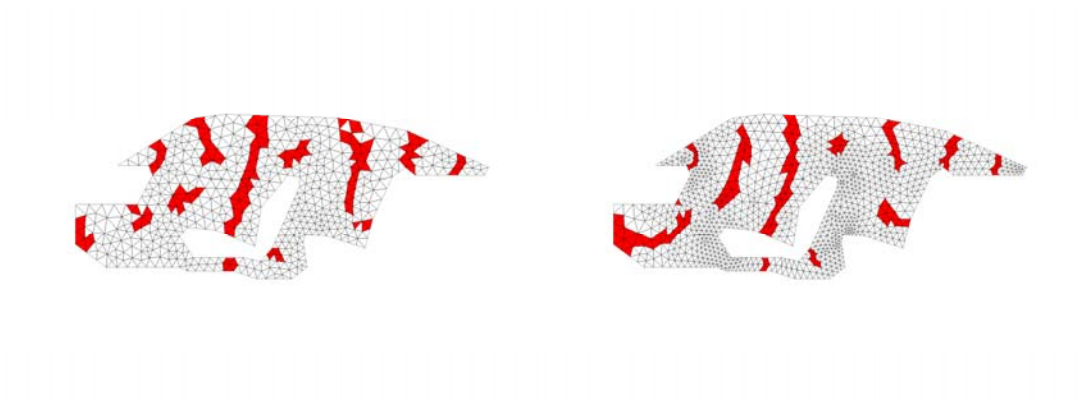

Figure 17. Example 4: Two unstructured triangular mesh where the red elements corresponding to solution fitting polynomial.

The reduction in the dispersion error obtained by using stabilization techniques is shown in table VIII. This table also shows the influence of the selection of the stabilization parameter. As can be seen the results of the GLS approximations with the three stabilization parameters are nearly identical for the two meshes, and provide significant improvement over the Galerkin method.

5. Conclusions

This paper introduces an error assessment technique for the numerical wave number κ_H of the Helmholtz problem, both for standard Galerkin and stabilized formulations. The strategy introduced in [28], which determines the numerical wave number κ_H as the one that better accommodates the

	GLS/FE		
$n_{\rm np}$	E	$E^*_{\rm pol}$	$\widehat{E}^*_{\rm exp}$
		$\theta = 0$	
568	0.03792	0.02267	0.03563
1092	0.00577	0.00653	0.00644
		$\theta = \pi/12$	
568	0.03808	0.02281	0.03583
1092	0.00583	0.00658	0.00651
		$\theta = \pi/6$	
568	0.03824	0.02294	0.03601
1092	0.00589	0.00663	0.00656

Table VIII. Example 4: Assessment of the dispersion error of the GLS method for an unstructured triangular mesh. The GLS approximations are shown for different stabilization directions θ.

numerical solution u_H in a modified problem, has been extended to deal with stabilized formulations. The numerical solution u_H and the reference modified problem are computed using stabilized methods to obtain both more accurate approximations of the solution and sharper estimates of the dispersion error.

The proposed strategy requires obtaining an inexpensive approximation of the modified problem, using post-processing techniques. Thus, the associated numerical wave number is readily recovered using a closed expression. A new improved recovery technique is developed to take advantage of the nature of the solutions of wave problems. The standard polynomial least squares techniques is replaced by an exponential fitting yielding much sharper results in most applications. However, both the error estimates computed using a polynomial and exponential fitting provide reasonable approximations of the true errors.

The estimates of the dispersion error reaffirm that using stabilized approximations substantially improves the performance of finite-element computations of time-harmonic acoustics at high wave numbers. The sensitivity of the choice of the stabilization parameter for the GLS method has been studied concluding that the change in the orientation of the stabilization parameter has little effect on the results of non-academic problems or when considering non-structured meshes.

REFERENCES

1. Mark Ainsworth. Discrete dispersion relation for hp-version finite element approximation at high wave number. *SIAM J. Numer. Anal.*, 42(2):553–575, 2004.
2. I. Babuška, F. Ihlenburg, E. T. Paik, and S. A. Sauter. A generalized finite element method for solving the Helmholtz equation in two dimensions with minimal pollution. *Comput. Methods Appl. Mech. Engrg.*, 128:325–359, 1995.
3. I. Babuška, F. Ihlenburg, T. Strouboulis, and K. Gangaraj. A posterori error estimation for finite element solutions of Helmholtz Part II: Estimation of the pollution error. *Internat. J. Numer. Methods Engrg.*, 40:3883–3900, 1997.
4. I. Babuška, F. lhlenburg, T. Strouboulis, and S. K. Gangaraj. A posteriori error estimation for finite element solutions of Helmholtz' equation. Part I: The quality of local indicators and estimators. *Internat. J. Numer. Methods Engrg.*, 40(18)(7):3443–3462, 1997.
5. I. Babuška and J. M. Melenk. The partition of unity method. *Internat. J. Numer. Methods Engrg.*, 40:727–758, 1997.
6. I. Babuška and S. A. Sauter. Is the pollution effect of the fem avoidable for the Helmholtz equation considering high wavenumber? *SIAM Review*, 42(3):451–484, 2000.
7. A. Bayliss, M. Gunzburger, and E. Turkel. Boundary conditions for the numerical solution of elliptic equations in exterior regions. *SIAM (Soc. Ind. Appl. Math.) J. Appl. Math.*, 42(2):430–451, 1982.

8. P. Bouillard. Admissible fields and error estimation for acoustic FEA with low wave numbers. *Comput. Struct.*, 73(1-5):227–237, 1999.
9. P. Bouillard. Influence of the pollution on the admissible field error estimation for fe solutions of the Helmholtz equation. *Internat. J. Numer. Methods Engrg.*, 45(7):783–800, 1999.
10. P. Bouillard and F. Ihlenburg. Error estimation and adaptivity for the finite element method in acoustics: 2D and 3D applications. *Comput. Methods Appl. Mech. Engrg.*, 176(1):147–163, 1999.
11. G. Calderón and P. Díez. Análisis de diferentes estimadores de error de postproceso para adaptatividad orientada al resultado. *Rev. Internac. Métod. Numér. Cálc. Diseñ. Ingr.*, 22(2):193–213, 2006.
12. P. Díez and G. Calderón. Goal-oriented error estimation for transient parabolic problems. *Comput. Mech.*, 39(5):631–646, 2007.
13. R. Djellouli, C. Farhat, A. Macedo, and R. Tezaur. Finite element solution of two-dimensional acoustic scattering problems using arbitrarily shaped convex artificial boundaries. *J. Comput. Acoust.*, 8(1):81–99, 2000.
14. J. Donea and A. Huerta. *Finite Element Methods for Flow Problems*. John Wiley & Sons, Chichester, 2003.
15. L.P. Franca and E.G. Dutra do Carmo. The Galerkin gradient least-squares method. *Comput. Methods Appl. Mech. Engrg.*, 74(1):41–54, 1989.
16. K. Gerdes and F. Ihlenburg. On the pollution effect in FE solutions of the 3D-Helmholtz equation. *Comput. Methods Appl. Mech. Engrg.*, 170(1-2):155–172, 1999.
17. I. Harari and T.J.R. Hughes. Galerkin/least-squares finite element methods for the reduced wave equation with nonreflecting boundary conditions in unbounded domains. *Comput. Methods Appl. Mech. Engrg.*, 98(3):411–454, 1992.
18. I. Harari and F. Magoulès. Numerical investigations of stabilized finite element computations for acoustics. *Wave Motion*, 39:339–349, 2004.
19. I. Harari and C. L. Nogueira. Reducing dispersion of linear triangular elements for the Helmholtz equation. *J. Engrg. Mech.*, 128(3):351–358, 2002.
20. T. J. R. Hughes and A. N. Brooks. A multi-dimensional upwind scheme with no crosswind diffusion. *Finite Element Methods for Convection Dominated Flows (Collection of Papers Pres at Winter Ann. Meeting Amer. Soc. Mech. Engrs(ASME), New York)*, 34:19–35, 1979.
21. T. J. R. Hughes, L. P. Franca, and G.M. Hulbert. A new finite element formulation for computational fluid dynamics. *Comput. Methods Appl. Mech. Engrg.*, 73:173–189, 1989.
22. F. Ihlenburg. *Finite Element Analysis of Acoustic Scattering*, volume 132 of *Applied Mathematical Sciences*. Springer-Verlarg, New York, 1998.
23. F. Ihlenburg and I. Babuška. Dispersion analysis and error estimation of Galerkin fininite element methods for the helmoholtz equation. *Internat. J. Numer. Methods Engrg.*, 38:3745–3774, 1995a.
24. F. Ihlenburg and I. Babuška. Finite element solution of the Helmholtz equation with high wave number. Part 1: The hp-version of the FEM. *Comput. Math. Appl.*, 38:9–37, 1995b.
25. S. Irimie and P. Bouillard. A residual a posteriori error estimator for the finite element solution of the Helmholtz equation. *Comput. Methods Appl. Mech. Engrg.*, 190(31):4027–4042, 2001.
26. J.T. Oden, S. Prudhomme, and L. Demkowicz. A posteriori error estimation for acoustic wave propagation problems. *Arch. Comput. Methods Engrg.*, 12(4):343–389, 2005.
27. J. Peraire and A. T. Patera. Asymptotic a posteriori finite element bounds for the outputs of noncoercive problems: The Helmholtz and Burgers equations. *Comput. Methods Appl. Mech. Eng.*, 171(1):77–86, 1999.
28. L.M. Steffens and P. Díez. A simple strategy to assess the error in the numerical wave number of the finite element solution of the Helmholtz equation. *Comput. Methods Appl. Mech. Engrg.*, 198:1389–1400, 2009.
29. J. R. Stewart and T.J.R. Hughes. Explicit residual-based a posteriori error estimation for finite element discretizations of the Helmholtz equation. computation of the constant and new measures of error estimator quality. *Comput. Methods Appl. Mech. Engrg.*, 131(3-4):335–363, 1996.
30. J. R. Stewart and T.J.R. Hughes. A posteriori error estimation and adaptive finite element computation of the Helmholtz equation in exterior domains. *Finite Elem. Anal. Des.*, 22(1):15–24, 1996.
31. S. Suleau, A. Deraemaeker, and P. Bouillard. Dispersion and pollution of meshless solutions for the Helmholtz equation. *Comput. Methods Appl. Mech. Engrg.*, 190:639–657, 2000.
32. N.-E. Wiberg, L.F. Zeng, and X.D. Li. Error estimation and adaptivity in elastodynamics. *Comput. Methods Appl. Mech. Eng.*, 101:369–395, 1992.

Goal-oriented *h*-adaptivity for the Helmhotz equation equation: error estimates, local indicators and refinement strategies

Steffens, L. M., Parés N., and Díez P.

Computational Mechanics

submitted for publication, 2010

Computational Mechanics manuscript No.
(will be inserted by the editor)

Goal-oriented *h*-adaptivity for the Helmholtz equation: error estimates, local indicators and refinement strategies

Lindaura Maria Steffens · Núria Parés · Pedro Díez

Received: date / Accepted: date

Abstract This paper introduces a new goal-oriented adaptive technique based on a simple and effective post-process of the finite element approximations. The goal-oriented character of the estimate is achieved by analyzing both the direct problem and an auxiliary problem, denoted as *adjoint* or *dual*, which is related to the quantity of interest. Thus, the error estimation technique proposed in this paper would fall into the category of recovery-type and explicit residual *a posteriori* error estimates. The procedure is valid for general linear quantities of interest and it is also extend to non-linear ones. The numerical examples demonstrate the efficiency of the proposed approach and discuss: 1) different error representations, 2) assessment of the dispersion error, and 3) different remeshing criteria.

1 INTRODUCTION

One of the major problems in acoustic simulations, and in particular in problems governed by the Helmholtz equation, is that the Galerkin method requires too fine meshes. This is computationally unaffordable and undermines the practical utility of the method. Often the *rule of the thumb*, which prescribes the minimal discretization per wavelength, is used. However, it is widely known that this rule is not sufficient to obtain reliable results for large wave numbers due to dispersion and pollution errors [1–5]. Furthermore, non-uniform meshes are required to resolve singularities or large gradients in the solution. This suggests using adaptivity to control accuracy and obtain *optimal* meshes refining at the right locations.

Lindaura Maria Steffens · Núria Parés · Pedro Díez
Laboratori de Càlcul Numèric
Departament de Matemàtica Aplicada III
Universitat Politècnica de Catalunya, Barcelona, Spain
E-mail: lindaura.steffens@upc.edu

The basic scheme of the adaptive procedure is: first, estimate the discretization error; second, develop the strategy associated with the *h*-adaptive refinement, which determines the elements to be refined; and finally, generate a new mesh. Obviously, the most important ingredient in any adaptive procedure is a reliable error estimation procedure.

Goal-oriented adaptivity is related with controlling the error in a given quantity of interest, and optimal refinement techniques should only refine the areas affecting this quantity. Moreover, error assessment for the quantity of interest provides both the global error quantity and the local contributions to the error in the quantity of interest in each element. These local quantities are used to design the adaptive procedure.

While some progress has been done in assessing the global accuracy of finite element approximations for the Helmholtz equation [6–10], there exist very few literature concerning a posteriori goal-oriented error estimation for the Helmholtz equation [11–14]. For instance, [12] provides a strategy to compute asymptotic bounds for linear and non-linear quantities of interest based on the equilibrated residual method. Another example is [13] which proposes a goal-oriented adaptive technique for modeling the external human auditory system by the boundary element method.

The remainder of the paper is structured as follows: section 2 introduces the description of the problem to the solved. Section 3 presents a general framework for assessing the error in general linear and non-linear quantities of interest. Different representations for the linear contribution to the output are introduced in section 4. Section 5 is devoted to obtain error estimates for general outputs using the different error representations given in section 4. The adaptive strategy is introduced in the section 6, where local indicators and several strategies of refinement are defined. Finally, in section 7 the proposed procedure for goal-oriented adaptivity is tested in some numerical examples. The relation between

the different error representations and the dispersion error of the direct and adjoint problems is also discussed.

2 PROBLEM STATEMENT

The propagation of acoustic waves is governed by the wave equation describing the evolution of the acoustic pressure p as a function of the position $\mathbf{x}$ and time t. The harmonic assumption states that for a given angular frequency ω, $p(\mathbf{x},t) = u(\mathbf{x})e^{i\omega t}$, where the new unknown $u(\mathbf{x})$ is the complex amplitude of the acoustic pressure. For an interior spatial domain Ω, $u(\mathbf{x})$ is the solution of the Helmholtz equation

$$-\Delta u - \kappa^2 u = f \quad \text{in } \Omega, \tag{1}$$

taking the acoustic wave number $\kappa = \omega/c$ where c is the speed of sound. Equation (1) is complemented with the following boundary conditions

$$u = u_D \qquad \text{on } \Gamma_D, \tag{2a}$$

$$\nabla u \cdot \mathbf{n} = g \qquad \text{on } \Gamma_N, \tag{2b}$$

$$\nabla u \cdot \mathbf{n} = mu + \beta \qquad \text{on } \Gamma_R, \tag{2c}$$

where Γ_D, Γ_N and Γ_R are a disjoint partition of the boundary where Dirichlet, Neumann and Robin boundary conditions are applied respectively. The outward unit normal is denoted by $\mathbf{n}$ and u_D, f, g, m and β are the prescribed data, which are assumed to be sufficiently smooth.

The boundary value problem defined by equations (1) and (2) is readily expressed in its weak form introducing the solution and test spaces $\mathscr{U} := \{u \in \mathscr{H}^1(\Omega), u|_{\Gamma_D} = u_D\}$ and $\mathscr{V} := \{v \in \mathscr{H}^1(\Omega), v|_{\Gamma_D} = 0\}$. Here $\mathscr{H}^1(\Omega)$ is the standard Sobolev space of complex-valued square integrable functions with square integrable first derivatives. The weak form of the problem then reads: find $u \in \mathscr{U}$ such that

$$a(u,v) = \ell(v) \quad \forall v \in \mathscr{V},$$

where the sesquilinear form $a(\cdot,\cdot)$ and antilinear functional $\ell(\cdot)$ are defined as

$$a(u,v) := \int_\Omega \nabla u \cdot \nabla \bar{v} d\Omega - \int_\Omega \kappa^2 u \bar{v} d\Omega - \int_{\Gamma_R} mu\bar{v} d\Gamma,$$

$$\ell(v) := \int_\Omega f\bar{v} d\Omega + \int_{\Gamma_N} g\bar{v} d\Gamma + \int_{\Gamma_R} \beta\bar{v} d\Gamma, \tag{3}$$

and the symbol $\bar{\cdot}$ denotes the complex conjugate.

The finite element approximation of u is found by first discretizing the domain Ω into triangular or quadrilateral elements Ω_k, $k = 1,\dots,\mathrm{n_{el}}$, $\mathrm{n_{el}}$ being the number of elements in the mesh. This mesh has an associated characteristic mesh size H and induces the discrete functional spaces $\mathscr{U}_H \subset \mathscr{U}$ and $\mathscr{V}_H \subset \mathscr{V}$. The finite element approximation $u_H \in \mathscr{U}_H$ is then such that

$$a(u_H,v) = \ell(v) \quad \forall v \in \mathscr{V}_H.$$

3 ERROR ASSESSMENT FOR GENERAL (NONLINEAR) QUANTITIES OF INTEREST

A posteriori error estimation techniques aim at assessing the error committed in the approximation of u, $e := u - u_H$, where $e \in \mathscr{V}$ is the solution of the primal residual problem

$$a(e,v) = \ell(v) - a(u_H,v) =: R^P(v) \quad \forall v \in \mathscr{V}, \tag{4}$$

$R^P(\cdot)$ standing for the weak residual associated to the finite element approximation u_H.

When applied to classical problems (in which $a(\cdot,\cdot)$ is coercive) a first step in a posteriori assessment is estimating the error measured in the energy norm, that is obtaining a good approximation of e and computing $a(e,e)$. However, in acoustic problems, since the Helmholtz equation is not elliptic, the form $||v||^2 = a(v,v)$ does not define a squared norm. There is no natural energy norm to measure the error.

Additionally, assessing the error measured in some functional norm is not sufficient for many applications. In practice, the finite element user is interested in specific magnitudes extracted from the global solution by some postprocess. These magnitudes are referred as quantities of interest or functional outputs. Goal-oriented error assessment strategies aim at estimating the error committed in these quantities and possibly providing bounds for it.

The quantities of interest considered here are nonlinear functional outputs of the solution, $J(u)$, and the aim is to assess the error committed when approximating these quantities using the finite element approximation. Specifically, the goal is to assess and control the quantity

$$J(u) - J(u_H).$$

For the purposes of this paper, it is convenient to make the linear, quadratic and higher order terms contributions of $J(u)$ more explicit. To this end, $J(u)$ is expanded introducing the Gateaux first and second derivatives of $J(\cdot)$ at u_H, namely

$$J(u_H+v) = J(u_H) + \ell^{\mathscr{O}}(v) + \mathscr{Q}(v,v) + \mathscr{W}(v), \tag{5}$$

where $\ell^{\mathscr{O}}(v) = [D_v J](u_H)\cdot(v)$ and $2\mathscr{Q}(v_1,v_2) = [D_v^2 J](u_H)\cdot(v_1,v_2)$, see [12,15]. Note that $\ell^{\mathscr{O}} : \mathscr{H}^1(\Omega) \to \mathbb{C}$ and $\mathscr{Q} : \mathscr{H}^1(\Omega)\times\mathscr{H}^1(\Omega) \to \mathbb{C}$ are the linear and bilinear contributions of $J(\cdot)$, respectively, and that the functional $\mathscr{W}$ contains the higher order terms. In the case of a linear output, notice that $\mathscr{Q} = \mathscr{W} = 0$.

Using this decomposition and taking into account that $u = u_H + e$, the error in the quantity of interest may be rewritten as

$$J(u) - J(u_H) = J(u_H+e) - J(u_H) = \ell^{\mathscr{O}}(e) + \mathscr{Q}(e,e) + \mathscr{W}(e). \tag{6}$$

Thus, it is clear that in order to estimate the error in the quantity of interest, it is sufficient to estimate the linear, quadratic and higher-order terms separately, $\ell^{\mathscr{O}}(e)$, $\mathscr{Q}(e,e)$ and $\mathscr{W}(e)$ respectively.

Requiring $\mathscr{Q}$ and $\mathscr{W}$ to be $\mathscr{L}^2$-continuous, which in this particular case is equivalent to $|\mathscr{Q}(v)| \leq c_1\|v\|_0^2$ and $|\mathscr{Q}(v)| \leq c_2\|v\|_0^3$ where $\|\cdot\|_0$ denotes the $\mathscr{L}^2$-norm, shows that the quadratic and higher-order contributions to the error, $\mathscr{Q}(e,e)$ and $\mathscr{W}(e)$, converge as $\mathscr{O}(H^4)$ and $\mathscr{O}(H^6)$ respectively, whereas the linear term $\ell^{\mathscr{O}}(e)$ converges quadratically – recall that the finite element method for a regular problem converges quadratically in the $\mathscr{L}^2$-norm. Thus, for sufficiently small H the linear term provides a good inside to the error in the output since the other terms are negligible.

The following sections are devoted to describe the error assessment techniques to estimate $J(e)$ (linear and higher order contributions) and to provide local error estimators able to effectively drive the adaptive procedures.

4 ERROR REPRESENTATION OF A LINEARIZED OUTPUT AND ADJOINT PROBLEM

This section presents alternative representations for the linear contribution to the error in the output $\ell^{\mathscr{O}}(e)$. This alternative representations do not directly yield computable expressions for the estimates of the output because they depend on the exact errors on the primal and adjoint problems. However, estimates may be easily recovered using existing techniques providing approximations for the errors, as described in the following section.

The quantities of interest considered here are such that their linear part is expressed as

$$\ell^{\mathscr{O}}(v) = \int_{\Omega} f^{\mathscr{O}} v\, d\Omega + \int_{\Gamma_N} g^{\mathscr{O}} v\, d\Gamma + \int_{\Gamma_R} \beta^{\mathscr{O}} v\, d\Gamma, \tag{7}$$

where $f^{\mathscr{O}}$, $g^{\mathscr{O}}$ and $\beta^{\mathscr{O}}$ are given functions characterizing the linearized quantity of interest. Note that $\ell^{\mathscr{O}}(v)$ has the same structure as $\ell(v)$, see equation (3), excepting the conjugate in its argument. Thus, $\ell^{\mathscr{O}}$ is a linear functional whereas ℓ is a anti-linear functional.

Most existing techniques to estimate the error in a quantity of interest introduce an alternative representation for $\ell^{\mathscr{O}}(e)$. In practice, different error representations are used to properly estimate $\ell^{\mathscr{O}}(e)$. These error representations require introducing an auxiliary problem, denoted as *adjoint* or *dual* problem which reads: find $\psi \in \mathscr{V}$ such that

$$a(v,\psi) = \ell^{\mathscr{O}}(v) \quad \forall v \in \mathscr{V}, \tag{8}$$

which is equivalent to determine the adjoint solution ψ verifying the Helmholtz equation

$$-\Delta\psi - \kappa^2\psi = \bar{f}^{\mathscr{O}} \quad \text{in } \Omega,$$

complemented with the boundary conditions

$$\psi = 0 \qquad \text{on } \Gamma_D, \tag{9a}$$

$$\nabla\psi\cdot\mathbf{n} = \bar{g}^{\mathscr{O}} \qquad \text{on } \Gamma_N, \tag{9b}$$

$$\nabla\psi\cdot\mathbf{n} = \bar{m}\psi + \bar{\beta}^{\mathscr{O}} \qquad \text{on } \Gamma_R. \tag{9c}$$

In order to assess the error in the quantity of interest the adjoint solution ψ is approximated numerically by $\psi_H \in \mathscr{V}_H$ such that

$$a(v,\psi_H) = \ell^{\mathscr{O}}(v) \quad \forall v \in \mathscr{V}_H,$$

introducing the adjoint error $\varepsilon := \psi - \psi_H$ solution of the adjoint residual problem

$$a(v,\varepsilon) = \ell^{\mathscr{O}}(v) - a(v,\psi_H) =: R^D(v) \quad \forall v \in \mathscr{V}_H, \tag{10}$$

where $R^D(\cdot)$ is the weak adjoint residual associated with ψ_H.

The adjoint problem is introduced such that the following error representation holds:

$$\ell^{\mathscr{O}}(e) = a(e,\psi) = a(e,\varepsilon)$$

where the Galerkin orthogonality of the adjoint approximation ψ_H is used in the last equality. In turn, this error representation allows assessing the error in terms of the residuals of the direct and adjoint problems, namely

$$\ell^{\mathscr{O}}(e) = a(e,\varepsilon) = R^P(\varepsilon) = R^D(e). \tag{11}$$

These representations are obtained substituting $v = \varepsilon$ in (4) and $v = e$ in (10) respectively.

5 RECOVERY TYPE: ERROR ESTIMATES FOR LINEAR AND NONLINEAR OUTPUTS

A posteriori assessment of quantities of interest relies on obtaining a good approximation of $J(u) - J(u_H)$. This translates in finding a new enhanced solution u^*, based on the information at hand, that is u_H, and such that u^* approximates the actual solution u much better than u_H. Thus, a computable error estimate is readily obtained

$$e \approx e^* = u^* - u_H$$

yielding also the corresponding estimate for the quantity of interest

$$J(u) - J(u_H) \approx \ell^{\mathscr{O}}(e^*) + \mathscr{Q}(e^*,e^*) + \mathscr{W}(e^*). \tag{12}$$

This approximation of the error in the quantity of interest is obtained from equation (6) substituting the actual error e by its approximation e^*.

Thus, the key issue in any error estimation technique is to produce a properly enhanced solution u^* (or in some cases obtaining an enhanced approximation of the gradient of the solution $q^* \approx \nabla u$ suffices). The strategies producing

the enhanced solution u^* (or q^* respectively) are classified into two categories: recovery type estimators and implicit residual type estimators. Recovery techniques, based on the ideas of Zienkiewicz and Zhu [16–18], are often preferred by practitioners because they are robust and simple to use. On the other hand, a posteriori implicit residual-type estimators have a sounder mathematical basis and produce estimates that are upper or lower bounds of the error [19–23]. At first glance on could think that, once the enhanced solutions u^* or q^* are obtained either using recovery or residual-type error estimators, estimates for the error in the quantity of interest may be directly obtained using equation (12). However, as mentioned in section (4), this representation does not provide sound results. This is because inserting the enhanced error e^* (or its gradient q^*) in the functionals $\ell^{\mathscr{O}}(\cdot)$, $\mathscr{Q}(\cdot,\cdot)$ and $\mathscr{W}(\cdot)$ may not yield accurate results even when the enhanced approximation u^* provides a reasonable approximation of u in terms of energy. In practice, since the most-contributing term to the error in the quantity of interest is the linear term, alternative representations are used for this term, as the ones described in section (4), whereas no additional effort is done in the higher-order terms.

The linear term $\ell^{\mathscr{O}}(e)$ may be assessed by any of the following strategies:

1. Compute the primal enhanced solution u^* to obtain $e^* = u^* - u_H$ and evaluate $\ell^{\mathscr{O}}(e^*)$. This option is readily discarded as announced previously
2. Compute the primal enhanced solution u^* to obtain e^* and evaluate $R^D(e^*)$.
3. Compute the adjoint enhanced solution ψ^* to obtain $\varepsilon^* = \psi^* - \psi_H$ and evaluate $R^P(\varepsilon^*)$.
4. Compute both the primal and enhanced errors e^* and ε^* and evaluate $a(e^*,\varepsilon^*)$.

In this work, the strategies presented in [24,25] are used to recover the enhanced solutions u^* and ψ^* from u_H and ψ_H respectively. A simple and inexpensive post-processing technique is used to recover the approximations u^* and ψ^* of u and ψ in a finer reference mesh of associated characteristic mesh size $h << H$. Thus, $u^* \in \mathscr{U}_h$ and $\psi^* \in \mathscr{V}_h$, where $\mathscr{U}_h$ and $\mathscr{V}_h$ are the discrete functional spaces associated to the finer reference mesh, $\mathscr{U}_H \subset \mathscr{U}_h \subset \mathscr{U}$ and $\mathscr{V}_H \subset \mathscr{V}_h \subset \mathscr{V}$.

As mentioned before, for sufficiently refined meshes, the error in the quantity of interest is controlled by the linear term, since the quadratic and higher-order contributions converge faster to zero, see section (3). For this, the proposed approach is to make use of the available estimate e^* to obtain a simple and inexpensive estimate of the non-linear contributions. Namely, the quadratic and higher-order contributions to the error in the output, $\mathscr{Q}(e,e)$ and $\mathscr{W}(e)$ respectively, are assessed using the reconstruction of the primal error e^* used to assess the linear part of the error, namely

$$\mathscr{Q}(e,e) \approx \mathscr{Q}(e^*,e^*) \quad \text{and} \quad \mathscr{W}(e) \approx \mathscr{W}(e^*).$$

6 LOCAL INDICATORS AND ADAPTIVITY CRITERIA

Adaptive mesh refinement is nowadays an essential tool to obtain high-fidelity simulations at the lesser cost. The main ingredients of the proposed adaptive procedure are: the *h-refinement*, that is, the new meshes are obtained by subdividing the elements of the mesh; *optimal indicators*, the refinement is organized with the aim of achieving equal error in each element of new mesh; *iterative process*, the target in each step of refinement is to reduce the global error until the calculated error drops below the tolerance specified by the user.

Additionally, assessing the error measured in some functional norm is not sufficient for many applications. In practice, the finite element user is interested in specific magnitudes extracted from the global solution by some post-process. These magnitudes are referred as quantities of interest or functional outputs. Goal-oriented error assessment strategies aim at estimating the error committed in these quantities and possibly providing bounds for it.

This requires obtaining local error indicators allowing to decide the elements to be marked for refinement – those with larger contribution to the total error. In order to determine the contribution of every element to the total error, spatial error distributions of the estimates are derived decomposing the global estimates into a sum of local contributions in each element of the mesh induced by $\mathscr{U}_H$.

The estimates for the error in the quantity of interest are of the form

$$J(u) - J(u_H) \approx \ell^{\mathscr{O}}(e^*) + \mathscr{Q}(e^*,e^*) + \mathscr{W}(e^*),$$

where the linear term $\ell^{\mathscr{O}}(e^*)$ is replaced by either $a(e^*,\varepsilon^*)$, $R^P(\varepsilon^*)$ or $R^D(e^*)$, depending on the selected representation of the linear term. Since the linear term is the driving term of the error in the quantity of interest, in this work, the adaptive procedure is chosen to be driven by $\ell^{\mathscr{O}}(e^*)$. That is, the global estimate for the linear term $\ell^{\mathscr{O}}$ is decomposed into a sum of local contributions in each element. These local quantities are used to design the adaptive procedure.

6.1 Local Indicators

The natural restriction to every element Ω_k of the integral forms $a(\cdot,\cdot)$, $\ell(\cdot)$ and $\ell^{\mathscr{O}}(\cdot)$ yield the elementary contributions denoted by $a_k(\cdot,\cdot)$, $\ell_k(\cdot)$ and $\ell^{\mathscr{O}}_k(\cdot)$ such that

$$a(u,v) = \sum_{k=1}^{\mathrm{n_{el}}} a_k(u,v), \;\; \ell(v) = \sum_{k=1}^{\mathrm{n_{el}}} \ell_k(v), \;\; \ell^{\mathscr{O}}(v) = \sum_{k=1}^{\mathrm{n_{el}}} \ell^{\mathscr{O}}_k(v).$$

Similarly, the primal and adjoint residuals are decomposed as

$$R^P(v) = \sum_{k=1}^{\mathrm{n_{el}}} R^P_k(v) \quad , \quad R^D(v) = \sum_{k=1}^{\mathrm{n_{el}}} R^D_k(v),$$

where $R_k^P(\cdot) := \ell_k(\cdot) - a_k(u_H,\cdot)$ and $R_k^D(\cdot) := \ell_k^{\mathscr{O}}(\cdot) - a_k(\cdot,\psi_H)$.

Hence, the error representations for the linear contribution of the error in the quantity of interest given in equation (11) are associated to the elementary error distributions

$$\ell^{\mathscr{O}}(e) = \sum_{k=1}^{\mathrm{n_{el}}} \ell_k^{\mathscr{O}}(e) = \sum_{k=1}^{\mathrm{n_{el}}} a_k(e,\varepsilon) = \sum_{k=1}^{\mathrm{n_{el}}} R_k^P(\varepsilon) = \sum_{k=1}^{\mathrm{n_{el}}} R_k^D(e).$$

It is worth mentioning that, while the global error quantities are equal in all the representations, the local quantities $\ell_k^{\mathscr{O}}(e)$, $a_k(e,\varepsilon)$, $R_k^P(\varepsilon)$ and $R_k^D(e)$ represent different elementary contributions to the error and, besides, they are not necessarily positive nor even real numbers.

From the four possible representations of the linear contribution of the error $\ell^{\mathscr{O}}(e)$, in this work only the two expressions involving the primal and adjoint residuals are used, thus yielding the global estimates

$$\eta^{\varepsilon} := R^P(\varepsilon^*) \quad \text{and} \quad \eta^{e} := R^D(e^*), \tag{13}$$

and its associated local error indicators $\eta_k^{\varepsilon} := R_k^P(\varepsilon^*)$ and $\eta_k^{e} := R_k^D(e^*)$, such that

$$\eta^{\varepsilon} := \sum_{k=1}^{\mathrm{n_{el}}} \eta_k^{\varepsilon} \quad \text{and} \quad \eta^{e} := \sum_{k=1}^{\mathrm{n_{el}}} \eta_k^{e}. \tag{14}$$

Remark 1 *The local elemental contributions η_k^{ε} and η_k^{e} are the natural decomposition of the estimates η^{ε} and η^{e} to the elements. However, the computation of the local contributions η_k^{ε} and η_k^{e} requires the computation of local integral forms. This can be done either by storing the elemental contributions to the system matrices and vectors or by recomputing these contributions in an elementary loop. A cheaper and more natural to implement alternative is to decompose the estimates η^{ε} and η^{e} into nodal contributions. This is because it uses the finite element nature of the estimates η^{ε} and η^{e}. In practice, the estimates e^* and ε^* are computed in a finer reference mesh associated with the space $\mathscr{V}_h$, namely $e^* = \sum_j e_j^* \phi_{h,j}$ and $\varepsilon^* = \sum_j \varepsilon_j^* \phi_{h,j}$, where $\phi_{h,j}$ are the shape functions associated with the nodes of the reference mesh, $\mathbf{x}_{h,j}$. Thus, a natural decomposition of the estimates η^{ε} and η^{e} into nodal contributions on the reference mesh holds*

$$\eta^{\varepsilon} = \sum_j \varepsilon_j^* R^P(\phi_{h,j}) =: \sum_j \eta_{\mathbf{x}_{h,j}}^{\varepsilon}$$

and

$$\eta^{e} = \sum_j e_j^* R^D(\phi_{h,j}) =: \sum_{j=1} \eta_{\mathbf{x}_{h,j}}^{e}.$$

Note that $\eta_{\mathbf{x}_{h,j}}^{\varepsilon}$ and $\eta_{\mathbf{x}_{h,j}}^{e}$ are readily computed multiplying the j-th components of the finite element vectors associated to ε^* and $R^P(\cdot)$ and e^* and $R^D(\cdot)$ respectively.
Then, the local elemental contributions associated to the element Ω_k of the coarse mesh are computed from a weighted average of the local nodal contributions $\eta_{\mathbf{x}_{h,j}}^{\varepsilon}$ and $\eta_{\mathbf{x}_{h,j}}^{e}$ associated to the nodes $\mathbf{x}_{h,j}$ belonging to Ω_k. To be specific

$$\eta^{\varepsilon} = \sum_j \eta_{\mathbf{x}_{h,j}}^{\varepsilon} = \sum_{k=1}^{\mathrm{n_{el}}} \sum_{\mathbf{x}_{h,j}\in\Omega_k} \sigma_{h,j} \eta_{\mathbf{x}_{h,j}}^{\varepsilon} =: \sum_{k=1}^{\mathrm{n_{el}}} \hat{\eta}_k^{\varepsilon}, \tag{15}$$

and

$$\eta^{e} = \sum_j \eta_{\mathbf{x}_{h,j}}^{e} = \sum_{k=1}^{\mathrm{n_{el}}} \sum_{\mathbf{x}_{h,j}\in\Omega_k} \sigma_{h,j} \eta_{\mathbf{x}_{h,j}}^{e} =: \sum_{k=1}^{\mathrm{n_{el}}} \hat{\eta}_k^{e}, \tag{16}$$

where $\sigma_{h,j}$ is the inverse of the number of elements in the coarse mesh to which a particular node $\mathbf{x}_{h,j}$ belongs. For a detailed description, see [26].

A simple adaptive strategy is employed, using the local indicators η_k^{ε} or η_k^{e} produced during the calculation of the estimate for the output, to drive the non-linear output to a prescribed precision. That is, the algorithm ends if

$$\sum_{k=1}^{\mathrm{n_{el}}} \eta_k^{\circledast} + \mathscr{Q}(e^*,e^*) + \mathscr{W}(e^*) < \Delta_{\mathrm{tol}},$$

where $\eta_k^{\circledast}$ stands for any of the following local contributions η_k^{ε}, η_k^{e}, $\hat{\eta}_k^{\varepsilon}$ or $\hat{\eta}_k^{e}$, Δ_{tol} is a user-prescribed desired final accuracy, and at each level of refinement, the elements marked for refinement are those with larger values of the local linear contribution $\eta_k^{\circledast}$.

6.2 Remeshing criterion

In acoustic problems, the local contributions are not necessarily positive and in fact, in contrast to what occurs in thermal or elasticity problems, they can be complex numbers. To select the elements with larger local contributions, the modulus of the values $\eta_k^{\circledast}$ is considered, and the elements selected to be refined are the ones verifying

$$|\eta_k^{\circledast}| \geq \frac{\sum_{k=1}^{\mathrm{n_{el}}} |\eta_k^{\circledast}|}{\mathrm{n_{el}}}. \tag{17}$$

Note that this marking algorithm aims at obtaining elements with equal local error contribution. However, this is not equivalent to obtaining a uniform spatial error distribution, since the elements with larger area are penalized. In order to obtain a uniform spatial error distribution, the local contributions are weighted by the element area yielding the following marking criterion: the elements to be subdivided are the ones verifying

$$\frac{|\eta_k^{\circledast}|}{\mathrm{A}_k} \geq \frac{\sum_{k=1}^{\mathrm{n_{el}}} |\eta_k^{\circledast}|}{\mathrm{A}_{\Omega}}, \tag{18}$$

where A_k is the area of the element Ω_k and A_{Ω} is the area of the whole domain Ω. Note that expressions (17) and (18) are equivalent in uniform meshes where all the elements have the same area since in this case $\mathrm{A}_k = \mathrm{A}_{\Omega}/\mathrm{n_{el}}$ is constant.

7 NUMERICAL EXAMPLES

The performance of the estimates and error indicators described above is illustrated in three numerical examples. The quantities of interest are expressed as linear and quadratic functionals of the solution u. In particular, three different engineering outputs are considered. The first output is the integral of the solution over a subdomain $\Omega^{\mathscr{O}} \subset \Omega$

$$J_1(u) = \int_{\Omega^{\mathscr{O}}} u \, d\Omega, \tag{19}$$

that is, the data entering in (7) are $g^{\mathscr{O}} = \beta^{\mathscr{O}} = 0$ and $f^{\mathscr{O}} = 1$ in $\Omega^{\mathscr{O}}$ and $f^{\mathscr{O}} = 0$ elsewhere. Since the output depends linearly on u, $\ell_1^{\mathscr{O}}(v) = J_1(v)$ and $\mathscr{Q}_1(v,v) = \mathscr{W}_1(v) = 0$ in (5). Note that eventually $\Omega^{\mathscr{O}}$ can be Ω to compute an average of the solution over the whole domain.

The second output is the average of the squared modulus of the solution over a boundary strip $\Gamma^{\mathscr{O}} \subset \Gamma_N \cup \Gamma_R$

$$J_2(u) = \frac{1}{l_{\Gamma^{\mathscr{O}}}} \int_{\Gamma^{\mathscr{O}}} u\bar{u} \, d\Gamma \tag{20}$$

where $l_{\Gamma^{\mathscr{O}}}$ is the length of the boundary strip. Since this output depends quadratically on u, $\mathscr{W}_2(v) = 0$ and the linear and quadratic contributions are

$$\ell_2^{\mathscr{O}}(v) = \frac{1}{l_{\Gamma^{\mathscr{O}}}} \int_{\Gamma^{\mathscr{O}}} (u_H \bar{v} + \bar{u}_H v) \, d\Gamma, \quad \mathscr{Q}_2(v,v) = J_2(v).$$

Indeed, appealing to (5)

$$\begin{aligned} J_2(u_H + v) &= \frac{1}{l_{\Gamma^{\mathscr{O}}}} \int_{\Gamma^{\mathscr{O}}} (u_H + v)(\overline{u_H + v}) \, d\Gamma \\ &= \frac{1}{l_{\Gamma^{\mathscr{O}}}} \int_{\Gamma^{\mathscr{O}}} (u_H \bar{u}_H + u_H \bar{v} + v\bar{u}_H + v\bar{v}) \, d\Gamma \\ &= J_2(u_H) + \frac{1}{l_{\Gamma^{\mathscr{O}}}} \int_{\Gamma^{\mathscr{O}}} (u_H \bar{v} + \bar{u}_H v) \, d\Gamma + J_2(v). \end{aligned}$$

It is worth noting that the error estimation procedure described above can not be directly applied to this output as it stands since the linear functional $\ell_2^{\mathscr{O}}(\cdot)$ can not be expressed in the form of (7). A simple workaround to overcome this limitation is adopted noting that $\ell_2^{\mathscr{O}}(v)$ is a real number coinciding with

$$\ell_2^{\mathscr{O}}(v) = 2\Re\mathrm{e}\left(\frac{1}{l_{\Gamma^{\mathscr{O}}}} \int_{\Gamma^{\mathscr{O}}} \bar{u}_H v \, d\Gamma \right).$$

The adjoint problem is then defined with respect to the auxiliary linear functional $\int_{\Gamma^{\mathscr{O}}} \bar{u}_H v \, d\Gamma / l_{\Gamma^{\mathscr{O}}}$ which corresponds to $f^{\mathscr{O}} = 0$, $\beta^{\mathscr{O}} = \bar{u}_H / l_{\Gamma^{\mathscr{O}}}$ on $\Gamma^{\mathscr{O}} \cap \Gamma_R$ and zero elsewhere and $g^{\mathscr{O}} = \bar{u}_H / l_{\Gamma^{\mathscr{O}}}$ on $\Gamma^{\mathscr{O}} \cap \Gamma_N$ and zero elsewhere.

The third output is the normalized squared $\mathscr{L}^2$-norm of the solution over a region $\Omega^{\mathscr{O}}$

$$J_3(u) = \frac{1}{A_{\Omega^{\mathscr{O}}}} \int_{\Omega^{\mathscr{O}}} u\bar{u} \, d\Omega \tag{21}$$

where $A_{\Omega^{\mathscr{O}}}$ stands for the area of the subdomain $\Omega^{\mathscr{O}}$. Again, since the output is quadratic, $\mathscr{W}_3(v) = 0$ and

$$\ell_3^{\mathscr{O}}(v) = \frac{1}{A_{\Omega^{\mathscr{O}}}} \int_{\Omega^{\mathscr{O}}} (u_H \bar{v} + \bar{u}_H v) \, d\Omega, \quad \mathscr{Q}_3(v,v) = J_3(v).$$

The derivation is analogous to the one provided for $J_2(\cdot)$ except for the integrals being placed over a subdomain of Ω instead of its boundary. As in the second output, the adjoint problem is defined with respect to the modified functional $\int_{\Omega^{\mathscr{O}}} \bar{u}_H v \, d\Omega / A_{\Omega^{\mathscr{O}}}$, for which the data entering in (7) are $g^{\mathscr{O}} = \beta^{\mathscr{O}} = 0$ and $f^{\mathscr{O}} = \bar{u}_H / A_{\Omega^{\mathscr{O}}}$ in $\Omega^{\mathscr{O}}$ and $f^{\mathscr{O}} = 0$ elsewhere.

Remark 2 *The second and third outputs $J_2(u)$ and $J_3(u)$ are real quantities since they only involve the squared modulus of the solution. In particular, all the involved functionals, are real functions of a single complex variable, that is, for instance $\ell_2^{\mathscr{O}} : \mathbb{C} \to \mathbb{R}$. As mentioned above, in this case, the adjoint problem is defined with respect to an auxiliary non-real linear functional output. The original linear functional (and all the required estimates and local indicators) is recovered from this auxiliary functional taking the real part and multiplying by a factor two.*

When reporting the numerical results, $\eta^{\varepsilon}_{\mathrm{pol}} = R^P(\varepsilon^*_{\mathrm{pol}})$, $\eta^{\varepsilon}_{\mathrm{exp}} = R^P(\varepsilon^*_{\mathrm{exp}})$, $\eta^{e}_{\mathrm{pol}} = R^D(e^*_{\mathrm{pol}})$ and $\eta^{e}_{\mathrm{exp}} = R^D(e^*_{\mathrm{exp}})$ denote the estimates of the linear contribution to the error in the quantity of interest $\eta := \ell^{\mathscr{O}}(e)$ obtained by using the post-processing strategy described in [24,25]. The subindeces exp and pol indicate the kind of approximation used in the least squares fitting: either polynomial both for the real and imaginary part of the solution or a complex-exponential fitting (polynomial fitting for the logarithm of the modulus and for the angle). In order to see how well the estimators perform, the value of the true error $J(u) - J(u_H)$ or $\ell^{\mathscr{O}}(e)$ are required, but the analytical solutions of the considered problems are not available. An accurate value for the true error is obtained by making use of a sufficiently accurate approximation u_h of u in a finer reference mesh, that is, the estimates are compared with the reference values $J(u_h) - J(u_H)$ and $\eta_h := \ell^{\mathscr{O}}(e_h)$ respectively.

Note that this reference value can also be recovered from a faithful representation of the adjoint problem ψ_h since $\eta_h = \ell^{\mathscr{O}}(e_h) = R^P(\psi_h) = R^P(\varepsilon_h)$. In the examples, the approximations u^* and ψ^* used to recover the estimates of the errors $e^* = u^* - u_H$ and $\varepsilon^* = \psi^* - \psi_H$ and its corresponding estimates for the output $\eta^e = R^D(e^*)$ and $\eta^{\varepsilon} = R^P(\varepsilon^*)$, are also computed using the same reference mesh. Noting that $\eta_h = R^D(e_h) = R^P(\varepsilon_h)$ reveals that the quality of the estimates depends on the quality of the approximations $e^* \approx e_h$ and $\varepsilon^* \approx \varepsilon_h$. The accuracy of these approximations is closely related to the so-called pollution or dispersion error. Since the approximations u^* and ψ^* are constructed using a constrained least-squares technique, the estimates for the error

e^* and ε^* vanish at the nodes of the coarse mesh, yielding crude approximations if the solutions presents large dispersion errors. In the examples, the influence of the dispersion error in the estimates for the quantity of interest is analyzed using the estimates for the dispersion error introduced in [24,25]. These estimates are denoted by E^e and E^ε for the primal and adjoint problems respectively. A detailed description of the computation of these estimates is given in [25].

7.1 Square with obstacle

The first example is the scattering of a plane wave by a rigid obstacle introduced in [12]. The incident wave travels in the negative y-direction inside a square domain which contains a rigid body, see figure 1.

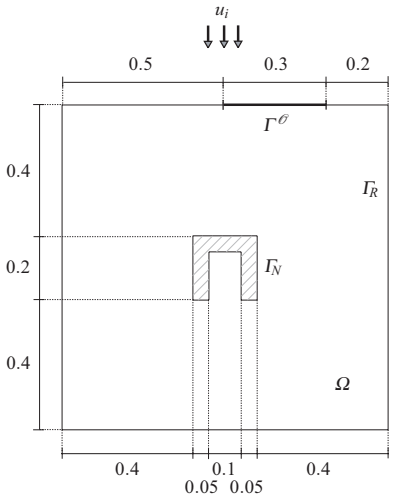

Fig. 1 Example 1: Description of the geometry and boundary conditions for the plane wave scattering by a rigid body.

The solution of the problem is composed of a prescribed incident wave plus a scattered wave, $u = u_r + u_i$, where u_r and u_i are the so-called reflected and incident waves respectively. The incident wave is of the form $u_i = e^{i\kappa(\cos\alpha x + \sin\alpha y)}$, where κ is the wave number and $\alpha = \pi/2$ is the incident wave direction. To reproduce the scattering nature of the problem, no essential boundary conditions are imposed and it is assumed that there are no sources in the domain, $f = 0$ in equation (1), and that the rigid obstacle is perfectly reflecting. This is, $\nabla u \cdot \mathbf{n} = 0$ or, in terms of the incident wave, $\nabla u_r \cdot \mathbf{n} = -\nabla u_i \cdot \mathbf{n}$ on Γ_N. On the exterior boundary, Robin absorbing boundary conditions are applied. Thus, the reflected wave u_r is the solution of the Helmholtz equation (1) for $f = 0$ and $\Gamma_D = \emptyset$ and where the data entering in (2) are $g = -\nabla u_i \cdot \mathbf{n}$, $m = -ik$ and $\beta = 0$.

To demonstrate the dependence of the results on the wave number, two values of the wave number are considered: $\kappa = \pi$ and $\kappa = 3\pi$. Both the reflected and total waves obtained for this problem in a mesh of 9825 nodes are shown in figure 2.

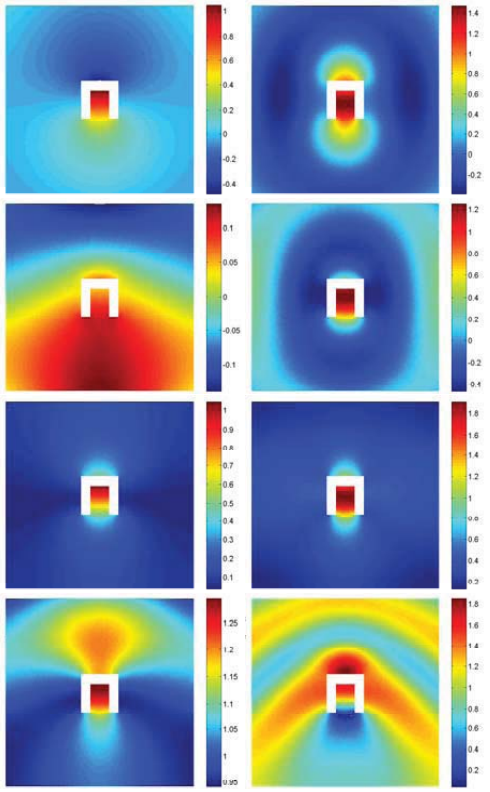

Fig. 2 Example 1: Real part (top), imaginary part (middle top) and modulus of the scattered solution u_r (middle bottom), that is, $\Re\mathrm{e}(u_r)$, $\Im\mathrm{m}(u_r)$ and $|u_r|$, and modulus of the total solution $|u|$ (bottom) for $\kappa = \pi$ (left) and $\kappa = 3\pi$ (right), computed using the Galerkin method and a mesh of 9852 nodes.

For this problem, two different quantities are considered: the average of the reflected solution over the whole domain, that is $J_1(u_r)$ for $\Omega^{\mathcal{O}} = \Omega$, which is a linear quantity of interest, and the average of the squared modulus of the reflected solution over the boundary strip $\Gamma^{\mathcal{O}}$ depicted in figure 1, that is, $J_2(u_r)$, which depends quadratically on u_r.

The behavior of the estimates for the linear quantity of interest $J_1(u_r)$ is first analyzed for a uniform mesh refinement in a series of unstructured triangular meshes for the value $\kappa = \pi$. Three triangular meshes are considered, start-

ing from an initial mesh of 636 nodes and obtaining the subsequent meshes by refining each triangle into four new ones, see figure 3.

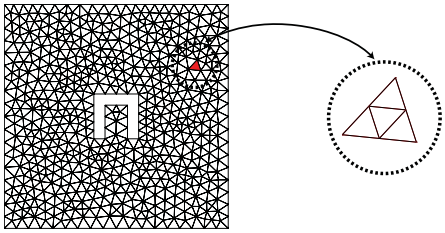

Fig. 3 Example 1: Initial mesh of 636 nodes and subdivision of each triangle into four new ones for the uniform mesh refinement.

The finite element approximation of the adjoint solution computed at the final mesh of the refinement procedure of 9825 nodes is shown in figure 4.

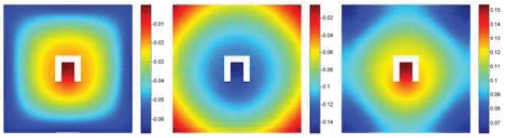

Fig. 4 Example 1: Real part (left), imaginary part (middle) and modulus (right) of the adjoint solution associated to the first quantity of interest $J_1(u_r)$ for $\kappa = \pi$ computed using the Galerkin method and a mesh of 9852 nodes.

Table 1 shows the estimates obtained for the error in the quantity of interest $J_1(u_r)$. Since the quantity of interest is linear, in this case, the estimates coincide with those for the linear term. Thus, the estimates given by the different error representations (13) are compared with the reference value η_h. For each coarse mesh, the reference value is obtained by computing and approximation u_h of u in a finer mesh (each element of the coarse mesh is subdivided into 16 new ones which corresponds to $h = H/4$). Also the table shows the estimates for the dispersion error for the primal and adjoint problem E^e and E^ε respectively.

As can be seen, the estimates for the error in the quantity of interest underestimate the reference value both for the polynomial and exponential fitting. However, as reported in [25] the exponential fitting provides better results, although in this example the improvement is not that substantial when compared to the reference value. The estimates for the dispersion error are also shown in the table. Looking at the dispersion errors provided by the exponential fitting, the dispersion for the primal problem ranges from a 28% for the first mesh to a 5% for the final mesh and for the adjoint problem are below 0.3% in all the meshes. Although the dispersion is larger in the primal problem, for both problems

	number of nodes		
	636	2445	9852
	$\kappa h_{\max} = 0.18$	$\kappa h_{\max} = 0.09$	$\kappa h_{\max} = 0.05$
η_h	5.06e-4 + 7.90e-4i	2.04e-4 + 3.09e-4i	8.14e-5 + 1.22e-4i
$\eta^\varepsilon_{\text{pol}}$	2.78e-4 + 5.41e-4i	1.03e-4 + 1.79e-4i	3.93e-5 + 6.23e-5i
$\eta^\varepsilon_{\text{exp}}$	3.49e-4 + 5.68e-4i	1.12e-4 + 1.85e-4i	4.00e-5 + 6.22e-5i
η^e_{pol}	2.32e-4 + 4.44e-4i	9.76e-5 + 1.68e-4i	3.82e-5 + 6.02e-5i
η^e_{exp}	2.72e-4 + 5.31e-4i	1.02e-4 + 1.77e-4i	3.92e-5 + 6.21e-5i
$E^\varepsilon_{\text{pol}}$	-3.17e-2	-3.25e-3	7.93e-4
$E^\varepsilon_{\text{exp}}$	-9.33e-3	1.84e-3	-3.43e-4
E^e_{pol}	-1.34e+0	-4.08e-1	-1.26e-1
E^e_{exp}	-8.95e-1	-3.15e-1	-1.50e-1

Table 1 Example 1: Estimates for the error in the linear quantity of interest $J_1(u_r) = \ell_1^{\mathcal{O}}(u_r)$. The table shows the reference value for the error in the quantity of interest η_h along with its different estimates. Also, the estimated dispersion error associated to the primal and adjoint problems are given, namely $E^\varepsilon_{\text{pol}}$ and E^e_{exp}.

the ratio $\kappa h_{\max} << 1$, in fact in average, $\kappa h_{\text{ave}} = 0.08, 0.04$ and 0.02. This explains that, although the dispersion error is significantly smaller in the adjoint problem, the difference between quality of the representations η^ε with respect to η^e are only slightly better. Indeed, since all the meshes properly satisfy the rule of thumb, the dispersion error is negligible in front of the errors appearing from the singular nature of the solution. The main source of error for this problem is not the dispersion error, and thus, even though the dispersion is smaller in the adjoint problem, the estimate ε^* does not provide a much better approximation of ε_h than e^* is of e_h. In fact, it is worth noting that most of the estimated dispersion errors are negative, yielding to finite element solutions with associated numerical wave number larger wave number than κ, opposing the predicted behavior given by a-priori estimates. This phenomena only appears when dispersion is not relevant for the problem at hand. When dispersion errors are important, the finite element method behaves as predicted by the a-priori estimates providing approximations with associated numerical wave number smaller than κ.

Figure 5 shows the local elementary contributions to the error in the quantity of interest for the initial mesh of 636 nodes. Both the local contributions of the reference values η^ε_h and η^e_h and its estimates (obtained using the polynomial and the exponential fitting) computed using the representations given in Remark 1, equations (15) and (16), are shown. Note that even though the global error quantities η^ε_h and η^e_h are equal, they represent different elementary contributions to the error. The spatial distribution of the estimates is in good agreement with the reference ones: they properly detect the elements with larger contributions to the error even though the obtained elemental contributions underestimate its reference value. The local contributions obtained using the natural restriction of the global estimates

to the elements given in equation (14) are also shown in figure 6 for η_h^ε, $\eta_{\text{pol}}^\varepsilon$ and $\eta_{\text{exp}}^\varepsilon$. Again, although the global values coincide with those computed distributing the nodal contributions over the elements, the obtained local distributions is not the same. As can be seen, the use of the easier and cheaper to compute local contributions described in remark 1 provides fairly good approximations to the natural restriction of the global quantities to the elements, yielding a nearly equivalent distribution of elements to be refined in the adaptive procedure. In this example, the natural decomposition yields higher values of the modulus of the elementary contributions $|\eta_k|$ since the local distribution presents larger positive and negative contributions η_k in neighboring elements. The averaging involved in the nodal-to-element representation, smoothes out this larger values yielding a more uniform distribution. Henceforth in this example, all the local contributions shown in the numerical examples are computed using the nodal-to-element representation instead of the natural representation.

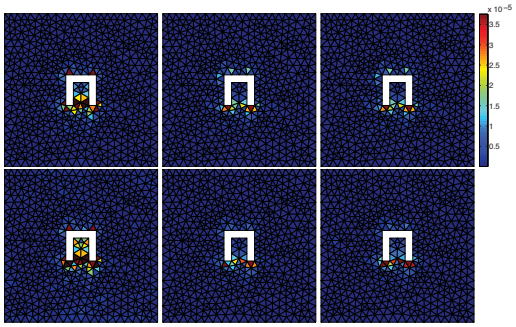

Fig. 5 Example 1: Local maps of the error in the linear quantity of interest $J_1(u_r)$. The distributions on the top are obtained using the representation η^ε, that is, η_h^ε (left), $\eta_{\text{pol}}^\varepsilon$ (middle) and $\eta_{\text{exp}}^\varepsilon$ (right) are shown. The distributions on the bottom correspond to η^e, that is, η_h^e (left), η_{pol}^e (middle) and η_{exp}^e (right) are shown.

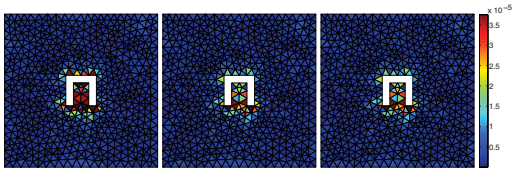

Fig. 6 Example 1: Local maps of the error in the linear quantity of interest $J_1(u_r)$ computed using the restrictions of the integrals over the elements (14). The distributions on the top are obtained using the integral representation η^ε, that is, η_h^ε (left), $\eta_{\text{pol}}^\varepsilon$ (middle) and $\eta_{\text{exp}}^\varepsilon$ are shown.

Figure 7 shows the elements with larger values of the estimates weighted by its area, $|\eta_k^{\circledast}|/\mathrm{A}_k$. In particular, the elements marked for refinement if 1%, 5%, 10% and 25% of the total elements are refined are shown respectively. Although the estimates underestimate the reference value for the error, they provide good information to guide the adaptive procedures.

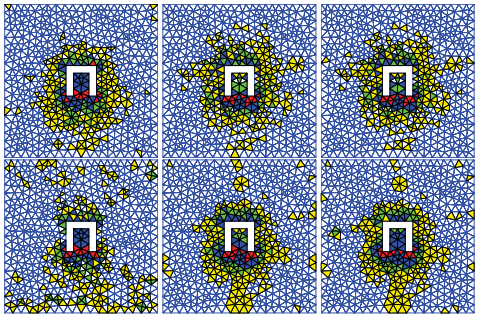

Fig. 7 Example 1: Elements marked for refinement if 1% (red), 5% (red+blue), 10% (red+blue+green) and 25% (red+blue+green+yellow) of the total elements are refined. The elements are selected using the local maps of the error in the linear quantity of interest $J_1(u_r)$ given in figure 5, namely: η_h^ε (top-left), $\eta_{\text{pol}}^\varepsilon$ (top-middle), $\eta_{\text{exp}}^\varepsilon$ (top-right), η_h^e (bottom-left), η_{pol}^e (bottom-middle) and η_{exp}^e (bottom-right).

The convergence of the estimates is shown in figure 8. Two refinement strategies are implemented: first, the meshes are uniformly refined whereby each triangle is subdivided into four sub-triangles at each step and second, the meshes are adaptively refined using the criterion given in equation (18). The singular nature of the solution yields an order of convergence for the uniform mesh refinement of $\mathcal{O}(H^{4/3})$ for the quantity of interest, which is equivalent to $\mathcal{O}((\mathrm{n_{np}})^{2/3})$ where $\mathrm{n_{np}}$ denotes the number of nodes of the mesh, instead of the standard convergence rate of $\mathcal{O}(H^4)$ obtained for regular solutions. As expected, the use of an adaptive refinement strategy leads to a faster reduction of the error in the quantity of interest than if a uniform refinement is used. Again it can be seen that, in this example, all the estimates provide similar results providing an underestimation of the reference values. For comparison, the adaptive algorithm guided by the reference errors η_h^e and η_h^ε are also run. Comparing the convergence curves obtained for these two local indicators and the ones produced by the estimates, it can be seen that the estimates perform optimally since they lead to even slightly better convergence ratios than the reference errors.

The series of adapted meshes produced by the local indicator associated to $\eta_{\text{exp}}^\varepsilon = R^P(\varepsilon_{\text{exp}}^*)$ subdividing at each remeshing step the elements satisfying the criterion given by equation (18) are shown in figure 9. The adaptive procedure is started from the initial mesh shown in figure 3 and pro-

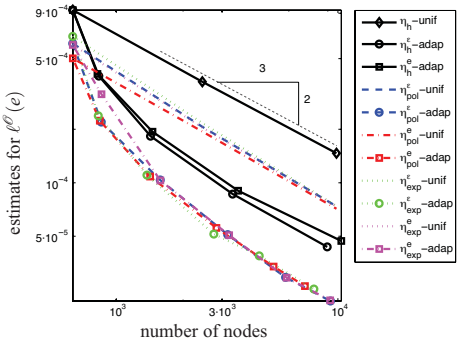

Fig. 8 Example 1: Performance of the estimators for the error in the quantity of interest $J_1(u_r)$ with a uniform and an adaptive refinement strategies. The estimates are compared with the reference values.

duces six new adapted meshes. The meshes obtained using the other local error indicators are virtually identical and are therefore not shown. Since the quantity of interest is the non-

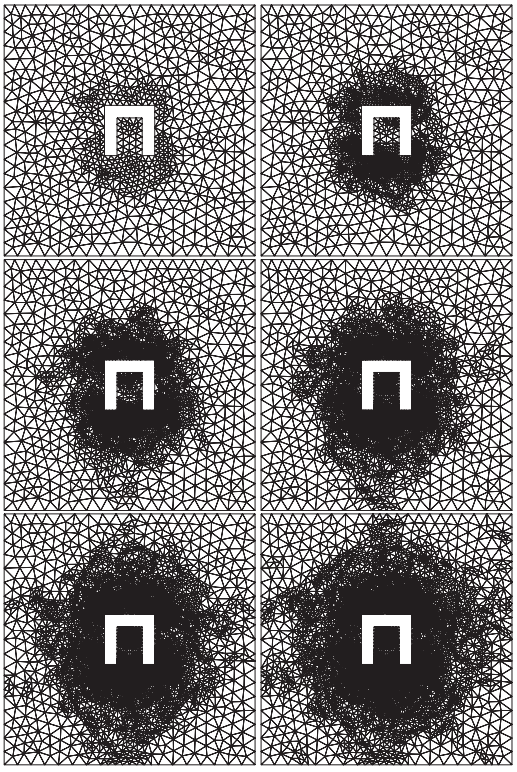

Fig. 9 Example 1: Sequence of adapted meshes obtained using the local error indicators provided by the estimate $\eta_{\text{exp}}^{\varepsilon}$ with 857, 1579, 3229, 5870, 9226 and 13852 nodes respectively, for the quantity of interest $J_1(u_r)$.

weighted average of the solution over the whole domain, the meshes are refined in the areas where the primal solution presents larger errors, that is, at the neighborhood of the obstacle where the singularities occur.

The performance of the estimates is also studied for the non-linear quantity of interest $J_2(u_r)$. Figure 10 shows the finite element approximation of the adjoint solution computed using a finite element mesh of 9825 nodes for the two wave numbers $\kappa = \pi$ and $\kappa = 3\pi$. Recall that, the adjoint solution associated with a non-linear output is defined using its linear approximation, and in this case, the r.h.s. of the adjoint problem (8) is given by the auxiliary linear functional $\int_{\Gamma^{\mathscr{O}}} \bar{u}_H v d\Gamma / l_{\Gamma^{\mathscr{O}}}$. Thus, the adjoint solution varies for each finite element approximation u_H and the adjoint solution shown in figure 10 only corresponds to the adjoint problem associated to the finite element approximation u_H computed using the mesh of 9825 nodes.

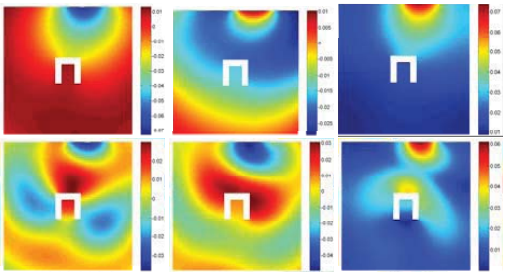

Fig. 10 Example 1: Real part (left), imaginary part (middle) and modulus (right) of the adjoint solution associated to the second quantity of interest $J_2(u_r)$ for the two parameters $\kappa = \pi$ on the figures on the top and $\kappa = 3\pi$ on the bottom figures computed using the Galerkin method and a mesh of 9852 nodes. The adjoint problem is defined with respect to the auxiliary functional $\int_{\Gamma^{\mathscr{O}}} \bar{u}_H v d\Gamma / l_{\Gamma^{\mathscr{O}}}$.

In order to illustrate the influence of the different terms contributing to the error in the quantity of interest, the linear and quadratic contributions to the error along with the "full" error are shown separately for the parameter $\kappa = \pi$. As predicted by the theory, the total error is guided by the linear contribution, whereas the quadratic contribution is negligible since it converges faster to zero. As occurs with the first quantity of interest $J_1(u_r)$, the rate of convergence of these two terms are not the expected since the solution is singular: the finite element approximation has a convergence rate of $\mathscr{O}(H^{2/3})$ and therefore the linear and quadratic contributions to the output converge as $\mathscr{O}(H^{4/3})$ and $\mathscr{O}(H^{8/3})$ respectively, as can be appreciated in the obtained results. The same behavior is observed when the reference values are substituted by its estimates.

Neglecting the higher order terms yields the following approximation of the reference value of the quantity of in-

n_{np}	$\ell_2^{\mathscr{O}}(e_h)$	$\mathscr{Q}_2(e_h,e_h)$	$J_2(u_h)-J_2(u_H)$
636	1.6572e-3	3.5279e-5	1.6925e-3
2445	6.8740e-4	5.7170e-6	6.9311e-4
9582	2.7799e-4	9.1190e-7	2.7891e-4

Table 2 Example 1: Influence of the linear and quadratic terms to the total error in the nonlinear quantity of interest $J_2(u_r)$ for $\kappa=\pi$.

terest

$$J_2(u_h) = J_2(u_H) + \ell_2^{\mathscr{O}}(e_h) + \mathscr{Q}_2(e_h,e_h)$$
$$\approx \ell_2^{\mathscr{O}}(u_H) + \ell_2^{\mathscr{O}}(e_h) = \ell_2^{\mathscr{O}}(u_H)\left(1+\frac{\ell_2^{\mathscr{O}}(e_h)}{\ell_2^{\mathscr{O}}(u_H)}\right).$$

Thus, the relative error $\rho_h := \ell^{\mathscr{O}}(e_h)/\ell^{\mathscr{O}}(u_H)$ provides a good inside of the error in the quantity of interest. Table 3 shows the values of the reference relative error and its corresponding estimates $\rho^{\varepsilon}_{\text{exp}} = \eta^{\varepsilon}_{\text{exp}}/\ell_2^{\mathscr{O}}(u_H)$ and $\rho^{e}_{\text{exp}} = \eta^{e}_{\text{exp}}/\ell_2^{\mathscr{O}}(u_H)$ along with the estimates for the relative dispersion error $\rho^{E^{\varepsilon}}_{\text{pol}} = E^{\varepsilon}_{\text{pol}}/\kappa$ and $\rho^{E^{e}}_{\text{pol}} = E^{e}_{\text{pol}}/\kappa$ both for $\kappa=\pi$ and for $\kappa=3\pi$.

$\kappa=\pi$

n_{np}	ρ_h	$\rho^{\varepsilon}_{\text{exp}}$	ρ^{e}_{exp}	$\rho^{E^{\varepsilon}}_{\text{exp}}$	$\rho^{E^{e}}_{\text{exp}}$
636	0.0411	0.0210	0.0189	-0.0247	-0.2849
2445	0.0170	0.0084	0.0080	-0.0089	-0.1003
9582	0.0069	0.0034	0.0033	-0.0039	-0.0479

$\kappa=3\pi$

n_{np}	ρ_h	$\rho^{\varepsilon}_{\text{exp}}$	ρ^{e}_{exp}	$\rho^{E^{\varepsilon}}_{\text{exp}}$	$\rho^{E^{e}}_{\text{exp}}$
636	0.1647	0.0584	0.0436	-0.0077	-0.0368
2445	0.0840	0.0387	0.0364	-0.0028	-0.0090
9582	0.0359	0.0167	0.0164	-0.0012	-0.0041

Table 3 Example 1: Estimates for the error in the linear term $\ell_2^{\mathscr{O}}(e_h)$ relative to $\ell^{\mathscr{O}}(u_H)$) and relative dispersion error for the primal and adjoint problem for a uniformly refined set of meshes.

The results are very similar to those obtained for the first quantity of interest. The two representations for the linear part of the quantity of interest $\eta^{\varepsilon}_{\text{exp}}$ and η^{e}_{exp} corresponding to the relative values $\rho^{\varepsilon}_{\text{exp}}$ and ρ^{e}_{exp}. The errors are larger for $\kappa=3\pi$ but the estimates behave similarly: the representation using the recovered adjoint error ε^* is slightly better than the representation using the recovered primal error e^* both underestimating the reference error. Also, since the values of κh_{ave} remains below 0.25 for all the meshes, the dispersion error is very small when compared to the errors due to the singular behavior of the solution. Note that increasing κ yields smaller negative dispersion errors since for larger κ's the numerical wave number underestimates the true value yielding positive dispersion errors.

The convergence of the estimates for a uniform and an adaptive procedure using the criterion given in equation (18) are shown in figure 11 starting with the finite element mesh shown in figure 3. As in the results for the first quantity of interest, the adaptive refinement leads to a faster reduction of the error and it can be seen that the local indicators associated to the estimates behave properly since the convergence curves of the estimates are in very good agreement with the reference ones. Only the estimates for the exponential fitting are shown since the polynomial fitting provide similar but slightly worst results. Comparing the results for the two different wave numbers reveals that for $\kappa=3\pi$ there is a short range where the solution is in its pre-asymptotic stage [7,27]. Note that the curves associated to the uniform refinements converge with a slightly smaller rate than the asymptotic one (0.5 instead of $\frac{2}{3}$).

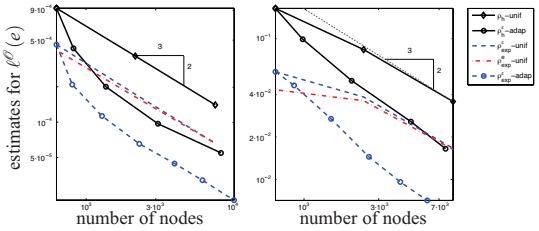

Fig. 11 Example 1: Convergence of the relative error for the quantity of interest J_2 for $\kappa=\pi$ (left) and $\kappa=3\pi$ (right) for uniform and adaptive processes in the reference solution compared with the enhanced solutions.

Figures 12 and 13 show the meshes produced by the adaptive procedure associated to the estimate $\eta^{\varepsilon}_{\text{exp}}$. The adaptive procedure refines the neighborhood of the obstacle but also refines around the boundary strip where the solution is evaluated to compute the quantity of interest. Additionally, for $\kappa=3\pi$, the procedure also refines the zones where the solution has a larger oscillatory behavior faraway from the obstacle.

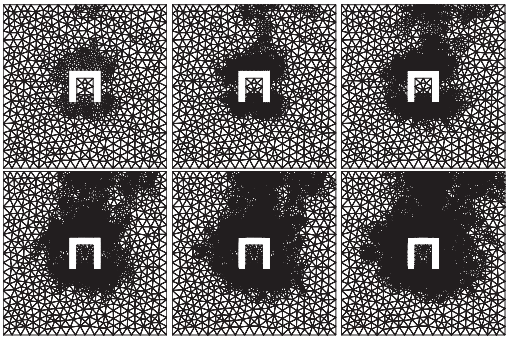

Fig. 12 Example 1: Sequence of adapted meshes with 834, 1384, 2619, 4781, 7709 and 13212 nodes, respectively. The adaptive process is driven by representation $\eta^{\varepsilon}_{\text{exp}}$, corresponding to the linear contribution $\ell_2^{\mathscr{O}}(\cdot)$ for $\kappa=\pi$.

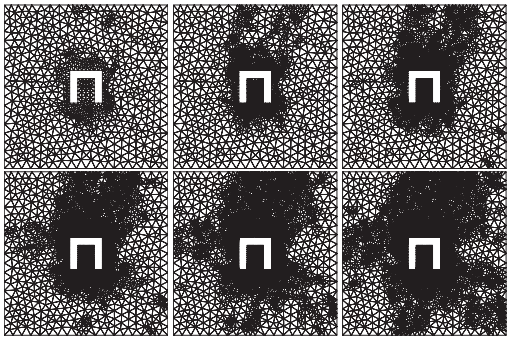

Fig. 13 Example 1: Sequence of adapted meshes with 846, 1486, 2649, 4277, 6457 and 9718 nodes. The adaptive process is driven by representation $\eta^{\varepsilon}_{\text{exp}}$, corresponding to the linear contribution $\ell_2^{\mathscr{O}}(\cdot)$ for $\kappa = 3\pi$.

7.2 Expansion chamber

The second example is a two-dimensional model of an expansion chamber with a perforated outlet pipe as shown in Figure 14. The source term entering in equation (1) is $f = 0$,

Fig. 14 Example 2: Description of the geometry and boundary conditions for the expansion chamber.

and the Neumann and Robin boundary conditions entering in equations (2b) and (2c) are of the form $g = -i\rho\kappa c v_n$ and $\nabla u \cdot \mathbf{n} = i\kappa u$, respectively, where in this case the material parameters are $c = 340\,m/s$ standing for the speed of sound of the medium and $\rho = 1.225\,kg/m^3$ standing for the mass density. An acoustic excitation is imposed at the inlet of the chamber, associated to a velocity $v_n = 0.1m/s$, whereas the chamber is assumed to be perfectly reflecting at the outlet, that is, Robin boundary conditions are applied to the outlet of the chamber. The rest of the boundary is assumed to be perfectly reflecting corresponding to $v_n = 0\,m/s$. In the computations, a wave number of $\kappa = 2\pi f/c \approx 12.936$, corresponding to a frequency of $700\,Hz$, has been considered.

The quantity of interest is the normalized $\mathscr{L}^2$-norm of the squared modulus of the solution over a region surrounding the outlet of the pipe, see the subdomain $\Omega^{\mathscr{O}}$ shown in figure 14, namely $J_3(u)$. Figures 26 and 27 show the Galerkin approximations of the primal and adjoint problems for a mesh of 1859 nodes respectively. Recall that the adjoint problem is defined using the auxiliary linear functional $\int_{\Omega^{\mathscr{O}}} \bar{u}_H v d\Omega / A_{\Omega^{\mathscr{O}}}$. Along with the finite element approximations, the reference solutions obtained by refining each element into 64 new ones and the reference errors are shown. The dispersion error for this mesh is one of the main sources

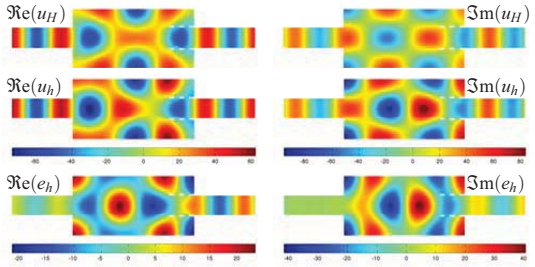

Fig. 15 Example 2: Galerkin finite element approximation of the primal problem for a mesh of 1859 nodes (top). The middle figures are the Galerkin approximation for a mesh obtained dividing each element into 64 new ones. The reference error with respect to this mesh is shown in the bottom.

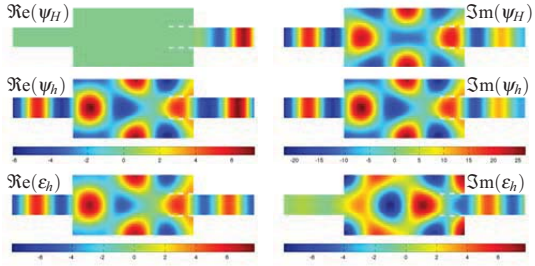

Fig. 16 Example 2: Galerkin finite element approximation of the adjoint problem for a mesh of 1859 nodes (top). The middle figures are the Galerkin approximation for a mesh obtained dividing each element into 64 new ones. The reference error with respect to this mesh is shown in the bottom.

of errors both for the primal and adjoint problem, as can be appreciated by the globally oscillating behavior of the errors.

Table 4 shows the estimates obtained for the quantity of interest $J_3(u)$ using three uniformly refined meshes, starting from the mesh shown in figure 17. As can be seen the estimates computed using the two proposed representations an exponential fitting are in very good agreement with the reference values, where the reference mesh is obtained from the finite element mesh subdividing each element into 16 new ones. Also, the errors for the quantity of interest are shown, highlighting the linear term contribution. As can be seen, the linear term provides a very good inside to the total error since the quadratic term converges rapidly to zero. Since the dispersion error is an important source of error for this problem, the dispersion error is closely associated to the

behavior of the representations η^{ε} and η^{e}. For the two first meshes, the dispersion error is smaller for the adjoint problem which causes the representation η^{ε} to be more accurate than η^{e}. Conversely, for the third mesh, the dispersion error is smaller for the primal problem and the representation which uses the enhanced primal error e^*, η^{e}, provide more accurate results. Thus, the dispersion error can be used to chose the error representation from which to obtain the approximation for the output.

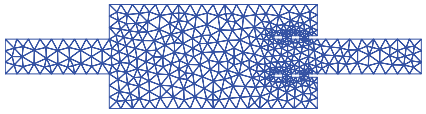

Fig. 17 Example 2: Initial mesh for the uniform and adaptive procedures of 494 nodes.

	number of nodes		
	494	1859	7193
$J(u_h)$	2.2067e+3	2.2588e+3	2.2763e+3
$J(u_H)$	1.8796e+3	2.1128e+3	2.2067e+3
$J(u_H)+\eta^{\varepsilon}+\mathcal{Q}(e^*,e^*)$	2.1548e+3	2.1967e+3	2.2611e+3
$J(u_H)+\eta^{e}+\mathcal{Q}(e^*,e^*)$	2.1082e+3	2.1961e+3	2.2622e+3
$J(u_h)$ - $J(u_H)$	3.2701e+2	1.4603e+2	6.9648e+1
$\eta^{\varepsilon}+\mathcal{Q}(e^*,e^*)$	2.7511e+2	8.3916e+1	5.4420e+1
$\eta^{e}+\mathcal{Q}(e^*,e^*)$	2.2854e+2	8.3293e+1	5.5533e+1
η^{ε}	2.7276e+2	8.3709e+1	5.4406e+1
η^{e}	2.2619e+2	8.3087e+1	5.5518e+1
E^{ε}	2.4556e-1	6.8103e-2	1.5967e-2
E^{e}	2.6351e-1	6.8293e-2	1.5780e-2

Table 4 Example 2: Estimates for the non-linear quantity of interest $J_3(u)$ and for the its error, including the linear contribution to the quantity of interest and the dispersion errors for the primal and adjoint problems. The meshes are obtained by refining each element into 16 new ones.

These results can also be appreciated in figure 18 where the estimates for the quantity of interest are depicted along with the finite element approximation and the reference value $J_3(u_h)$. Although the estimates underestimate the true error $J_3(u)$, they provide a much better approximation to the quantity of interest than $J_3(u_H)$ with very few effort.

The behavior of the estimate η^{ε} and its suitability for guiding an adaptive refinement algorithm is illustrated by applying different adaptive procedures. Starting from the mesh given in figure 17 the following six strategies are implemented to refine the elements at each step.

- *Strategy 1:* the elements to be refined are the ones verifying criterion (17).
- *Strategy 2:* the elements to be refined are the ones verifying criterion (18).
- *Strategy 3:* at each step, 10% of the elements are refined, those with larger contributions $|\eta_k^{\varepsilon}|$.

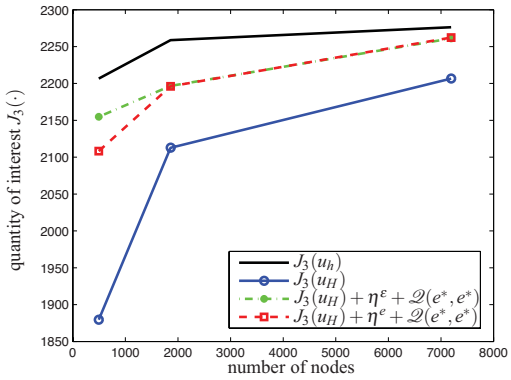

Fig. 18 Example 2: Behavior for the estimates for the quantity of interest $J_3(u)$ with respect to a uniform mesh refinement.

- *Strategy 4:* at each step, 10% of the elements are refined, those with larger contributions $|\eta_k^{\varepsilon}|/A_k$.
- *Strategy 5:* the smallest number of elements such that the sum of the contributions $|\eta_k^{\varepsilon}|$ toward the global error $\sum_{k=1}^{n_{el}}|\eta_k^{\varepsilon}|$ from these elements exceeds 25% of its value.
- *Strategy 6:* all elements on which the local error estimate $|\eta_k^{\varepsilon}|$ exceeds 50% of the largest local error estimate are refined at each step.

The results are shown in figure 19.

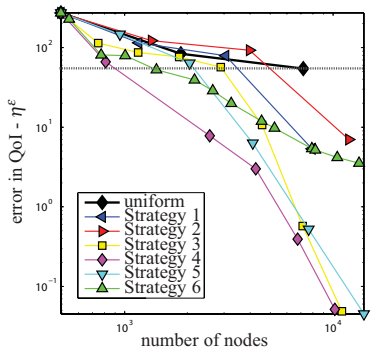

Fig. 19 Example 2: Convergence of the error in the quantity of interest for the different adaptive strategies using the local error indicators associated to η^{ε}.

Strategy four produces the best results, with those obtained using strategies three and five running a close second and third. The indicators based on strategies one and two produce noticeably poorer accuracy since they over refine the meshes at each step. Note that in the initial steps the behavior is similar to a uniform refinement. Penalizing the elements with smaller area provides an improvement of the

accuracy as can be seen comparing strategies one and two and strategies three and four. Note also that strategies three and four yield to similar accuracies, but at the initial steps, strategy three yield poorer results since it produces nearly uniformly refined meshes. Thus, analogous strategies to five and six could be develop taking into account for the area of the elements. From the graph it is clear that using a criterion that controls the ratio of elements to be refined (preventing the possibility of a uniform refinement) produces optimal adapted meshes, that is, meshes with the least number of elements for a prescribed given accuracy. Increasing the percentages in strategies three, four and six or decreasing it in the sixth, increases the number of elements to be refined producing not so optimal meshes. Hence a compromise between number of adaptive steps and accuracy is required. Finally, strategy six does not provide very good results in problems where the error is substantially larger in some parts of the domain. As can be seen in the figure, the ratio of convergence of this strategy is better than the ratio of a uniform refinement, but provides poorer results than other strategies. Note also that very few elements are refined in each iteration.

The intermediate meshes with precision closer to the one obtained in the second iteration of the uniform refinement procedure are shown in figure 20 for the six strategies. The second iteration of the uniform refinement provides a mesh of 7193 nodes and achieves a precision of $\eta^{\varepsilon} = 54.41$.

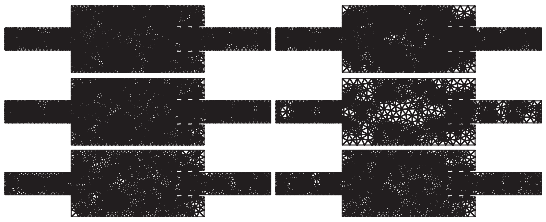

Fig. 20 Example 2: Intermediate meshes of the adaptive procedures for the six different strategies: third step of strategy 1 (top-left) with 3047 nodes and $\eta^{\varepsilon} = 79.11$, third step of strategy 2 (top-right) with 3976 nodes and $\eta^{\varepsilon} = 92.71$, fifth step of strategy 3 (middle-left) with 2892 nodes and $\eta^{\varepsilon} = 56.77$, second step of strategy 4 (middle-right) with 810 nodes with $\eta^{\varepsilon} = 66.62$, third step of strategy 5 (bottom-left) with 2050 nodes and $\eta^{\varepsilon} = 63.86$ and fifth step of strategy 6 (bottom-right) with 1005 nodes and $\eta^{\varepsilon} = 52.56$.

It can be observed that the meshes produced using strategies one and two tend to exhibit a more uniform refinement compared with those obtained using strategy four, which accounts for the poorer accuracy of the resulting approximation. Also, from the intermediate meshes, it can be observed that, as mentioned before, although strategies four, three and five achieve similar results for the final mesh, at the intermediate steps, joining the control of the elements to be refined along with penalizing the elements with smaller area, namely, strategy four, provides the best results. This is clearly appreciated in the intermediate meshes, where the mesh produced by strategy four is clearly more adapted to the features of the solution that all the other strategies. Adding the area factor to strategies five and six would produce similar results, although in the case of strategy 6 also a control on the minimal elements to be refined would be also advisable. It is worth mentioning, also, that strategies one and two can be adapted to control the elements to be refined by introducing a constant factor into criterions (17) and (18) as follows: $|\eta_k^{\varepsilon}| \geq C \sum_{k=1}^{\mathrm{n_{el}}} |\eta_k^{\varepsilon}|/\mathrm{n_{el}}$ and $|\eta_k^{\varepsilon}|/\mathrm{A}_k \geq C \sum_{k=1}^{\mathrm{n_{el}}} |\eta_k^{\varepsilon}|/\mathrm{A}_{\Omega}$. A value of $C = 1$ corresponds to strategies one and two respectively. Note that, however, increasing the value of C does not ensure that the set of elements to be refined is a non-empty set (for instance if a uniform mesh with uniform distribution of the error is obtained).

The final mesh of 10200 nodes obtained using strategy four is shown in figure 21. Strategies three and four produce meshes with similar accuracy but with a more diffuse or uniform refinement. The predicted quantity of interest for this final mesh is $J(u) \approx 2319.1$ associated to the errors $\eta^{\varepsilon} = 0.051528$ and $\mathscr{Q}(e^*, e^*) = 0.0000375$. Again, the quadratic contribution to the error is negligible in front of the linear contribution.

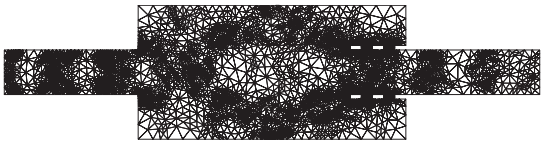

Fig. 21 Example 2: Final mesh obtained using the adaptive procedure described in strategy four with 10200 nodes.

Finally, figure 22 shows the local elementary contributions of η^{ε} to the error in the quantity of interest for the initial mesh and figure 23 shows the elements marked to be refined for each of the proposed adaptive strategies, reaffirming the behavior observed in the convergence curves and the intermediate meshes.

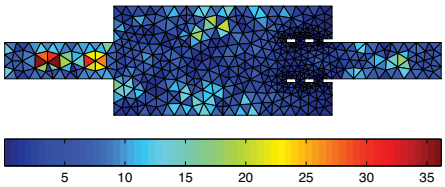

Fig. 22 Example 2: Local maps of the error in the linear term contribution to the quantity of interest $J_3(u)$ using the representation η^{ε}.

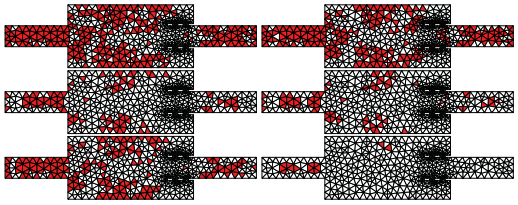

Fig. 23 Example 2: Elements to be refined in the first step highlighted for the six different strategies (from top-left to bottom-right): strategy 1 (top-left) with 303 elements, strategy 2 (top-right) with 316 elements, strategy 3 (middle-left) with 87 elements, strategy 4 (middle-right) with 87 elements, strategy 5 (bottom-left) with 183 elements and strategy 6 (bottom-right) with 14 elements.

7.3 Car cavity

This example studies the noise transmission inside a two-dimensional section of the cabin of a car which is excited by vibrations of the front panel and damped by Robin boundary conditions. This example is frequently used as a benchmark problem in error assessment for interior acoustic problems [9,28,29]. The geometry of the cabin is shown in figure 24. The size of the domain is characterized by the maximum horizontal and vertical lengths, $L_x = 2.7m$ and $L_y = 1.1m$, respectively. The source term entering in equation (1) is $f = 0$, and the Neumann and Robin boundary conditions entering in equations (2b) and (2c) are of the form $g = -i\rho c\kappa v_n$ and $mu = -i\rho c\kappa A_n u$, where in this case the material parameters are $c = 340m/s$ and $\rho = 1.225kg/m^3$. The vibrating front panel is excited with a unit normal velocity $v_n = 1m/s$ whereas the roof is considered to be an absorbent panel with associated admittance $A_n = 1/2000m.(Pa.s)^{-1}$. The normal boundary velocity is set to be zero at the other sides, $v_n = 0m/s$. Finally, a wave number of $\kappa \approx 9.7$, equivalent to a frequency of 525 Hz, has been considered in the computations.

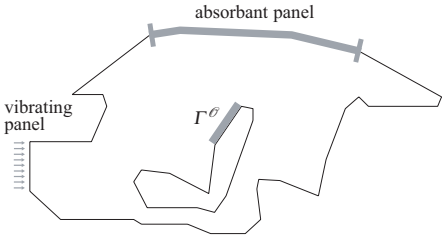

Fig. 24 Example 3: Description of the two-dimensional section of the cabin of a car and its associated boundary conditions.

The output of interest is the average of the squared modulus of the solution over the boundary strip Γ^o shown in figure 24, namely $J_2(u)$. The initial mesh used for this example is shown in figure 25. Figures 26 and 27 show the Galerkin approximations of the primal and adjoint problems for the initial mesh along with the finite element approximations computed in a reference mesh obtained by refining each element into 256 new ones. The figures also show the approximation of the true errors obtained by subtracting the two finite element approximations. The dispersion errors associated to the primal and adjoint problems are $E^{\epsilon} = 0.075$ and $E^e = 0.130$, respectively. Thus, the adjoint problem presents smaller dispersion errors and it is expected that in this mesh, the estimate η^{ϵ} provides better approximations to the error in the quantity of interest than η^e.

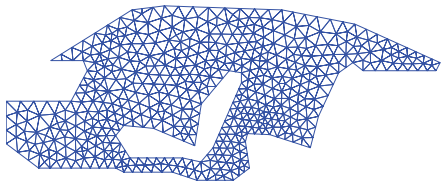

Fig. 25 Example 3: Initial mesh for the adaptive procedure with 568 nodes.

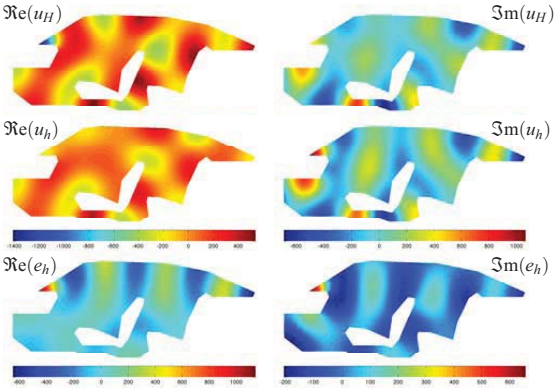

Fig. 26 Example 3: Galerkin finite element approximation of the primal problem for the initial mesh of 568 nodes (top). The middle figures are the Galerkin approximation for a mesh obtained dividing each element into 256 new ones. The reference error with respect to this mesh is shown in the bottom.

The mesh is adaptively refined using the refinement algorithm named after *strategy 4* in the previous example. The adaptive procedure is guided by the indicators provided by η^{ϵ}. However, in each step, the estimate η^e is also computed to compare the results.

The initial mesh of 568 elements provides the approximation of the quantity of interest $J_2(u_H) = 27093.7$ while the error estimation procedures described in this work provide the estimates for the error in the quantity of interest $\eta^{\epsilon} = 32461.3$, $\eta^e = 31966.4$ and $\mathcal{Q}(e^*, e^*) = 5.6$.

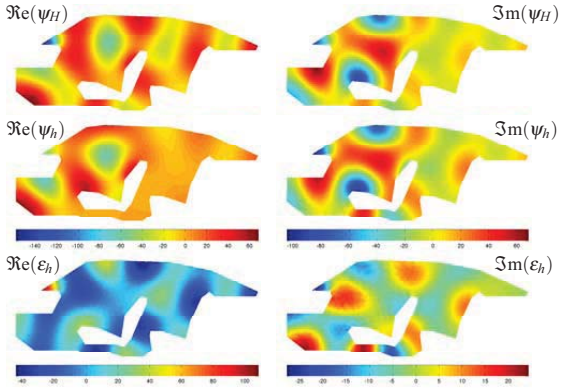

Fig. 27 Example 3: Galerkin finite element approximation of the adjoint problem for a mesh of 568 nodes (top). The middle figures are the Galerkin approximation for a mesh obtained dividing each element into 64 new ones. The reference error with respect to this mesh is shown in the bottom.

Thus, the estimates for the quantity of interest in the first mesh are $J_2(u) \approx 59560.6$ and 59065.8 for the two different representations, respectively. The reference value for the quantity of interest $J_2(u_h) = 65821.7$ confirming that, since the dispersion error is smaller in the adjoint problem, the estimate provided by η^{ε} is better than the one provided by η^{e}, although since the underestimation is quite large in both cases, both estimates produce similar accuracy of the estimates. It can also be seen that even for the initial mesh, the contribution of the quadratic term to the quantity of interest is negligible in front of the linear contribution. After remeshing, the final mesh provides the approximation for the quantity of interest $J_2(u_H) = 67076.3$ and the estimates $J_2(u) \approx 69089.6$ and 69098.1 provided by η^{ε} and η^{e} respectively. Note that in this case, since the estimates for the dispersion errors are $E^{\varepsilon} = 0.00358$ and $E^{e} = 0.00487$, the second estimates is expected to be more reliable.

The convergence of the estimates is shown in figure 28. As can be seen, both representations for the quantity of interest provide similar results improving the accuracy of the finite element approximation with very little computational effort (they only involve an inexpensive post-processing of the finite element solutions).

Figure 29 shows the intermediate and final adaptively refined meshes. As can be seen, the adaptive procedure refines the corners where the solution presents larger singularities and also the front part of the mesh which is the region most affecting the quantity of interest. This is confirmed by the fact that the mesh beside the seat is only refined in a reentrant corner where the solution is singular.

The same example is considered in [9] and [30] where mesh adaptivity aiming at reducing global measures of the error are considered. Although the examples shown therein

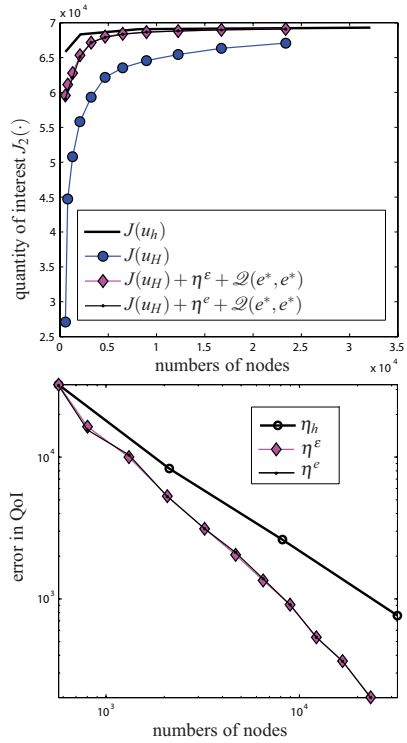

Fig. 28 Example 3: Behavior of the estimates for the nonlinear quantity of interest $J_2(u)$ (top) and convergence of the linear contributions to the error (bottom). c

refer to lower wave numbers, a close comparison with the results obtained with the goal-oriented strategy presented in this work reveals that our technique properly resolves the singularities of the primal problem (refining the regions of the domain where the primal error is larger) while refining, at the same time, the areas relevant for the quantity of interest.

Fig. 29 Example 3: Intermediate and final meshes obtained using the adaptive process associated to strategy 4. Iteration fourth (left) with 3235 nodes and final with 23380 nodes.

8 CONCLUSIONS

A simple and effective strategy for guiding goal-oriented adaptive procedures has been presented, based on the post-

processing techniques introduced in [24,25]. Two different representations of the error in the quantities of interest have been studied which provide similar results. It has been shown that the accuracy of these representations, which involve the post-processing of either the primal or adjoint finite element approximations, is related to the dispersion error of the corresponding problems. The adaptive procedure is valid both linear and non-linear quantities of interest. The non-linear case is solved using a linear approximation and neglecting quadratic terms. In all the analyzed examples the linear part of the quantity of interest is the leading term, since the higher order contribution converge faster to zero.

References

1. Ihlenburg, F., Babuška, I.: Dispersion analysis and error estimation of Galerkin fininite element methods for the Helmohltz equation. Internat. J. Numer. Methods Engrg. **38**, 3745–3774 (1995a)
2. Ihlenburg, F., Babuška, I.: Finite element solution of the Helmholtz equation with high wave number. Part 1: The *hp*-version of the FEM. Comput. Math. Appl. **38**, 9–37 (1995b)
3. Ihlenburg, F.: Finite Element Analysis of Acoustic Scattering, *Applied Mathematical Sciences*, vol. 132. Springer-Verlarg, New York (1998)
4. Deraemaeker, A., Babuška, I., Bouillard, P.: Dispersion and pollution of the FEM solution for the Helmholtz equation in one, two and three dimensions. Internat. J. Numer. Methods Engrg. **46**(4), 471–499 (1999)
5. Babuška, I., Sauter, S.A.: Is the pollution effect of the FEM avoidable for the Helmholtz equation considering high wavenumber? SIAM Rev. **42**(3), 451–484 (2000)
6. Stewart, J.R., Hughes, T.J.R.: Explicit residual-based a posteriori error estimation for finite element discretizations of the Helmholtz equation. computation of the constant and new measures of error estimator quality. Comput. Methods Appl. Mech. Engrg. **131**(3-4), 335–363 (1996)
7. Babuška, I., Ihlenburg, F., Strouboulis, T., Gangaraj, S.K.: A posterori error estimation for finite element solutions of Helmholtz' equation Part I: The quality of locar indicators and estimators. Internat. J. Numer. Methods Engrg. **40**, 3443–3462 (1997)
8. Bouillard, P.: Admissible fields and error estimation for acoustic fea with low wave numbers. Comput. Struct. **73**(1-5), 227–237 (1999)
9. Bouillard, P., Ihlenburg, F.: Error estimation and adaptivity for the finite element method in acoustics: 2d and 3d applications. Comput. Methods Appl. Mech. Engrg. **176**(1), 147–163 (1999)
10. Irimie, S., Bouillard, P.: A residual a posteriori error estimator for the finite element solution of the Helmholtz equation. Comput. Methods Appl. Mech. Engrg. **190**(31), 4027–4042 (2001)
11. Peraire, J., Patera, A.T.: Asymptotic a posteriori finite element bounds for the outputs of noncoercive problems: The Helmholtz and burgers equations. Comput. Methods Appl. Mech. Engrg. **171(1)**, 77–86 (1999)
12. Sarrate, J., Peraire, J., Patera, A.T.: A posteriori finite element error bounds for non-linear outputs of the Helmholtz equation. Internat. J. Numer. Methods Engrg. **31**(1), 17–36 (1999)
13. Walsh, T., Demkowicz, T.: *hp* boundary element modeling of the external human auditory system - Goal oriented adaptivity with multiple load vectors. Comput. Methods Appl. Mech. Engrg. **192**(1-2), 125–146 (2003)
14. Strouboulis, T., Babuška, I., Hidajat, R.: The generalized finite element method for Helmholtz equation theory, computation, and open problems. Comput. Methods Appl. Mech. Engrg. **195**, 4711–4731 (2006)
15. Maday, Y., Patera, A.T., Peraire, J.: A general formulation for a posteriori bounds for output functionals of partial differential equations; application to the eigenvalue problem. C. R. Acad. Sci. Paris - Anal. Numér. **328**(1), 823–828 (1999)
16. Zienkiewicz, O., Zhu, J.: A simple error estimator and adaptive procedure for practical engineering analysis. Int. J. Numer. Methods Engrg. **24**, 337–357 (1987)
17. Zienkiewicz, O., Zhu, J.: The superconvergent patch recovery (SPR) and adaptive finite element refinement. Comput. Methods Appl. Mech. Engrg. **101**, 207–224 (1992)
18. Díez, P., Rodenas, J.J., Zienkiewicz, O.C.: Equilibrated patch recovery error estimates: simple and accurate upper bounds of the error. Internat. J. Numer. Methods Engrg. **69**(10), 2075–2098 (2007)
19. Ainsworth, M., Oden, J.T.: A posteriori error estimation in finite element analysis. John Wiley & Sons, Chichester (2000)
20. Ladevèze, P., Leguillon, D.: Error estimate procedure in the finite element method and applications. SIAM J. Numer. Anal. **20**(3), 485–509 (1983)
21. Díez, P., Parés, N., Huerta, A.: Recovering lower bounds of the error by postprocessing implicit residual a posteriori error estimates. Internat. J. Numer. Methods Engrg. **56**(10), 1465–1488 (2003)
22. Parés, N., Díez, P., Huerta, A.: Subdomain-based flux-free a posteriori error estimators. Comput. Methods Appl. Mech. Engrg. **195**(4-6), 297–323 (2006)
23. Parés, N., Santos, H., Díez, P.: Guaranteed energy error bounds for the Poisson equation using a flux-free approach: solving the local problems in subdomains. Internat. J. Numer. Methods Engrg. **79**(10) (2009)
24. Steffens, L.M., Díez, P.: A simple strategy to assess the error in the numerical wave number of the finite element solution of the Helmholtz equation. Comput. Methods Appl. Mech. Engrg. **198**, 1389–1400 (2009)
25. Steffens, L.M., Parés, N., Díez, P.: Estimation of the dispersion error in the numerical wave number of standard and stabilized finite element approximations of the Helmholtz equation. Internat. J. Numer. Methods Engrg. **to appear**
26. Díez, P., Calderón, G.: Remeshing criteria and proper error representations for goal oriented *h*-adaptivity. Comput. Methods Appl. Mech. Engrg. **196**(4-6), 719–733 (2007)
27. Babuška, I., Ihlenburg, F., Strouboulis, T., Gangaraj, K.: A posterori error estimation for finite element solutions of Helmholtz' Part II: Estimation of the pollution error. Internat. J. Numer. Methods Engrg. **40**, 3883–3900 (1997)
28. Suleau, S., Deraemaeker, A., Bouillard, P.: Dispersion and pollution of meshless solutions for the Helmholtz equation. Comput. Methods Appl. Mech. Engrg. **190**, 639–657 (2000)
29. Harari, I., Magoulès, F.: Numerical investigations of stabilized finite element computations for acoustics. Wave Motion **39**, 339–349 (2004)
30. Bausys R., H.P., Wiberg, N.E.: Postprocessing techniques and *h*-adaptive finite element-eigenproblem analysis. Comput. Struct. **79**, 2039–2052 (2001)